2013-04-19

GNSS Interference Mitigation Using Antenna Array Processing

Daneshmand, Saeed

UNIVERSITY OF CALGARY

GNSS Interference Mitigation Using Antenna Array Processing

by

Saeed Daneshmand

A THESIS

SUBMITTED TO THE FACULTY OF GRADUATE STUDIES

IN PARTIAL FULFILMENT OF THE REQUIREMENTS FOR THE

DEGREE OF DOCTOR OF PHILOSOPHY

DEPARTMENT OF GEOMATICS ENGINEERING

CALGARY, ALBERTA

APRIL, 2013

Abstract

Although hundreds of millions receivers are used worldwide, the performance of location-based services provided by GNSS is still compromised by interference which can range from unintentional distortion due to multipath propagation to intentionally menacing spoofing signals. Hence, the requirement for proper mitigation techniques becomes a must in GNSS receivers for robust, accurate and reliable positioning.

Recently, interference mitigation techniques utilizing antenna arrays have gained significant attention in GNSS communities. Although at the time of this thesis, employing antenna array in GNSS applications is mostly limited to academic research and possibly sophisticated military applications, it is expected that in the near future, antenna array-based receivers will become widespread in civilian markets as well. Rapid advances in electronic systems and antenna design technology make previously hardware and software challenging problems easier to solve. Furthermore, due to the significant effort devoted to miniaturization of RF front-ends and antennas, the size of antenna array-based receivers will no longer be an issue.

Given the above, this thesis investigates the use of antenna arrays in GNSS interference mitigation applications. It starts by proposing a new spatial processing technique capable of mitigating both high power interference and coherent and correlated GNSS multipath signals. It then follows by introducing three new methods that take advantage of spatial and temporal processing in three different GNSS applications.

In the first method, the use of spatial-temporal processing for multipath mitigation in the form of a synthetic array is studied. A new method utilizing a moving antenna array is proposed to deal with highly correlated multipath components and also to increase the

degree of freedom of the beamformer by synthesizing a larger antenna array. Thus, the array's degree of freedom is not limited to the number of physical antenna elements. This method can be employed to mitigate multipath signals in vehicular navigation applications.

The second method investigates benefits of spatial-temporal processing algorithms for improving narrowband interference mitigation performance. The limitations of previous space-time filters are analyzed and a new approach that employs the inherent periodic feature of GNSS signals in conjunction with the spatial-temporal processing to improve the performance of existing space-time filters is proposed. It is shown that in some interference scenarios, a space-time filter subject to the distortionless constraint may cause a significant degradation to the signal-to-noise ratio (SINR), which can be alleviated by employing the periodicity in the structure of the filter.

In the third method the advantage of spatial-temporal processing for the purpose of GNSS spoofing mitigation is studied. A new mitigation approach, which removes the spoofing signal LOS component as well as its multipath reflections before the despreading process of GNSS signals, is introduced. This in turn decreases the computational complexity and processing time. Therefore, this method can be either employed as an inline standalone pre-processing unit for conventional GNSS receivers or it could easily be integrated in the next generation of receivers.

Several simulations and real data analyses are used to evaluate and show the effectiveness of the proposed methods.

Preface

This thesis includes some materials (e.g. figures, tables, formulas and texts) previously published, accepted or submitted in three conference papers, one magazine paper, three journal papers and one pending patent as follows:

Daneshmand, **S.,** A. Broumandan, J. Nielsen and G. Lachapelle (2013a) "Interference and multipath mitigation utilising a two-stage beamformer for global navigation satellite systems applications" *IET Radar, Sonar and Navigation Journal,* vol 7, no 1, January, pp. 55-66

Daneshmand, **S.,** A. Broumandan, N. Sokhandan and G. Lachapelle (2013b) "GNSS Multipath Mitigation with a Moving Antenna Array" *IEEE Transactions on Aerospace and Electronic Systems*, vol 49, no 1, January, pp. 693-698

Daneshmand, **S.,** A. Jafarnia, A. Broumandan and G. Lachapelle (2013c) "GNSS spoofing mitigation in multipath environments using space-time processing" *accepted to the European Navigation Conference (ENC) 2013*, 23-25 April, Vienna, Austria, 10 pages

Daneshmand, **S.,** A. Broumandan, and G. Lachapelle (2013d) "Distortionless Space-Time Interference Mitigation for GNSS Applications" *Submitted to IEEE Transactions on Aerospace and Electronic Systems*, 17 pages

Daneshmand, **S.,** A. Jahromi, A. Broumandan and G. Lachapelle (2012)"A Low-Complexity GPS Anti-Spoofing Method Using a Multi-Antenna Array" *in Proceedings of the 25th International Technical Meeting of The Satellite Division of the Institute of Navigation (ION GNSS 2012)*, 17-21 September, Nashville TN, 11 pages

Daneshmand, S., A. Jafarnia-Jahromi, A. Broumandan, J. Nielsen, G. Lachapelle (2012) *Global Navigation Satellite System (GNSS) Anti-Interference using Array Processing* Submitted to the U.S. Bureau of Patents and Trademarks, November

Daneshmand, **S.,** A. Broumandan and G. Lachapelle (2011a) "GNSS Interference and Multipath Suppression Using Array Antenna," *in Proceedings of the 24th International Technical Meeting of the Satellite Division of the Institute of Navigation (ION GNSS 2011)*, 20-23 September, Portland, OR, pp. 1183-1192

Daneshmand, **S.,** A. Jafarnia, A. Broumandan and G. Lachapelle (2011b) "A Low Complexity GNSS Spoofing Mitigation Technique Using a Double Antenna Array" *GPS World*, vol 22, no 12, December, pp. 44-46

The above papers were produced by the author during the research phase of this thesis.

The co-authors' valuable feedback on the above materials is acknowledged.

Acknowledgements

I would like to express my gratitude to my supervisor, Professor Gérard Lachapelle for his expertise, kindness, constant guidance and encouragement during my PhD studies. I will never forget his sound advice and support, which have helped me to shape my professional career.

Special thanks to my advisor, Dr. Ali Broumandan for sharing his insights and helping me in the theoretical work of this thesis. This dissertation would not have been possible without his guide and knowledge. I would also like to thank Professor John Nielsen, Professor Mark Petovello, Dr. Cillian O'Driscoll, Dr. Daniele Borio, and Dr. Vahid Dehghanian for their valuable advice during my studies.

I owe special thanks to my graduate student colleagues Mohammad Abdizadeh, Anup Dhital, Elmira Amirloo, Nima Sadrieh and other friends who have provided me with an enjoyable and peaceful environment for study. In particular, I would like to thank my colleague and friend Ali Jafarnia whose positive comments and help were of upmost importance in completing this research.

I am incredibly thankful to have my parents and my brother. They are always supporting and encouraging me with their best wishes. I could never have gotten this far without them.

Finally and most important, I wish to thank Negin Sokhandan, my beloved wife and wonderful colleague. I would never have been able to finish my dissertation without her support both in academia and in life.

Dedication

To my wife Negin,

& my parents, Mahin and Fereidoon

& my brother Ali

Table of Contents

List of Tables

List of Figures

List of Acronyms

AG	Array Gain
AM	Amplitude Modulation
AOA	Angle Of Arrival
CAF	Cross Ambiguity Function
CDMA	Code Division Multiple Access
CS	Correlator Spacing
CW	Continuous Wave
DF	Direction Finding
DLL	Delay Locked Loop
DOF	Degree Of Freedom
DSSS	Direct Sequence Spread Spectrum
ED	Eigenvalue Decomposition
FM	Frequency Modulation
GED	Generalized Eigen Decomposition
GNSS	Global Navigation Satellite System
HRC	High Resolution Correlator
IFS	Interference Frequency Span
IMU	Inertial Measurement Unit
INR	Interference to Noise Ratio
LCMP	Linear Constrained Minimum Power
LCMV	Linear Constrained Minimum Variance
LOS	Line Of Sight
LPA	Linear Prediction Algorithm
MDOP	Minimum Difference Output Power
ML	Maximum Likelihood
MPDR	Minimum Power Distortionless Response
MSINR	Maximum Signal-to-Interference-plus-Noise Ratio
MUSIC	MUltiple Signal Classification
MVDR	Minimum Variance Distortionless Response
OPDA	Outer Product Decomposition Algorithm
PPD	Personal Privacy Device
PRN	Pseudo Random Noise
RF	Radio Frequency
RHCP	Right Hand Circularly Polarized
SAPR	Spoofing to Authentic Power Ratio
SDR	Software Defined Radio
SFAP	Space-Frequency Adaptive Processing
SINR	Signal to Interference-plus-Noise Ratio
SNR	Signal to Noise Ratio
SOS	Second Order Statistics
STAP	Space-Time Adaptive Processing
SVD	Singular Value Decomposition
TOA	Time Of Arrival
TDL	Tapped Delay Line

UWB	Ultra Wide Band
WAAS	Wide Area Augmentation System

List of Symbols

φ_{Az}	Azimuth angle
θ_{El}	Elevation angle
$\mathbf{d}_i^{ant}$	Vector pointing from the origin of the coordinate system to the *i*th antenna element
B_s	Signal bandwidth
$\Delta t_{\max}$	Maximum possible delay of incident signals between two antennas in the array
t_i	Propagation delay of the *i*th antenna with respect to the origin of the coordinate
f_c	Carrier frequency
N	Number of antenna elements in the array
t	Time
$s_{ant}(t)$	Complex envelope of the signal
$\mathbf{s}_{ant}(t)$	Complex envelope of the signal vector
$x_{ant}(t)$	Received signal at the antenna element
$\mathbf{x}_{ant}(t)$	Received signal vector at the antenna array
$z(t)$	Beamformer output signal
$h_i(t)$	Impulse response of the *i*th branch of the beamformer
$\mathbf{h}(t)$	Impulse response vector of the array
$\boldsymbol{S}_{ant}(f)$	Complex envelope of the signal vector in frequency domain
$\boldsymbol{H}(f)$	Impulse response vector of the array in frequency domain
$Z(f)$	Beamformer output signal in frequency domain
$\hat{\mathbf{e}}$	Unitary vector pointing the direction of the incident signal
$\mathbf{a}_{\hat{\mathbf{e}}}$	Array manifold vector or array steering vector for the signal coming from direction $\hat{\mathbf{e}}$
c	Propagation speed
$\Upsilon(f,\hat{\mathbf{e}})$	Beamformer response
BP	Array beam pattern (in dB)
$\mathbf{w}$	Weighting vector or gain vector
N_{de}	Number of the desired signals

I	Number of the undesired signals
$\boldsymbol{\eta}$	Noise vector
σ^2	Noise variance
$\mathbf{R}_{\mathbf{r}}$	Spatial correlation matrix for the signal vector $\mathbf{r}$
$\tilde{\mathbf{R}}_{\mathbf{v}}$	Temporal correlation matrix for the signal vector $\mathbf{v}$
σ_s^2	Desired signal variance
$\mathbf{R}_{\mathbf{v},\boldsymbol{\eta}}$	Spatial correlation matrix of the undesired signals-plus-noise
$\mathbf{w}_{MVDR}$	Gain vector obtained from MVDR optimization
$\mathbf{w}_{ML}$	Gain vector obtained from the ML criterion
$p_{\mathbf{r}\|s}\left(\mathbf{r}(t)\middle\|s(t)\right)$	Conditional PDF of $\mathbf{r}(t)$ given $s(t)$
$\mathbf{w}_{MSINR}$	Gain vector obtained from MSINR criterion
$\mathbf{w}_{MPDR}$	Gain vector obtained from MPDR optimization
$\mathbf{C}_{const.}$	Constraint matrix
$\mathbf{C}_{const.\perp}$	Orthogonal projection to the constraint subspace
$\mathbf{w}_{LCMV}$	Gain vector obtained from LCMV optimization
$\mathbf{w}_{LCMP}$	Gain vector obtained from LCMP optimization
$\mathbf{U}_{Int}$	Eigen vector matrix of the interference subspace
$\mathbf{U}_{S+N}$	Eigen vector matrix of the noise-plus-signal subspace
$\boldsymbol{\Lambda}_{Int}$	Eigen value matrix of the interference subspace
$\boldsymbol{\Lambda}_{S+N}$	Eigen value matrix of the noise-plus-signal subspace
$\mathbf{w}_{Eig.}$	Gain vector obtained in Eigen beamformer
$\mathbf{P}_{N+S}$	Projection matrix in to the noise-plus-signal subspace
$\tilde{\mathbf{R}}_{\mathbf{v}s}$	Temporal cross correlation matrix between signal vectors $\mathbf{v}$ and $\mathbf{s}$
ρ	Normalized correlation coefficient
σ_I^2	Interference signal variance
C	Number of subarrays
K	Number of taps in a FIR filter
P_s	Power of the desired signal at the beamformer output
P_v	Power of the interference at the beamformer output
P_η	Power of the noise at the beamformer output
M_{ref}	Number of multipath reflections

$M_{Coh.}$	Number of coherent multipath components
$g(t)$	PRN code
τ	Code delay
ϕ	Phase shift
Δf	Carrier frequency offset
α	Attenuation factor
$\mathbf{a}_0$	Steering vector of the GNSS LOS signal
$\hat{\mathbf{s}}$	Signal vector $\mathbf{s}$ after despreading
$\hat{\mathbf{R}}$	Spatial correlation matrix after despreading
$\hat{\sigma}^2$	Noise variance at the correlator output
$\bar{\mathbf{A}}$	Steering matrix of the multipath signals
$\tilde{\mathbf{S}}$	Temporal correlation matrix of multipath signals after despreading
$\hat{\mathbf{r}}$	Received array signal vector $\mathbf{r}$ after despreading
$\hat{\boldsymbol{\eta}}$	Noise vector after despreading
$\boldsymbol{\zeta}$	Noise vector after applying differencing between subarrays
$\hat{\mathbf{R}}_D$	Spatial correlation matrix after despreading and differencing between subarrays
$\mathbf{U}_s$	Eigen vector matrix of the signal subspace
$\mathbf{U}_n$	Eigen vector matrix of the noise subspace
$\mathbf{\Lambda}_s$	Eigen value matrix of the signal subspace
T_c	Coherent integration time
$\mathbf{v}_{vel}$	Velocity vector of a moving array
λ	Carrier wavelength
K_{win}	Number of the consecutive widows for forming correlation matrix
λ_{GE}	Generalized Eigen value
M	Number of GNSS signals
I_N	Number of the narrowband interfering signals
I_W	Number of the wideband interfering signals
$x_i(t)$	Waveforms of the *i*th narrowband interfering signal
$y_q(t)$	Waveforms of the *q*th wideband interfering signal
T_e	Period of the GNSS signal
$S_m'(f)$	Power spectrum of one period of the GNSS signal

L_p	Number of GNSS signal periods employed in space-time filtering
T_s	Sampling duration
P	Number of samples per epoch
L_{FIR}	Total number of tabs in space-time processing
N_0	Power noise spectral density
AG	Array gain
L_{ch}	Maximum available delay for multipath components among all desired and undesired signals
K_s	Number of consecutive snapshots to form the augmented space-time correlation matrix
σ_{sp}^2	Power of the spoofing signal
$\mathrm{L}(\mathbf{w}, \boldsymbol{\lambda}_L)$	Lagrange function
$\boldsymbol{\lambda}_L$	Lagrangian multiplier

List of Notations

$(\cdot)^H$:	Complex conjugate transpose
$(\cdot)^T$:	Transpose
$(\cdot)^*$:	Conjugate
$(\cdot)^{\#}$:	Pseudo Inverse
$\|\cdot\|$:	Vector norm
$E\{\cdot\}$:	Statistical expectation
$F^{-1}\{\cdot\}$:	Invers Fourier transform
$F\{\cdot\}$:	Fourier transform
$\|a\|$:	Absolute value of scalar a
$\otimes$:	Kronecker product
$\underset{M}{\mathbf{1}}$:	$M \times 1$ all-one vector
$\underset{M}{\mathbf{I}}$:	$M \times M$ identity matrix
$\underset{M \times N}{\mathbf{0}}$:	$M \times N$ all-zero matrix
$\det(\mathbf{A})$	Determinant of matrix $\mathbf{A}$
$rk(\mathbf{A})$:	Rank of matrix $\mathbf{A}$

Furthermore, bold letters, capital bold letters, capital italic letters and bold capital italic letters stand for vectors in time domain, matrices in time domain, scalar in frequency domain and vector in frequency domain, respectively.

Chapter One: INTRODUCTION

Despite the ever increase in demand for accurate and reliable global navigation satellite system (GNSS) dependent services, one of the main drawbacks of GNSS signals is their susceptibility to interference. Interference ranges from unintentional distortion due to multipath propagation to intentionally menacing spoofing signals. Generally, interference decreases the effective signal-to-noise ratio (SNR) of received satellite signals such that a receiver may not be able to measure the true values of pseudoranges and carrier phases. Therefore, even a low-power interfering signal can easily deny GNSS services within a radius of several kilometres.

Interference can generally be detected and suppressed by using time, frequency and spatial domain processing or a combination of them. Time/frequency narrowband interference detection and suppression methods have been widely studied and reported in the literature. However, their performance degrades when dealing with wideband interference or rapid changes of interference centre frequency. On the contrary, interference mitigation techniques utilizing an antenna array can effectively detect and suppress both narrowband and wideband interfering signals regardless of their time and frequency characteristics.

Rapid advancements in electronic systems and antenna technology are resulting in powerful antenna array based solutions to further enhance the performance of GNSS receivers in terms of signal to interference-plus-noise ratio (SINR). This chapter begins with a brief introduction of GNSS interference, mitigation strategies and antenna array

processing. Those constitute the motivation for this research. It then goes on to objectives and contributions of this thesis and ends with the dissertation outline.

1.1 Background and motivation

Positioning and timing systems such as GPS and GLONASS are widespread in today's human life. Currently, most mobile phones as well as vehicles are equipped with GNSS receivers. GNSS applications include safety of life, tracking of animals and vehicles, air, marine and ground transportation, criminal offenders' surveillance, police and rescue services, timing synchronization, surveying, electrical power grids, space applications, agricultural and so many other applications. In fact, it is not an exaggeration to say that GNSS is now affecting in any aspect of human life. However, GNSS signals are vulnerable to in–band interference because of being extremely weak received signals. For instance, GPS includes satellites orbiting at approximately 20,000 km above the Earth, transmitting signals which are received on the Earth's surface with a power of approximately -158.5 dBW for L1 C/A and -160 dBW for L2 (Kaplan & Hegarty 2006). Such signals have spectral power densities far below that of the ambient thermal noise (for L1 C/A signal, 16.5 dB below the noise floor for a receiver with a 2 MHz bandwidth). Although the despreading process performed in both acquisition and tracking stages brings these signals above the background noise, they are still susceptible to interference. The spread spectrum technique applied in the structure of GNSS signals provides a certain degree of protection against interference for narrowband interfering signals and multipath (Pickholtz et el 1982); however, the spreading gain alone is not

sufficient to avoid interference whose power is much stronger than the GNSS signal power or to mitigate non-resolvable multipath components[1].

GNSS interference can be classified in two groups, namely intentional and unintentional interference. Intentional interference can be generated by GNSS jammers (e. g. by a transmission of a strong continuous wave (CW) signal, strong Gaussian noise in GNSS frequency bands or by smart jammers such as spoofers). Unintentional interference can be generated by a variety of electronic devices working on their non-linear region so as to emit strong electromagnetic harmonics in GNSS frequency bands or from broadband communication systems such as television and radio broadcasting stations which have also harmonics in GNSS frequency bands (Borio 2008). Considering bandwidth, interfering signals can be categorized into narrowband and wideband. In the case of narrowband interference, only a small portion of the GNSS frequency bands is affected whereas wideband interference almost occupies the entire frequency band. For example, CW interference is a narrowband interfering signal and Gaussian noise jammers produce wideband interfering signals.

Past decades have seen significant advances in electronic technology. However, these rapid changes have also had some drawbacks influencing GNSS. In recent years, low cost GNSS jammers have become available such as so-called personal privacy devices (PPDs). The main target of these devices is to disturb GNSS receivers within a radius of a few metres; however, this is not always the case due to the poor quality of electronic elements used in PPDs. For instance, it has been observed that these jammers can

[1] multipath components whose delays are less than one chip duration

dangerously impact GNSS receivers and wide area augmentation systems (WAASs) employed in air navigation (Grabowski 2012). Therefore, interference not only degrades the performance of GNSS receivers but also can seriously jeopardize the security and safety of human life. This makes GNSS interference detection and mitigation a high research and development priority in GNSS communities. Different types of interference adversely impacting GNSS are tabulated in Table 1-1.

Table 1-1: Types of interference and typical sources (Kaplan & Hegarty 2006)

Types of Interference		Typical sources
Narrowband	Continuous wave	Intentional sinusoidal jammers or near-band unmodulated transmitter's carriers
	Swept continuous wave	Intentional CW jammers or frequency modulation (FM) transmitter's harmonics
	Phase/frequency modulation	Intentional chirp jammers or harmonics from an amplitude modulation (AM) radio station, citizens band radio or amateur radio transmitter
Wideband	Band-limited Gaussian	Intentional matched bandwidth noise jammers
	Phase/frequency modulation	Television transmitter's harmonics of near-band microwave link transmitters
	Matched spectrum	Intentional matched spectrum jammers or near-field of pseudolites
	Wide-band-pulse	Any type of burst transmitters such as radar or ultra wide band (UWB)
	Multipath	Reflection, diffraction and diffusion of signals off nearby objects
	Spoofing signal	spoofer structured to resemble a set of counterfeit GNSS signals to mislead receivers

From this thesis' point of view, interfering signals mentioned in Table 1-1 are categorized into three groups: namely "strong narrowband and wideband interference", "multipath" and "spoofing signals". The first group consists of any high power interfering signal which is not correlated with GNSS signals such that it is spread during acquisition and tracking stages in a GNSS receiver. Therefore, this type of interference can be more conveniently

detected and mitigated before despreading. On the other hand, multipath signals are inherently correlated with the GNSS signals. Although long-delay or resolvable multipath signals are essentially suppressed during the despreading process, non-resolvable or short-delay ones may significantly degrade the performance of receivers. The last group encompasses spoofing signals which mimic the authentic GNSS signals. Therefore they are correlated with the GNSS signals as well as multipath. However, their navigation bits are different and their ranges are intelligently controlled. A spoofing signal includes several counterfeit pseudo random noise (PRN) codes which carry false time and position solutions to deceive receivers.

The main objective of this thesis is to introduce new algorithms and methods for suppressing these three types of interfering signals based on the antenna array processing. These three groups and their mitigation approaches currently studied in the literature are briefly introduced in the following subsections.

1.1.1 Strong narrowband and wideband interference

Generally, interference can be suppressed using each one or a combination of the time, frequency and spatial domain processing. Interference suppression methods based on time and frequency processing have been broadly studied in the literature; however, their performance degrades when they deal with wideband interference (e. g. Gaussian jammers or harmonics from television transmissions) or when interfering signals change fast in time or frequency. On the other hand, interference mitigation techniques utilizing an antenna array can effectively suppress narrowband and wideband interference signals independent of their time and frequency characteristics. Herein, strong narrowband and wideband

interference is referred to as any unwanted radio frequency (RF) signal such as tones, swept waveforms, pulse and broadband noise and any other multi-frequency and time-varying version thereof (Poisel 2004). They are called strong because they must have enough power to be adversely effective on the receiver performance even after despreading and Doppler removal. In fact, in the context of array processing, all these interfering signals are considered narrowband plane waves as long as the reciprocal of a maximum propagation delay across the array is much greater than the signal bandwidth (Van Trees 2002). This is explained in the next chapter. Therefore, regardless of the characteristics of these interfering signals, they can be suppressed by applying a proper spatial filter.

1.1.2 Multipath

Another type of interference in GNSS applications is caused by multipath propagation. This phenomenon in outdoors is mostly caused by reflection and diffraction of the signals off nearby objects such as buildings, mountains, trees and so on. Although the spread spectrum technique is also resistant to multipath, it is only able to mitigate the resolvable multipath components whose delays are more than 1.5 chip duration. Multipath may cause significant errors in pseudorange measurements (e.g. for L1 C/A, up to 100 m). Multipath results in one or more additional propagation paths which always have longer propagation time than the line of sight (LOS) signal and the same as the LOS signal their power density is far below the noise floor. This leads to the distortion of the correlation ambiguity function (CAF) and produces negative or positive biases on pseudorange and carrier phase measurements depending of the received phases of multipath components.

Multipath propagation is generally modeled as specular or diffuse. In diffuse multipath scattering environments such as indoor, the magnitudes of the signals arriving by the various paths can be approximately modeled by a Rayleigh distribution (Rensburg & Friedlander 2004). On the other hand, in the specular multipath model, multipath can be assumed as several deterministic replicas of the LOS signal with unknown delays and attenuation factors. This thesis only focuses on mitigation strategies for specular multipath environments. Multipath signals should be considered as wideband interference since their power spread over the GNSS frequency bands. However, due to the high correlation between these signals and the LOS one, in acquisition and tracking stages, these signals are also despread which causes the distortion of CAF and degradation of the receiver's performance. They may induce significant errors in pseudorange measurements. Therefore, multipath generally should be mitigated after despreading process. Multipath effects can be reduced in hardware, software or both parts of a GNSS receiver. In hardware, multipath can be mitigated by using a special antenna design such as choke-ring to put mask on low elevation multipath signals and prevent reflected signals from below the local horizon from reaching the antenna, or employing right hand circularly polarized (RHCP) antennas to at least suppress those multipath components reflected once. In software, there is a large volume of published studies describing time-frequency domain algorithms. The most famous ones widely implemented in commercial GNSS receivers are correlation-based multipath mitigation methods (Irsigler & Eissfeller 2003, McGraw & Braasch 1999, Van Dierendonck et al 1992). Correlation-based methods were developed and studied over the years such as the double-delta technique (Irsigler & Eissfeller 2003), the strobe correlator (Garin & Rousseau, 1997), high resolution correlator (HRC) (McGraw & Braasch 1999),

and the multipath estimation delay locked loop (MEDLL) (Van Nee 1992, Townsend et al 1995). Although correlation-based techniques achieve much better results than the conventional standard delay locked loop (DLL) in terms of multipath timing bias, they may fail to mitigate the effect of closely spaced multipath components or when a multipath component that is stronger than the LOS signal exists (e. g. foliage obstructions). In these situations, the performance of GNSS receivers degrades significantly and the timing synchronization may fail (Closas et al 2006). In general, the important common property between most of these correlation-based techniques is that their stable lock point is at the maximum power of the correlation function (Townsend & Fenton 1994), no matter how much this peak has been shifted with respect to the peak which corresponds to the actual LOS. On the other hand, multipath mitigation methods based on spatial processing are theoretically able to mitigate multipath components stronger than the LOS signal, no matter how much the multipath components are close to each other and the LOS one. Section 1.2.2 briefly reviews the research conducted on GNSS multipath mitigation employing an antenna array.

1.1.3 Spoofing

GNSS signals are defenseless against high power in–band interference signals such as jamming and spoofing. Spoofing is well-known to be the most hazardous intentional interfering signal that targets GNSS receivers and forces them into generating false time and position solutions. A spoofing attack is more treacherous than jamming since the target receiver is not aware of the threat. Ever-increasing advances in electronic technology have made GNSS spoofers and jammers more flexible and less costly such that interferers

impacting GNSS can be developed at a low cost for civilian misapplications (Humphreys et al 2008).

Several anti-spoofing techniques have been recently proposed in the open literature. These methods can be generally divided into two main categories, namely spoofing detection and spoofing mitigation. Spoofing detection algorithms concentrate on discriminating the spoofing attack while spoofing mitigation techniques aim to neutralize the spoofing threat. Most of the previously proposed techniques focus on spoofing detection rather than spoofing mitigation. Amplitude discrimination, time of arrival (TOA) discrimination, consistency cross-check of the solution with inertial measurement units (IMU), polarization discrimination, angle of arrival (AOA) discrimination and cryptographic authentication are some of the most popular spoofing detection techniques documented in the recent literature (Jafarnia et al. 2012, Ledvina et al 2010, Montgomery et al 2009, Humphreys et al 2008, Wen et al 2005).

Spoofing countermeasure using multiple antennas is one of the powerful techniques that have been devised against this threat (Daneshmand et al 2013c, Daneshmand et al 2012, Daneshmand et al 2011b, Nielsen et al 2010, Montgomery et al 2009, McDowell 2007, Hartman 1996). These techniques generally rely on the fact that a spoofer usually transmits several PRN codes from the same antenna while the authentic signals are transmitted from different satellites from different directions.

1.2 Antenna array processing in GNSS

A large and growing body of literature has investigated antenna array processing as a powerful tool for GNSS interference suppression. This section provides a background on antenna array-based methods for mitigating GNSS interference introduced in the previous

section. Some previous work and associated limitations for interference mitigation using antenna array processing are briefly described.

1.2.1 Strong narrowband and wideband interference suppression

Antenna array processing in GNSS applications has been mostly centered on interference suppression (Amin & Sun 2005, Amin et al 2004, Fante & Vaccaro 2000, Brown & Gerein 2001, e. g. Fante & Vaccaro 1998a, Fante & Vaccaro 1998b, Zoltowski & Gecan 1995). Zoltowski & Gecan (1995) draws the attention on utilizing the minimum power distortionless response (MPDR) beamforming for GPS applications to reject interference signals whose power is significantly higher than that of GPS signals, these being below the noise floor. Amin & Sun (2005) and Sun & Amin (2005a) took advantage of the periodicity of GPS signals and also highlighted the usefulness of eigenvector beamformers for GNSS applications with this difference that contrary to the conventional subspace beamformer, which projects the received signal onto the signal subspace, the received signal is projected onto the noise-plus-GNSS signal subspace. Received signals will be then enhanced such that the beamformer maximizes the desired signal to interference-plus-noise ratio (SINR).

Despite the effectiveness of antenna array-based methods, they suffer from hardware complexity. Considering the fact that the number of antennas determines the number of undesired signals that can be mitigated, limitation on the number of the antennas, size and shape of the array can be considered as the main problem for these methods. To deal with this problem, techniques employing both time/frequency and spatial domain processing such as space-time adaptive processing (STAP) and space-frequency adaptive processing (SFAP) previously employed for radar and wireless applications have been studied and

developed for GNSS as well in the literature (e. g. Gupta & Moore 2004, Fante & Vaccaro 2002, Myrick et el 2001, Hatke 1998). These methods combine spatial and temporal filters to suppress more radio frequency interfering signals by increasing the degree of freedom without increasing physically the antenna array size. However, a number of considerations should be taken into account in designing a space-time filter in order to prevent distortions in pseudorange and carrier phase measurements. The term "adaptive" is employed as opposed to "deterministic" and means that the filter follows the changes in environment and constantly adapts its own pattern by means of a feedback control. Studying adaptive methods is outside the scope of this dissertation.

Moving antenna arrays and synthetic array processing are other solutions to increase the degree of freedom (DOF) without increasing the number of physical antenna elements. Recently, the antenna motion in the form of synthetic antenna array processing has been utilized to augment the correlation matrix for the purpose of angle of arrival estimation, multipath mitigation and other applications (Daneshmand et al 2013b, Broumandan et al 2008, Draganov et al 2011).

1.2.2 Multipath mitigation

In the context of multipath mitigation using an antenna array in GNSS applications, much work has been proposed. Seco-Granados et el (2005) and Brown (2000) studied the maximum likelihood (ML) criterion in order to mitigate multipath components. Seco-Granados et el (2005) models an equivalent zero-mean Gaussian noise that includes the contribution of all undesired signals such as reflections, interferences, and thermal noise and applied the ML function to this model. Therefore, a simple model for interference is

obtained at the expense of a mismatch with the actual interface model. Brown (2000) applied the ML function to estimate the amplitude, delay and direction of multipath components. Sahmoudi & Amin (2007) developed the Capon beamformer to deal with multipath when the steering vector, delay and amplitude of multipath components are known. These assumptions may not be realistic in practice for some applications. Another group of methods first finds direction of multipath components by direction finding (DF) methods such as the multiple signal classification (MUSIC) algorithm and then puts nulls in these directions (e. g. Moelker 1997) which may be computationally complex in some applications. The most difficulty for multipath mitigation arises from this fact that there is a high degree of correlation between the LOS signal and multipath components and, thus, the conventional antenna array processing techniques fail to cope with multipath propagation. The correlation between the LOS signal and the undesired signals causes the signal cancelation phenomenon and the rank deficiency of the temporal correlation matrix (Van Trees 2002). In other words, steering the beam pattern in the direction of the LOS signal and simultaneously suppressing the highly correlated multipath components in other directions requires special considerations. To deal with this problem, decorrelating methods have been proposed in the literature. These methods can be categorized into three groups including spatial smoothing (e. g. Pillai & Kwon 1989, Shan & kailath 1985, Evans et el 1982), spatial pre-filtering (Haimovich & Bar-Ness 1991, Citron & Kailath 1984, Duvall 1983, Widrow et el 1982) or antenna array motion (Haber & Zoltowski 1986) which are explained later in the next chapter.

1.2.3 Spoofing countermeasures

Position solutions provided by GNSS can be completely misled by spoofing attacks. Recently, several anti-spoofing techniques have been introduced to combat spoofing attacks. However, in most cases the available anti-spoofing techniques are computationally complicated or limited to a specific spoofing scenario. Anti-spoofing using antenna array processing is one of the most powerful techniques and it has been studied in the literature (e. g. Nielsen et al 2011, Nielsen et al 2010, Montgomery et al 2009, McDowell 2007, Hartman & Minn 1996). The antenna array based anti-spoofing techniques mostly focus on detecting the spoofing threat where limited research has been conducted on spoofing mitigation. Although spoofing countermeasures using an antenna array constitute powerful techniques against this threat, the proposed methods generally operate after acquisition and tracking stages of a GNSS receiver and they need to separately acquire and track all authentic and spoofing signals. This imposes a high computational burden and processing time on the GNSS receivers. For example, McDowell (2007) has proposed a mitigation approach that utilizes an antenna array. This method compares the estimated AOA of both authentic and spoofing PRNs after they are fully tracked by the GNSS receiver. Although this is an effective method, it requires the receiver to perform high computational process. Moreover, most of the previously proposed techniques have been studied under open sky conditions and they may fail in multipath environments where the resolvable and non-resolvable reflections of the spoofing signal are also received by an antenna array-based GNSS receiver.

Both spoofing and authentic signals use the direct sequence spread spectrum (DSSS) modulation by employing PRN codes and their power is far below the noise floor when

they are received by the antenna array. However, a spoofer is a point source transmitter propagating several PRN codes, each of which having a comparable power level to that of the authentic signals and therefore, the spatial power of the spoofing signal is considerably higher than that of the authentic ones. This common feature of spoofers was previously utilized in order to design a beamformer to steer a null toward the direction where the spoofing signal impinges on an antenna array in open-sky environments (Daneshmand et al 2012, Daneshmand et al 2011b). However, this mitigation strategy becomes more challenging and may not operate properly in multipath environments.

1.3 Objectives and contributions

The main goal of this thesis is to investigate the use of an antenna array to combat different kinds of interference. Herein, interference refers to strong narrowband and wideband interfering signals, GNSS multipath components or smart jamming signals such as GNSS spoofing. This dissertation investigates how spatial processing can be employed to deal with the interfering signals which are correlated with the LOS signal such as multipath components and spoofing signals. Moreover, distortionless space-time processing for strong wideband and narrowband GNSS interfering signals will be investigated. To this end, the following objectives are outlined for this thesis:

a) Two-stage multipath and interference mitigation technique

In this section, a general scheme of a beamformer for dealing with both high power interference and GNSS multipath is proposed. As mentioned, the performance of beamforming techniques employing antenna arrays severely degrades to cope with correlated and coherent multipath components. A two-stage beamforming technique is

proposed to suppress high power interference before despreading and to mitigate multipath signals after despreading.

The first stage has two main goals, namely interference suppression to let acquisition perform successfully in order to provide a coarse estimation of Doppler and code delay, and finding the interference subspace used as a constraint for further analyses in the second stage. In the second stage a modified version of the minimum power distortionless response (MPDR) beamformer employing several overlapping subarrays is utilized to mitigate the correlated multipath and coherent multipath components. Therefore, the proposed beamformer is able to deal with the signal cancelation phenomenon and temporal correlation matrix rank deficiency.

b) Multipath mitigation using a moving antenna array

This part of thesis highlights the advantages of antenna array motion for enhancing GNSS multipath mitigation in terms of the degree of freedom of the antenna array and the decorrelating property. A method relying on the array motion is then proposed to deal with highly correlated multipath components without employing several subarrays. Moreover, by employing this method, the degree of freedom of the antenna array is increased without adding physical antenna elements. In fact, this method synthesizes a larger array to mitigate a number of multipath components higher than the number of physical antenna elements. Antenna array motion can be employed not only to decorrelate the coherent multipath components but also to further increase the array degree of freedom by implementing a synthetic array and augmenting the correlation matrix. In the suggested method, a spatial filter is applied to the augmented correlation matrix to estimate the multipath subspace.

Afterwards, in a constraint optimization problem, an optimal gain vector is obtained to maximize the SNR of the LOS signal whereby it suppresses the multipath signals.

c) GNSS distortionless space-time processing

Besides the advantages of space-time processing, the distortion due to this filtering reduces the accuracy of the measurements and can even generate large errors in the time and position solutions (O'Brien & Gupta 2011, Fante et al 2004, Myrick et al 2001). The focus of this part of the thesis is on the mitigation of high power interference signals based on distortionless space-time processing. The effect of space-time filtering on the cross correlation function is studied. Furthermore, the periodicity of the GNSS signals is utilized in order to increase the degree of freedom of the antenna array and to enhance the SINR. It is shown that the periodicity of GNSS signals due to the DSSS modulation can be employed in space-time filter structures for increasing the degree of freedom of the space-time filter without decreasing the SINR and distorting the cross correlation function.

d) Anti-spoofing using antenna array processing

In this part, the antenna array processing is used to mitigate spoofing signals. It is shown how the spatial characteristics of spoofing and authentic signals can be used to design a beamforming method that puts nulls in the direction of the spoofing signal.

This part of the thesis introduces a spoofing mitigation approach in the multipath environments where several resolvable and non-resolvable reflections of the spoofer signal also impinge on the antenna array. Although the reflected components usually have lower power than the LOS spoofing signal, they may mislead the GNSS receivers if they are not properly detected and mitigated. Detecting/mitigating these multipath components is more

difficult than suppressing only the spoofing LOS component since they are coming from different directions and the number of multipath components is essentially unknown. Furthermore, considering the fact that the spoofing and authentic signals are received far below the noise floor, it is difficult to discriminate between resolvable multipath components of the spoofing signal and the authentic signals by only employing spatial processing when there is no knowledge about their number.

Herein, a spatial processing approach in conjunction with time domain processing is utilized to estimate spoofing multipath channel coefficients, which can then be employed to nullify the spoofing signal and its reflections. In doing so, a blind channel estimation technique based on second order statistics (SOS) is employed to estimate the channel coefficients. It is shown that the spatial power dominance of the spoofing signal leads to easy decomposition of the channel coefficients of the spoofing signal and its multipath components from authentic GNSS signals by analyzing the space-time covariance matrix.

1.4 Thesis outline

This dissertation consists of seven chapters. The remainder of this thesis is organized as follows:

Chapter 2 starts by introducing background knowledge for the antenna array processing technique and the signal model received by an antenna array in the presence of interference. This is followed by a brief review on conventional optimization methods for designing a beamformer and then by introducing difficulties arising for mitigating correlated incident signals. To deal with correlated signals, three approaches are introduced which are special smoothing, spatial pre-filtering and antenna array motion. Finally, this chapter ends by

introducing space-time processing as an approach for enhancing interference mitigation capability of an antenna array.

Chapter 3 presents a two-stage beamformer to deal with high power interference signals and GNSS multipath signals. Eigen beamformer is introduced for the first stage and the special filtering in conjunction with spatial smoothing is utilized as a remedy to deal with highly correlated GNSS multipath in the second stage. To this end, an array with a linear configuration consisting of several overlapping subarrays is utilized. Simulations are provided to illustrate the capability of this method to suppress both high power interference and multipath. Moreover, to evaluate performance in dealing with multipath signals, the proposed method has been compared with other beamformers. Finally results of a practical test are brought to demonstrate the error and bias correction in the cross correlation function by employing this method.

Chapter 4 deals with multipath mitigation whereby antenna array motion is employed to not only decorrelate the multipath components but also synthesize an augmented array to increase the degree of freedom of the array. The chapter consists of two main parts, namely synthetic array processing and multipath mitigation. The first part explains the formation of a larger correlation matrix and the resulting increase in the degree of freedom by employing temporal and spatial samples of a moving antenna array and the second part is devoted to designing a space-time filter applied to mitigate multipath without causing the signal cancelation phenomenon. Simulation results demonstrate the validity of this approach.

Chapter 5 focuses on enhancing the SINR by studying the space-time filtering and its advantages and drawbacks. Some efforts are devoted to evaluate distortionless space-time filtering in terms of SINR, interference to noise ratio (INR) and the degree of freedom of the array. Furthermore, it is shown how the inherent periodicity of the GNSS signals can be employed to further improve the existing space-time beamformers. Several simulation and experimental results are used to evaluate the performance of this method.

Chapter 6 studies the use of space-time processing for anti-spoofing applications. It is shown that the spatial characteristics of any incident spoofing signal can be employed as an effective way to discriminate between authentic and fake GNSS signals in open-sky and specular multipath environments. Simulations are provided to evaluate the spoofing multipath channel coefficients estimation and null steering stages and Monte-Carlo simulations are used to evaluate the performance of this method for different scenarios.

Chapter 7 summarizes the contributions and key findings of the thesis and presents recommendations for future work.

Chapter Two: ANTENNA ARRAY PROCESSING AND BEAMFORMING

This chapter concisely brings together the fundamentals of antenna array processing focused on the topics related to GNSS applications. Section 2.1 provides a brief background on antenna array processing and beamforming, a general signal model and basic principles. Section 2.2 presents a number of important optimum beamformers which are referred to or employed in the succeeding chapters. Section 2.3 studies the failure in beamforming applications arising from correlated incident signals and presents three different countermeasures, namely spatial smoothing, spatial pre-filtering and antenna array motion. Finally, space-time array processing and array calibration are briefly introduced in Section 2.4 and Section 2.5, respectively.

2.1 Background on antenna arrays and beamformers

Although nowadays employing antenna array processing in GNSS applications is becoming a breakthrough technique especially for interference suppression (e. g. Kappen et al 2012, Basta et al 2012, Cuntz et al 2011), beamforming and antenna array processing have been studied for several decades in other areas (Van Trees 2002, Van Veen & Buckley 1998, Krim & Viberg 1996). There are numerous applications for array processing in radar, sonar, navigation, wireless communications, direction finding, acoustics, radio astronomy, seismology and biomedicine, to name some.

Beamforming is referred to as a spatial domain signal processing method employing an array of sensors or antennas (Van Veen & Buckley 1998). The received signals of antenna elements are gained or delayed differently to provide desired spatial characteristics. Usually

the received signals from different antennas are combined to attenuate the undesired signals (null steering) and to amplify the desired signals.

One of the earliest beamforming methods was derived by Capon (1969) which has been referred to as the Capon beamformer or the minimum variance distortionless response (MVDR) beamformer (Van Trees 2002). This beamformer has been considered a popular method for a variety of signal processing applications such as radar, wireless communications, and speech enhancement. The MVDR beamformer has a distortionless response for the desired signal whereas suppressing all signals arriving from other directions. Over the years, many other beamformers have been introduced in the literature. Some important beamformers are addressed in Section 2.2.

Figure 2-1 provides an example to demonstrate the antenna array processing concept. Two signals from two different directions are impinging on an antenna array consisting of N antenna elements. It is assumed that the transmitters are located in a far-field region of the array and therefore the received signals are plane waves. Consider that one of them is a desired signal (e.g. a GNSS signal) and the other one is an unwanted signal (e.g. a CW interfering, multipath or spoofing signal). Since they have different incident angles, they are received with different delays and phases at each antenna. The antenna array processor aims to assign extra delays or phases (array gains) to the received signal of each antenna so that the desired signal is passed through the beamformer whereas the undesired one is suppressed or significantly attenuated. Optimal phases and delays can be obtained in terms of different criteria. Generally, they are obtained from a constraint optimization problem which depends on the model chosen to describe the system and required objectives.

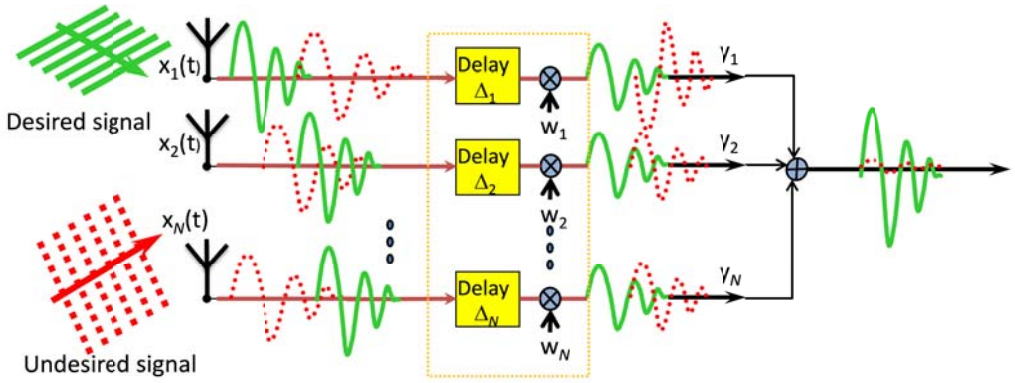

Figure 2-1: General block diagram of a beamformer

By employing array processing techniques, spatial discrimination among signals coming from different directions is possible. This feature of antenna array processing cannot be realized by any temporal/spectral processing techniques.

The combination of antennas' output results in a new gain pattern called antenna array beam pattern. In fact, it is possible to shape this beam pattern (electronically or in software) by changing the array gain vector such that the beam pattern with desired features is achieved. Therefore, there is no need to physically change the orientation of antennas. Moreover, the main lobe, side lobes, nulls and directivity of the array can be controlled by array gains. This is especially useful to suppress interfering signals in particular directions by nullifying them and to steer the main lobe in the direction of the desired signal. Figure 2-2 illustrates an antenna array beam pattern for a scenario in which one interfering signal and one LOS GNSS signal impinge on an antenna array. The beam pattern has been shaped to put a null in the direction of interference and to steer the main lobe toward the GNSS signal direction.

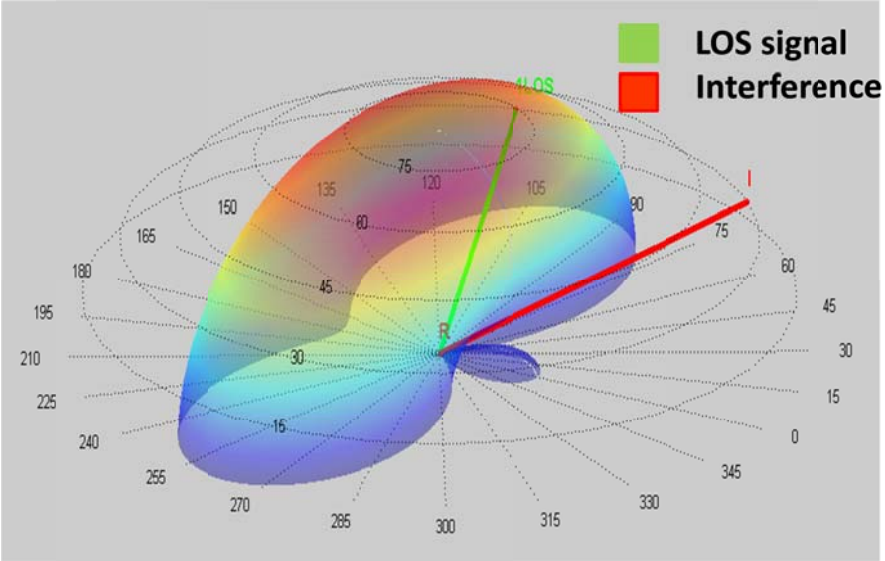

Figure 2-2: Three dimensional antenna array beam pattern

2.1.1 Signal model

In this subsection, a general signal model of an antenna array and some basic principles are presented.

Assume a GNSS signal impinges on an antenna array with N isotropic antennas [1]. Arbitrary positions are assumed for antenna elements. In a Cartesian coordinate system, the positions of these elements are shown with vectors $\mathbf{d}_1^{ant}$, $\mathbf{d}_2^{ant}$, … $\mathbf{d}_N^{ant}$ which are pointing from the origin of the coordinate system to the antenna elements as shown in Figure 2-3. Without loss of generality, it can be assumed that the origin of the coordinate system is located at the position of the first antenna element.

[1] Isotropic antenna is defined as an antenna which has no preferred direction of reception. It receives signals uniformly in all directions over a sphere centered on the antenna.

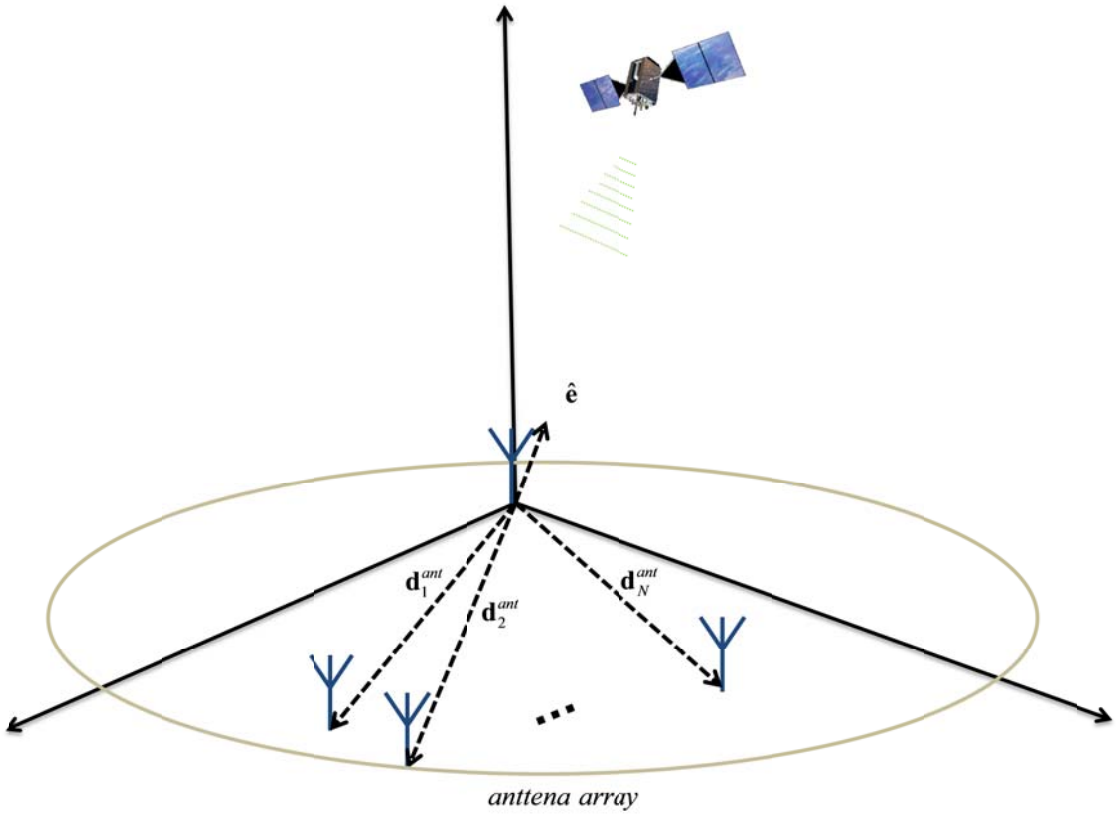

Figure 2-3: Plane wave impinging on an antenna array with *N* elements

Assume that the received signal is a band pass signal (e. g. GPS L1 C/A). The signal received by the first antenna can be modeled as

$$x_{ant}(t) = \mathrm{Re}\left\{ s_{ant}(t) e^{j2\pi f_c t} \right\} \tag{2.1}$$

where f_c is the carrier frequency and $s_{ant}(t)$ is the complex envelope signal which is band limited as

$$\left| f - f_c \right| \le \frac{B_s}{2} \tag{2.2}$$

where B_s is a bandwidth of the complex envelope signal (for GPS L1 C/A, $f_c = 1575.42MHz$ and $B_s = 2.046MHz$). The set of received signals of all antennas can be expressed in vector form as

$$\underset{N\times 1}{\mathbf{x}_{ant}}(t) = \begin{bmatrix} \mathrm{Re}\left\{ s_{ant}(t-t_1)e^{j2\pi f_c(t-t_1)} \right\} \\ \mathrm{Re}\left\{ s_{ant}(t-t_2)e^{j2\pi f_c(t-t_2)} \right\} \\ \vdots \\ \mathrm{Re}\left\{ s_{ant}(t-t_N)e^{j2\pi f_c(t-t_N)} \right\} \end{bmatrix} \tag{2.3}$$

where $t_1, t_2, ..., t_N$ are the received signal delays with respect to the first antenna where $t_1 = 0$. The generic structure of the beamformer is shown in Figure 2-4. Assume that the maximum travel time across the antenna elements is $\Delta t_{\max}$. It can be easily verified that if

$$B_s \Delta t_{Max} << 1, \tag{2.4}$$

then the following approximation is valid (Van Trees 2002):

$$s_{ant}(t) \simeq s_{ant}(t-t_i) \qquad i = 1,2,...,N. \tag{2.5}$$

(For GPS L1 C/A and for an antenna array with maximum antenna elements separation equal to 1 m, $B_s \Delta t_{Max}$ is approximately equal to 0.007). Hence, by substituting (2.5) in (2.3), one obtains

$$\mathbf{x}_{ant}(t) \approx \begin{bmatrix} \mathrm{Re}\left\{ s_{ant}(t)e^{j2\pi f_c(t-t_1)} \right\} \\ \mathrm{Re}\left\{ s_{ant}(t)e^{j2\pi f_c(t-t_2)} \right\} \\ \vdots \\ \mathrm{Re}\left\{ s_{ant}(t)e^{j2\pi f_c(t-t_N)} \right\} \end{bmatrix}. \tag{2.6}$$

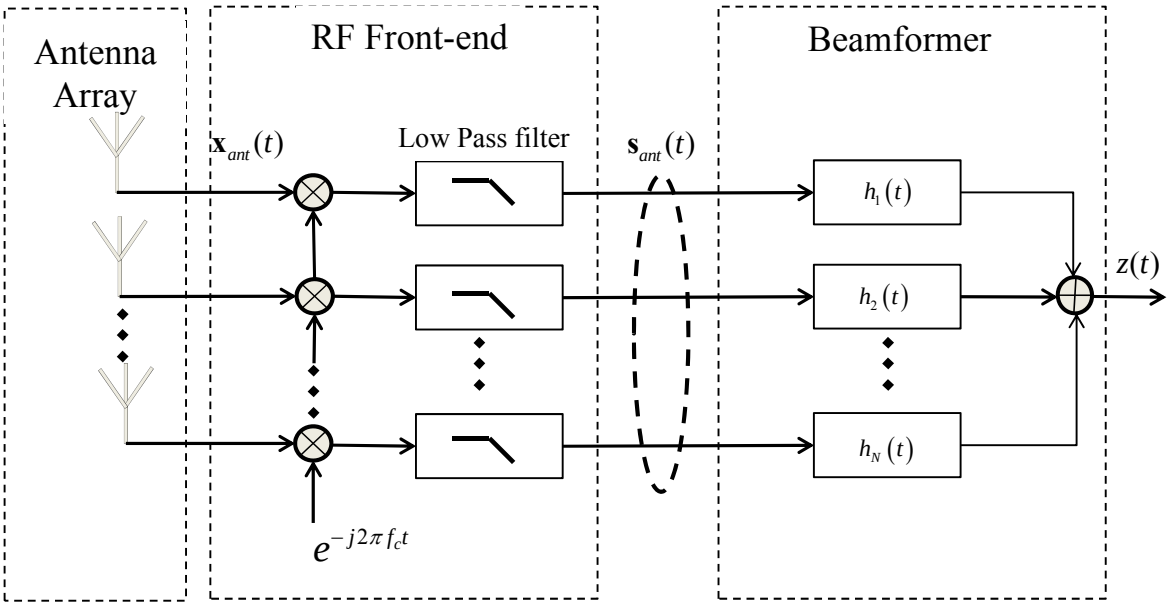

Figure 2-4: General structure of a beamformer

These signals are then down converted [1] (see Figure 2-4). It can be easily verified that the received signal vector after down conversion becomes

$$\underset{N\times 1}{\mathbf{s}_{ant}}(t) \approx \begin{bmatrix} s_{ant}(t)e^{-j2\pi f_c t_1} \\ s_{ant}(t)e^{-j2\pi f_c t_2} \\ \vdots \\ s_{ant}(t)e^{-j2\pi f_c t_N} \end{bmatrix} \tag{2.1}$$

For beamforming, the down-converted signal of each antenna element passes through a time-invariant filter. The way of designing these filters will be discussed in Section 2.2 and 2.4. The beamformer output is obtained as

[1] For the sake of simplicity, analog to digital (ADC) converter and intermediate frequency conversion are not considered.

$$z(t) = \sum_{i=1}^{N} \int_{-\infty}^{-\infty} h_i(t-\tau) s_{ant}(\tau) e^{-j2\pi f_c t_i} d\tau \tag{2.2}$$

which can be expressed in a compact form as

$$z(t) = \int_{-\infty}^{-\infty} \mathbf{h}^T(t-\tau) \mathbf{s}_{ant}(\tau) d\tau \tag{2.3}$$

where $\mathbf{s}_{ant}$ is defined in (2.1) and $\mathbf{h}$ is defined as

$$\mathbf{h}(t) \triangleq \begin{bmatrix} h_1(t) \\ h_2(t) \\ \vdots \\ h_N(t) \end{bmatrix}. \tag{2.4}$$

It is also convenient to express (2.3) in the frequency domain as

$$Z(f) = \boldsymbol{H}^T(f) \boldsymbol{S}_{ant}(f) \tag{2.5}$$

where

$$\begin{aligned} \boldsymbol{S}_{ant}(f) &\triangleq F\{\boldsymbol{s}_{ant}(t)\} \\ \boldsymbol{H}(f) &\triangleq F\{\boldsymbol{h}(t)\} \\ Z(f) &\triangleq F\{z(t)\}. \end{aligned} \tag{2.6}$$

It can be readily verified that delays t_i $, i = 1,2,...,N,$ in (2.1) are related to the relative positions of the antenna elements and the direction of the incident signal (shown with unit vector $\hat{\mathbf{e}}$ in Figure 2-3) by the relation

$$t_i = \frac{\hat{\mathbf{e}}^T \mathbf{d}_i^{ant}}{c}, \quad i = 1,2,...,N \tag{2.7}$$

where c is the propagation speed in the medium. In (2.5), $\boldsymbol{S}_{ant}(f)$ can be written as

$$\boldsymbol{S}_{ant}(f)=\begin{bmatrix} F\{s_{ant}(t)\}e^{-j2\pi f_c t_1} \\ F\{s_{ant}(t)\}e^{-j2\pi f_c t_2} \\ \vdots \\ F\{s_{ant}(t)\}e^{-j2\pi f_c t_N} \end{bmatrix}. \tag{2.8}$$

By substituting (2.7) in (2.8), $\boldsymbol{S}_{ant}(f)$ can be expressed as

$$\boldsymbol{S}_{ant}(f)=\mathbf{a}_{\hat{\mathbf{e}}}F\{s_{ant}(t)\} \tag{2.9}$$

and in the time domain as

$$\mathbf{s}_{ant}(t)=\mathbf{a}_{\hat{\mathbf{e}}}s_{ant}(t) \tag{2.10}$$

where $\mathbf{a}_{\hat{\mathbf{e}}}$ is defined as

$$\underset{N\times 1}{\mathbf{a}_{\hat{\mathbf{e}}}} \triangleq \begin{bmatrix} e^{-j2\pi f_c \frac{\hat{\mathbf{e}}^T\mathbf{d}_1^{ant}}{c}} \\ e^{-j2\pi f_c \frac{\hat{\mathbf{e}}^T\mathbf{d}_2^{ant}}{c}} \\ \vdots \\ e^{-j2\pi f_c \frac{\hat{\mathbf{e}}^T\mathbf{d}_N^{ant}}{c}} \end{bmatrix}. \tag{2.11}$$

The vector $\mathbf{a}_{\hat{\mathbf{e}}}$ includes all spatial information of the incident signal, which is a function of the carrier frequency, the direction of the incident signal and the array configuration. In the literature, this vector is referred to as the array manifold vector or the steering vector. By substituting (2.9) in (2.5),

$$Z(f)=\Upsilon(f,\hat{\mathbf{e}})F\{s_{ant}(t)\} \tag{2.12}$$

where $\Upsilon(f,\hat{\mathbf{e}})$ is defined as

$$\Upsilon(f,\hat{\mathbf{e}}) \triangleq \boldsymbol{H}^T(f)\mathbf{a}_{\hat{\mathbf{e}}}. \tag{2.13}$$

$\Upsilon(f,\hat{\mathbf{e}})$ is the beamformer response to the impinging signal with incident direction of $\hat{\mathbf{e}}$. For an antenna array, the array beam pattern (in dB) is defined as

$$BP \triangleq 10\log\left(\left|\Upsilon(f,\hat{\mathbf{e}})\right|^2\right). \tag{2.14}$$

In fact, array beam pattern determines the beamformer gain in a specific frequency and direction.

As long as (2.4) and, consequently, (2.5) hold, vector $\mathbf{h}(t)$ can be modeled by a set of phase shifts (complex values) to weight the received signals. In this case, the response of the beamformer $\mathbf{h}(t)$ in (2.13) can be simplified to

$$\Upsilon(\hat{\mathbf{e}}) = \mathbf{w}^H\mathbf{a}_{\hat{\mathbf{e}}} \tag{2.15}$$

in which $\mathbf{w}$ is a complex-value vector referred to as the weighting vector or gain vector. This implementation is referred to as a phased array beamformer and is widely employed in practice. In this case, the beamformer response only depends on the direction of the incident signal.

On the other hand, the general model shown in Figure 2-4 by carrying out spatial-temporal processing utilizes some properties of the incident signals received by the antenna array. For example, this model can be employed when the approximation in (2.5) does not hold or for enhancing interference mitigation methods. Generally, filters in a beamformer are implemented by finite impulse response (FIR) filters. Section 2.4 discusses this in more details.

After introducing the basic concepts, (2.10) is now generalized to the case of N_{de} desired signals (e. g. GNSS satellite signals) and I undesired ones (e. g. interfering signals) as

$$\mathbf{r}(t)=\sum_{m=1}^{N_{de}}\mathbf{a}_m s_m(t)+\sum_{i=1}^{I}\mathbf{b}_i v_i(t)+\boldsymbol{\eta} \tag{2.16}$$

where $\mathbf{a}_m$ and $\mathbf{b}_i$ are the steering vector of the *m*th desired signal and *i*th undesired signal, respectively. Correspondingly, $s_m(t)$ and $v_i(t)$ are the complex envelopes of the *m*th and *i*th desired and undesired signals and $\boldsymbol{\eta}$ is the noise vector. $\mathbf{r}(t)$ in (2.16) can be expressed in matrix form as

$$\mathbf{r}(t)=\mathbf{A}\mathbf{s}+\mathbf{B}\mathbf{v}+\boldsymbol{\eta}. \tag{2.17}$$

where the steering matrices $\mathbf{A}$ and $\mathbf{B}$ consider all spatial characteristics of the signals received by an array and are defined as

$$\begin{aligned}\mathbf{A}&\triangleq\begin{bmatrix}\mathbf{a}_1 & \mathbf{a}_2 & \cdots & \mathbf{a}_{N_{de}}\end{bmatrix}\\ \mathbf{B}&\triangleq\begin{bmatrix}\mathbf{b}_1 & \mathbf{b}_2 & \cdots & \mathbf{b}_I\end{bmatrix}.\end{aligned} \tag{2.18}$$

$\mathbf{A}$ and $\mathbf{B}$ are assumed to be full column rank matrices. This assumption implies that the incident signals are not coming from the same direction. In (2.17), $\mathbf{s}$ and $\mathbf{v}$ are the desired and interfering waveform vectors respectively and are defined as

$$\mathbf{v} \triangleq \begin{bmatrix} v_1(t) \\ v_2(t) \\ \vdots \\ v_I(t) \end{bmatrix} \qquad \mathbf{s} \triangleq \begin{bmatrix} s_1(t) \\ s_2(t) \\ \vdots \\ s_{N_{de}}(t) \end{bmatrix} \tag{2.19}$$

The following assumptions are used in the rest of this thesis:

Assumption 1: the noise term in (2.16) is a spatially-temporally white zero-mean complex vector with covariance matrix $\sigma^2 \mathbf{I}_N$.

Assumption 2: both the desired signals (GNSS signals) and undesired signals (interfering signals) are considered as unknown deterministic signals.

Based on these assumptions, in the following section, a number of well-known beamformers are described.

2.2 Optimum beamformers

An *N*-antenna phase array implementation is considered in this section. For the sake of simplicity, assume that only one desired signal exists.

2.2.1 Minimum variance distortionless response (MVDR) beamformer

By assuming one desired signal, (2.17) becomes

$$\mathbf{r}(t) = \mathbf{a}s(t) + \mathbf{B}\mathbf{v} + \boldsymbol{\eta} \tag{2.20}$$

The spatial correlation matrix of the received signal vector is obtained as

$$\mathbf{R}_{\mathbf{r}} = E\left\{\mathbf{r}(t)\mathbf{r}^{H}(t)\right\} \tag{2.21}$$

Considering (2.20), $\mathbf{R}_{\mathbf{r}}$ can be expressed as

$$\mathbf{R}_{\mathbf{r}} = \mathbf{a}\sigma_s^2\mathbf{a}^{H} + \mathbf{B}\tilde{\mathbf{R}}_{\mathbf{v}}\mathbf{B}^{H} + \sigma^2\mathbf{I} \tag{2.22}$$

where σ_s^2, and $\tilde{\mathbf{R}}_{\mathbf{v}}$ are the desired signal variance (power) and temporal correlation matrix of the interference (for simplicity, interfering and desired signals are assumed to have zero mean)and are defined as

$$\begin{aligned} \sigma_s^2 &\triangleq E\left\{s(t)s^{H}(t)\right\} \\ \tilde{\mathbf{R}}_{\mathbf{v}} &\triangleq E\left\{\mathbf{v}(t)\mathbf{v}^{H}(t)\right\} \end{aligned} \tag{2.23}$$

Assume that $\mathbf{R}_{\mathbf{v},\boldsymbol{\eta}}$ is defined as

$$\mathbf{R}_{\mathbf{v},\boldsymbol{\eta}} \triangleq \mathbf{B}\tilde{\mathbf{R}}_{\mathbf{v}}\mathbf{B}^{H} + \sigma^2\mathbf{I} \tag{2.24}$$

which is the spatial correlation matrix of the undesired signals. The distortionless criterion is considered for the MVDR beamformer, which implies

$$z(t) = s(t) \tag{2.25}$$

where $z(t)$ is the beamformer output. Considering (2.15), the constraint of no distortion can be also expressed as

$$\mathbf{w}^{H}\mathbf{a} = 1. \tag{2.26}$$

The goal is to minimize $\mathbf{R}_{\mathbf{v},\boldsymbol{\eta}}$ subject to the constraint in (2.26). This minimization problem can be solved by using a Lagrange multiplier approach (see appendix A). The optimal gain vector is obtained as

$$\mathbf{w}_{MVDR} = \mathbf{R}_{\mathbf{v},\boldsymbol{\eta}}^{-1}\mathbf{a}\left(\mathbf{a}^H\mathbf{R}_{\mathbf{v},\boldsymbol{\eta}}^{-1}\mathbf{a}\right)^{-1}. \tag{2.27}$$

This beamformer is called minimum variance distortionless response (MVDR) beamformer and it was first derived by Capon (1969). In Van Trees (2002), this optimal gain vector is obtained in the frequency domain and further analyses have been performed.

2.2.2 Maximum likelihood (ML) estimator

It can be easily verified that the MVDR beamformer is the maximum likelihood (ML) estimator under the assumption that the noise distribution is a circular complex Gaussian random vector (Van Trees 2002). Under this assumption, the conditional probability density function of the received signal, given $s(t)$, would be

$$p_{\mathbf{r}|s}\left(\mathbf{r}(t)\middle|s(t)\right) = \frac{\mathrm{e}^{-\left(\mathbf{r}^H(t)-\mathbf{a}^H s^*(t)\right)\mathbf{R}_{\mathbf{v},\boldsymbol{\eta}}^{-1}\left(\mathbf{r}(t)-\mathbf{a}s(t)\right)}}{\det\left(\pi\mathbf{R}_{\mathbf{v},\boldsymbol{\eta}}\right)}. \tag{2.28}$$

Then maximizing the log-likelihood function requires minimizing the following term:

$$\underset{s(t)}{Min}\left(\mathbf{r}^H(t)-\mathbf{a}^H s^*(t)\right)\mathbf{R}_{\mathbf{v},\boldsymbol{\eta}}^{-1}\left(\mathbf{r}(t)-\mathbf{a}s(t)\right). \tag{2.29}$$

By taking the complex gradient with respect to $s(t)$ and setting the result equal to zero, the maximum likelihood estimate of $s(t)$ is obtained as

$$s(t)_{ML} = \left(\mathbf{a}^H \mathbf{R}_{\mathbf{v},\boldsymbol{\eta}}^{-1} \mathbf{a}\right)^{-1} \mathbf{a}^H \mathbf{R}_{\mathbf{v},\boldsymbol{\eta}}^{-1} \mathbf{r}(t) \tag{2.30}$$

which indicates that the optimal gain vector applied to the received signal is

$$\mathbf{w}_{ML} = \mathbf{R}_{\mathbf{v},\boldsymbol{\eta}}^{-1} \mathbf{a}\left(\mathbf{a}^H \mathbf{R}_{\mathbf{v},\boldsymbol{\eta}}^{-1} \mathbf{a}\right)^{-1}. \tag{2.31}$$

It can be observed that this result is the same as (2.27).

2.2.3 Maximum signal-to-noise plus-interference ratio (MSINR) beamformer

In this beamformer, the optimization criterion is maximizing the signal-to-noise-plus-interference ratio (SINR) of the beamformer signal output. The SINR of the beamformer output is

$$\underset{\mathbf{w}}{Max} \frac{\left|z(t)\right|^2}{Noise + Interference\,Power} = \underset{\mathbf{w}}{Max} \frac{\mathbf{w}^H \mathbf{R}_{\mathbf{r}} \mathbf{w}}{\mathbf{w}^H \mathbf{R}_{\mathbf{v},\boldsymbol{\eta}} \mathbf{w}} \tag{2.32}$$

This is a generalized Eigen decomposition problem (GED). In order to estimate $\mathbf{w}$, the following problem should be solved:

$$\mathbf{R}_{\mathbf{r}} \mathbf{w} = \lambda_{GE} \mathbf{R}_{\mathbf{v},\boldsymbol{\eta}} \mathbf{w} \tag{2.33}$$

where λ_{GE} is the largest generalized eigenvalue and $\mathbf{w}$ is its corresponding eigenvector. It is also possible to come up with the closed form solution for $\mathbf{w}$. To this end, considering that $\mathbf{R}_{\mathbf{v},\boldsymbol{\eta}}$ is a full rank matrix and it is invertible, $\bar{\mathbf{w}}$ can be defined as

$$\bar{\mathbf{w}}^H \triangleq \mathbf{w}^H \mathbf{R}_{\mathbf{v},\boldsymbol{\eta}}^{\frac{1}{2}} \tag{2.34}$$

By substituting (2.34) in (2.32), the maximization problem is transformed into

$$\underset{\bar{\mathbf{w}}}{Max}\frac{\bar{\mathbf{w}}^H\mathbf{R}_{\mathbf{v},\boldsymbol{\eta}}^{\frac{-1}{2}}\mathbf{R}_{\mathbf{r}}\bar{\mathbf{w}}^H\mathbf{R}_{\mathbf{v},\boldsymbol{\eta}}^{\frac{-1}{2}}\bar{\mathbf{w}}}{\bar{\mathbf{w}}^H\mathbf{R}_{\mathbf{v},\boldsymbol{\eta}}^{\frac{-1}{2}}\mathbf{R}_{\mathbf{v},\boldsymbol{\eta}}\mathbf{R}_{\mathbf{v},\boldsymbol{\eta}}^{\frac{-1}{2}}\bar{\mathbf{w}}}=\underset{\bar{\mathbf{w}}}{Max}\frac{\bar{\mathbf{w}}^H\mathbf{R}_{\mathbf{v},\boldsymbol{\eta}}^{\frac{-1}{2}}\mathbf{R}_{\mathbf{r}}\mathbf{R}_{\mathbf{v},\boldsymbol{\eta}}^{\frac{-1}{2}}\bar{\mathbf{w}}}{\bar{\mathbf{w}}^H\bar{\mathbf{w}}}. \tag{2.35}$$

Substituting (2.22) and (2.24) in (2.35) results in

$$\underset{\bar{\mathbf{w}}}{Max}\frac{\bar{\mathbf{w}}^H\mathbf{R}_{\mathbf{v},\boldsymbol{\eta}}^{\frac{-1}{2}}\left(\mathbf{a}\sigma_s^2\mathbf{a}^H+\mathbf{R}_{\mathbf{v},\boldsymbol{\eta}}\right)\bar{\mathbf{w}}^H\mathbf{R}_{\mathbf{v},\boldsymbol{\eta}}^{\frac{-1}{2}}\bar{\mathbf{w}}}{\bar{\mathbf{w}}^H\bar{\mathbf{w}}}=\underset{\bar{\mathbf{w}}}{Max}\frac{\bar{\mathbf{w}}^H\mathbf{R}_{\mathbf{v},\boldsymbol{\eta}}^{\frac{-1}{2}}\mathbf{a}\sigma_s^2\mathbf{a}^H\mathbf{R}_{\mathbf{v},\boldsymbol{\eta}}^{\frac{-1}{2}}\bar{\mathbf{w}}}{\bar{\mathbf{w}}^H\bar{\mathbf{w}}}. \tag{2.36}$$

Assuming $\|\bar{\mathbf{w}}\|=1$, this maximization becomes

$$\underset{\|\bar{\mathbf{w}}\|=1}{Max}\bar{\mathbf{w}}^H\mathbf{R}_{\mathbf{v},\boldsymbol{\eta}}^{\frac{-1}{2}}\mathbf{a}\sigma_s^2\mathbf{a}^H\mathbf{R}_{\mathbf{v},\boldsymbol{\eta}}^{\frac{-1}{2}}\bar{\mathbf{w}}. \tag{2.37}$$

It can be readily verified that

$$\bar{\mathbf{w}}=\frac{\mathbf{R}_{\mathbf{v},\boldsymbol{\eta}}^{\frac{-1}{2}}\mathbf{a}}{\left(\mathbf{a}^H\mathbf{R}_{\mathbf{v},\boldsymbol{\eta}}^{-1}\mathbf{a}\right)} \tag{2.38}$$

and by substituting in (2.34), $\mathbf{w}_{MSINR}$ is obtained as

$$\mathbf{w}_{MSINR}=\mathbf{R}_{\mathbf{v},\boldsymbol{\eta}}^{-1}\mathbf{a}\left(\mathbf{a}^H\mathbf{R}_{\mathbf{v},\boldsymbol{\eta}}^{-1}\mathbf{a}\right)^{-1}. \tag{2.39}$$

The same result was also derived in the frequency domain (Van Trees 2002). It can be seen that the obtained gain vector is the same as the previously introduced beamformers. In fact, for a wide class of criteria the optimal gain vector is obtained from (2.27) followed by a scalar that depends on the criterion (Van Trees 1966)

2.2.4 Minimum power distortionless response (MPDR) beamformer

The main problem with the MVDR beamformer is that the interference-plus-noise spatial correlation matrix is assumed to be known which is difficult or impossible to estimate in some applications. To deal with this problem, the minimum power distortionless response (MPDR) beamformer was developed. In this beamformer, instead of using $\mathbf{R}_{\mathbf{v},\boldsymbol{\eta}}$, $\mathbf{R}_{\mathbf{r}}$ is employed in the beamforming process. Hence, the gain vector for a MPDR beamformer is obtained as

$$\mathbf{w}_{MPDR} = \mathbf{R}_{\mathbf{r}}^{-1}\mathbf{a}\left(\mathbf{a}^{H}\mathbf{R}_{\mathbf{r}}^{-1}\mathbf{a}\right)^{-1}. \tag{2.40}$$

MVDR and MPDR are equivalent as long as there is no mismatch between the estimated steering vector of the desired signal and the actual value. However, in the case of a steering vector mismatch, the MVDR beamformer outperforms the MPDR beamformer (Van Trees 2002). The MPDR beamformer was first pointed for GPS by Zoltowski & Gecan (1995), who also extended the concept for the case when the steering vectors of the GPS signals are unknown.

2.2.5 Linear constrained minimum variance and linear constrained minimum power beamformers

In the MVDR and MPDR beamformers, only one constraint is considered. These beamformers can be generalized to the cases in which several constraints are imposed in the optimization problem. This can be advantageous for multi-constraint optimization problems or for beam shaping (Van Trees 2002, Buckley & Griffits 1986, Er & Cantoni 1983). The extended versions of MVDR and MPDR beamformers are referred to as linear constrained

minimum variance (LCMV) and linear constrained minimum power (LCMP), respectively. Assume that there are several linear constraints put in matrix $\mathbf{C}_{const.}$ whose columns are linearly independent. These constraints can be expressed as

$$\mathbf{w}^H\mathbf{C}_{const.} = \mathbf{f}^H. \tag{2.41}$$

The value of $\mathbf{f}$ depends on the problem at hand. Therefore, the optimization problem in LCMV is

$$\underset{\substack{\mathbf{w} \\ \mathbf{w}^H\mathbf{C}_{const.}=\mathbf{f}^H}}{Min}\ \mathbf{w}^H\mathbf{R}_{\mathbf{v},\boldsymbol{\eta}}\mathbf{w} \tag{2.42}$$

and similarly for LCMP is

$$\underset{\substack{\mathbf{w} \\ \mathbf{w}^H\mathbf{C}_{const.}=\mathbf{f}^H}}{Min}\ \mathbf{w}^H\mathbf{R}_{\mathbf{r}}\mathbf{w} \tag{2.43}$$

The Lagrange multiplier method can be also employed to solve the optimization problem in (2.42) and (2.43) (Van Trees 2002, Frost 1972). The results are given as follows (see Appendix A):

$$\begin{aligned}\mathbf{w}_{LCMV} &= \mathbf{R}_{\mathbf{v},\boldsymbol{\eta}}^{-1}\mathbf{C}_{const.}\left(\mathbf{C}_{const.}{}^H\mathbf{R}_{\mathbf{v},\boldsymbol{\eta}}^{-1}\mathbf{C}_{const.}\right)^{-1}\mathbf{f} \\ \mathbf{w}_{LCMP} &= \mathbf{R}_{\mathbf{r}}^{-1}\mathbf{C}_{const.}\left(\mathbf{C}_{const.}{}^H\mathbf{R}_{\mathbf{r}}^{-1}\mathbf{C}_{const.}\right)^{-1}\mathbf{f}\end{aligned} \tag{2.44}$$

2.2.6 Eigenvector beamformer

In order to reduce the computational complexity of beamforming, eigenvector beamformers were introduced. In addition, they can be also useful for applications in which the environment is stationary only over a short period and the number of samples is limited in

order to form the spatial correlation matrix (Van trees 2002). Generally, these beamformers project the received signals into the reduced rank subspace including the desired signal and interference. Then, the beamforming methods are applied to this subspace. Therefore, there is no need to completely calculate the spatial correlation matrix $\mathbf{R}_r$ or $\mathbf{R}_{v,\eta}$. This approach was studied under different names although they are essentially the same. Under the eigenvector name, there are algorithms introduced by Hung & Tunder (1983), Citron & Kailath (1984), Friedlander (1988), Haimovich & Bar-ness (1988), Haimovich & Bar-ness (1991), Van Veen & Buckley (1988), Chang & Yeh (1992), Youn & Un (1994) and Yu & Yeh (1995). Under the name of reduced covariance matrix, this beamformer was studied by Kirstein & Tufts (1985), and under the projection name, this approach was studied by Feldman & Griffiths (1991, 1994) and there are so many other papers in this context. Eigenvector beamformers have been extensively studied in Van Trees (2002) where more references are provided.

In GNSS applications, beamforming can be performed in two different ways: before despreading and after despreading. If a beamformer is applied after despreading, the conventional eigenvector can be applied (for example for multipath mitigation). On the other hand, for mitigating high power interfering signals, since the desired signal is below the noise floor, the eigenvector beamforming should be modified and applied before despreading. In this case, the desired signal belongs to the noise subspace. Therefore, instead of projecting the received signal into the interference-plus-signal subspace, the received signal should be projected to the noise-plus-signal subspace (e. g. Sun & Amin 2005b). Herein, the eigenvector beamformer is reformulated for this case.

The spatial correlation matrix $\mathbf{R}_\mathbf{r}$ is first decomposed in terms of its eigenvalues and eigenvectors as

$$\mathbf{R}_\mathbf{r} = \begin{bmatrix} \underset{N\times I}{\mathbf{U}_{Int}} & \underset{N\times(N-I)}{\mathbf{U}_{S+N}} \end{bmatrix} \begin{bmatrix} \underset{I\times I}{\mathbf{\Lambda}_{Int}} & \underset{I\times(N-I)}{\mathbf{0}} \\ \underset{(N-I)\times I}{\mathbf{0}} & \underset{(N-I)\times(N-I)}{\mathbf{\Lambda}_{S+N}} \end{bmatrix} \begin{bmatrix} \mathbf{U}_{Int}^H \\ \mathbf{U}_{S+N}^H \end{bmatrix} = \mathbf{U}_{Int}\mathbf{\Lambda}_{Int}\mathbf{U}_{Int}^H + \mathbf{U}_{S+N}\mathbf{\Lambda}_{S+N}\mathbf{U}_{S+N}^H \tag{2.45}$$

where $\mathbf{U}_{Int}$ and $\mathbf{U}_{S+N}$ are the eigenvector matrices of the interference and noise-plus-signal subspaces respectively, and $\mathbf{\Lambda}_{Int}$ and $\mathbf{\Lambda}_{S+N}$ are the corresponding eigenvalue matrices. It can be easily verified that

$$\mathbf{R}_\mathbf{r}^{-1} = \mathbf{U}_{Int}\mathbf{\Lambda}_{Int}^{-1}\mathbf{U}_{Int}^H + \mathbf{U}_{S+N}\mathbf{\Lambda}_{S+N}^{-1}\mathbf{U}_{S+N}^H. \tag{2.46}$$

In order to be effective, an interfering signal should have stronger power than that of the noise and GNSS signals. Consequently, the eigenvalues of the interference subspace are much larger than those of the noise-plus-GNSS subspace. Hence, $\mathbf{R}_\mathbf{r}^{-1}$ in (2.46) can be approximated as

$$\mathbf{R}_\mathbf{r}^{-1} \simeq \mathbf{U}_{S+N}\mathbf{\Lambda}_{S+N}^{-1}\mathbf{U}_{S+N}^H \tag{2.47}$$

By substituting (2.47) in (2.40), the optimal gain vector for the eigenvector beamformer becomes

$$\mathbf{w}_{Eig.} = \beta\mathbf{U}_{S+N}\mathbf{\Lambda}_{S+N}^{-1}\mathbf{U}_{S+N}^H\mathbf{a} \tag{2.48}$$

in which β is a scale factor equal to

$$\beta = \left(\mathbf{a}^H\mathbf{U}_{S+N}\mathbf{\Lambda}_{S+N}^{-1}\mathbf{U}_{S+N}^H\mathbf{a}\right)^{-1} \tag{2.49}$$

To study this from the projection concept point of view, assume that $\bar{\mathbf{a}}$ is the projected steering vector of the desired signal into the noise-plus-GNSS subspace and is defined as

$$\bar{\mathbf{a}} \triangleq \mathbf{P}_{N+S}\mathbf{a} \tag{2.50}$$

where $\mathbf{P}_{N+S}$ is the projection matrix into the noise-plus-GNSS subspace defined as

$$\mathbf{P}_{N+S} \triangleq \mathbf{U}_{S+N}^{H} \tag{2.51}$$

The optimal gain vector in (2.48) can be simplified as

$$\begin{aligned} \mathbf{w}_{\mathrm{Proj.}}^{H} &= \beta \mathbf{P}_{S+N}^{H} \boldsymbol{\Lambda}_{S+N}^{-1} \mathbf{P}_{S+N} \\ \beta &= \left(\bar{\mathbf{a}}^{H} \boldsymbol{\Lambda}_{S+N}^{-1} \bar{\mathbf{a}} \right)^{-1}. \end{aligned} \tag{2.52}$$

If the obtained gain vector is applied to the received signal vector, the beamformer output is equal to

$$y(t) = \beta \mathbf{P}_{S+N}^{H} \boldsymbol{\Lambda}_{S+N}^{-1} \bar{\mathbf{r}}(t) \tag{2.53}$$

where $\bar{\mathbf{r}}(t)$ is the projected received signal in to the noise-plus-GNSS subspace defined as

$$\bar{\mathbf{r}}(t) \triangleq \mathbf{P}_{N+S}\mathbf{r}(t) \tag{2.54}$$

2.3 Beamforming for correlated signals

Up to this point, for MPDR and LCMP beamformers, it is implicitly assumed that the desired signal is uncorrelated with the unwanted signals. The performance of the beamformers can be significantly degraded if correlation exists. In GNSS applications, this situation may occur in multipath environments (e.g. urban canyon) or in smart jamming such as spoofing attacks. This issue was addressed and analyzed in the literature over the

years (e. g. Van Trees 2002, Tsai et al 1995, Raghunath & Reddy 1992, Godara 1990, Bresler et al 1988, Zoltowski 1988, Reddy et al 1987, Shan & Kialath 1985, Widrow et al 1982).

This degradation also can be inferred from expanding the spatial correlation matrix. To this end, (2.22) should be revised by considering the cross correlation terms as

$$\mathbf{R}_{\mathbf{r}} = \mathbf{a}\sigma_s^2\mathbf{a}^H + \underbrace{\mathbf{a}\tilde{\mathbf{R}}_{\mathbf{vs}}\mathbf{B}^H + \mathbf{B}\tilde{\mathbf{R}}_{\mathbf{vs}}\mathbf{a}^H}_{Cross\ \ correlation\ \ terms} + \mathbf{B}\tilde{\mathbf{R}}_{\mathbf{v}}\mathbf{B}^H + \sigma^2\mathbf{I}. \tag{2.55}$$

Due to the existence of cross correlation terms, the minimization of $\mathbf{R}_{\mathbf{r}}$ does not necessarily lead only to the minimization of interfering signals. Although the beamformer has a distortionless response for the desired signal, the whole power is minimized when some amount of undesired signals power passes through the beamformer to cancel out the desired signal. The following example illustrates how this correlation can dramatically decrease the performance of the MPDR beamformer (Van Trees 2002).

Assume that there is a single interfering signal along with a desired signal where the spatial correlation matrix is expressed as

$$\mathbf{R}_{\mathbf{r}} = \begin{bmatrix}\mathbf{a} & \mathbf{b}\end{bmatrix}\begin{bmatrix}\sigma_S^2 & \sigma_I\sigma_S\rho \\ \sigma_I\sigma_S\rho^* & \sigma_I^2\end{bmatrix}\begin{bmatrix}\mathbf{a}^H \\ \mathbf{b}^H\end{bmatrix} + \sigma^2\mathbf{I} \tag{2.56}$$

where ρ is the normalized correlation coefficient ($|\rho| \le 1$) between the desired and the interfering signal and $\mathbf{b}$ is the steering vector of the interfering signal. Considering (2.56), the received signal vector can be written as

$$\mathbf{r}(t) = \left(\sigma_S\mathbf{a} + \sigma_I\rho^*\mathbf{b}\right)s(t) + \sigma_I\sqrt{1-|\rho|^2}\,\mathbf{b}v(t) + \boldsymbol{\eta} \tag{2.57}$$

such that the three terms in (2.57) are uncorrelated. By applying the gain vector $\mathbf{w}$, the MPDR beamformer output is equal to

$$z(t)=\left(\sigma_S+\sigma_I\rho^*\mathbf{w}^H\mathbf{b}\right)s(t)+\sigma_I\sqrt{1-|\rho|^2}\,\mathbf{w}^H\mathbf{b}v(t)+\mathbf{w}^H\boldsymbol{\eta}. \tag{2.58}$$

Considering the fact that for an MPDR beamformer, $\mathbf{w}^H\mathbf{a}=1$, the following relations can be easily obtained (Van Trees 2002):

$$\begin{aligned} P_s &= \sigma_S^2\left|1+\mathbf{w}^H\mathbf{b}\frac{\sigma_I\rho^*}{\sigma_S}\right|^2 \\ P_v &= \left|\mathbf{w}^H\mathbf{b}\right|^2\left(1-\left|\rho^*\right|^2\sigma_I^2\right) \\ P_\eta &= \sigma^2\left\|\mathbf{w}\right\| \end{aligned} \tag{2.59}$$

where P_s, P_v and P_η are the power of the desired signal, interference and noise at the beamformer output, respectively. It can be obtained that the SINR, interference to noise ratio (INR) and SNR at the beamformer output are approximately equal to (Van Trees 2002)

$$\begin{aligned} SINR &= \frac{P_s}{P_v+P_\eta}\simeq\frac{\sigma_S^2\left(1-|\rho|^2\right)^2}{\left(1-|\rho|^2\right)|\rho|^2+\dfrac{\sigma^2}{N}} \\ INR &= \frac{P_v}{P_\eta}\simeq\frac{\left(1-|\rho|^2\right)|\rho|^2}{\dfrac{\sigma^2}{N}} \\ SNR &= \frac{P_s}{P_\eta}\simeq\frac{\sigma_S^2\left(1-|\rho|^2\right)^2}{\dfrac{\sigma^2}{N}}. \end{aligned} \tag{2.60}$$

Approximations hold when the desired signal and interference power are high and the interfering signal is coming from a sidelobe. It can be observed that when the $|\rho|$ (correlation between the desired signal and the interfering signal) increases, SINR decreases. For the case of coherent signals[1], SINR is equal to zero, which signifies the severe signal cancellation in the presence of a correlated signal.

The previous example revealed the effect of correlation among received signals on the performance of beamformers. In the following subsections, three well-known approaches namely spatial smoothing, spatial pre-filtering and antenna array motion are introduced to deal with this issue. These methods are employed in Chapter 3 and 4 for GNSS multipath mitigation.

2.3.1 Spatial smoothing

Preliminary work on spatial smoothing was undertaken by Evans et al (1982) for direction of arrival (DOA) estimation and was later modified and developed for beamforming by Shan & Kailath (1985) and then by Pillai & Kwon (1989). This method has been used over the years as pre-processing for direction finding (DF) and beamforming applications in order to reduce the signal cancellation phenomenon due to the correlation between unwanted signals and the desired ones. In this method, the antenna array is grouped into several subarrays and the spatially smoothed covariance matrix is obtained by averaging the covariance matrices of all subarrays. This approach requires certain array configurations such as a linear uniform array. It has been shown that this leads to the increase of the rank of the noise-free spatially smoothed covariance matrix and by choosing the proper number

[1] Two signals are coherent if one is a scaled and delayed replica of the other or in the other words $\rho = 1$.

of subarrays, this matrix becomes full rank. After fulfilling this condition, the traditional antenna array processing can be applied for DF, interference mitigation and other applications.

The following simple example shows the essential of the spatial smoothing methods. Consider C identical subarrays of the antenna elements with the same configuration (see Figure 2-5). In fact, each subarray is a regularly shifted version of the previous one without changing the orientation.

For the ith group, assume that the received signal vector is expressed as

$$\mathbf{r}_i(t) = \mathbf{A}\mathbf{s}_i + \boldsymbol{\eta}_i \quad i = 1,2,...,C. \tag{2.61}$$

where $\mathbf{A}$ and $\mathbf{s}$ are the steering matrix and signal waveform vector. It can be easily confirmed that

$$\mathbf{s}_{i+1} = \boldsymbol{\Pi}_i \mathbf{s}_i \qquad i = 1,2,...,C-1 \tag{2.62}$$

where $\boldsymbol{\Pi}_i$ is a diagonal matrix. In fact, received signals at subarrays only differ in phases which are considered in the diagonal elements of this matrix. In this case, the spatial correlation matrices of these subarrays are equal to

$$\mathbf{R}_{\mathbf{r}_i} = \mathbf{A}\left(\boldsymbol{\Pi}_i\right)^{i-1} E\left\{\mathbf{s}_1\mathbf{s}_1^H\right\}\left(\boldsymbol{\Pi}_i^H\right)^{i-1}\mathbf{A}^H + \sigma^2\mathbf{I} \quad i = 1,2,...,C. \tag{2.63}$$

The spatially smoothed correlation matrix is formed by performing the summation of all subarray spatial correlation matrices as

$$\mathbf{R}_{\mathbf{r}} = \mathbf{A}\tilde{\mathbf{R}}\mathbf{A}^H + \sigma^2\mathbf{I} \tag{2.64}$$

where $\tilde{\mathbf{R}}$ is the de-correlated temporal correlation matrix defined as

$$\tilde{\mathbf{R}} = \sum_{i=1}^{C} \left(\mathbf{\Pi}_i\right)^{i-1} E\left\{\mathbf{s}_1 \mathbf{s}_1^H\right\} \left(\mathbf{\Pi}_i^H\right)^{i-1}. \tag{2.65}$$

It can be observed that by performing this averaging the rank of the temporal correlation matrix increases. In other words, the spatial correlation matrix is de-correlated. As a drawback, it can be seen that the degree of freedom of the array is decreased by at least the number of subarrays. Employing configurations with overlapping subarrays can improve the DOF loss due to spatial smoothing. More analyses can be found in Van Trees (2002).

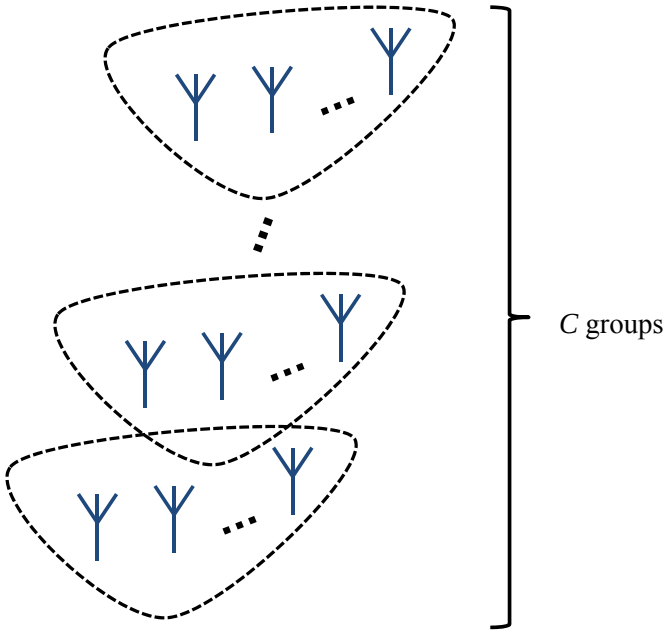

Figure 2-5: an antenna array including *C* identical subarrays

2.3.2 Spatial pre-filtering

Spatial smoothing is not able to completely mitigate the degradation due to the correlation between desired and undesired signals (Van Trees 2002). In fact, de-correlating methods increase the rank of the signal correlation matrix (at most to the number of signals impinging on the antenna array) and prevent rank deficiency of this matrix for DF applications; however, it might not be adequate for interference mitigation purposes. To

successfully mitigate this degradation, the spatial pre-filtering method was suggested (Duvall 1983, Widrow et el 1982). Widrow et el (1982) and Duvall (1983) studied this problem under the name of signal cancellation phenomenon. Citron & Kailath (1984) applied this pre-filtering in conjunction with the eigenvector beamformer and further analyses were carried out by Haimovich & Bar-Ness (1991). The signal cancelation phenomenon and the spatial pre-filtering are simply explained in the following example.

Consider the MPDR beamformer is employed in a GNSS application in order to have a distortionless response for a LOS signal and to suppress its multipath reflections. Although the beamformer can satisfy the distortionless condition for the LOS signal, due to the correlation between the LOS signal and multipath ones, the entire power is minimized when some amount of multipath components' power also passes through the beamformer such that the LOS signal and multipath components cancel each other out. Thus the SNR of the LOS signal may reduce dramatically. In the spatial pre-filtering technique, by knowing the LOS signal direction, complex gains are applied to the linearly spaced N-antenna array such that the LOS signal is received with the same phase and amplitude by all antennas. Afterwards, by differencing between the adjacent elements and summation over these differenced signals, the counterpart of the LOS signal is removed from the resulting signal and only the multipath components are passed through this spatial filter. Thus the multipath signals' subspace can be estimated from the output of this filter and employed to suppress the multipath component without attenuating the LOS signal (Haimovich & Bar-Ness 1991, Haimovich & Bar-Ness 1988, Citron & Kailath 1984). Therefore, by losing one degree of freedom due to the subtraction process, the conventional optimization methods, subject to the constraint that the optimal gain is orthogonal to the obtained multipath signals'

subspace, can be performed to design a beamformer that is able to completely suppress the multipath signals and pass the LOS signal without distortion. In the spatial pre-filtering technique, it is implicitly assumed that there is not more than one coherent multipath component. In the general case, the spatial smoothing and the spatial filtering methods should be combined to completely suppress the correlated and coherent multipath components (Daneshmand et al 2013a, Daneshmand et al 2011a). This is explained in Chapter 3 in details.

2.3.3 Antenna array motion

Another approach to deal with the correlated signals is employing a moving antenna array (Haber & Zoltowski 1986). This is briefly described in the following example.

In a multipath environment, a GNSS receiver likely receives several reflections from nearby objects such as buildings. Assume a moving antenna array scenario where a GNSS signal and its reflections are received by the antenna array. Moving the antenna array decorrelates coherent and correlated multipath components coming from different directions (similar to spatial smoothing methods). This can be explained by considering the extra term of the Doppler shifts induced on the received signal vector due to the motion as (Haber & Zoltowski 1986)

$$\underset{\left(M_{ref}+1\right)\times 1}{\mathbf{s}}(t) \approx \begin{bmatrix} s_{ant}(t)e^{\frac{\|\mathbf{v}_{vel}\|}{\lambda}\cos(\omega_0)t} \\ s_{ant}(t)e^{\frac{\|\mathbf{v}_{vel}\|}{\lambda}\cos(\omega_1)t} \\ \vdots \\ s_{ant}(t)e^{\frac{\|\mathbf{v}_{vel}\|}{\lambda}\cos\left(\omega_{M_{ref}}\right)t} \end{bmatrix} \tag{2.66}$$

where M_{ref} is the number of the reflections and $\mathbf{v}_{vel}$ is the antenna array velocity vector. $\omega_i, i = 0,1,...M_{ref}$ is the angle between the signal direction and the velocity vector. In (2.66), λ is the wavelength of the signal and index zero stands for the LOS component. This formula shows how the velocity and the angle of arrival are related to the Doppler frequency term. Therefore, the multipath components coming from different directions have different Doppler frequencies.

Considering (2.66), the received baseband signal (for the sake of simplicity, noise is not considered) can be written as

$$\mathbf{r}(t) = \sum_{m=0}^{M_{ref}} \mathbf{a}_m s_{ant}(t) e^{\frac{\|\mathbf{v}_{vel}\|}{\lambda}\cos(\omega_m)t} \tag{2.67}$$

where $\mathbf{a}_m$ is the steering vector of the mth incident signal. $\mathbf{r}(t)$ in (2.67) can be written in a compact matrix form as

$$\mathbf{r}(t) = \mathbf{A}\mathbf{s} \tag{2.68}$$

where

$$\mathbf{A} = \begin{bmatrix} \mathbf{a}_0 & \mathbf{a}_1 & \cdots & \mathbf{a}_{M_{ref}} \end{bmatrix}$$
$$\mathbf{s} = \begin{bmatrix} s(t)e^{\frac{\|\mathbf{v}_{vel}\|}{\lambda}\cos(\omega_0)t} \\ s(t)e^{\frac{\|\mathbf{v}_{vel}\|}{\lambda}\cos(\omega_1)t} \\ \vdots \\ s(t)e^{\frac{\|\mathbf{v}_{vel}\|}{\lambda}\cos(\omega_{M_{ref}})t} \end{bmatrix} \tag{2.69}$$

By forming the spatial correlation matrix as

$$\mathbf{R}_{\mathbf{r}} = \mathbf{A}E\left\{\mathbf{s}\mathbf{s}^{H}\right\}\mathbf{A}^{H}, \tag{2.70}$$

it can be easily verified that if $\left\|\mathbf{v}_{vel}\right\| = 0$, the rank of the temporal correlation matrix $E\left\{\mathbf{s}\mathbf{s}^{H}\right\}$ is equal to one whereas the array motion increases the rank of this matrix by generating different Doppler frequencies. By increasing the velocity, multipath components become more uncorrelated. Nevertheless, as for spatial smoothing, the degradation due to the signal cancelation phenomenon may not be avoided. To alleviate this, the combination of the spatial pre-filtering and antenna array motion can be employed to avoid the degradation due to the multipath signals (Daneshmand et al 2013b). A comprehensive explanation of this can be found in Chapter 4.

2.4 Space-Time processing

Space-time processing techniques take advantage of both spatial and temporal processing domains. This is a mature field of study that has been in existence for several decades and originates from radar applications for increasing SINR (Melvin 2004, Klemm 2004, Applebaum 1976, Brennan & Reed 1974, Frost 1972). It was later employed for channel equalization and multiuser code division multiple access (CDMA) in order to decrease the bit error rate of the transmitted data and to increase the capacity of the system (Paulraj & Papadias 1997). These techniques are generally referred to as space-time adaptive processing (STAP) or space-frequency adaptive processing (SFAP), which is its corresponding use in the frequency domain. STAP and SFAP approaches have been employed and implemented in many applications. Utilizing these techniques in GNSS applications, however, requires a number of considerations in order to prevent induced

biases in pseudorange and carrier phase measurements (Fante et al 2004). Considering STAP for GNSS backs to early 1990s (Moelker et al 1996, Ramos et al 1996, Agamata 1991). Especially, the distortion and bias caused on the cross correlation function due to space-time filtering and the related countermeasure techniques have been of great interest in the literature (O'Brien & Gupta 2011, Lorenzo 2007, McGraw et al 2006, Lorenzo et al 2006, Falcone et al 2000, Fante et al 2004, McGraw et al 2004, Fante & Vaccaro 1998a, Fante & Vaccaro 1998b, Hatke 1998, Myrick et al 2001).

Generally, the term "Adaptive array" means that the array follows the changes in environment (e. g. alteration in the characteristics of interference signals) and constantly adapts its own pattern by means of a feedback control. This term is employed as opposed to the deterministic beamformer introduced in the previous sections. Adaptivity is not the only benefit of STAP techniques. In addition to this feature, increasing the degree of freedom of the antenna array is also an important advantage which is the topic of interest in this thesis. In the remainder of this section, space-time processing from the view point of increasing the degree of freedom of the array is introduced.

The standard implementation of the STAP methods consists of an antenna array in which each antenna element is followed by a temporal filter or a tapped delay line (TDL) with the tap delay time typically equal to the sampling duration (see Figure 2-6).

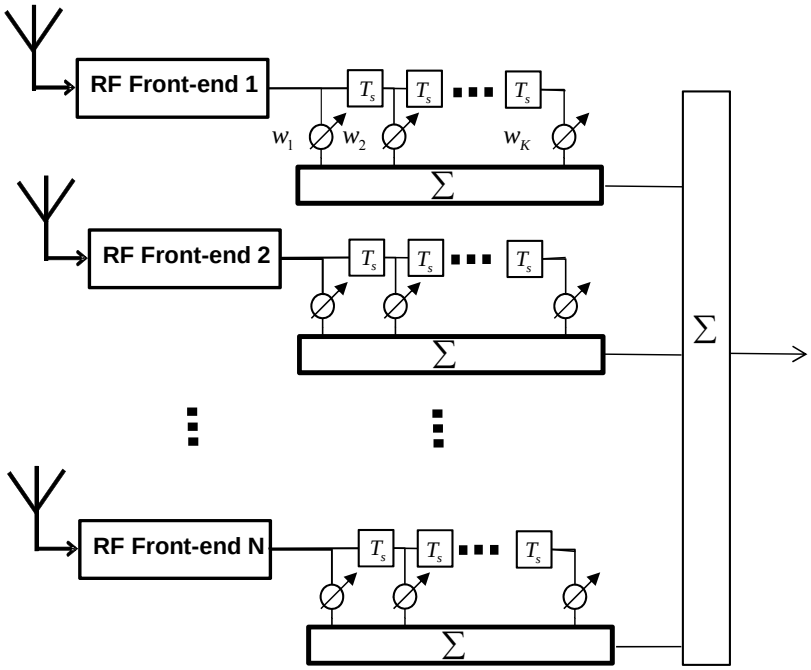

Figure 2-6: Generic structure of a space-time processor

A space-time antenna array with N antenna elements and TDLs with K taps leaves KN unknown gains which should be determined. For each time snapshot, KN samples of all TDL taps form a $NK \times 1$ received signal vector as

$$\vec{\mathbf{r}} = \begin{bmatrix} r_{1,1} & r_{1,2} & \cdots & r_{1,N} & r_{2,1} & r_{2,2} & \cdots & r_{2,N} & \cdots & r_{K,1} & r_{K,2} & \cdots & r_{K,N} \end{bmatrix}^T \tag{2.71}$$

in which $r_{k,n}$ is the time sample of the kth tap, $k = 1, 2, ..., K$, for the nth antenna element, $n = 1, 2, ..., N$. Then the augmented spatial correlation matrix can be formed as

$$\underset{KN \times KN}{\mathbf{R}_{\vec{\mathbf{r}}}} = E\left\{\vec{\mathbf{r}}(t)\vec{\mathbf{r}}^H(t)\right\}. \tag{2.72}$$

Considering the dimension of $\mathbf{R}_{\vec{\mathbf{r}}}$, the array degree of freedom becomes at most $KN - 1$ which is increased by the factor of K compared to only-space processing. The augmented correlation matrix can be utilized in the beamforming methods introduced in Section 2.2.

Nevertheless, more constraints should be put on optimization problems in order to avoid the bias and distortion in the cross correlation function (e. g. Myrick et al 2001).

In Chapter 5, it is shown that how the inherent periodicity of GNSS signals in conjunction with space-time processing can be employed to improve the performance of the existing methods.

2.5 Array calibration

Array calibration is one of the main challenges in employing antenna arrays. (Gupta et al 2003). Due to mutual coupling between antennas, antenna gain/phase mismatches, antenna phase center variations and RF front-end distortions and etc., there are additional unknown phase offsets that should be taken into account during most antenna array-based applications. Array calibration becomes a critical stage of the antenna array processing if in the beamformer structure the array manifold vector of one or more incident signals are assumed to be known or to be estimated. Much research on array calibration has been pursued since the antenna array and beamforming techniques were introduced. In GNSS applications, there are also several publications that have studied different array calibration methods (e. g. Church & Gupta 2009, Backen et al. 2008, Gupta et al. 2003, Ng & See 1996). Studying calibration methods is out of the scope of this research. In this dissertation, if the steering vector of the incident signals are explicitly employed in optimization problems, it is assumed that array calibration is already performed otherwise there is no need for array calibration. Herein, a blind beamformer is referred to the beamformer that does need require any array calibration. In other words, the array manifold vectors of the incident signals are not employed in the beamforming process.

Chapter Three: TWO-STAGE BEAMFORMING FOR GNSS INTERFERENCE AND MULTIPATH MITIGATION

As mentioned in previous chapters, the performance of location-based services provided by GNSS is compromised by interference and multipath propagation. It is well known that time/frequency interference suppression methods fail to cope with wideband interference signals. Instead, techniques utilizing several antenna elements can be employed to mitigate both narrowband and wideband interference signals. However, as mentioned in Chapter 2, the performance of beamforming techniques utilizing antenna arrays severely degrades in dealing with correlated and coherent multipath components which cause the signal cancelation phenomenon and temporal correlation matrix rank deficiency. This chapter proposes a two-stage beamformer to jointly deal with interference and multipath which is correlated with the GNSS line of sight (LOS) signals. In the first stage, before despreading process, by applying the eigenvector decomposition the interference subspace is estimated and used as a constraint for the optimization problem in the next stage. In the second stage a modified version of the minimum power distortionless response (MPDR) beamformer employing several overlapping sub-arrays called the minimum difference output power (MDOP) method is utilized to mitigate the correlated multipath and coherent multipath components such that the proposed beamformer is able to deal with the signal cancelation phenomenon and temporal correlation matrix rank deficiency. The first stage of the proposed method mitigates the interference signals and their reflections, which are all uncorrelated with the LOS signals. Herein, interference is referred to as any unwanted radio frequency (RF) signal such as tones, swept waveforms, pulse and wideband noise and any other multi-frequency and time-varying versions of them (Poisel 2004). In fact, in the

context of antenna array processing, all these interfering signals are considered narrowband plane waves as long as the reciprocal of a maximum propagation delay across the array is much greater than the signal bandwidth (see relation in (2.4)). Therefore, regardless of their characteristics, they can be suppressed by applying a proper spatial filter. The first stage follows two main goals namely interference suppression to provide a coarse estimation of Doppler and code delay, and finding the interference subspace to be used as a constraint for further analyses in the second stage. Therefore, the eigen beamformers can be a good choice to fulfill both objectives. In the second stage, spatial filtering and spatial smoothing are implemented by using the differences between signals of several overlapping subarrays to place deep nulls in the direction of the undesired signals. In this stage, the minimum power criterion is applied to the difference between the signals of adjacent subarrays subject to the constraint that the optimal gain vector is orthogonal to the interference subspace and has a distortionless response for the LOS signal. It will be shown that the resulting gain vector alleviates the signal cancelation phenomenon and rank deficiency of the temporal correlation matrix.

The chapter is organized as follows: In Section 3.1, the problem formulation is stated. Section 3.2 provides the structure of the proposed two-stage beamformer and the interference and multipath suppression techniques are presented. Illustrative simulations and practical test results are provided in Section 3.3 and 3.4, respectively, and finally Section 3.5 summarizes the chapter.

3.1 Problem formulation

Considering (2.16), the complex baseband representation of *N* received spatial samples of a GNSS signal, its reflections and interference signals impinging on an *N*-element linear antenna array before despreading can be written in vector form as

$$\mathbf{r}(t) = \sum_{m=0}^{M_{ref}} \mathbf{a}_m \alpha_m g(t-\tau_m) e^{j\phi_m + j2\pi\Delta f_m t} + \sum_{i=1}^{I} \mathbf{b}_i v_i(t) + \boldsymbol{\eta}(t). \tag{3.1}$$

Here M_{ref} stands for the number of multipath reflections and the subscript zero stands for the LOS signal. Furthermore, τ_m, ϕ_m, α_m and Δf_m are code delay, phase shift, attenuation factor and carrier offset of the *m*th signal component respectively. $g(t)$ stands for the pseudo random noise (PRN) code.

In this chapter, the focus has been devoted to an individual GNSS signal and its multipath reflections while ignoring the presence of simultaneous GNSS signals. The proposed method can be readily extended to the general case. Moreover, it is assumed that the navigation data is estimated and wiped off. Hence, it is not considered herein. Similar to (2.17), the received signal vector $\mathbf{r}$ (for simplicity, t is omitted) can be put in a more compact form as

$$\mathbf{r} = \mathbf{A}\mathbf{s} + \mathbf{B}\mathbf{v} + \boldsymbol{\eta} \tag{3.2}$$

where $\mathbf{A}$ and $\mathbf{s}$ are the steering matrix of the LOS and multipath components and their waveform vectors defined as

$$\mathbf{A} \triangleq \begin{bmatrix} \mathbf{a}_0 & \cdots & \mathbf{a}_{M_{ref}} \end{bmatrix}$$
$$\mathbf{s} \triangleq \begin{bmatrix} \alpha_0 g(t-\tau_0) e^{j\phi_0 + j2\pi\Delta f_0 t} \\ \vdots \\ \alpha_{M_{ref}} g(t-\tau_{M_{ref}}) e^{j\phi_{M_{ref}} + j2\pi\Delta f_{M_{ref}} t} \end{bmatrix} \tag{3.3}$$

and $\mathbf{B}$ and $\mathbf{v}$ are defined in (2.18) and (2.19), respectively.

3.2 Two-stage interference and multipath mitigation approach

This section describes the proposed interference and multipath mitigation technique.

3.2.1 Interference suppression

The eigenvector beamformer can be a proper choice for this stage since it not only provides a coarse estimation of Doppler and code delay but also estimates the interference subspace that is used as a constraint for further analyses in the second stage. As mentioned in Section 2.2.6, for GNSS applications, the received signal before the despreading process is projected onto the noise subspace, which includes the GNSS signals and their reflections, and then will be enhanced such that the beamformer achieves the maximum SINR criterion (Amin et al 2004, Sun & Amin 2005b). Noise-plus-GNSS signal and interference subspaces can be obtained by Eigen value decomposition (EVD) of the spatial correlation matrix (see (2.45)). In Section 2.2.6, it has been shown that the beamformer achieves maximum SINR by choosing the array gain vector as

$$\mathbf{w}_{Eig.} = \beta \mathbf{U}_{S+N} \mathbf{\Lambda}_{S+N}^{-1} \mathbf{U}_{S+N}^{H} \mathbf{a}_0 \tag{3.4}$$

where $\mathbf{U}_{S+N}$ and $\mathbf{\Lambda}_{S+N}$ are the eigenvector and eigenvalue matrices of the signal-plus-noise subspace. It should be noticed that the optimal gain vector $\boldsymbol{\mu}$ maximizes the SINR with the condition that all undesired signals belong to the interference subspace. Since multipath components are not considered as undesired signals at this stage, the obtained gain vector does not necessarily suppress the multipath components. However, this gain vector is used to remove the interference components in order to obtain coarse estimates of the code delay and Doppler frequency, which are accurate enough for despreading the received signals.

3.2.2 Multipath mitigation

To suppress the multipath components in the second stage, the correlation matrix after despreading is utilized and denoted by

$$\widehat{\mathbf{R}} = \mathbf{A}E\left\{\widehat{\mathbf{s}}\widehat{\mathbf{s}}^H\right\}\mathbf{A}^H + \widehat{\sigma}^2\mathbf{I} \tag{3.5}$$

where $\widehat{\mathbf{s}}$ denotes the vector $\mathbf{s}$ after despreading and $E\left\{\widehat{\mathbf{s}}\widehat{\mathbf{s}}^H\right\}$ is its temporal correlation matrix after despreading. In (3.5), the remaining interference after mitigation is considered in noise term. $\mathbf{A}$ and $E\left\{\widehat{\mathbf{s}}\widehat{\mathbf{s}}^H\right\}$ can be partitioned as

$$E\left\{\widehat{\mathbf{s}}\widehat{\mathbf{s}}^H\right\} = \begin{bmatrix} s_0 & \overline{\widehat{\mathbf{s}}}^H \\ \underset{M_{ref}\times 1}{\overline{\widehat{\mathbf{s}}}} & \underset{M_{ref}\times M_{ref}}{\tilde{\mathbf{S}}} \end{bmatrix}$$
$$\mathbf{A} = \begin{bmatrix} \mathbf{a}_0 & \overline{\mathbf{A}} \end{bmatrix}. \tag{3.6}$$

Hence, $\widehat{\mathbf{R}}$ can be written as

$$\widehat{\mathbf{R}} = \mathbf{a}_0 s_0 \mathbf{a}_0^H + \overline{\mathbf{A}}\tilde{\mathbf{S}}\overline{\mathbf{A}}^H + \mathbf{a}_0\overline{\widehat{\mathbf{s}}}^H\overline{\mathbf{A}}^H + \overline{\mathbf{A}}^H\overline{\widehat{\mathbf{s}}}\mathbf{a}_0^H + \tilde{\sigma}^2\mathbf{I}. \tag{3.7}$$

The first term in (3.7) is the spatial correlation matrix of the desired signal. The second term is the correlation matrix of the multipath components and the two other terms are the cross-correlation matrices between the desired signal and the multipath components. Herein, the problem of interest is to find an optimal weighting vector $\boldsymbol{\mu}$ to satisfy the following relations:

$$\begin{aligned} \boldsymbol{\mu}^H \mathbf{U}_{Int} &\simeq \mathbf{0}^T \\ \boldsymbol{\mu}^H \bar{\mathbf{A}} &\simeq \mathbf{0}^T \\ \boldsymbol{\mu}^H \mathbf{a}_0 &\simeq 1 \ . \end{aligned} \tag{3.8}$$

Therefore $\boldsymbol{\mu}$ puts nulls in the directions of the interference and multipath components and has a distortionless response in the direction of the LOS signal.

As mentioned before, if the conventional optimization techniques such as MPDR are used, the signal cancelation phenomenon will happen due to the correlation between the LOS signal and multipath components. This also can be inferred from (3.7).

Minimizing the second, third and fourth term of (3.7) is of interest when the whole power of the correlation matrix is minimized. However, due to existing cross-correlation terms, this minimization does not only lead to minimization of the undesired terms. Hence, a pre-processing is needed to separate the LOS signal from its reflections such that only the undesired terms are minimized, which is addressed extensively in (Widrow et al 1982, Duvall 1983). As stated in Chapter 2, in order to prevent the signal cancelation phenomenon, an array gain vector orthogonal to the multipath component steering vectors should be employed. It cannot be realized unless $\tilde{\mathbf{S}}$ is full rank. This can be stated as

$$\left.\begin{array}{l} \underset{\boldsymbol{\mu}}{Min}\ \boldsymbol{\mu}^H \overline{\mathbf{A}}\tilde{\mathbf{S}}\overline{\mathbf{A}}^H\boldsymbol{\mu} \\ \tilde{\mathbf{S}}\ is\ \ full\ rank \end{array}\right\} \Rightarrow \boldsymbol{\mu}^H\overline{\mathbf{A}} \simeq \mathbf{0}^T. \tag{3.9}$$

To compensate for the rank deficiency of the temporal correlation matrix caused by coherent multipath components, the spatial smoothing method is applied. In the proposed method, to avoid the rank deficiency and the signal cancelation phenomenon together, the spatial smoothing and spatial filtering techniques have been considered. To do this, an array configuration consisting of several overlapping linear subarrays is required. Figure 3-1 shows the proposed array configuration consisting of $C+1$ overlapping subarrays. (It will be shown that C is determined by the maximum number of available coherent multipath components).

Here the main goal is to obtain an optimal gain vector that minimizes the multipath and interference power and has a distortionless response in the direction of the LOS signal. This can be realized in three steps. The first step is called pre-gaining in which, based on knowledge of the LOS signal direction and array configuration, a proper gain vector can be obtained such that all antenna elements receive the LOS signal with the same phase and amplitude. In the next step, the LOS signal power is removed in the correlation matrix by taking the difference between the signals of the adjacent subarrays. Considering (3.7), the correlation matrix obtained from these subtracted signals does not include first, third and fourth terms and, thus, the signal cancelation phenomenon is prevented. Since the differencing is performed over several subarrays, rank deficiency of the temporal correlation matrix is also prevented.

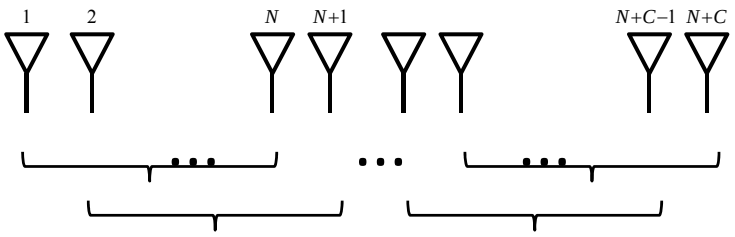

Figure 3-1: Array configuration with *C*+1 overlapping subarrays with *N* elements in each subarray

In the final step, the optimal gain vector can be obtained by performing a constraint minimization problem on this correlation matrix. This gain vector is constrained to be orthogonal to the interference subspace, obtained in the first stage, and also to have a distortionless response toward the direction of the LOS signal. Herein, this optimization problem is called minimum difference output power (MDOP). The details are explained as follows.

Assume that the received signals at the *i*th subarray after despreading is shown as

$$\hat{\mathbf{r}}_i = \mathbf{A}_i \hat{\mathbf{s}} + \hat{\boldsymbol{\eta}}_i, \qquad i = 1,...,C+1 \tag{3.10}$$

where $\mathbf{A}_i$ and $\hat{\boldsymbol{\eta}}_i$ are the steering matrix and the zero-mean white noise vector of the correlator output with covariance matrix $\tilde{\sigma}^2 \underset{N\times N}{\mathbf{I}}$ for the *i*th subarray. By pre-gaining subarrays and then calculating the difference between adjacent subarrays, $\hat{\mathbf{z}}_i$ is obtained as

$$\hat{\mathbf{z}}_i = \mathbf{G}_i \hat{\mathbf{r}}_i - \mathbf{G}_{i+1} \hat{\mathbf{r}}_{i+1} \qquad i = 1,...,C \tag{3.11}$$

where $\mathbf{G}_i$ is the diagonal matrix with diagonal elements equal to the conjugate of the elements of the LOS signal steering vector for the *i*th subarray. This steering vector can be obtained when the locations of the antennas and satellites ephemeris are known a priori. The problem addressed here is stated as the following constraint minimization problem:

$$\begin{aligned} &\min_{\mathbf{w}} \quad \mathbf{w}^H \widehat{\mathbf{R}}_D \mathbf{w} \\ &subject\ to \qquad \mathbf{w}^H \mathbf{C}_{Const.} = \mathbf{f}^H \end{aligned} \tag{3.12}$$

where $\mathbf{w}$ is the optimal gain vector and $\widehat{\mathbf{R}}_D$, $\mathbf{f}$ and $\mathbf{C}_{Const.}$ are defined as

$$\begin{aligned} \widehat{\mathbf{R}}_D &\triangleq E\left\{\sum_{i=1}^{C} \widehat{\mathbf{z}}_i \widehat{\mathbf{z}}_i^{\,H}\right\} \\ \mathbf{f} &\triangleq \begin{bmatrix} 1 \\ \mathbf{0}_{I\times 1} \end{bmatrix} \\ \mathbf{C}_{Const.} &\triangleq \begin{bmatrix} \mathbf{G}_1 \mathbf{a}_0 & \mathbf{G}_1 \mathbf{U}_{Int} \end{bmatrix} \end{aligned} \tag{3.13}$$

where $\mathbf{a}_0$ is the LOS signal steering vector for the first subarray. The term $\widehat{\mathbf{z}}_i$ can be written as

$$\widehat{\mathbf{z}}_i = \mathbf{G}_i \widehat{\mathbf{r}}_i - \mathbf{G}_{i+1} \widehat{\mathbf{r}}_{i+1} = \left(\mathbf{G}_i \mathbf{A}_i - \mathbf{G}_{i+1} \mathbf{A}_{i+1}\right) \widehat{\mathbf{s}} + \mathbf{G}_i \widehat{\boldsymbol{\eta}}_i - \mathbf{G}_{i+1} \widehat{\boldsymbol{\eta}}_{i+1} \qquad i = 1,\ldots,C. \tag{3.14}$$

Considering the configuration of the antenna elements in Figure 3-1, it can be concluded that

$$\begin{aligned} \mathbf{G}_{i+1} &= \mathbf{G}_i e^{j\Psi} \\ \mathbf{A}_{i+1} &= \mathbf{A}_i \boldsymbol{\Omega}, \end{aligned} \tag{3.15}$$

where $e^{j\Psi}$ is a complex scalar and $\boldsymbol{\Omega}$ is a diagonal matrix whose elements depend on the antenna elements configuration and the direction of the LOS and multipath components; hence

$$\mathbf{G}_i \mathbf{A}_i - \mathbf{G}_{i+1} \mathbf{A}_{i+1} = \mathbf{G}_i \mathbf{A}_i - \mathbf{G}_i \mathbf{A}_i \boldsymbol{\Omega} e^{j\Psi} = \mathbf{G}_1 \mathbf{A}_1 \boldsymbol{\Delta}_i \tag{3.16}$$

where $\boldsymbol{\Delta}_i$ is a diagonal matrix defined as

$$\boldsymbol{\Delta}_i \triangleq \left(e^{j\Psi}\boldsymbol{\Omega}\right)^{(i)}\left(\mathbf{I}-\boldsymbol{\Omega}e^{j\Psi}\right) \quad i=1,...,C. \tag{3.17}$$

The values of this matrix depend on the antenna array configuration Assume that $\boldsymbol{\Delta}_i$ is partitioned as

$$\boldsymbol{\Delta}_i = \begin{bmatrix} \underset{1\times 1}{\delta_0} & \mathbf{0} \\ \mathbf{0} & \underset{(M_{ref})\times(M_{ref})}{\bar{\boldsymbol{\Delta}}_i} \end{bmatrix}. \tag{3.18}$$

Hence, by substituting (3.6), (3.7), (3.16) and (3.18) in (3.12), the optimization problem becomes

$$\begin{aligned} &\underset{\mathbf{w}}{Min}\ \mathbf{w}^H\hat{\mathbf{R}}_D\mathbf{w}= \\ &\mathbf{w}^H\left(\sum_{i=1}^{C}\begin{pmatrix}\mathbf{G}_1\mathbf{a}_0\delta_0 s_0\delta_0{}^H\mathbf{a}_0^H\mathbf{G}_1{}^H+\mathbf{G}_1\bar{\mathbf{A}}_1\bar{\boldsymbol{\Delta}}_i\tilde{\mathbf{S}}\bar{\boldsymbol{\Delta}}_i{}^H\bar{\mathbf{A}}_1^H\mathbf{G}_1{}^H \\ +\mathbf{G}_1\mathbf{a}_0\delta_0\bar{\bar{\mathbf{s}}}^H\bar{\boldsymbol{\Delta}}_i^H\bar{\mathbf{A}}_1{}^H\mathbf{G}_1{}^H+\mathbf{G}_1\bar{\mathbf{A}}_1\bar{\boldsymbol{\Delta}}_i\bar{\bar{\mathbf{s}}}\delta_0{}^H\mathbf{a}_0^H\mathbf{G}_1{}^H\end{pmatrix}+E\left\{\zeta\zeta^H\right\}\right)\mathbf{w} \\ &\quad subject\ to\ \ \mathbf{C}_{Const.}^H\mathbf{w}=\mathbf{f}\end{aligned} \tag{3.19}$$

where ζ is the noise vector and $\bar{\mathbf{A}}_1$ is the steering matrix of the multipath components for the first subarray (See definition of $\bar{\mathbf{A}}_1$ in (3.6)). Because all antenna elements become co-phased with respect to the LOS signal, δ_0 is equal to zero and in (3.19), three terms are omitted and the optimization problem becomes

$$\begin{aligned} &\min_{\mathbf{w}}\ \mathbf{w}^H\hat{\mathbf{R}}_D\mathbf{w}=\mathbf{w}^H\left(\mathbf{G}_1\bar{\mathbf{A}}_1\sum_{i=1}^{C}\bar{\boldsymbol{\Delta}}_i\tilde{\mathbf{S}}\bar{\boldsymbol{\Delta}}_i{}^H\bar{\mathbf{A}}_1{}^H\mathbf{G}_1{}^H+E\left\{\zeta\zeta^H\right\}\right)\mathbf{w} \\ &\qquad subject\ to\ \mathbf{C}_{Const.}^H\mathbf{w}=\mathbf{f}\end{aligned} \tag{3.20}$$

In fact, the pre-gaining of the array elements results in the received signal of each channel to be in phase for the LOS signal and, therefore, with differencing signals from adjacent

subarrays, the LOS signal power becomes significantly small and is not considered in the optimization problem. Thus, the signal cancelation phenomenon does not happen. Furthermore, using several overlapping subarrays results in $\sum_{i=1}^{C}\overline{\mathbf{\Delta}}_i\tilde{\mathbf{S}}\overline{\mathbf{\Delta}}_i^H$ to be full rank although $\tilde{\mathbf{S}}$ may not be. Therefore, the rank deficiency problem is avoided. In fact, if $M_{Coh.}$ coherent multipath components exist, $\tilde{\mathbf{S}}$ has a rank deficiency with the order of $M_{Coh.}-1$. Therefore, by choosing a proper value for C, $\sum_{i=1}^{C}\overline{\mathbf{\Delta}}_i\tilde{\mathbf{S}}\overline{\mathbf{\Delta}}_i^H$ with different $\overline{\mathbf{\Delta}}_i$ s becomes full rank. The method of Lagrange multipliers can be used to solve the constrained optimization of (3.12) (see Appendix A). The optimal gain vector is obtained as

$$\mathbf{w}=\left(\hat{\mathbf{R}}_D\right)^{-1}\mathbf{C}_{Const.}\left(\mathbf{C}_{Const.}{}^H\left(\hat{\mathbf{R}}_D\right)^{-1}\mathbf{C}_{Const.}\right)^{-1}\mathbf{f}. \tag{3.21}$$

The necessary conditions for the number of subarrays and the number of antenna elements in each subarray are

$$\begin{aligned} &N-M_{ref}-I-1\geq 0\\ &C\geq 1\\ &C\geq M_{Coh.}\end{aligned} \tag{3.22}$$

It is straightforward to verify that the relations in (3.8) hold if $\boldsymbol{\mu}=\mathbf{G}_1^H\mathbf{w}$. To this end, the following analyses are performed. In (3.20), assume that $E\left\{\boldsymbol{\zeta}\boldsymbol{\zeta}^H\right\}$ is decomposed as

$$E\left\{\boldsymbol{\zeta}\boldsymbol{\zeta}^H\right\}=\tilde{\sigma}^2\mathbf{T}\mathbf{T}^H \tag{3.23}$$

where $\mathbf{T}$ is an arbitrary normalized full rank matrix. Hence, $\hat{\mathbf{R}}_D$ can be written as

$$\begin{aligned}\hat{\mathbf{R}}_D &= \mathbf{G}_1\bar{\mathbf{A}}_1\sum_{i=1}^{C}\bar{\mathbf{\Delta}}_i\tilde{\mathbf{S}}\bar{\mathbf{\Delta}}_i^H\bar{\mathbf{A}}_1^{HH}\mathbf{G}_1^{\ H} + E\left\{\boldsymbol{\zeta}\boldsymbol{\zeta}^H\right\} \\ &= \mathbf{G}_1\bar{\mathbf{A}}_1\sum_{i=1}^{C}\bar{\mathbf{\Delta}}_i\tilde{\mathbf{S}}\bar{\mathbf{\Delta}}_i^H\bar{\mathbf{A}}_1^{H}\mathbf{G}_1^{\ H} + \tilde{\sigma}^2\mathbf{T}\mathbf{T}^H \\ &= \mathbf{T}\left(\mathbf{T}^{-1}\mathbf{G}_1\bar{\mathbf{A}}_1\sum_{i=1}^{C}\bar{\mathbf{\Delta}}_i\tilde{\mathbf{S}}\bar{\mathbf{\Delta}}_i^H\bar{\mathbf{A}}_1^{H}\mathbf{G}_1^{\ H}\left(\mathbf{T}^{-1}\right)^H + \tilde{\sigma}^2\mathbf{I}\right)\mathbf{T}^H\ .\end{aligned} \tag{3.24}$$

Since $\sum_{i=1}^{C}\bar{\mathbf{\Delta}}_i\tilde{\mathbf{S}}\bar{\mathbf{\Delta}}_i^H$ and $\mathbf{T}^{-1}$ have full rank, $\bar{\mathbf{A}}_1$ is full column rank and $\mathbf{G}_1$ is a diagonal matrix with no zero diagonal elements, then the rank of matrix $\mathbf{T}^{-1}\mathbf{G}_1\bar{\mathbf{A}}_1\sum_{i=1}^{C}\bar{\mathbf{\Delta}}_i\tilde{\mathbf{S}}\bar{\mathbf{\Delta}}_i^H\bar{\mathbf{A}}_1^{H}\mathbf{G}_1^{\ H}\left(\mathbf{T}^{-1}\right)^H$ is equal to M_{ref}.

The EVD of $\mathbf{T}^{-1}\mathbf{G}_1\bar{\mathbf{A}}_1\sum_{i=1}^{C}\bar{\mathbf{\Delta}}_i\tilde{\mathbf{S}}\bar{\mathbf{\Delta}}_i^H\bar{\mathbf{A}}_1^{H}\mathbf{G}_1^{\ H}\left(\mathbf{T}^{-1}\right)^H + \tilde{\sigma}^2\mathbf{I}$ can be expressed as

$$\begin{aligned}&\mathbf{T}^{-1}\mathbf{G}_1\bar{\mathbf{A}}_1\sum_{i=1}^{C}\bar{\mathbf{\Delta}}_i\tilde{\mathbf{S}}\bar{\mathbf{\Delta}}_i^H\bar{\mathbf{A}}_1^{H}\mathbf{G}_1^{\ H}\left(\mathbf{T}^{-1}\right)^H + \tilde{\sigma}^2\mathbf{I} \\ &= \begin{bmatrix}\mathbf{U}_s & \mathbf{U}_n\end{bmatrix}\begin{bmatrix}\mathbf{\Lambda}_s + \tilde{\sigma}^2\underset{M_{ref}\times M_{ref}}{\mathbf{I}} & \mathbf{0} \\ \mathbf{0} & \tilde{\sigma}^2\underset{N-M_{ref}\times N-M_{ref}}{\mathbf{I}}\end{bmatrix}\begin{bmatrix}\mathbf{U}_s^H \\ \mathbf{U}_n^H\end{bmatrix},\end{aligned} \tag{3.25}$$

where $\mathbf{\Lambda}_s$ and $\mathbf{U}_s$ are the eigenvalue and eigenvector matrices of the signal subspace and $\mathbf{U}_n$ is referred as the eigenvector matrix of the noise subspace. Therefore

$$\begin{aligned}\left(\hat{\mathbf{R}}_D\right)^{-1} &= \left(\mathbf{T}^H\right)^{-1}\left(\mathbf{T}^{-1}\mathbf{G}_1\bar{\mathbf{A}}_1\sum_{i=1}^{C}\bar{\mathbf{\Delta}}_i\tilde{\mathbf{S}}\bar{\mathbf{\Delta}}_i^H\bar{\mathbf{A}}_1^{H}\mathbf{G}_1^{\ H}\left(\mathbf{T}^{-1}\right)^H + \tilde{\sigma}^2\mathbf{I}\right)^{-1}\left(\mathbf{T}\right)^{-1} \\ &= \left(\mathbf{T}^H\right)^{-1}\mathbf{U}_s(\mathbf{\Lambda}_s + \tilde{\sigma}^2\mathbf{I})^{-1}\mathbf{U}_s^H\left(\mathbf{T}\right)^{-1} + \frac{1}{\tilde{\sigma}^2}\left(\mathbf{T}^H\right)^{-1}\mathbf{U}_n\mathbf{U}_n^H\left(\mathbf{T}\right)^{-1} \\ &\approx \frac{1}{\tilde{\sigma}^2}\left(\mathbf{T}^H\right)^{-1}\mathbf{U}_n\mathbf{U}_n^H\left(\mathbf{T}\right)^{-1}\ .\end{aligned} \tag{3.26}$$

The approximation in (3.26) comes from the fact that after despreading the power of the multipath component is significantly larger than $\tilde{\sigma}^2$. By substituting (3.26) in (3.21), $\mathbf{w}$ is obtained as

$$\mathbf{w} \simeq \left(\mathbf{T}^H\right)^{-1} \mathbf{U}_n \mathbf{U}_n^H \left(\mathbf{T}\right)^{-1} \mathbf{C}_{Const.} \left(\mathbf{C}_{Const.}^H \left(\mathbf{T}^H\right)^{-1} \mathbf{U}_n \mathbf{U}_n^H \left(\mathbf{T}\right)^{-1} \mathbf{C}_{Const.}\right)^{-1} \mathbf{f}. \tag{3.27}$$

It can be found out that $\mathbf{w}^H \mathbf{G}_1$ is orthogonal to the multipath and interference subspaces and also allows the LOS signal to pass from the beamformer without distortion. From (3.25), it is concluded that

$$\mathbf{U}_s = \mathbf{T}^{-1} \mathbf{G}_1 \bar{\mathbf{A}}_1 \left(\sum_{i=1}^{C} \bar{\mathbf{\Delta}}_i \tilde{\mathbf{S}} \bar{\mathbf{\Delta}}_i^H \right)^{\frac{1}{2}} \mathbf{Q} (\mathbf{\Lambda}_s)^{-\frac{1}{2}} \tag{3.28}$$

where $\mathbf{Q}$ is an unknown $M_{ref} \times M_{ref}$ unitary matrix. In addition, as a result of the signal and noise eigenvector orthogonality, $\mathbf{U}_n^H \mathbf{U}_s = 0$ and therefore

$$\begin{aligned} &\mathbf{w}^H \mathbf{T} \mathbf{U}_s \\ &= \mathbf{f}^H \left(\mathbf{C}_{Const.}^H \left(\mathbf{T}^H\right)^{-1} \mathbf{U}_n \mathbf{U}_n^H \left(\mathbf{T}\right)^{-1} \mathbf{C}_{Const.}\right)^{-1} \mathbf{C}_{Const.}^H \left(\mathbf{T}^H\right)^{-1} \mathbf{U}_n \mathbf{U}_n^H \left(\mathbf{T}\right)^{-1} \mathbf{T} \mathbf{U}_s = 0 \ . \end{aligned} \tag{3.29}$$

By substituting $\mathbf{U}_s$ from (3.28) into (3.29), one obtains

$$\mathbf{w}^H \mathbf{T} \mathbf{T}^{-1} \mathbf{G}_1 \bar{\mathbf{A}}_1 \left(\sum_{i=1}^{C} \bar{\mathbf{\Delta}}_i \tilde{\mathbf{S}} \bar{\mathbf{\Delta}}_i^H \right)^{\frac{1}{2}} \mathbf{Q} (\mathbf{\Lambda}_s)^{-\frac{1}{2}} = 0 \, . \tag{3.30}$$

As assumed, $\sum_{i=1}^{C} \bar{\mathbf{\Delta}}_i \tilde{\mathbf{S}} \bar{\mathbf{\Delta}}_i^H$ has full rank and also $\mathbf{Q}$ and $\mathbf{\Lambda}_s^{-\frac{1}{2}}$ have full rank. Therefore $\bar{\mathbf{A}}_1 \left(\sum_{i=1}^{C} \bar{\mathbf{\Delta}}_i \tilde{\mathbf{S}} \bar{\mathbf{\Delta}}_i^H \right)^{\frac{1}{2}} \mathbf{Q} (\mathbf{\Lambda}_s)^{-\frac{1}{2}}$ and $\bar{\mathbf{A}}_1$ share the same M_{ref} dimensional space and thus

$$\mathbf{w}^H \mathbf{G}_1 \bar{\mathbf{A}}_1 = 0 \tag{3.31}$$

which means that gain vector $\mathbf{w}^H \mathbf{G}_1$ is orthogonal to the steering matrix of multipath components. In other words, the beamformer puts nulls in the direction of multipath components. It is straightforward to show that $\mathbf{w}^H \mathbf{G}_1$ has a distortionless response for the LOS signal and is orthogonal to the interference subspace. In order to show this, it is proven that $\mathbf{w}^H \mathbf{C}_{Const.} = \mathbf{f}^H$ as

$$\begin{aligned} &\mathbf{w}^H \mathbf{C}_{Const.} = \\ &\mathbf{f}^H \left(\mathbf{C}_{Const.}^H \left(\mathbf{T}^H \right)^{-1} \mathbf{U}_n \mathbf{U}_n^H \left(\mathbf{T} \right)^{-1} \mathbf{C}_{Const.} \right)^{-1} \mathbf{C}_{Const.}^H \left(\mathbf{T}^H \right)^{-1} \mathbf{U}_n \mathbf{U}_n^H \left(\mathbf{T} \right)^{-1} \mathbf{C}_{Const.} = \mathbf{f}^H, \end{aligned} \tag{3.32}$$

since as long as (3.22) holds, $\mathbf{C}_{Const.}^H \left(\mathbf{T}^H \right)^{-1} \mathbf{U}_n \mathbf{U}_n^H \left(\mathbf{T} \right)^{-1} \mathbf{C}_{Const.}$ has full rank and hence

$$\left(\mathbf{C}_{Const.}^H \left(\mathbf{T}^H \right)^{-1} \mathbf{U}_n \mathbf{U}_n^H \left(\mathbf{T} \right)^{-1} \mathbf{C}_{Const.} \right)^{-1} \mathbf{C}_{Const.}^H \left(\mathbf{T}^H \right)^{-1} \mathbf{U}_n \mathbf{U}_n^H \left(\mathbf{T} \right)^{-1} \mathbf{C}_{Const.} = \mathbf{I} \tag{3.33}$$

Regarding computational complexity, the formation of the correlation matrices, matrix inversions and EVD carry the major parts of the computational load of the proposed method. The correlation matrices are $N \times N$ and, therefore, EVD in the first stage and the matrix inversions in (3.21) require a computational load of $O\left(N^3\right)$. Since the value of N is limited to the number of the antenna elements of the subarrays, which is limited in practice, EVD and matrix inversions can be implemented in a real time operation without significantly increasing computational complexity. The formation of the correlation matrices for the first and second stages requires computation complexities of $O\left(K_{win} N^2\right)$ and $O\left(K_{win} C N^2\right)$ respectively, where K_{win} is the number of samples employed to form

these matrices and C is the number of extra antenna elements to make $C+1$ overlapping subarrays. In the first stage, the samples are collected before despreading whereas in the second stage the correlator outputs are utilized to form the correlation matrix. For the latter, the multipath should be assumed constant during the process, which is realistic for static GNSS receivers. The summary of the proposed technique consists of the following steps:

1 Calculate the interference subspace by performing EVD of the correlation matrix before the despreading process

2 Mitigate interference and obtain the coarse estimates of Doppler frequency and code delay in the first stage utilizing (3.4).

3 Calculate the modified correlation matrix after pre-gaining from (3.13)

4 Calculate the optimal gain vector $\mathbf{w}$ from (3.21)

5 Apply the gain vector $\boldsymbol{\mu}$, which is equal to $\mathbf{G}_1^H\mathbf{w}$, to the first subarray

3.3 Simulation results

In order to evaluate the effectiveness of the proposed interference and multipath mitigation technique, three simulation scenarios are considered. In all scenarios, a linear uniform spacing antenna array consisting of seven elements is considered. A GPS L1 C/A code with a chipping rate of 1.023 MHz and a sampling rate of 10 MHz are used for the simulations.

In the first simulation scenario, the performance of the proposed MDOP beamformer for interference and multipath suppression is examined. In this simulation, a LOS signal, one coherent multipath component and two interference signals are considered. The first interference signal is a multi-tone signal consisting of eleven sinusoidal signals, which are uniformly distributed over a 2 MHz bandwidth centered at L1 (1575.42 MHz). The second

interference signal is a broadband Gaussian noise spread over a 2 MHz bandwidth of L1. The multipath component is simulated with the same Doppler frequency as that of the LOS component and a delay of 0.4 chip. The received power and direction of these signals are shown in Table 3-1. Herein, the array configuration consists of two overlapping subarrays with six elements in each subarray. In the first and second stage of the beamformer, the optimal gain vectors are obtained from (3.4) and (3.21), respectively. The resulting beam patterns are shown in Figure 3-2. It can be observed that the beamformer puts deep nulls in the direction of the interference signals (approximately -151 dB for the multi-carrier interference and -116 dB for the broadband Gaussian interference). These attenuations plus the attenuation due to the despreading process lead to suppression of the interfering signals. After interference suppression, the multipath component is attenuated by 24 dB in the second stage.

Table 3-1: Signal characteristics in the first simulation scenario

	LOS signal	Multipath	Multi-carrier interference	Broadband Gaussian interference
Received Power (dBW)	-159	-162	-80	-80
Direction of arrival (degree) For elevation angle 0°	60	45	120	90

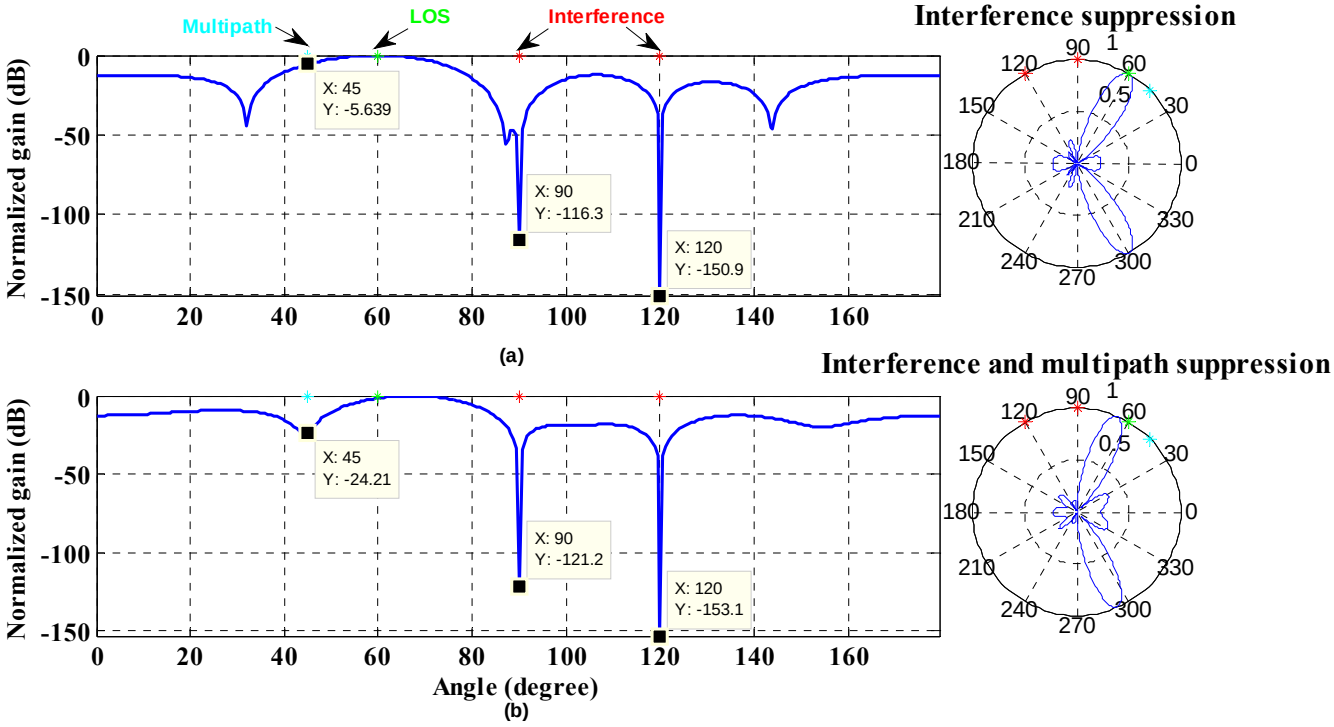

Figure 3-2: MDOP beam patterns, a) interference mitigation in the first stage b) multipath mitigation in the second stage

In GNSS applications, pseudorange measurements are obtained by tracking the correlation peak. Multipath propagation distorts the correlation peak and causes a bias in the pseudo-range estimation. In the ideal case (zero error due to multipath and the filtering effect of the RF front-end), this peak is an isosceles triangle. In Figure 3-3, the normalized correlation functions are shown after the first and second stages (normalized with respect to the value of the second satge correlation peak). It can be observed that the proposed beamformer puts null in the direction of the multipath component in the second stage and, therefore, almost an ideal correlation peak can be achieved.

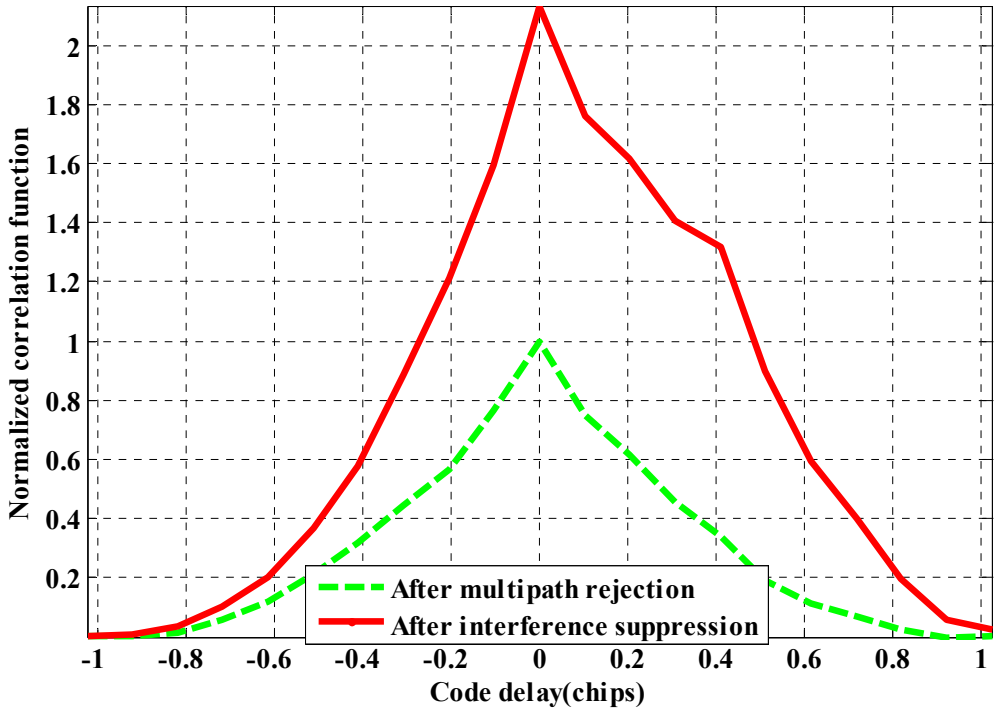

Figure 3-3: Correlation functions after the first and second stage

In the second simulation scenario, the performance of the proposed method to deal with correlated multipath components is examined. In this simulation one LOS signal and a broadband Gaussian interference and two coherent multipath components are simulated. The utilized interference signal parameters are the same as in the previous simulation. The multipath components have a 0.1 and 0.3 chip delay with respect to the LOS component. Table 3-2 provides the characteristics of the simulated signals.

Table 3-2: Signals characteristics in the second simulation scenario

	LOS signal	Multipath1	Multipath2	Broadband Gaussian interference
Received Power (dBW)	-159	-160	-161	-80
Direction of arrival (degree) For elevation angle 0°	60	45	120	90

In this simulation, the performances of three different beamforming configurations to deal with the multipath signals have been characterized. In the first case, MDOP is applied where the antenna configuration includes three overlapping subarrays, each of which has five antenna elements. According to (3.22), this configuration can deal with both the signal cancelation phenomenon and the rank deficiency of the temporal correlation matrix. In the second case, again the MDOP method is employed however, the antenna configuration consists of two overlapping subarrays with six elements in each subarray. This case cannot compensate for the rank deficiency of the temporal correlation matrix. In the third case, a conventional beamformer namely Linear Constraint Minimum Power (LCMP) beamformer is applied to compare its performance with the proposed method. For this case, the antenna configuration is the same as the first case. Therefore, it is expected that, despite the rank deficiency compensation, the beamformer will fail due to the signal cancelation phenomenon. The beam patterns and correlation functions for the aforementioned three cases are shown in Figure 3-4 and Figure 3-5, respectively. As expected, only the first case properly puts nulls in the direction of the multipath components.

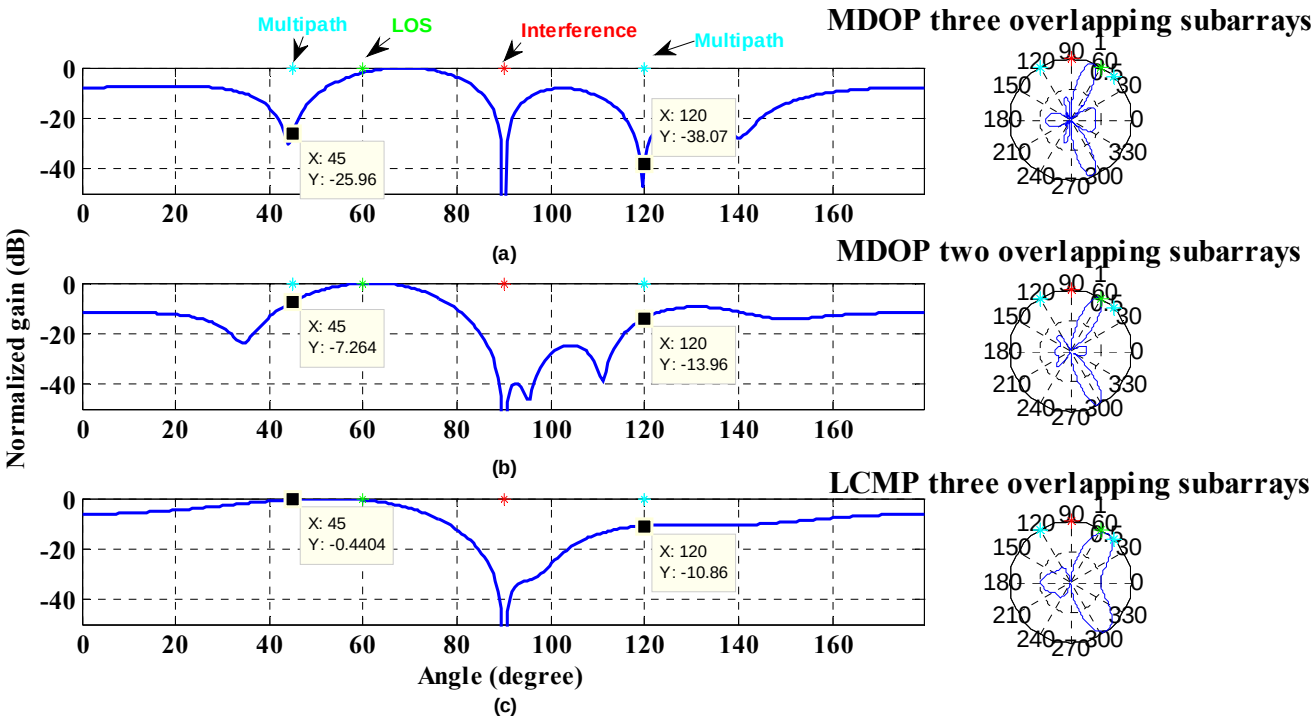

Figure 3-4: Beam patterns, a) MDOP with three overlapping subarrays, b) MDOP with two overlapping subarrays, c) LCMP with three overlapping subarrays

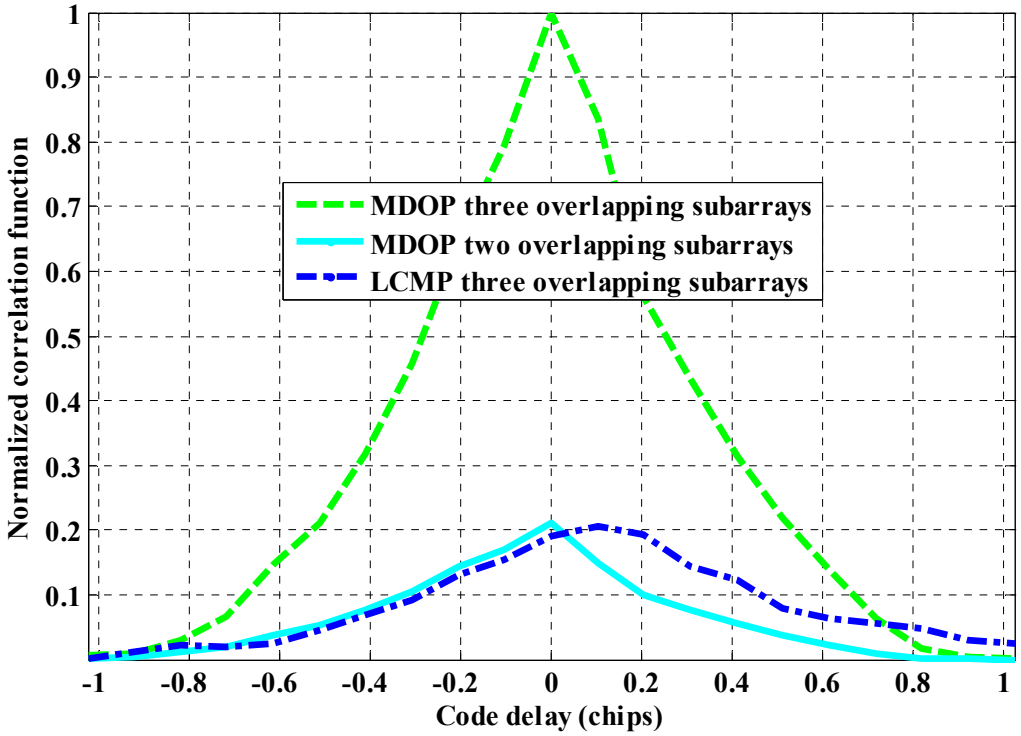

Figure 3-5: Correlation functions for the MDOP method with three overlapping subarrays, the MDOP method with two overlapping subarrays and the LCMP beamformer with three overlapping subarrays

In the last simulation scenario, the multipath error envelope concept was utilized for further evaluation of the performance of this method. In this scenario, a LOS signal arriving from an azimuth angle of 90º and one multipath component have been considered. The multipath error has been plotted as a function of the multipath signal direction of arrival and its delay with respect to the LOS signal. This simulation compares the multipath error performance of three different receivers which have employed the Early-Minus-Late (EML) discriminator. The first and second receivers employ the MDOP and LCMP beamformer with the same array configuration described

in the second simulation scenario and the third receiver utilizes a single antenna receiver. The multipath errors for correlator spacings (CS) of 0.1, 0.5 and 1 chips are shown in Figure 3-6. For the single antenna receiver, the multipath signal is assumed to be in phase with the LOS signal whereas for the other receivers, the relative phase between the multipath and LOS signals is dependent on their directions. As observed, in the single antenna receiver case, the multipath error does not depend on the direction of the multipath component and the LCMP beamformer fails to mitigate multipath in all directions due to signal cancelation whereas the MDOP beamformer only fails when the direction of the multipath component is close to that of the LOS signal such that the MDOP beamformer is not able to spatially discriminate between these two signals.

It is worth mentioning that the proposed method performs well even when the LOS power is weaker than the multipath power (for example by foliage obstructions) whereas in this situation the conventional single channel multipath mitigation methods fail to reduce the error due to multipath in pseudorange measurements (Broumandan & Lin 2008).

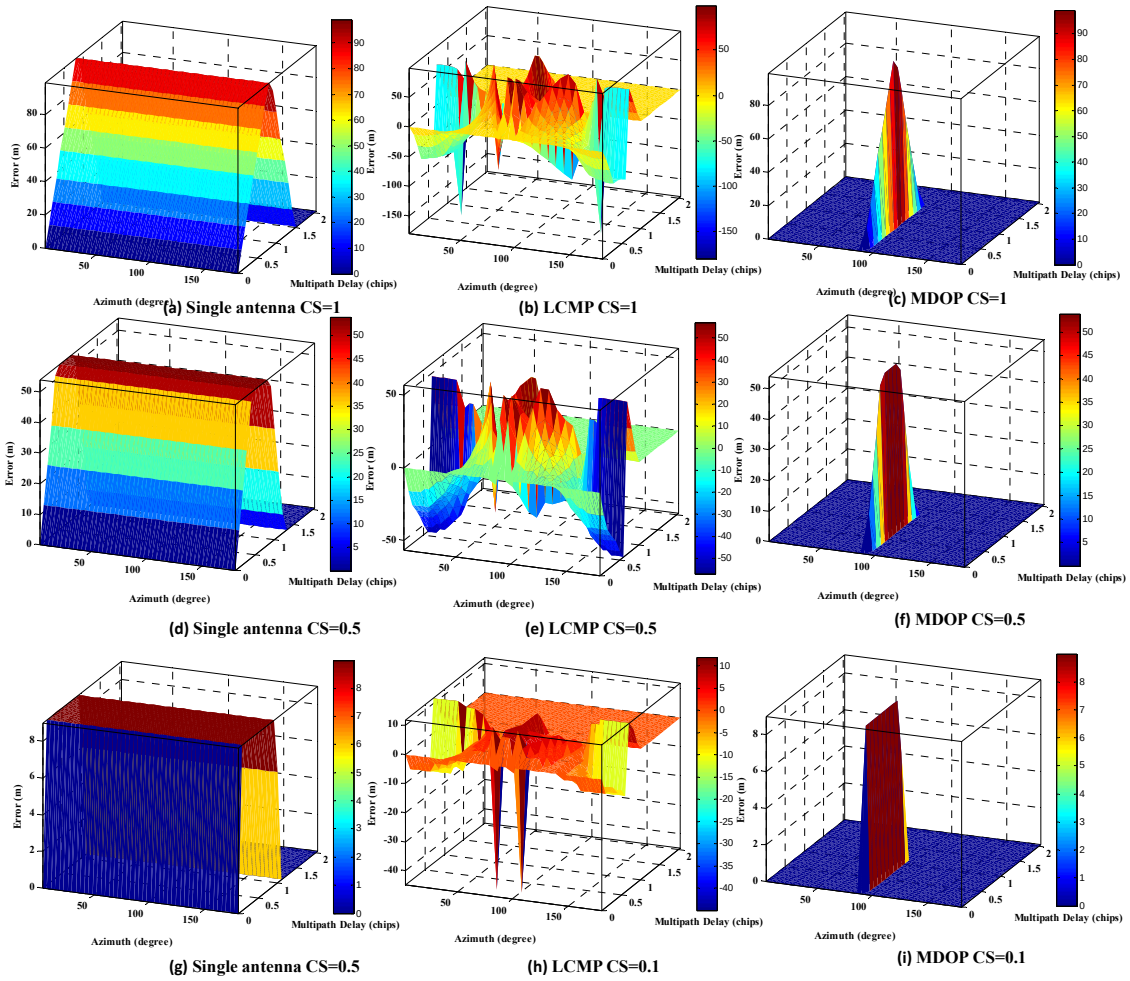

Figure 3-6: Multipath error as a function of the multipath signal direction of arrival and its delay with respect to the LOS signal for a) single antenna CS=1, b) LCMP CS=1, and c) MDOP receivers CS=1 d) single antenna CS=0.5, e) LCMP CS=0.5, and f) MDOP receivers CS=0.5 g) single antenna CS=0.1, h) LCMP CS=0.1, and i) MDOP receivers CS=0.1

3.4 Experimental results

To verify that the proposed method is indeed applicable to real-world scenarios, a practical test was performed in a controlled environment with a Spirent GSS 7700 hardware simulator and a signal generator to simulate the GPS signals and one sinusoidal

waveform as interference. These signals were propagated on a rooftop by several directional antennas where their power was controlled by amplifiers and attenuators to affect only a small controlled test area. The transmitted signals were received by a linear antenna array with five elements and were passed to a five channel RF front-end. A hardware simulator was used to simulate an unavailable PRN at the propagating time with a controlled power to cover a small area of the rooftop. The generated GPS signal was split into two parts to generate one LOS signal and one multipath component. Practical implementation issues including array calibration had been considered. In this test by utilizing the attenuator and amplifier, the power of the multipath component in a long cable was controlled in order to have proper power with respect to the LOS component. During the measurements, the power of both multipath and LOS components was chosen to be received with a carrier-to-noise ratio (C/N0) of 45 dB-Hz. The received signal power was measured using the GSNRx™ GNSS software receiver (Petovello et al 2008). Using a long cable, the delay of the multipath was adjusted to be around 0.2 chip duration (about 60 m). The data collection setup and the block diagram of the scenario are shown in Figure 3-7 a and b, respectively.

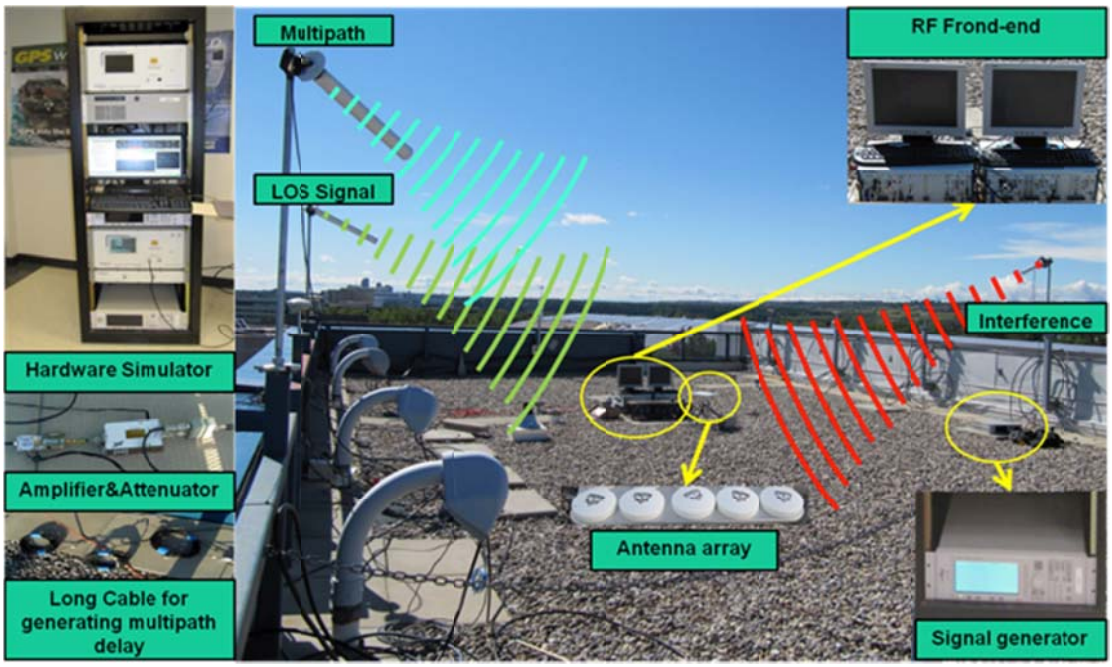

(a)

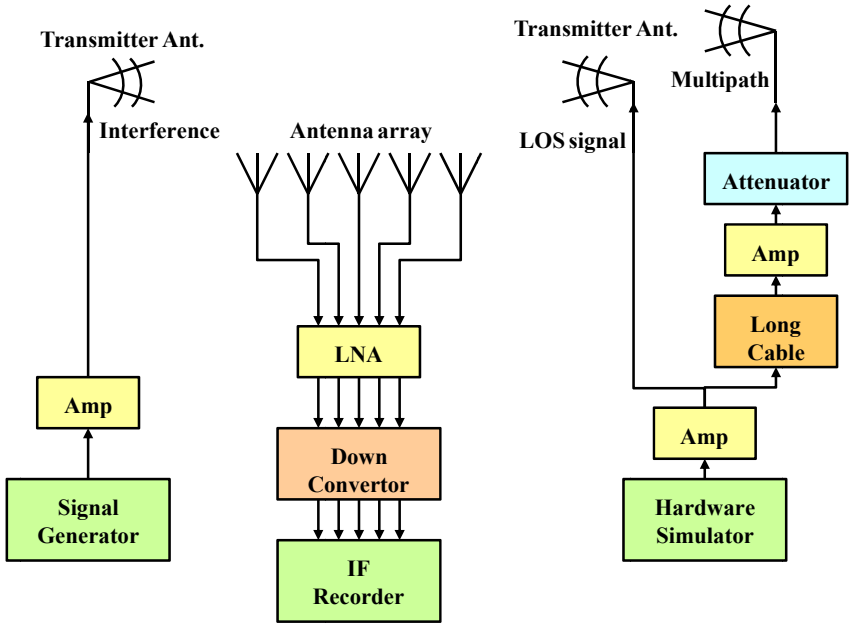

(b)

Figure 3-7: a) data collection set up, b) Block diagram of signal connections

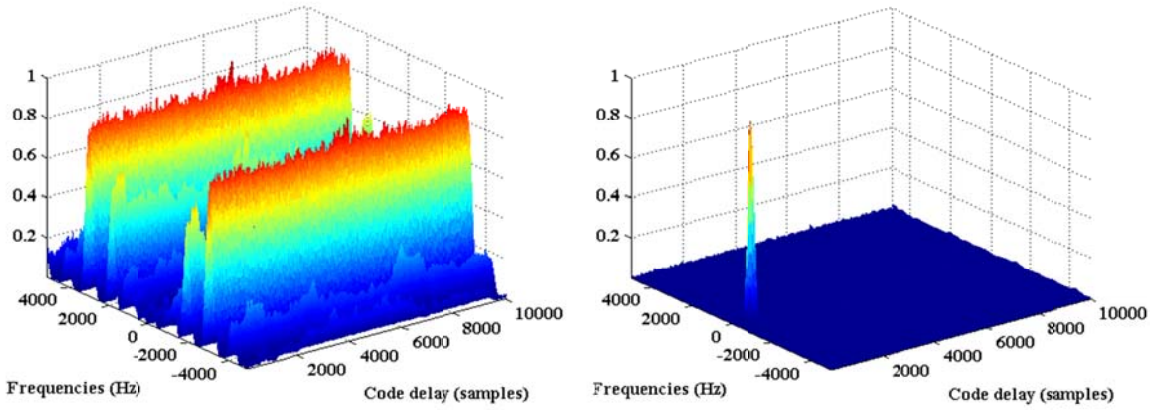

(a) (b)

Figure 3-8: Normalized CAFs (a) before interference rejection (b) after interference rejection

According to (3.22), in order to mitigate one multipath component and one interfering signal and have a distortionless response in the direction of the LOS signal, two overlapping subarrays with four antenna elements in each subarray were chosen. In the interference rejection stage, the optimal weight is obtained from (3.4). In Figure 3-8, the normalized correlation peak before and after interference suppression are shown. It can be seen that the acquisition process cannot be performed without the interference suppression stage. However, after interference rejection, the multipath component still exists which can be mitigated in the second stage by obtaining the optimal gain vector from (3.21).

In order to evaluate the performance of the proposed multipath mitigation stage, a test was performed over one second observation for the coherent integration time 1 ms. In this test, the multipath component was tuned to be stronger than the LOS component and almost in-phase with it. The normalized correlation peaks are shown in Figure 3-9 before

and after multipath mitigation. An examination of the relative amplitude, delay and width of these correlation peaks reveal that the time of arrival error due to multipath is successfully mitigated by the proposed method. The Double Delta Correlator technique was applied for comparing the pseudorange measurements before and after multipath mitigation. Over one second of observations, the average of the errors that can be corrected by the proposed method was 50 m. The experimental results reveal that the proposed algorithm is effective for both interference suppression and multipath mitigation.

The experimental results show that the proposed algorithm is effective for both interference suppression and multipath mitigation.

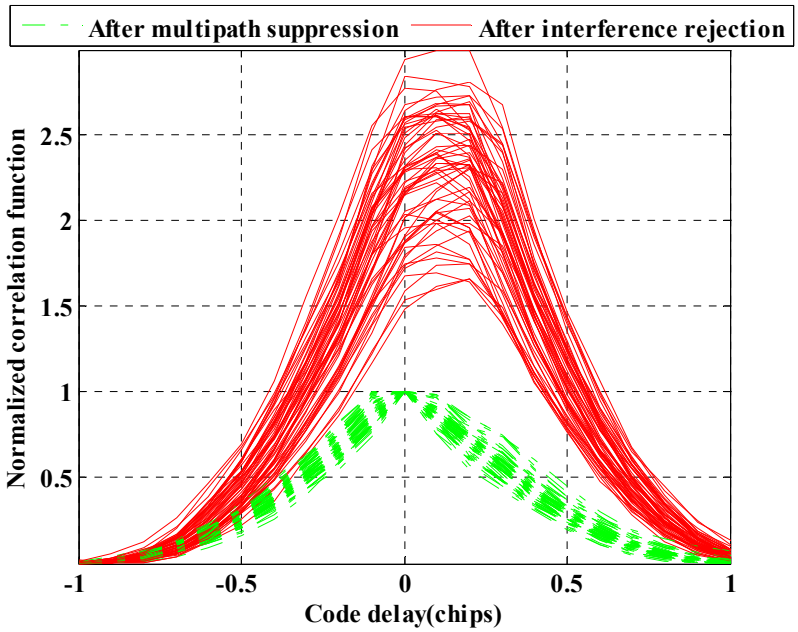

Figure 3-9: Correlation peaks after the first and second stage

3.5 Summary

A new beamformer technique to suppress both interference and multipath signals with distortionless response in the direction of the LOS signal has been proposed. In the interference suppression stage the subspace method has been used to mitigate wideband and narrowband interference signals. In the multipath mitigation stage the proposed technique utilizes several overlapping subarrays. Afterwards, by pre-gaining and taking the difference between signals of subarrays the proposed method minimizes the power of the multipath components. As shown, the proposed method is robust against the signal cancelation phenomenon and rank deficiency of the temporal correlation matrix. This method can be implemented in vehicular or high precision navigation applications operating in urban environments where multipath and wideband/narrowband interference signals degrade or completely fail the position solution. The simulation and experimental results reported above show the effectiveness of the method for interference suppression and multipath mitigation.

Chapter Four: GNSS MULTIPATH MITIGATION WITH A MOVING ANTENNA ARRAY

As mentioned in previous chapters, besides the size and shape of antenna arrays, the correlation between multipath components and a desired signal restricts the use of array processing techniques for GNSS multipath mitigation. In Chapter 3, spatial smoothing in conjunction with pre-spatial filtering was proposed to deal with highly correlated multipath components applicable for both static and mobile applications.

This chapter proposes a method based on a moving antenna array to deal with multipath propagation. Furthermore, the proposed method synthesizes a larger array and increases its degree of freedom such that without increasing the number of the physical antenna elements, the number of multipath components that can be suppressed is increased.

4.1 Introduction

Multipath propagation is one of the main error sources in GNSS applications. Antenna array processing has been widely utilized for GNSS multipath mitigation (Sahmoudi & Amin 2007, Seco-Granados et el 2005, Brown 2000, Moelker 1997). However, the size and the structure of antenna arrays limit their usage in both pedestrian and vehicular applications. Furthermore, mutual coupling among antennas and array calibration become challenging for large antenna arrays. On the other hand, the number of undesired signals that can be mitigated (degree of freedom of the array) increases if the number of antenna elements is increased. Recently, antenna motion and synthetic array processing have been studied to deal with this problem (Broumandan et al 2008, Draganov et al 2011). Antenna

Array motion has been also utilized as a decorrelating technique in array processing methods (Haber & Zoltowski 1986). As mentioned previously, one of the main difficulties in dealing with multipath propagation is the high correlation with the LOS signal. In this chapter, antenna array motion is utilized to decorrelate multipath components and to further increase the array degree of freedom by implementing a synthetic array and forming a spatial-temporal correlation matrix. A spatial filter is applied to this correlation matrix to estimate the multipath steering vectors (the same concept of the spatial pre-filtering introduced in Chapters 2 and 3). Afterwards, in a constraint optimization problem, an optimal gain vector is obtained to maximize the signal-to-noise ratio (SNR) of the LOS signal whereby mitigating the multipath signals.

4.2 Proposed method

Assume a uniform linear antenna array consisting of N antennas. The complex baseband representation of a GNSS signal and its reflections impinging on the antenna array for each satellite signal after despreading can be written in a $N \times 1$ vector as

$$\hat{\mathbf{r}} = \mathbf{A}\hat{\mathbf{s}} + \hat{\boldsymbol{\eta}} \tag{4.1}$$

where $\hat{\boldsymbol{\eta}}$ models the spatial-temporal white zero-mean complex noise vector and $\mathbf{A}$ is defined in (3.3). The steering matrix $\mathbf{A}$ is assumed to have a full column rank, which means that incident signals impinge on the array from different directions. In (4.1), $\hat{\mathbf{s}}$ can be represented as

$$\widehat{\mathbf{s}} = \begin{bmatrix} \alpha_0 e^{j\phi_0 + j2\pi\Delta f_0 nT_c} \\ \alpha_1 e^{j\phi_1 + j2\pi\Delta f_1 nT_c} \\ \vdots \\ \alpha_{M_{ref}} e^{j\phi_{M_{ref}} + j2\pi\Delta f_{M_{ref}} nT_c} \end{bmatrix} \tag{4.2}$$

in which M_{ref} is the number of multipath components, n is the discrete time index, T_c is the coherent integration time and ϕ_m, α_m and Δf_m are the phase shift, the attenuation factor and the frequency offset of the *m*th multipath component after despreading, respectively. The subscript zero indicates the LOS signal. As the number of multipath components increases $\left(M_{ref} > N-1\right)$ conventional beamforming methods fail to suppress undesired signals. Furthermore, the high correlation between multipath components and the LOS signal causes a rank deficiency of the temporal correlation matrix and the signal cancellation phenomenon. In the following subsections, a moving antenna array in the form of a synthetic array processing is employed to not only decorrelate the received signals but also to increase the degree of freedom of the antenna array. In addition, the spatial pre-filtering technique investigated in (Citron & Kailath 1984, Haimovich & Bar-Ness 1991) is extended in the proposed method to prevent the signal cancellation phenomenon.

4.2.1 Synthetic array processing

It is assumed that the antenna array moves with a constant unknown velocity $\mathbf{v}_{vel}$. The output of each antenna element after down-conversion is despread by the locally

generated PRN code and coherently integrated over T_c seconds. The synthetic array realization and the spatial/temporal sampling process are depicted in Figure 4-1. Consider K_s consecutive snapshots separated by L_s samples as shown in this figure. K_s is determined with respect to the required degree of freedom and L_s is an integer design parameter which is a function of the antenna array velocity and is typically selected such that

$$2T_c \left\| \mathbf{v}_{vel} \right\| L_s \approx \lambda \tag{4.3}$$

in which λ is the carrier wavelength. A super-vector can be formed from these $K_s N$ samples as

$$\vec{\mathbf{r}}_n = \left[\hat{\mathbf{r}}^T[n] \quad \hat{\mathbf{r}}^T[n+L_s] \quad \cdots \quad \hat{\mathbf{r}}^T[n+L_s(K_s-1)] \right]^T . \tag{4.4}$$

It can be shown that

$$\vec{\mathbf{r}}_n = \mathcal{A}\mathbf{s} + \vec{\boldsymbol{\eta}}_n \tag{4.5}$$

where $\vec{\boldsymbol{\eta}}_n$ is the $K_s N \times 1$ noise vector with the covariance matrix of $\hat{\sigma}^2 \underset{K_s N \times K_s N}{\mathbf{I}}$ and $\mathcal{A}$ is the augmented steering matrix that can be stated as

$$\mathcal{A} = \begin{bmatrix} \mathbf{A} \\ \mathbf{AD} \\ \vdots \\ \mathbf{AD}^{K_s-1} \end{bmatrix} \tag{4.6}$$

in which the diagonal matrix $\mathbf{D}$ is defined as

$$\mathbf{D} = \begin{bmatrix} e^{j2\pi \frac{\mathbf{v}_{vel} \bullet \hat{\mathbf{e}}_0}{\lambda} L_s T_c} & \cdots & 0 \\ \vdots & \ddots & \vdots \\ 0 & \cdots & e^{j2\pi \frac{\mathbf{v}_{vel} \bullet \hat{\mathbf{e}}_{M_{ref}}}{\lambda} L_s T_c} \end{bmatrix}. \tag{4.7}$$

In (4.7), $\hat{\mathbf{e}}_m$ $(m = 0,...,M_{ref})$ is a unit vector pointing from the antenna array to the direction of arrival of the *m*th signal component and "•" stands for dot product.

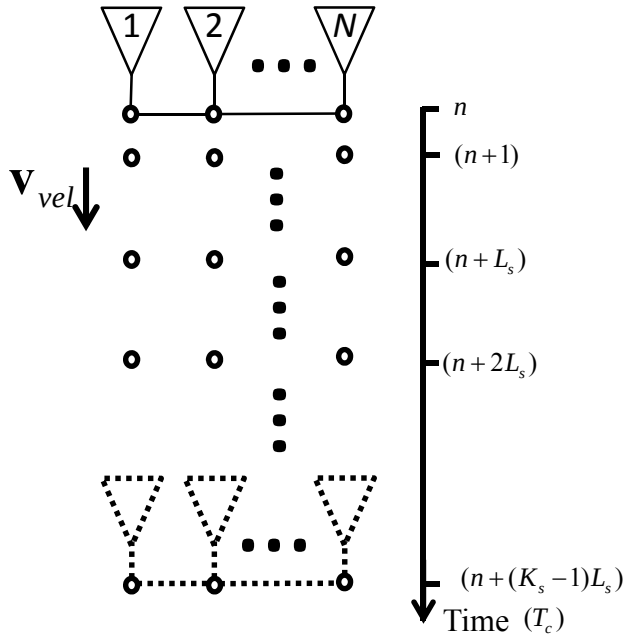

Figure 4-1: Illustration of a moving array sampling process

In fact, since different signal components arrive from different directions, their corresponding Doppler frequency shifts due to the antenna array motion differ from each other and therefore, the diagonal elements of **D** are different. According to (4.6) and (4.7), since **D** has a rank order of $M_{ref}+1$, if $K_s N > M_{ref}$, augmenting the

steering matrix increases the degree of freedom in the beamforming process to mitigate a number of multipath components larger than that of the antenna elements. In order to mitigate the multipath components, the augmented correlation matrix will be used for further analyses. This matrix can be represented as

$$\widehat{\mathbf{R}} = E\left\{\vec{\mathbf{r}}_n \vec{\mathbf{r}}_n^{\,H}\right\} = \mathcal{A} E\left\{\widehat{\mathbf{s}}\widehat{\mathbf{s}}^H\right\}\mathcal{A}^H + \widehat{\sigma}^2\,\mathbf{I}. \tag{4.8}$$

If the constant phases are ignored (they do not affect the final result), $\widehat{\mathbf{s}}$ can be stated as follows for a moving antenna array:

$$\widehat{\mathbf{s}} = \begin{bmatrix} \alpha_0 e^{j2\pi \frac{\mathbf{v}_{vel}\bullet\hat{\mathbf{e}}_0}{\lambda} nT_c} \\ \alpha_1 e^{j2\pi \frac{\mathbf{v}_{vel}\bullet\hat{\mathbf{e}}_1}{\lambda} nT_c} \\ \vdots \\ \alpha_{M_{ref}} e^{j2\pi \frac{\mathbf{v}_{vel}\bullet\hat{\mathbf{e}}_{M_{ref}}}{\lambda} nT_c} \end{bmatrix}. \tag{4.9}$$

According to (4.9), the array motion also results in decorrelation of the temporal correlation matrix $E\left\{\widehat{\mathbf{s}}\widehat{\mathbf{s}}^H\right\}$ via $\mathbf{v}_{vel}\bullet\hat{\mathbf{e}}_m$ terms. In (4.8), $\widehat{\mathbf{R}}$ can be approximately estimated by averaging over K_{win} consecutive widows of the received spatial samples as

$$\widehat{\mathbf{R}} = \frac{1}{K_{win}} \sum_{n=0}^{K_{win}-1} \vec{\mathbf{r}}_n \vec{\mathbf{r}}_n^{\,H}. \tag{4.10}$$

$\mathbf{A}$, $\mathbf{D}$ and $E\left\{\widehat{\mathbf{s}}\widehat{\mathbf{s}}^H\right\}$ can be partitioned as

$$\mathbf{D} = \begin{bmatrix} d_0 & \mathbf{0} \\ \underset{M_{ref}\times 1}{\mathbf{0}} & \underset{M_{ref}\times M_{ref}}{\overline{\mathbf{D}}} \end{bmatrix}$$
$$E\left\{\hat{\mathbf{s}}\hat{\mathbf{s}}^H\right\} = \begin{bmatrix} S_0 & \overline{\hat{\mathbf{s}}}^H \\ \underset{M_{ref}\times 1}{\overline{\hat{\mathbf{s}}}} & \underset{M_{ref}\times M_{ref}}{\hat{\mathbf{S}}} \end{bmatrix} \tag{4.11}$$
$$\mathbf{A} = \begin{bmatrix} \mathbf{a}_0 & \overline{\mathbf{A}} \end{bmatrix}.$$

Hence, $\hat{\mathbf{R}}$ can be written as

$$\hat{\mathbf{R}} = \vec{a}s_0\vec{a}^H + \overline{\mathcal{A}}\hat{\mathbf{S}}\overline{\mathcal{A}}^H + \vec{a}\overline{\hat{\mathbf{s}}}^H\overline{\mathcal{A}}^H + \overline{\mathcal{A}}\overline{\hat{\mathbf{s}}}\vec{a}^H + \hat{\sigma}^2\mathbf{I} \tag{4.12}$$

where

$$\overline{\mathcal{A}} = \begin{bmatrix} \overline{\mathbf{A}} \\ \overline{\mathbf{A}}\overline{\mathbf{D}} \\ \vdots \\ \overline{\mathbf{A}}\overline{\mathbf{D}}^{K_s-1} \end{bmatrix} \qquad \vec{a} = \begin{bmatrix} \mathbf{a}_0 \\ \mathbf{a}_0 d_0 \\ \vdots \\ \mathbf{a}_0 d_0^{K_s-1} \end{bmatrix}. \tag{4.13}$$

In (4.12), the first term is the correlation matrix of the desired signal (LOS signal), the second term is the correlation matrix of the multipath components and the two other terms are the cross-correlation between the desired signal and the multipath components. Herein, the problem of interest is to find an optimal weighting vector $\mathbf{w}$ that maximizes the SNR of the LOS signal subject to the constraint that $\mathbf{w}$ is orthogonal to the steering matrix of the multipath components as

$$\max_{\substack{\|\mathbf{w}\|=1 \\ \mathbf{w}^H\overline{\mathcal{A}} = \underset{1\times M_{ref}}{\mathbf{0}}}} \frac{\mathbf{w}^H\vec{a}s_0\vec{a}^H\mathbf{w}}{\mathbf{w}^H\hat{\sigma}^2\mathbf{I}\mathbf{w}}. \tag{4.14}$$

Due to the correlation between the LOS signal and the multipath components, the multipath steering matrix $\bar{\mathcal{A}}$ cannot be directly estimated from $\hat{\mathbf{R}}$. However, a spatial pre-filter can be employed to estimate $\bar{\mathcal{A}}$ as explained in the following subsection.

4.2.2 Multipath mitigation

Extending the spatial pre-filtering in (Citron & Kailath 1984, Haimovich & Bar-Ness 1991) for a synthetic array is straightforward. To this end, a filtering matrix $\mathbf{H}_f$ is designed such that $\mathbf{H}_f \vec{a} = \mathbf{0}$. Hence, the correlation matrix after applying this filter to $\vec{\mathbf{r}}$ becomes

$$\begin{aligned}&\hat{\mathbf{R}}_D = \mathbf{H}_f \hat{\mathbf{R}} \mathbf{H}_f^H = \\ &\mathbf{H}_f \vec{a} s_0 \vec{a}^H \mathbf{H}_f^H + \mathbf{H}_f \bar{\mathcal{A}} \hat{\mathbf{S}} \bar{\mathcal{A}}^H \mathbf{H}_f^H + \mathbf{H}_f \vec{a} \bar{\vec{s}}^H \bar{\mathcal{A}}^H \mathbf{H}_f^H + \mathbf{H}_f \bar{\mathcal{A}} \bar{\vec{s}} \vec{a}^H \mathbf{H}_f^H + \hat{\sigma}^2 \mathbf{H}_f \mathbf{H}_f^H .\end{aligned} \tag{4.15}$$

$\mathbf{H}_f$ can be formed using two known matrices as $\mathbf{H}_f = \mathcal{F}\mathcal{G}$ where $\mathcal{F}$ and $\mathcal{G}$ are $K_s \times K_s$ block matrices defined as

$$\mathcal{F} \triangleq \begin{bmatrix} \underset{N-1\times N}{\mathbf{F}} & \cdots & \underset{N-1\times N}{\mathbf{0}} \\ \vdots & \ddots & \mathbf{0} \\ \mathbf{0} & \cdots & \mathbf{F} \end{bmatrix} \quad \mathcal{G} \triangleq \begin{bmatrix} \underset{N\times N}{\mathbf{G}} & \cdots & \underset{N\times N}{\mathbf{0}} \\ \vdots & \ddots & \mathbf{0} \\ \mathbf{0} & \cdots & \mathbf{G} \end{bmatrix} \tag{4.16}$$

where $\mathbf{G}$ is a $N \times N$ diagonal gaining sub-matrix and $\mathbf{F}$ is a $(N-1)\times N$ differencing sub-matrix defined as

$$\mathbf{F} \triangleq \begin{bmatrix} 1 & -1 & 0 & \cdots & 0 & 0 \\ 0 & 1 & -1 & \ddots & & \vdots \\ \vdots & & \ddots & \ddots & -1 & 0 \\ 0 & 0 & 0 & \cdots & 1 & -1 \end{bmatrix}. \tag{4.17}$$

If $\mathbf{G}$ is designed such that $diag(\mathbf{G}) = \mathbf{a}_0^*$, then $\mathbf{H}_f \vec{a} = \mathbf{0}$ and, therefore,

$$\hat{\mathbf{R}}_D = \mathcal{F}\mathcal{G}\bar{\mathcal{A}}\tilde{\mathbf{S}}\bar{\mathcal{A}}^H\mathcal{G}^H\mathcal{F}^H + \hat{\sigma}^2\mathcal{F}\mathcal{F}^H \ . \tag{4.18}$$

In order to estimate $\bar{\mathcal{A}}$, the following generalized eigen-decomposition (GED) problem should be solved:

$$\hat{\mathbf{R}}_D\mathbf{u} = \lambda_{GE}\mathcal{F}\mathcal{F}^H\mathbf{u} \tag{4.19}$$

where λ_{GE} is any generalized eigenvalue and $\mathbf{u}$ is its corresponding eigenvector. It can be shown that, when $\tilde{\mathbf{S}}$ is full rank, the following relation holds (Haimovich &. Bar-Ness 1991)

$$span(\mathcal{F}\mathcal{G}\bar{\mathcal{A}}) \perp span(\mathbf{U}_n) \tag{4.20}$$

where $\mathbf{U}_n$ consists of $(N-1)K_s - M_{ref}$ eigenvectors corresponding to the $(N-1)K_s - M_{ref}$ smallest generalized eigenvalues. In order to suppress the multipath components whereas the LOS signal is allowed to pass through the beamformer, the augmented correlation matrix obtained from (4.8) and (4.10) is replaced by the one constructed from the samples of the first $(N-1)$ antenna elements. The correlation matrix for this case is expressed as

$$\underset{K_s(N-1)\times K_s(N-1)}{\widehat{\mathbf{R}}'} = \vec{\boldsymbol{a}}' s_0 \vec{\boldsymbol{a}}'^H + \overline{\boldsymbol{\mathcal{A}}}' \tilde{\mathbf{S}} \overline{\boldsymbol{\mathcal{A}}}'^H + \vec{\boldsymbol{a}}' \hat{\mathbf{s}}^H \overline{\boldsymbol{\mathcal{A}}}'^H + \overline{\boldsymbol{\mathcal{A}}}' \hat{\mathbf{s}} \vec{\boldsymbol{a}}'^H + \hat{\sigma}^2 \mathbf{I} \tag{4.21}$$

where $\vec{\boldsymbol{a}}'$ and $\overline{\boldsymbol{\mathcal{A}}}'$ are defined as

$$\overline{\boldsymbol{\mathcal{A}}}' = \begin{bmatrix} \overline{\mathbf{A}}' \\ \overline{\mathbf{A}}' \overline{\mathbf{D}} \\ \vdots \\ \overline{\mathbf{A}}' \overline{\mathbf{D}}^{K_s-1} \end{bmatrix} \qquad \vec{\boldsymbol{a}}' = \begin{bmatrix} \mathbf{a}_0' \\ \mathbf{a}_0' d_0 \\ \vdots \\ \mathbf{a}_0' d_0^{K_s-1} \end{bmatrix} \tag{4.22}$$

in which $\mathbf{a}_0'$ and $\overline{\mathbf{A}}'$ are formed by omitting the last element of $\mathbf{a}_0$ and the last row of $\overline{\mathbf{A}}$, respectively. Considering a uniform linear array configuration, it can be concluded that (Citron & Kailath 1984, Haimovich & Bar-Ness 1991)

$$\mathcal{F}\mathcal{G}\overline{\boldsymbol{\mathcal{A}}} = \mathcal{G}' \overline{\boldsymbol{\mathcal{A}}}' \boldsymbol{\Omega} \tag{4.23}$$

where $\boldsymbol{\Omega}$ is a diagonal matrix which depends on signal directions and $\mathcal{G}'$ is a $K_s \times K_s$ block diagonal matrix as

$$\mathcal{G}' = \begin{bmatrix} \underset{N-1\times N-1}{\mathbf{G}'} & \cdots & \underset{N-1\times N-1}{\mathbf{0}} \\ \vdots & \ddots & \mathbf{0} \\ \mathbf{0} & \cdots & \mathbf{G}' \end{bmatrix} \tag{4.24}$$

where $\mathbf{G}'$ is a diagonal matrix in which $diag\left(\mathbf{G}'\right) = \left(\mathbf{a}_0'\right)^*$. Hence from (4.20), $span(\mathcal{G}' \overline{\boldsymbol{\mathcal{A}}}' \boldsymbol{\Omega}) \perp span(\mathbf{U}_n)$ holds. Since $\boldsymbol{\Omega}$ is a full rank matrix, $span(\mathcal{G}' \overline{\boldsymbol{\mathcal{A}}}') \perp span(\mathbf{U}_n)$ holds as well. It is required that the optimal gain vector $\mathbf{w}$ for the array be a vector in

$span(\mathcal{G}^{'H}\mathbf{U}_n)$, which means that it should be orthogonal to the multipath steering matrix $\vec{\mathcal{A}}'$. Let $\boldsymbol{\beta}$ be an arbitrary vector with $\|\boldsymbol{\beta}\|=1$ such that

$$\mathbf{w}=\mathcal{G}^{'H}\mathbf{U}_n\boldsymbol{\beta}. \tag{4.25}$$

In order to maximize the SNR of the LOS signal and simultaneously suppressing the multipath components, the following optimization should be performed

$$\begin{aligned}&\max_{\|\mathbf{w}\|=1}\ \frac{\mathbf{w}^H\vec{\boldsymbol{a}}'s_0\vec{\boldsymbol{a}}'^H\mathbf{w}}{\mathbf{w}^H\hat{\sigma}^2\mathbf{I}\mathbf{w}}\\ =&\max_{\|\boldsymbol{\beta}\|=1}\ \frac{\boldsymbol{\beta}^H\mathbf{U}_n^H\mathcal{G}'\vec{\boldsymbol{a}}'s_0\vec{\boldsymbol{a}}'^H\mathcal{G}'^H\mathbf{U}_n\boldsymbol{\beta}}{\boldsymbol{\beta}^H\mathbf{U}_n^H\mathcal{G}'\hat{\sigma}^2\mathbf{I}\mathcal{G}'^H\mathbf{U}_n\boldsymbol{\beta}}\\ =&\max_{\|\boldsymbol{\beta}\|=1}\ \frac{\boldsymbol{\beta}^H\mathbf{U}_n^H\mathcal{G}'\hat{\mathbf{R}}'\mathcal{G}'^H\mathbf{U}_n\boldsymbol{\beta}}{\hat{\sigma}^2}.\end{aligned} \tag{4.26}$$

The maximization in (4.26) is an Eigen decomposition (ED) problem in which $\boldsymbol{\beta}$ is the eigenvector corresponding to the largest eigenvalue of $\mathbf{U}_n^H\mathcal{G}'\hat{\mathbf{R}}'\mathcal{G}'^H\mathbf{U}_n$. Therefore, the optimal gain vector $\mathbf{w}$ is obtained from (4.25). Considering (4.26), by applying this method, the degree of freedom is increased to

$$DoF=\left(N-1\right)K_s-1. \tag{4.27}$$

The summary of the proposed technique consists of the following steps:

1 Construct the correlation matrix $\hat{\mathbf{R}}$ from (4.10).

2 Compute $\hat{\mathbf{R}}_D$ by applying $\mathbf{H}_f$ to $\hat{\mathbf{R}}$ from (4.15).

3 Compute $\mathbf{U}_n$ by solving the GED problem of (4.19).

4 Construct $\hat{\mathbf{R}}'$ by removing the last row and column of $\hat{\mathbf{R}}$.

5 Obtain $\boldsymbol{\beta}$ by solving the ED problem of (4.26).

6 Obtain the optimal gain vector $\mathbf{w}$ from (4.25).

4.3 Simulation results

To verify the effectiveness of the proposed beamformer, a simulation test was performed. In this simulation, a GPS L1 C/A code with a chipping rate of 1.023 MHz and a sampling rate of 10 MHz was used. The coherent integration time (T_c) was 1 ms and it is assumed that the antenna array moves with a constant velocity of 30 km/h perpendicular to the array axis. Five multipath components impinging on the array from different directions were assumed. The signals characteristics are tabulated in Table 4-1.

Three different cases are considered, namely: A uniform linear antenna array with two elements and $K_s = 7$, three elements where $K_s = 6$ and four elements and $K_s = 5$. Considering (4.27), the degree of freedom for these cases becomes 6, 11 and 14, respectively. For each case, L_s is differently chosen such that (4.3) holds.

GNSS pseudorange measurements are obtained by tracking the correlation peak. Multipath signals distort the correlation peak and cause a bias in pseudorange measurements. In the absence of multipath and the filtering effect of the RF front-end, the correlation function should be an isosceles triangle due to the square pulse shape. In Figure 4-2, the normalized cross correlation functions for the three cases and a single antenna receiver are shown (herein, the dynamic effects on the receiver tracking loops are

not accounted for. The sensitivity to multipath can be reduced due to dynamics even for the single antenna case, e.g. Kelly & Braasch 1999, Kalyanaraman et al 2006). It is observed that the proposed method removes the multipath effects in all the cases and almost distortionless correlation peaks are obtained. Furthermore, it is observed that increasing the degree of freedom increases the SNR values and, therefore, a stronger correlation peak is attained. In Figure 4-3, normalized polar beam patterns versus azimuth and elevation angles are shown for the three cases. It can be observed that deep nulls are placed in the direction of the multipath components whereas the LOS component has a maximum gain.

Table 4-1: Signals characteristics used in simulations

	Received power (dBW)	Code delay (Chips)	Azimuth (degree)	Elevation (degree)
LOS	-160	0	180	60
Multipath 1	-160	0.1	60	45
Multipath 2	-160	0.2	15	15
Multipath 3	-160	0.2	300	45
Multipath 4	-160	0.3	105	30
Multipath 5	-160	0.3	195	15

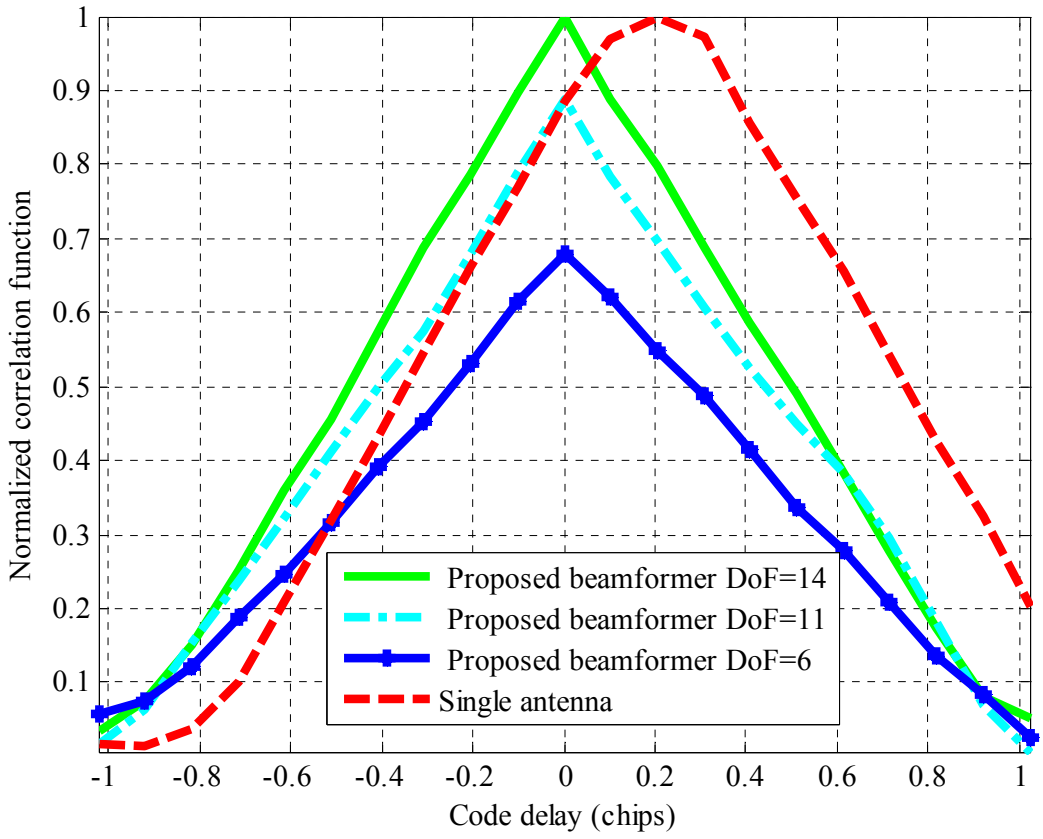

Figure 4-2: Comparison of correlation peaks for the proposed beamformer with a single antenna receiver

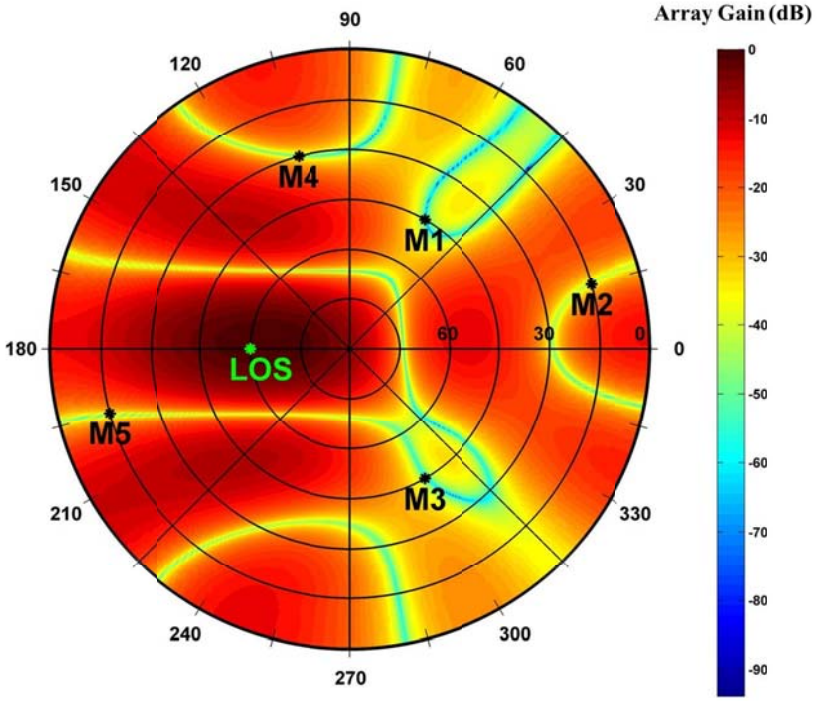
Array Gain (dB)
90
120
60
150
30
180
0
210
330
240
300
270
M4
M1
M2
LOS
M5
M3
60
30
0
0
-10
-20
-30
-40
-50
-60
-70
-80
-90

(a)

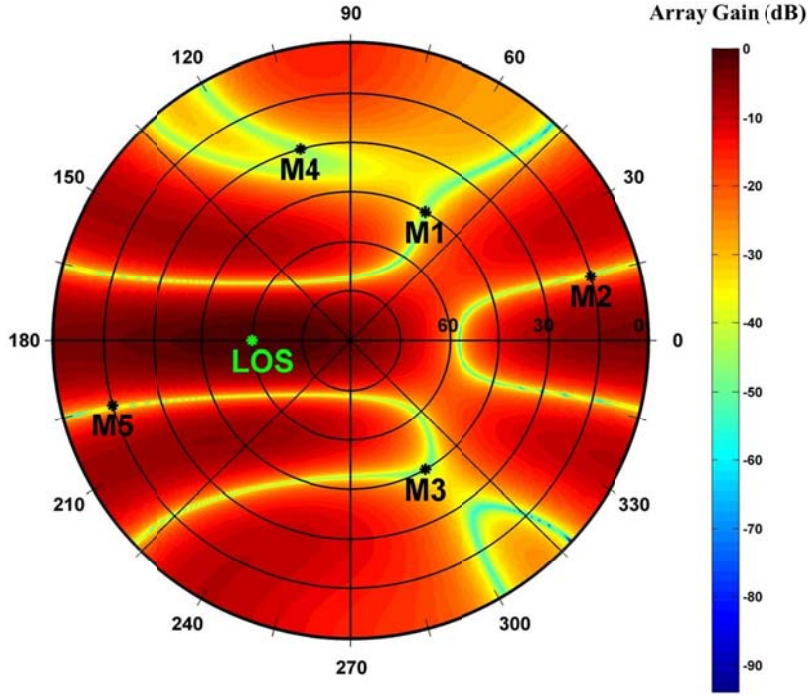
Array Gain (dB)
90
120
60
150
30
180
0
210
330
240
300
270
M4
M1
M2
LOS
M5
M3
60
30
0
0
-10
-20
-30
-40
-50
-60
-70
-80
-90

(b)

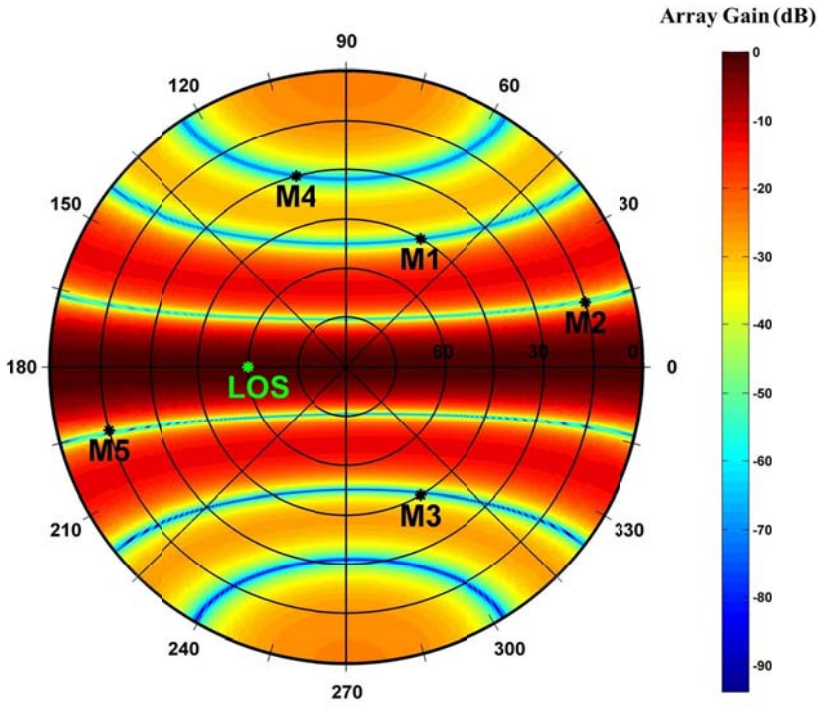

(c)

Figure 4-3: Beam pattern versus azimuth and elevation angles (M stands for Multipath signals) for a uniform linear antenna array with a) four elements and K_s=5 b) three elements and K_s=6 c) two elements and K_s=7.

In the last simulation, the effect of the array velocity for decorrelating multipath components was evaluated. A uniform linear antenna array with three elements was considered. Multipath components are the same as Table 4-1. Figure 4-4 plots the normalized correlation functions after applying the proposed method for the antenna array velocities of $\mathbf{v}_{vel}$, $\mathbf{v}_{vel}-\delta\mathbf{v}_{vel}$, $\mathbf{v}_{vel}-2\delta\mathbf{v}_{vel}$, $\mathbf{v}_{vel}-3\delta\mathbf{v}_{vel}$ and $\mathbf{v}_{vel}-4\delta\mathbf{v}_{vel}$ where $\mathbf{v}_{vel}=50\,\mathrm{km/h}$ and $\delta\mathbf{v}_{vel}=10\,\mathrm{km/h}$. In all cases, the array moves perpendicular to the array axis, $K_s=6$ and $L_s=10$. It can be observed that as the velocity decreases, the correlation function distortion increases such that for the last case the beamformer was

not able to mitigate the multipath components and the peak of the correlation function was shifted right from the true position. This is due to the relation between the velocity of the array and the decorrelation of multipath components, which is shown in (4.9). The array motion results in decorrelation of the temporal correlation matrix $E\left\{\widetilde{\mathbf{s}}\widetilde{\mathbf{s}}^H\right\}$. Otherwise, $E\left\{\widetilde{\mathbf{s}}\widetilde{\mathbf{s}}^H\right\}$ becomes rank deficient and the beamformer fails to mitigate multipath components.

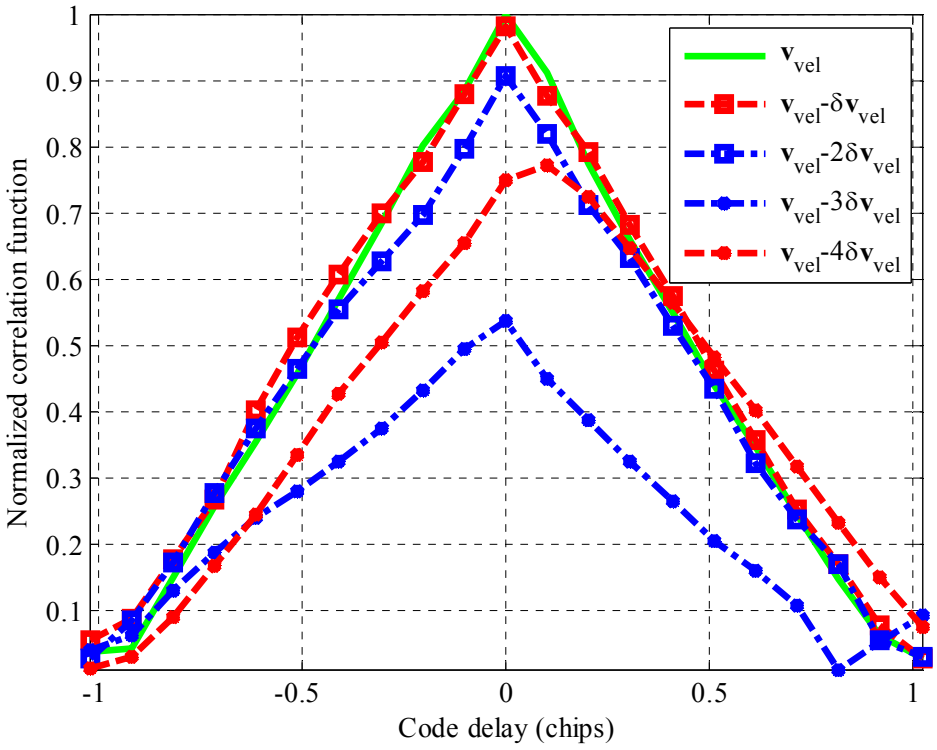

Figure 4-4: Comparison of correlation peaks for the proposed beamformer for different array velocities

4.4 Summary

By taking advantage of antenna array motion and spatial filtering, a multipath mitigation method in which the array degree of freedom is not limited to the number of the antenna elements, was successfully designed and tested. In addition, a spatial filter was applied to the synthesis array to estimate the multipath steering vectors and maximize the SNR of the LOS signal. Simulation results show the practicality of this method. The proposed method can be implemented to reduce multipath errors in vehicular navigation applications.

Chapter Five: SPACE-TIME INTERFERENCE MITIGATION EMPLOYING THE PERIODICITY OF GNSS SIGNALS

Space-time processing methods are widely studied in the literature as an effective approach for narrowband and wideband interference suppression. Recently the use of space-time filtering techniques in GNSS applications has gained significant attention due to their effectiveness in both narrowband and wideband interference suppression. Concurrently, the distortion and bias caused on the cross correlation function due to space-time filtering and countermeasure techniques have also been of significant interest especially for high precision GNSS applications. This chapter analyses the limitation of the previous work in terms of interference mitigation capability, induced bias and distortion in the cross correlation function, and then proposes a new approach which employs the inherent periodicity of GNSS signals in conjunction with the space-time processing to improve the performance of the existing space-time filters. Several simulations and a practical test are provided to analyze the applicability of the proposed method.

The rest of this chapter is organized as follows. In Section 5.1, an introduction on space-time processing in GNSS interference mitigation is provided and in Section 5.2 the problem formulation is introduced. Section 5.3 describes the proposed space-time filtering approach employing the periodicity of GNSS signals without distorting the cross correlation function. Simulation results and a real data test are presented in Section 5.4 and finally, Section 5.5 concludes the chapter.

5.1 Introduction

As mentioned before, despite the ever increasing demand for reliable positioning and timing services provided by GNSS for a variety of civilian and military applications, interfering signals still compromise positioning and navigation accuracy or completely disrupt signal quality and overall system performance such that conventional GNSS receivers may not be able to obtain the pseudorange and carrier phase measurements. The interference effects on GNSS receivers have been widely studied in the literature (e. g. Jang et al 2012, Motella et al 2011, Borio 2010).

In the last 10 years, several GNSS interference suppression methods in time, frequency and spatial domains (e. g. Hwang & Shynk 2006, Amin et al 2004, Madhani 2003, Badke & Spanias 2002, Zoltowski & Gecan 1995) or any combination of these processing domains have been proposed (e. g. Deergha & Swamy 2006, Kim & Iltis 2004). Among them, methods based on space-time (or space-frequency) processing are of great interest since in contrast to time/frequency based methods, they are able to deal with both wideband and narrowband interference. They also surpass only space-based methods by providing enhancement in interference mitigation methods. These techniques generally are referred to as space-time adaptive processing (STAP) methods (e. g. Kim & Iltis 2004, Fante & Vaccaro 2000). They are usually implemented by placing a tapped delay line (TDL) after each antenna element. A space-time filter assigns tap gains and combines all TDL outputs. The term “adaptive” means that the array follows the changes in environment and constantly adapts its own pattern by means of a feedback control. The

main focus of this chapter is on space-time processing techniques where studying on adaptive methods is out of the scope of this chapter. Nevertheless, the proposed method can be extended for the adaptive cases as well.

Besides superior advantages of space-time filtering, some considerations should be taken into account in designing such filters (e. g. O'Brien & Gupta 2011, Fante 2004). The output of the space-time filter is basically a direction-frequency dependent response. Even if the filter completely nullifies interfering signals, the non-linearity behavior of its frequency response results in bias error in measurements, distortion[1] or the broadness of the cross correlation function in GNSS receiver acquisition and tracking stages. This may not be tolerable especially for high precision GNSS applications. The effects of this distortion on GNSS signals were recently studied (De Lorenzo et al 2012, O'Brien & Gupta 2011, Fante 2004, Fante & Vaccaro 2000, Myrick et al 2001). To reduce this distortion, one approach is to employ special structures in the design of TDLs. In Fante & Vaccaro (2000), it is suggested that if TDLs are designed to have a real frequency response (formed from a filter multiplied by its conjugate), the bias can be suppressed although the cross correlation function is broadened. In Myrick et al (2001), by putting a distortionless constraint on the optimization problem for finding the filter tap gains, a distortionless filter was suggested. However, the signal-to-interference plus noise ratio (SINR) may be significantly degraded, as shown later in this chapter. Although in Myrick et al (2001) a suboptimum approach was also suggested which is more robust and has

[1] Herein, distortion is defined as a process that disfigures the shape of the cross correlation function. Either time or spatial processing may cause a distortion in the shape of the cross correlation function.

less computational complexity, this method is not able to avoid distortion completely. There are other effective approaches to reduce the induced bias error; however, they do not guarantee to have a distortionless response for GNSS signals (e. g. O'Brien & Gupta 2011, De Lorenzo et al 2012). During past years, these techniques have been implemented in practice and their performance has been evaluated in much literature (De Lorenzo et al 2007, 2005, McDonald, et al 2006, 2004, Falcone et al 2000, Hatke 1998).

As stated before, the direct sequence spread spectrum (DSSS) technique applied in the structure of the GNSS signals provides a certain degree of protection against narrowband interference (Pickholtz et al 1982). However, the spreading gain alone is not sufficient to prevent interference with much stronger power than the GNSS signal power. DSSS modulation utilizes periodic codes such as Gold and M-sequences known as pseudo random noise (PRN). In addition to provide a certain degree of protection against interference and multipath, this modulation is essential for measuring pseudoranges in any satellite positioning systems. The periodicity of GNSS signals was employed for interference mitigation in the spatial domain (Amin & Sun 2005) or maximum likelihood GNSS multipath mitigation (Sahmoudi & Amin 2008).

In this chapter, the inherent periodicity of GNSS signals is employed to design a distortionless space-time filter. The proposed filter reduces the induced bias and distortion due to space-time filtering to the insignificant level and also increases the space-time filter degree of freedom (DOF) without decreasing the SINR. Furthermore, analyses and simulations are performed to show that the modified linear constraint minimum power (LCMP) beamformer for the space-time processing subject to the

distortionless constraint may cause a complete failure in optimizing the solution and result in severe degradation in SINR in some operation scenarios. The main contribution of this chapter is to design and implement a new filter which employs the periodicity of GNSS signals in the structure of the space-time filter to avoid SINR degradation and satisfy the distortionless condition.

5.2 Problem formulation

Assume that I_N narrowband interfering signals, I_W wideband interfering signals including their multipath components and M GNSS signals impinge on an *N*-element antenna array. The signal vector received by the antenna array in the complex baseband representation is given by $\mathbf{r}(t)$ as

$$\underset{N\times 1}{\mathbf{r}}(t)=\sum_{m=1}^{M}\alpha_m g_m(t-\tau_m)\underset{N\times 1}{\mathbf{a}_m}e^{j2\pi\Delta f_m t}+\sum_{i=1}^{I_N}x_i(t)\underset{N\times 1}{\mathbf{b}_i}+\sum_{q=1}^{I_W}y_q(t)\underset{N\times 1}{\mathbf{c}_q}+\underset{N\times 1}{\boldsymbol{\eta}}(t) \tag{5.1}$$

where $\mathbf{a}_m$, $\mathbf{b}_i$ and $\mathbf{c}_q$ are steering vectors of the *m*th GNSS signal, *i*th narrowband interfering signal and *q*th wideband interfering signal, respectively. In (5.1), τ_m, α_m and Δf_m are code delay, attenuation factor and carrier frequency offset of the *m*th GNSS signal respectively, and $g_m(t)$ stands for the PRN code. $x_i(t)$ and $y_q(t)$ are the waveforms of the *i*th narrowband and *q*th wideband interfering signals and $\boldsymbol{\eta}(t)$ models the noise vector with covariance matrix $\sigma^2\mathbf{I}$. For the sake of simplicity, it is assumed

that the navigation data bits are removed in advance and hence in (5.1), the navigation data bits are omitted. The vector $\mathbf{r}(t)$ can be written in a more compact form as

$$\mathbf{r}(t) = \mathbf{A}\mathbf{s}(t) + \mathbf{B}\mathbf{x}(t) + \mathbf{C}\mathbf{y}(t) + \boldsymbol{\eta}(t) \tag{5.2}$$

where

$$\begin{aligned} \underset{N\times M}{\mathbf{A}} &\triangleq \begin{bmatrix} \mathbf{a}_1 & \cdots & \mathbf{a}_M \end{bmatrix} \\ \underset{N\times I_N}{\mathbf{B}} &\triangleq \begin{bmatrix} \mathbf{b}_1 & \cdots & \mathbf{b}_{I_N} \end{bmatrix} \\ \underset{N\times I_W}{\mathbf{C}} &\triangleq \begin{bmatrix} \mathbf{c}_1 & \cdots & \mathbf{c}_{I_W} \end{bmatrix} \end{aligned} \tag{5.3}$$

and

$$\begin{aligned} \underset{M\times 1}{\mathbf{s}}(t) &\triangleq \begin{bmatrix} \alpha_1 g(t-\tau_1) e^{j2\pi\Delta f_1 t} \\ \vdots \\ \alpha_M g(t-\tau_M) e^{j2\pi\Delta f_M t} \end{bmatrix} \\ \underset{I_N\times 1}{\mathbf{x}}(t) &\triangleq \begin{bmatrix} x_1(t) \\ \vdots \\ x_{I_N}(t) \end{bmatrix} \\ \underset{I_W\times 1}{\mathbf{y}}(t) &\triangleq \begin{bmatrix} y_1(t) \\ \vdots \\ y_{I_W}(t) \end{bmatrix} \end{aligned} \tag{5.4}$$

where $\mathbf{A}$, $\mathbf{B}$ and $\mathbf{C}$ are the steering matrices of the GNSS signals, narrowband and wideband interfering signals, and $\mathbf{s}(t)$, $\mathbf{x}(t)$ and $\mathbf{y}(t)$ represent the GNSS, narrowband and wideband interfering received waveform vectors, respectively. The problem of

interest is to design a space-time filter that suppresses undesired signals and does not disrupt GNSS signals. This filter can be interpreted in the frequency domain as

$$Z(f) = \boldsymbol{H}^T(f)\boldsymbol{R}(f) \tag{5.5}$$

where $\underset{N\times 1}{\boldsymbol{H}}(f)$ is the frequency response vector of filters applied to the down-converted signals received by the antenna array such that the *i*th element of this vector corresponds to the frequency response of the filter of the *i*th branch. In (5.5), $Z(f)$ and $\boldsymbol{R}(f)$ are frequency responses of the filter output $z(t)$ and received signal vector $\mathbf{r}(t)$, respectively. The filter weighting vector $\boldsymbol{H}(f)$ should be designed so as to filter out the interfering signal and keep the GNSS ones undistorted. In doing so, two approaches can be considered.

In the first approach, it is assumed that the steering vectors of GNSS signals are known and $\boldsymbol{H}(f)$ is separately designed for each GNSS signal to suppress interfering signals and to have a distortionless response for that particular GNSS signal. Therefore, for the *m*th GNSS signal, if $\boldsymbol{H}_m(f)$ is applied to the received signal vector, then

$$\begin{aligned} Z(f) &= \boldsymbol{H}_m^T(f)\boldsymbol{R}(f) \\ &= \boldsymbol{H}_m^T(f)\mathbf{A}\boldsymbol{S}(f) + \underbrace{\boldsymbol{H}_m^T(f)\mathbf{B}\boldsymbol{X}(f) + \boldsymbol{H}_m^T(f)\mathbf{C}\boldsymbol{Y}(f)}_{\simeq 0} + \boldsymbol{H}_m^T(f)\boldsymbol{\eta}(f) \end{aligned} \tag{5.6}$$

where

$$\begin{aligned} \boldsymbol{S}(f) &= F\{\mathbf{s}(t)\} \\ \boldsymbol{X}(f) &= F\{\mathbf{x}(t)\} \\ \boldsymbol{Y}(f) &= F\{\mathbf{y}(t)\} \\ \boldsymbol{\eta}(f) &= F\{\boldsymbol{\eta}(t)\}. \end{aligned} \tag{5.7}$$

In (5.6), $\boldsymbol{H}_m^T(f)\mathbf{A}\boldsymbol{S}(f)$ should not cause any distortion for the *m*th GNSS signal.

In the second approach, a space-time filter is obtained for all GNSS signals in order to suppress interfering signals without causing any bias and distortion. This approach increases the DOF of the space-time filter and does not employ the GNSS signal steering vectors. This method has less practical complexity compared to the previous method; however, unintentional nulls cannot be avoided and the overall SINR is decreased. Both approaches have been considered in the following section, which utilizes the inherent periodicity of GNSS signals for space-time filtering.

5.3 Proposed distortionless space-time filter

In this section, it is shown that utilizing the periodicity of GNSS signals can be employed in conjunction with temporal-spatial processing without distorting the cross correlation function.

5.3.1 Known steering vectors

Without loss of generality, only the gain vector for the *m*th GNSS signal is obtained in this section. One can apply the same method to the other GNSS signals. Assume that the steering vector of the *m*th GNSS signal is known and the carrier frequency offset and data

bits are removed. For the *m*th GNSS signal, the frequency response function of the array is denoted by $\Upsilon(f,\boldsymbol{a}_m)$ and is expressed as

$$\Upsilon(f,\boldsymbol{a}_m)=\boldsymbol{H}^T(f)\boldsymbol{a}_m \tag{5.8}$$

where $\mathbf{a}_m$ is the array manifold vector of the *m*th GNSS signal. If the power spectrum of the GNSS signal after despreading is defined as $S_m(f)$, the cross correlation function is obtained as (Fante & Vaccaro 2000)

$$R(\tau,\mathbf{a}_m)=\int_{-\infty}^{\infty}\Upsilon(f,\mathbf{a}_m)S_m(f)e^{-j2\pi f\tau}df. \tag{5.9}$$

Assume that the GNSS signal is modulated by a periodic spreading code, in which case $S_m(f)$ can be expressed as

$$S_m(f)=\sum_{n=-\infty}^{\infty}S_m^{'}(f)e^{j2\pi fnT_e} \tag{5.10}$$

where $S_m^{'}(f)$ is the power spectrum of one period (T_e) of the GNSS signal. By substituting (5.10) into (5.9), the cross correlation function for the *m*th signal is

$$R(\tau,\boldsymbol{a}_m)=\int_{-\infty}^{\infty}\boldsymbol{H}_m^T(f)\boldsymbol{a}_m\left(\sum_{n=-\infty}^{\infty}S_m^{'}(f)e^{j2\pi fnT_e}\right)e^{-j2\pi f\tau}df. \tag{5.11}$$

It can be readily verified that for a distortionless response for the *m*th GNSS incident signal, the following relation should hold:

$$\boldsymbol{H}_m^T(f)\boldsymbol{a}_m = \sum_{i=0}^{L_p-1} e^{-j2\pi fiT_e} \tag{5.12}$$

where L_p is a design parameter (number of the period employed in designing the filter). Eq (5.12) means that the frequency response of the array in the direction of the *m*th signal should be formed only from the certain exponential terms. One implementation to satisfy (5.12) can be realized by designing $\boldsymbol{H}_m^T(f)\boldsymbol{a}_m$ in the time domain as

$$F^{-1}\left\{\boldsymbol{H}_m^T(f)\boldsymbol{a}_m\right\} = \sum_{i=0}^{L_p-1} \delta(t - iT_e) \tag{5.13}$$

Implementing this filter by TDLs is straightforward. The structure shown in Figure 5-1 is one possible implementation to have a distortionless filter that takes advantage of the periodicity of GNSS signals.

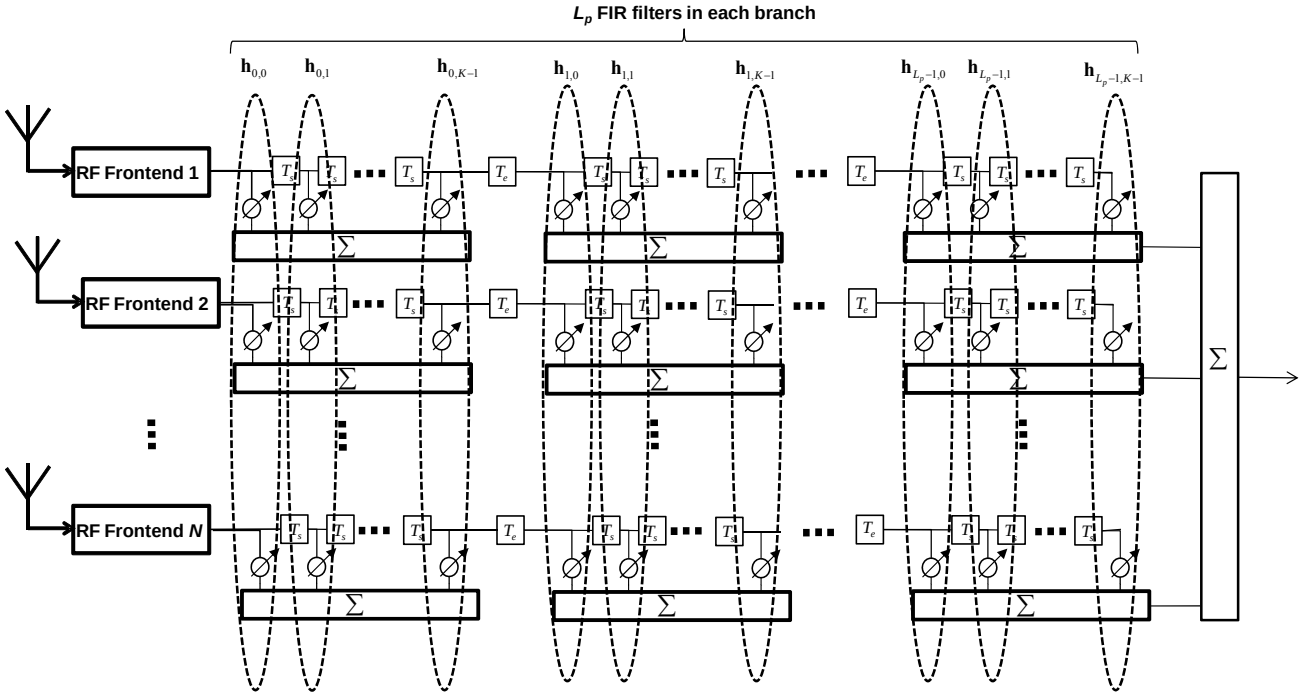

Figure 5-1: FIR implementation of the proposed space-time filter

This structure includes N banks of TDLs, each one consisting of L_p consecutive K-tapped delay lines where the delay between the neighboring TDLs is selected equal to T_e and the delay between each tap is equal to the sampling duration denoted by T_s. In order to satisfy the relation in (5.13), the following constraints on filter coefficients are required:

$$\begin{aligned} &\mathbf{h}_{l,k}^T \mathbf{a}_m = 1, \quad k = 0,\ l = 0,1,...,L_p - 1 \\ &\mathbf{h}_{l,k}^T \mathbf{a}_m = 0, \quad k = 1,2,...,K-1,\ l = 0,1,...,L_p - 1 \end{aligned} \tag{5.14}$$

where tap gains $\mathbf{h}_{l,k}, \quad k = 0,1,...,K-1,\ l = 0,1,...,L_p - 1$ are shown in the figure. The next step is to find these filter coefficients to suppress interfering signals whereas (5.14) holds.

To this end, assume that there are $P = \frac{T_e}{T_s}$ samples in each period of the despreading code where P is an integer number. Therefore, considering (5.2), the sampled signal vector received by the antenna array can be expressed as

$$\mathbf{r}(nT_s) = \mathbf{A}\mathbf{s}(nT_s) + \mathbf{B}\mathbf{x}(nT_s) + \mathbf{C}\mathbf{y}(nT_s) + \boldsymbol{\eta}(nT_s). \tag{5.15}$$

For simplicity, T_s is omitted and $\mathbf{r}(nT_s)$ is written as

$$\mathbf{r}_n = \mathbf{A}\mathbf{s}_n + \mathbf{B}\mathbf{x}_n + \mathbf{C}\mathbf{y}_n + \boldsymbol{\eta}_n. \tag{5.16}$$

Assume that vector $\vec{\mathbf{r}}_n$ is formed from $L_p N$ space-time digitized samples as

$$\underset{L_p N \times 1}{\vec{\mathbf{r}}_n} = \begin{bmatrix} \mathbf{r}_n^T & \mathbf{r}_{n+P}^T & \cdots & \mathbf{r}_{n+(L_p-1)P}^T \end{bmatrix}^T. \tag{5.17}$$

Then assume that a $L_p NK \times 1$ vector of space-time samples is formed by concatenating K consecutive $\vec{\mathbf{r}}_n$ as

$$\vec{r}_n = \begin{bmatrix} \vec{\mathbf{r}}_n^T & \vec{\mathbf{r}}_{n+1}^T & \cdots & \vec{\mathbf{r}}_{n+K-1}^T \end{bmatrix}^T. \tag{5.18}$$

In the same order, filter tap gains are defined as a $L_p NK \times 1$ vector as

$$\vec{h}_n = \begin{bmatrix} \mathbf{h}_{0,0}^T & \mathbf{h}_{1,0}^T & \cdots & \mathbf{h}_{L_p-1,0}^T & \mathbf{h}_{0,1}^T & \mathbf{h}_{1,1}^T & \cdots & \mathbf{h}_{L_p-1,1}^T & \cdots & \mathbf{h}_{0,K-1}^T & \mathbf{h}_{1,K-1}^T & \cdots & \mathbf{h}_{L_p-1,K-1}^T \end{bmatrix}^T \tag{5.19}$$

Therefore, the output of the filter at the nth time instant becomes

$$z_n = \vec{h}_n^T \vec{r}_n. \tag{5.20}$$

Hence, the power of the output signal is obtained as

$$E\left\{|z_n|^2\right\} = E\left\{\left|\vec{h}_n^T \vec{r}_n\right|^2\right\} = \vec{h}_n^H \mathbf{R}_{\vec{r}} \vec{h}_n \tag{5.21}$$

where $\mathbf{R}_{\vec{r}}$ is the time-space correlation matrix defined as

$$\mathbf{R}_{\vec{r}} = E\left\{\vec{r}_n \vec{r}_n^H\right\} \tag{5.22}$$

In order to satisfy the relation in (5.14) and suppressing interference, the following constrained optimization can be performed which is the linear constraint minimum power (LCMP) optimization problem (Van Trees 2002) (for the sake of simplicity, the time index *n* is omitted):

$$\begin{aligned} \underset{\vec{h}}{Min}\ & \vec{h}^H \mathbf{R}_{\vec{r}}\, \vec{h} \\ & \mathbf{C}_{const.}^H\, \vec{h} = \mathbf{f} \end{aligned} \tag{5.23}$$

where

$$\underset{NL_pK \times K}{\mathbf{C}_{const.}} = \begin{bmatrix} \underset{NL_p \times 1}{\mathbf{d}} & \mathbf{0} & \cdots & \mathbf{0} \\ \mathbf{0} & \underset{NL_p \times 1}{\mathbf{d}} & \ddots & \vdots \\ \vdots & \ddots & \ddots & \mathbf{0} \\ \mathbf{0} & \cdots & \mathbf{0} & \mathbf{d} \end{bmatrix}, \quad \underset{K \times 1}{\mathbf{f}} = \begin{bmatrix} 1 \\ 0 \\ \vdots \\ 0 \end{bmatrix} \tag{5.24}$$

and

$$\mathbf{d} = \underset{L_p}{\mathbf{1}} \otimes \mathbf{a}_m \tag{5.25}$$

The method of Lagrange multipliers can be used to solve this constrained optimization problem (see Appendix A). The optimal gain vector $\vec{\boldsymbol{h}}$ is obtained as

$$\vec{\boldsymbol{h}} = \mathbf{R}_{\vec{\mathbf{r}}}^{-1}\mathbf{C}_{const.}\left(\mathbf{C}_{const.}^{H}\mathbf{R}_{\vec{\mathbf{r}}}^{-1}\mathbf{C}_{const.}\right)^{-1}\mathbf{f}. \tag{5.26}$$

It can be proven that the obtained gain vector removes the interference terms and has a distortionless response in the direction of the GNSS signal. To this end, considering (5.16) and (5.17), $\vec{\mathbf{r}}_n$ can be written as

$$\vec{\mathbf{r}}_n = \overline{\mathbf{A}}\vec{\mathbf{s}}_n + \overline{\mathbf{B}}\vec{\mathbf{x}}_n + \overline{\mathbf{C}}\vec{\mathbf{y}}_n + \vec{\boldsymbol{\eta}}_n \tag{5.27}$$

where $\vec{\boldsymbol{\eta}}_n$ is the noise super vector, $\overline{\mathbf{A}}$, $\overline{\mathbf{B}}$ and $\overline{\mathbf{C}}$ are augmented steering matrices and, $\vec{\mathbf{s}}_n$, $\vec{\mathbf{x}}_n$ and $\vec{\mathbf{y}}_n$ are super vectors defined as

$$
\begin{aligned}
\underset{L_pN\times L_pM}{\overline{\mathbf{A}}} &\triangleq \begin{bmatrix} \underset{N\times M}{\mathbf{A}} & \mathbf{0} & \cdots & \mathbf{0} \\ \mathbf{0} & \mathbf{A} & \ddots & \mathbf{0} \\ \vdots & \ddots & \ddots & \vdots \\ \mathbf{0} & \mathbf{0} & \cdots & \mathbf{A} \end{bmatrix} \\
\underset{L_pN\times L_pI_N}{\overline{\mathbf{B}}} &\triangleq \begin{bmatrix} \underset{N\times I_N}{\mathbf{B}} & \mathbf{0} & \cdots & \mathbf{0} \\ \mathbf{0} & \mathbf{B} & \ddots & \mathbf{0} \\ \vdots & \ddots & \ddots & \vdots \\ \mathbf{0} & \mathbf{0} & \cdots & \mathbf{B} \end{bmatrix} \\
\underset{L_pN\times L_pI_W}{\overline{\mathbf{C}}} &\triangleq \begin{bmatrix} \underset{N\times I_W}{\mathbf{C}} & \mathbf{0} & \cdots & \mathbf{0} \\ \mathbf{0} & \mathbf{C} & \ddots & \mathbf{0} \\ \vdots & \ddots & \ddots & \vdots \\ \mathbf{0} & \mathbf{0} & \cdots & \mathbf{C} \end{bmatrix} \\
\vec{\mathbf{x}}_n &\triangleq \begin{bmatrix} \mathbf{x}_n^T & \mathbf{x}_{n+P}^T & \cdots & \mathbf{x}_{n+(L_p-1)P}^T \end{bmatrix}^T \\
\vec{\mathbf{y}}_n &\triangleq \begin{bmatrix} \mathbf{y}_n^T & \mathbf{y}_{n+P}^T & \cdots & \mathbf{y}_{n+(L_p-1)P}^T \end{bmatrix}^T \\
\vec{\mathbf{s}}_n &\triangleq \begin{bmatrix} \mathbf{s}_n^T & \mathbf{s}_{n+P}^T & \cdots & \mathbf{s}_{n+(L_p-1)P}^T \end{bmatrix}^T \\
\vec{\boldsymbol{\eta}}_n &\triangleq \begin{bmatrix} \boldsymbol{\eta}_n^T & \boldsymbol{\eta}_{n+P}^T & \cdots & \boldsymbol{\eta}_{n+(L_p-1)P}^T \end{bmatrix}^T
\end{aligned}
\tag{5.28}
$$

where $\mathbf{x}_n$, $\mathbf{y}_n$ and $\mathbf{s}_n$ are defined in (5.4). Consequently, $\vec{r}_n$ in (5.18) can be written as

$$\vec{r}_n = \mathcal{A}\vec{s}_n + \mathcal{B}\vec{x}_n + \mathcal{C}\vec{y}_n + \vec{\eta}_n \tag{5.29}$$

where

$$
\begin{aligned}
\underset{L_pNK\times L_pMK}{\mathcal{A}} &\triangleq \begin{bmatrix} \underset{NL_p\times ML_p}{\bar{\mathbf{A}}} & \mathbf{0} & \cdots & \mathbf{0} \\ \mathbf{0} & \bar{\mathbf{A}} & \ddots & \mathbf{0} \\ \vdots & \ddots & \ddots & \vdots \\ \mathbf{0} & \mathbf{0} & \cdots & \bar{\mathbf{A}} \end{bmatrix} \\
\underset{L_pNK\times KL_pI_N}{\mathcal{B}} &\triangleq \begin{bmatrix} \underset{NL_p\times L_pI_N}{\bar{\mathbf{B}}} & \mathbf{0} & \cdots & \mathbf{0} \\ \mathbf{0} & \bar{\mathbf{B}} & \ddots & \mathbf{0} \\ \vdots & \ddots & \ddots & \vdots \\ \mathbf{0} & \mathbf{0} & \cdots & \bar{\mathbf{B}} \end{bmatrix} \\
\underset{L_pNK\times KL_pI_W}{\mathcal{C}} &\triangleq \begin{bmatrix} \underset{NL_p\times L_pI_W}{\bar{\mathbf{C}}} & \mathbf{0} & \cdots & \mathbf{0} \\ \mathbf{0} & \bar{\mathbf{C}} & \ddots & \mathbf{0} \\ \vdots & \ddots & \ddots & \vdots \\ \mathbf{0} & \mathbf{0} & \cdots & \bar{\mathbf{C}} \end{bmatrix} \\
\vec{\mathcal{X}}_n &\triangleq \begin{bmatrix} \vec{\mathbf{x}}_n^T & \vec{\mathbf{x}}_{n+1}^T & \cdots & \vec{\mathbf{x}}_{n+(K-1)}^T \end{bmatrix}^T \\
\vec{\mathcal{Y}}_n &\triangleq \begin{bmatrix} \vec{\mathbf{y}}_n^T & \vec{\mathbf{y}}_{n+1}^T & \cdots & \vec{\mathbf{y}}_{n+(K-1)}^T \end{bmatrix}^T \\
\vec{\mathcal{S}}_n &\triangleq \begin{bmatrix} \vec{\mathbf{s}}_n^T & \vec{\mathbf{s}}_{n+1}^T & \cdots & \vec{\mathbf{s}}_{n+(K-1)}^T \end{bmatrix}^T \\
\vec{\boldsymbol{\eta}}_n &\triangleq \begin{bmatrix} \vec{\boldsymbol{\eta}}_n^T & \vec{\boldsymbol{\eta}}_{n+1}^T & \cdots & \vec{\boldsymbol{\eta}}_{n+(K-1)}^T \end{bmatrix}^T .
\end{aligned}
\tag{5.30}
$$

Assume that for the narrowband signals $x_i, i = 1,2,...,I_N$, such as CW tones, the following approximation holds:

$$
x_i(nT_s + PL_pT_s) \approx x_i(nT_s)e^{j2\pi\Delta f_i' PL_pT_s} \tag{5.31}
$$

where $\Delta f_i'$ is the carrier frequency offset of the *i*th narrowband interfering signal. Hence, $\mathcal{B}\vec{\mathcal{X}}_n$ in (5.29) can be approximately written as

$$\mathcal{B}\vec{\chi}_n = \begin{bmatrix} \begin{bmatrix} \mathbf{B} \\ \mathbf{B\Phi} \\ \vdots \\ \mathbf{B\Phi}^{L_p-1} \end{bmatrix} & \mathbf{0} & \cdots & \mathbf{0} \\ \mathbf{0} & \begin{bmatrix} \mathbf{B} \\ \mathbf{B\Phi} \\ \vdots \\ \mathbf{B\Phi}^{L_p-1} \end{bmatrix} & \ddots & \mathbf{0} \\ \vdots & \ddots & \ddots & \vdots \\ \mathbf{0} & \mathbf{0} & \cdots & \begin{bmatrix} \mathbf{B} \\ \mathbf{B\Phi} \\ \vdots \\ \mathbf{B\Phi}^{L_p-1} \end{bmatrix} \end{bmatrix} \begin{bmatrix} \mathbf{x}_n \\ \mathbf{x}_{n+1} \\ \vdots \\ \mathbf{x}_{n+K-1} \end{bmatrix} \tag{5.32}$$

and it can be further simplified to $\bar{\mathcal{B}}\mathbf{x}_n$ where $\bar{\mathcal{B}}$ is defined as

$$\bar{\mathcal{B}} \triangleq \begin{bmatrix} \begin{bmatrix} \mathbf{B} \\ \mathbf{B\Phi} \\ \vdots \\ \mathbf{B\Phi}^{L_p-1} \end{bmatrix} \\ \begin{bmatrix} \mathbf{B} \\ \mathbf{B\Phi} \\ \vdots \\ \mathbf{B\Phi}^{L_p-1} \end{bmatrix} \mathbf{\Theta} \\ \vdots \\ \begin{bmatrix} \mathbf{B} \\ \mathbf{B\Phi} \\ \vdots \\ \mathbf{B\Phi}^{L_p-1} \end{bmatrix} \mathbf{\Theta}^{K-1} \end{bmatrix} \tag{5.33}$$

in which the diagonal matrices $\mathbf{\Phi}$ and $\mathbf{\Theta}$ are defined as

$$\begin{aligned}\mathbf{\Phi} &\triangleq \begin{bmatrix} e^{j2\pi\Delta f_1^{'}PT_s} & 0 & \cdots & 0 \\ 0 & e^{j2\pi\Delta f_2^{'}PT_s} & & 0 \\ \vdots & & \ddots & \vdots \\ 0 & 0 & \cdots & e^{j2\pi\Delta f_{I_N}^{'}PT_s} \end{bmatrix} \\ \Theta &\triangleq \begin{bmatrix} e^{j2\pi\Delta f_1^{'}T_s} & 0 & \cdots & 0 \\ 0 & e^{j2\pi\Delta f_2^{'}T_s} & & 0 \\ \vdots & & \ddots & \vdots \\ 0 & 0 & \cdots & e^{j2\pi\Delta f_{I_N}^{'}T_s} \end{bmatrix}\end{aligned} \tag{5.34}$$

Therefore, considering $\vec{r}_n$ in (5.29), $\mathbf{R}_{\vec{r}}$ in (5.22) can be expressed as

$$\mathbf{R}_{\vec{r}} = \mathcal{A}E\left\{\vec{s}_n\vec{s}_n^H\right\}\mathcal{A}^H + \overline{\mathcal{B}}E\left\{\mathbf{x}_n\mathbf{x}_n^H\right\}\overline{\mathcal{B}}^H + \mathcal{C}E\left\{\vec{y}_n\vec{y}_n^H\right\}\mathcal{C}^H + \sigma^2\mathbf{I}. \tag{5.35}$$

Since the power of the GNSS signals is far below the noise floor, in the rest of the process their correlation matrix is included in the noise term and $\mathbf{R}_{\vec{r}}$ is expressed as

$$\mathbf{R}_{\vec{r}} = \overline{\mathcal{B}}E\left\{\mathbf{x}_n\mathbf{x}_n^H\right\}\overline{\mathcal{B}}^H + \mathcal{C}E\left\{\vec{y}_n\vec{y}_n^H\right\}\mathcal{C}^H + \sigma^2\mathbf{I}. \tag{5.36}$$

In the following part, it is shown that the gain vector obtained from (5.26) is approximately orthogonal to the interference subspace and also satisfies the constraint in (5.23), which guarantees the distortionless response for the GNSS signal. It is obvious that

$$\begin{aligned} &rk\left\{\overline{\mathcal{B}}E\left\{\mathbf{x}_n\mathbf{x}_n^H\right\}\overline{\mathcal{B}}^H\right\} \le I_N \\ &rk\left\{\mathcal{C}E\left\{\vec{y}_n\vec{y}_n^H\right\}\mathcal{C}^H\right\} \le KL_pI_W. \end{aligned} \tag{5.37}$$

In (5.37), the equalities hold if $\bar{\mathcal{B}}$ and $\mathcal{C}$ are full column rank matrices and $E\left\{\mathbf{x}_n\mathbf{x}_n^H\right\}$ and $E\left\{\vec{y}_n\vec{y}_n^H\right\}$ are full rank matrices. In addition, it can be readily verified that

$$r = rk\left\{\bar{\mathcal{B}}E\left\{\mathbf{x}_n\mathbf{x}_n^H\right\}\bar{\mathcal{B}}^H + \mathcal{C}E\left\{\vec{y}_n\vec{y}_n^H\right\}\mathcal{C}^H\right\} \le I_N + KL_pI_W. \tag{5.38}$$

The Eigen value decomposition (EVD) of $\mathbf{R}_{\vec{r}}$ can be expressed as

$$\mathbf{R}_{\vec{r}} = \begin{bmatrix}\mathbf{U}_I & \mathbf{U}_n\end{bmatrix}\begin{bmatrix}\underset{r\times r}{\mathbf{\Lambda}_I + \sigma^2\,\mathbf{I}} & \mathbf{0} \\ \mathbf{0} & \sigma^2\,\underset{KN-r\times KN-r}{\mathbf{I}}\end{bmatrix}\begin{bmatrix}\mathbf{U}_I^H \\ \mathbf{U}_n^H\end{bmatrix}, \tag{5.39}$$

where $\mathbf{\Lambda}_I$ and $\mathbf{U}_I$ are the eigenvalue and eigenvector matrices of the interference subspace and $\mathbf{U}_n$ is referred to as the eigenvector matrix of the noise subspace (including the GNSS signals). As a result of the eigenvectors orthogonality of symmetric matrices, one concludes that

$$\mathbf{U}_n^H\mathbf{U}_I = \mathbf{0}. \tag{5.40}$$

From (5.39), it is concluded that

$$\mathbf{R}_{\vec{r}} = \mathbf{U}_I\left(\underset{r\times r}{\mathbf{\Lambda}_I + \sigma^2\,\mathbf{I}}\right)\mathbf{U}_I^H + \sigma^2\mathbf{U}_n\mathbf{U}_n^H \tag{5.41}$$

and hence

$$\begin{aligned}\mathbf{R}_{\vec{r}}^{-1} &= \mathbf{U}_s \left(\underset{r\times r}{\mathbf{\Lambda}_I} + \sigma^2 \underset{r\times r}{\mathbf{I}} \right)^{-1} \mathbf{U}_I^H + \mathbf{U}_n \frac{1}{\sigma^2} \mathbf{U}_n^H \\ &\simeq \frac{1}{\sigma^2} \mathbf{U}_n \mathbf{U}_n^H \end{aligned} \tag{5.42}$$

The approximation in (5.42) comes from the fact that the power of the noise is significantly less than that of the interfering signals. By substituting (5.42) in (5.26),

$$\vec{\boldsymbol{h}} = \frac{1}{\sigma^2} \mathbf{U}_n \mathbf{U}_n^H \mathbf{C}_{const.} \left(\mathbf{C}_{const.}^H \frac{1}{\sigma^2} \mathbf{U}_n \mathbf{U}_n^H \mathbf{C}_{const.} \right)^{-1} \mathbf{f}. \tag{5.43}$$

Considering (5.43) and (5.40), it can be concluded that

$$\begin{aligned}\vec{\boldsymbol{h}}^H \mathbf{U}_I &= \mathbf{f}^H \mathbf{C}_{const.} \left(\mathbf{C}_{const.}^H \mathbf{U}_n \mathbf{U}_n^H \mathbf{C}_{const.} \right)^{-1} \mathbf{U}_n \mathbf{U}_n^H \mathbf{U}_I \\ &= \underset{KNL_p \times 1}{\mathbf{0}}^T \end{aligned} \tag{5.44}$$

In addition, from (5.41) and (5.36), it is obtained that

$$\mathbf{U}_I \mathbf{\Lambda}_I \mathbf{U}_I^H = \bar{\boldsymbol{\mathcal{B}}} E\left\{ \mathbf{x}_n \mathbf{x}_n^H \right\} \bar{\boldsymbol{\mathcal{B}}}^H + \boldsymbol{C} E\left\{ \vec{\boldsymbol{y}}_n \vec{\boldsymbol{y}}_n^H \right\} \boldsymbol{C}^H. \tag{5.45}$$

Since both terms of (5.45) are positive semi-definite and considering (5.44), the following relations are obtained:

$$\begin{aligned}\vec{\boldsymbol{h}}^H \bar{\boldsymbol{\mathcal{B}}} E\left\{ \mathbf{x}_n \mathbf{x}_n^H \right\} \bar{\boldsymbol{\mathcal{B}}}^H &= \mathbf{0}^T \\ \vec{\boldsymbol{h}}^H \boldsymbol{C} E\left\{ \vec{\boldsymbol{y}}_n \vec{\boldsymbol{y}}_n^H \right\} \boldsymbol{C}^H &= \mathbf{0}^T. \end{aligned} \tag{5.46}$$

If it is assumed that $E\left\{\mathbf{x}_n\mathbf{x}_n^H\right\}\bar{\mathcal{B}}^H$ and $E\left\{\vec{y}_n\vec{y}_n^H\right\}C^H$ are full row rank matrices, then $\bar{\mathcal{B}}E\left\{\mathbf{x}_n\mathbf{x}_n^H\right\}\bar{\mathcal{B}}^H$ and $\bar{\mathcal{B}}$ share the same KNL_p dimensional space and similarly $CE\left\{\vec{y}_n\vec{y}_n^H\right\}C^H$ and C. Thus

$$\begin{aligned}\vec{h}^H\bar{\mathcal{B}} &= \mathbf{0}^T \\ \vec{h}^H C &= \mathbf{0}^T.\end{aligned} \tag{5.47}$$

Therefore if the gain vector obtained in (5.26) is applied to the received signal vector in (5.27), it can be verified that the interference terms are discarded as

$$\begin{aligned}\vec{h}^H\vec{r}_n &= \vec{h}^H\mathcal{A}\vec{s}_n + \vec{h}^H\mathcal{B}\vec{x}_n + \vec{h}^H C\vec{y}_n + \vec{h}^H\vec{\eta}_n \\ &= \vec{h}^H\mathcal{A}\vec{s}_n + \underbrace{\vec{h}^H\bar{\mathcal{B}}\vec{\mathbf{x}}_n + \vec{h}^H C\vec{y}_n}_{\mathbf{0}^T} + \vec{h}^H\vec{\eta}_n \\ &= \vec{h}^H\mathcal{A}\vec{s}_n + \vec{h}^H\vec{\eta}_n.\end{aligned} \tag{5.48}$$

Even if $E\left\{\mathbf{x}_n\mathbf{x}_n^H\right\}\bar{\mathcal{B}}^H$ and $E\left\{\vec{y}_n\vec{y}_n^H\right\}C^H$ are not full row rank matrices (when the interfering signals are correlated), although (5.47) does not hold, interference still can be mitigated since the following relations hold:

$$\begin{aligned}\vec{h}^H\mathcal{B}\vec{x}_n &= 0 \\ \vec{h}^H C\vec{y}_n &= 0\end{aligned} \tag{5.49}$$

It is straightforward to show that this gain vector has a distortionless response for the GNSS signal. In order to show this, it is shown that the gain vector obtained in (5.26) satisfies the constraint in (5.23) as

$$\mathbf{C}_{const.}^{H}\vec{\boldsymbol{h}}=\mathbf{C}_{const.}^{H}\mathbf{R}_{\vec{r}}^{-1}\mathbf{C}\left(\mathbf{C}_{const.}^{H}\mathbf{R}_{\vec{r}}^{-1}\mathbf{C}_{const.}\right)^{-1}\mathbf{f}=\mathbf{f}. \tag{5.50}$$

In the rest of the analyses, it is shown that the filter fails to suppress the interfering signals if the following condition, which is implicitly assumed in the previous analyses, is not met:

$$\mathbf{C}_{const.}^{H}\bar{\mathbf{U}}_{n}\bar{\mathbf{U}}_{n}^{H}\mathbf{C}_{const.}\ \ is\ \ full\ \ rank. \tag{5.51}$$

To this end, (5.41) without approximation is substituted in (5.26) as

$$\begin{aligned}\vec{\boldsymbol{h}}=&\left(\mathbf{U}_{I}\left(\underset{r\times r}{\boldsymbol{\Lambda}_{I}}+\sigma^{2}\underset{r\times r}{\mathbf{I}}\right)^{-1}\mathbf{U}_{I}^{H}+\mathbf{U}_{n}\frac{1}{\sigma^{2}}\mathbf{U}_{n}^{H}\right)\mathbf{C}_{const.}\\&\left(\mathbf{C}_{const.}^{H}\mathbf{U}_{I}\left(\underset{r\times r}{\boldsymbol{\Lambda}_{I}}+\sigma^{2}\underset{r\times r}{\mathbf{I}}\right)^{-1}\mathbf{U}_{I}^{H}\mathbf{C}_{const.}+\mathbf{C}_{const.}^{H}\mathbf{U}_{n}\frac{1}{\sigma^{2}}\mathbf{U}_{n}^{H}\mathbf{C}_{const.}\right)^{-1}\mathbf{f}.\end{aligned} \tag{5.52}$$

Assuming that $\mathbf{C}_{const.}^{H}\mathbf{U}_{n}\frac{1}{\sigma^{2}}\mathbf{U}_{n}^{H}\mathbf{C}_{const.}$ is not a full rank matrix and considering the fact that $\sigma^{2}\mathbf{I}\ll\boldsymbol{\Lambda}_{I}$, the following eigenvalue decomposition can be performed:

$$\begin{aligned}&\mathbf{C}_{const.}^{H}\mathbf{U}_{I}\left(\underset{r\times r}{\boldsymbol{\Lambda}_{I}}+\sigma^{2}\underset{r\times r}{\mathbf{I}}\right)^{-1}\mathbf{U}_{I}^{H}\mathbf{C}_{const.}+\mathbf{C}_{const.}^{H}\mathbf{U}_{n}\frac{1}{\sigma^{2}}\mathbf{U}_{n}^{H}\mathbf{C}_{const.}\\&=\mathbf{V}_{s}\boldsymbol{\Lambda}_{s}\mathbf{V}_{s}^{H}+\mathbf{V}_{n}\Pi_{n}\mathbf{V}_{n}^{H},\end{aligned} \tag{5.53}$$

where $\mathbf{U}_{s}$ and $\mathbf{V}_{n}$ are the eigenvector matrices of the signal and noise (null) subspaces and the $\boldsymbol{\Lambda}_{s}$ and Π_{n} are the corresponding eigenvalue matrices. It can be verified that the following approximation holds:

$$\mathbf{C}_{const.}^{H}\mathbf{U}_n\frac{1}{\sigma^2}\mathbf{U}_n^{H}\mathbf{C}_{const.}\mathbf{V}_n \approx \mathbf{0}. \tag{5.54}$$

Eq (5.52) can be simplified to

$$\begin{aligned}\vec{\boldsymbol{h}} &\approx \left(\mathbf{U}_I\left(\underset{r\times r}{\boldsymbol{\Lambda}_I}+\sigma^2\underset{r\times r}{\mathbf{I}}\right)^{-1}\mathbf{U}_I^{H}+\mathbf{U}_n\frac{1}{\sigma^2}\mathbf{U}_n^{H}\right)\mathbf{C}_{const.}\mathbf{V}_n\Pi_n^{-1}\mathbf{V}_n^{H}\mathbf{f}\\ &\approx \mathbf{U}_I\left(\underset{r\times r}{\boldsymbol{\Lambda}_I}+\sigma^2\underset{r\times r}{\mathbf{I}}\right)^{-1}\mathbf{U}_I^{H}\mathbf{C}_{const.}\mathbf{V}_n\Pi_n^{-1}\mathbf{V}_n^{H}\mathbf{f}.\end{aligned} \tag{5.55}$$

It can be readily verified that in this case the optimal gain vector is not orthogonal to the interference subspace and the filter fails to suppress interference.

In the case of the conventional distortionless space-time processing method where $L_p = 1$, the condition in (5.51) is not met in some interference scenarios. In such cases, although the distortionless condition is satisfied, the filter is not able to suppress interference, which causes significant degradation in the SINR. By employing the GNSS signal periodic feature, the chance of this failure is reduced. Employing the periodicity reduces the rank deficiency of $\mathbf{C}_{const.}^{H}\mathbf{U}_n\frac{1}{\sigma^2}\mathbf{U}_n^{H}\mathbf{C}_{const.}$ for a wider range of interference scenarios. This is supported with several Monte-Carlo simulations in Section 5.4. In order to satisfy the condition in (5.51), the necessary but not sufficient condition is that

$$NKL_p - r \geq K \tag{5.56}$$

Therefore, if the condition in (5.51) is met, the filter DOF is obtained as

$$DOF = KL_pN - K. \tag{5.57}$$

Considering (5.37), in order to suppress each narrowband interfering signal, one degree of freedom is consumed and for each wideband interfering signal KL_p degrees of freedom is consumed. Similar to the conventional space-time filtering methods, time processing contribution only increases the DOF for narrowband interference mitigation.

It is worth mentioning that although the obtained $\vec{h}$ causes the GNSS signal to pass through the filter undistorted, the SINR is not necessarily maximized. In fact, although for a spatial filter only, the distortionless and the maximum SINR beamformers are the same in essence (Van Trees 2002), it is important to notice that having a distortionless response and attaining the maximum SINR does not happen at the same time in a distortionless spatial-temporal filter (Myrick et al 2001). To highlight this fact, the filter gain for the GNSS signal direction is calculated in the following analysis. It can be shown that for a distortionless filter increasing the number of taps decrease the filter gain for the GNSS signal. It is due to the distortionless constraint that forces the filter to only pass the GNSS signal from certain taps.

In order to calculate the array gain in the direction of the GNSS signal, it is convenient to express $\vec{h}$ in terms of the projection and orthogonal projection to the constraint subspace as (Myrick et al 2001)

$$\vec{h} = \mathbf{C}_{const.}\vec{h}_{\parallel} + \mathbf{C}_{const.\perp}\vec{h}_{\perp} \tag{5.58}$$

where

$$\mathbf{C}_{const.}^{H}\mathbf{C}_{const.\perp} = \underset{K\times KNL_p-K}{\mathbf{0}}. \tag{5.59}$$

$\mathbf{C}_{const.\perp}$ can be obtained by singular value decomposition (SVD) of $\mathbf{C}_{const.}$ as

$$\mathbf{C}_{const.} = \begin{bmatrix} \underset{KNL_p\times K}{\mathbf{U}} & \underset{KNL_p\times\left(KNL_p-K\right)}{\mathbf{C}_{const.\perp}} \end{bmatrix} \begin{bmatrix} \underset{K\times K}{\mathbf{\Lambda}} & \underset{K\times\left(KNL_p-K\right)}{\mathbf{0}} \\ \underset{\left(KNL_p-K\right)\times K}{\mathbf{0}} & \underset{\left(KNL_p-K\right)\times\left(KNL_p-K\right)}{\mathbf{0}} \end{bmatrix} \mathbf{V}^H \tag{5.60}$$

where $\mathbf{C}_{const.\perp}$ is the singular vector matrix of the null space of $\mathbf{C}_{const.}$. It can be readily verified that

$$\begin{aligned} \mathbf{C}_{const.}^{H}\mathbf{C}_{const.} &= L_p \underset{K\times K}{\mathbf{I}} \\ \mathbf{C}_{const.\perp}^{H}\mathbf{C}_{const.\perp} &= \underset{\left(NL_pK-K\right)\times\left(NL_pK-K\right)}{\mathbf{I}}. \end{aligned} \tag{5.61}$$

Moreover, one can show

$$\begin{aligned} \vec{\boldsymbol{h}}_{\parallel} &= \frac{\mathbf{f}}{L_p} \\ \vec{\boldsymbol{h}}_{\perp} &= \mathbf{C}_{const.\perp}^{H}\mathbf{R}_{\vec{\boldsymbol{r}}}^{-1}\mathbf{C}_{const.}\left(\mathbf{C}_{const.}^{H}\mathbf{R}_{\vec{\boldsymbol{r}}}^{-1}\mathbf{C}_{const.}\right)^{-1}\mathbf{f}. \end{aligned} \tag{5.62}$$

The array gain (AG) for the *m*th GNSS signal is defined as

$$AG \triangleq \frac{\bar{\mathbf{d}}^H\vec{\boldsymbol{h}}}{\left\|\bar{\mathbf{d}}\right\|\left\|\vec{\boldsymbol{h}}\right\|} \tag{5.63}$$

where

$$\bar{\mathbf{d}} = \underset{L_p K}{\mathbf{1}} \otimes \mathbf{a}_m \tag{5.64}$$

By substituting (5.58), (5.62) and (5.65) in (5.63), one obtains

$$AG = \frac{\bar{\mathbf{d}}^H \vec{\boldsymbol{h}}}{\left\|\bar{\mathbf{d}}\right\| \left(\dfrac{\mathbf{f}^H \mathbf{f}}{L_p} + \mathbf{f}^H \left(\mathbf{C}_{const.}^H \mathbf{R}_{\bar{\boldsymbol{r}}}^{-1} \mathbf{D} \right)^{-1} \mathbf{C}_{const.}^H \mathbf{R}_{\bar{\boldsymbol{r}}}^{-1} \mathbf{C}_{const.\perp} \mathbf{C}_{const.\perp}^H \mathbf{R}_{\bar{\boldsymbol{r}}}^{-1} \mathbf{C}_{const.} \left(\mathbf{C}_{const.}^H \mathbf{R}_{\bar{\boldsymbol{r}}}^{-1} \mathbf{C}_{const.} \right)^{-1} \mathbf{f} \right)^{\frac{1}{2}}} \tag{5.65}$$

It can be readily verified that

$$\begin{aligned} &\left\|\bar{\mathbf{d}}\right\| = \sqrt{KL_p} \\ &\bar{\mathbf{d}}^H \vec{\boldsymbol{h}} = \bar{\mathbf{d}}^H \mathbf{C}_{const.} \vec{\boldsymbol{h}}_{\parallel} - \bar{\mathbf{d}}^H \mathbf{C}_{const.\perp} \vec{\boldsymbol{h}}_{\perp} = \bar{\mathbf{d}}^H \mathbf{C}_{const.} \vec{\boldsymbol{h}}_{\parallel} = \bar{\mathbf{d}}^H \mathbf{C}_{const.} \frac{\mathbf{f}}{L_p} = 1 \end{aligned} \tag{5.66}$$

Therefore, *AG* can be simplified as

$$AG = \frac{1}{\sqrt{K} \left(1 + L_p \mathbf{f}^H \mathbf{R}_{\bar{\boldsymbol{r}}}^{-1} \mathbf{C}_{const.\perp} \left[\mathbf{C}_{const.\perp}^H \mathbf{R}_{\bar{\boldsymbol{r}}}^{-1} \mathbf{C}_{const.\perp} \right]^{-1} \left[\mathbf{C}_{const.\perp}^H \mathbf{R}_{\bar{\boldsymbol{r}}}^{-1} \mathbf{C}_{const.\perp} \right]^{-1} \mathbf{C}_{const.\perp}^H \mathbf{R}_{\bar{\boldsymbol{r}}}^{-1} \mathbf{f} \right)^{\frac{1}{2}}} \tag{5.67}$$

It can be observed that *AG* is a function of K, L_p, constraint matrix and the space-time correlation matrix.

5.3.2 Unknown steering vector

Knowing the steering vector of GNSS signals require antenna array calibration and knowledge of the array configuration and orientation, which cannot be realized in some GNSS applications. In this case, designing a blind space-time filter is of interest. The proposed method can be extended for such a blind case. The optimal gain vector is obtained to suppress bias and distortion due to time filtering although the spatial processing may distort some GNSS signals by putting unintentional nulls in for these signals. It can be easily verified that in this case employing the periodicity of the GNSS signals is essential since K should be chosen to be 1 (employing distortionless constraints needs the knowledge of steering vectors). In other words, the structure of the filter in Figure 5-1 reduces to the N TDLs, each of which consists of L_p taps where the delay between the taps is T_e. In this case, the optimization problem becomes

$$\begin{aligned} \underset{\vec{h}}{Min}\ & \vec{h}^H \mathbf{R}_{\tilde{r}} \vec{h} \\ & \boldsymbol{\beta}^H \vec{h} = 1 \end{aligned} \tag{5.68}$$

where $\boldsymbol{\beta}$ is a $NL_p \times 1$ vector defied as

$$\underset{NL_p \times 1}{\boldsymbol{\beta}} = \begin{bmatrix} 1 \\ 0 \\ \vdots \\ 0 \end{bmatrix} \tag{5.69}$$

where vector $\boldsymbol{\beta}$ is employed to avoid the trivial solution $\vec{h} = \underset{NL_p \times 1}{\mathbf{0}}$. In fact, this approach can be considered as an extension of the method introduced in Zoltowski & Gecan (1995) to the case of employing the periodicity to increase the DOF of the space-time filter. By employing the method of Lagrange multipliers, the optimal gain vector $\vec{h}$ is obtained as

$$\vec{h} = \mathbf{R}_{\vec{r}}^{-1}\boldsymbol{\beta}\left(\boldsymbol{\beta}^H \mathbf{R}_{\vec{r}}^{-1}\boldsymbol{\beta}\right)^{-1}. \tag{5.70}$$

In order to improve performance, one can employ the subspace method to estimate the interference subspace and then by projecting the received signal into the interference-free subspace the SINR can be maximized after the despreading process (Daneshmand et al 2013b, Sun & Amin 2005b, Amin et al 2004). Therefore, the attenuation due to unintentional nulls can be considerably reduced.

5.4 Simulation results

In order to evaluate the performance of the proposed method, several simulation scenarios were performed. In all simulation scenarios, a three-element antenna array with the equatorial configuration was considered. A GPS L1 C/A code with a chipping rate of 1.023 MHz and a sampling rate of 20 MHz was employed. In the following sub-sections the performance of the proposed space-time filter is investigated and contrasted with conventional space-time filters.

A. Gain pattern of the proposed space-time filter

In the first simulation scenario, the effectiveness of the proposed method for narrowband and wideband interference mitigation is illustrated. In doing so, the gain pattern is shown after applying the proposed method. For a space-time filtering, the gain pattern (in dB) is calculated as

$$BP \triangleq 10\log\left(\left|\Upsilon\left(f,\hat{\mathbf{e}}\right)\right|^2\right) \tag{5.71}$$

where $\Upsilon\left(f,\hat{\mathbf{e}}\right)$ is a response of the filter to the impinging signal with the incident direction of $\hat{\mathbf{e}}$ and frequency *f* where it is defined in (5.8) and expanded as

$$\Upsilon\left(f,\hat{\mathbf{e}}\right) \triangleq \boldsymbol{H}^T\left(f\right)\begin{bmatrix} e^{-j2\pi f_c \frac{\hat{\mathbf{e}}^T\mathbf{d}_1^{ant}}{c}} \\ e^{-j2\pi f_c \frac{\hat{\mathbf{e}}^T\mathbf{d}_2^{ant}}{c}} \\ \vdots \\ e^{-j2\pi f_c \frac{\hat{\mathbf{e}}^T\mathbf{d}_N^{ant}}{c}} \end{bmatrix} \tag{5.72}$$

where

$$\hat{\mathbf{e}} \triangleq \begin{bmatrix} \cos\theta_{El}\cos\varphi_{Az} \\ \cos\theta_{El}\sin\varphi_{Az} \\ \sin\theta_{El} \end{bmatrix} \tag{5.73}$$

and $\mathbf{d}_i^{ant}, i = 1,2,..N$ are vectors pointing from the origin of the coordinate system to the antenna elements. In (5.73), θ_{El} and φ_{Az} are elevation and azimuth angles of the received signal, respectively. In fact, this gain pattern determines the space-time filter gain in

specific frequency, azimuth and elevation angles. For this simulation, seven narrowband and one wideband interfering signals were considered. Parameters L_p and K are both four. One GPS signal (with a known steering vector) received at azimuth 120º and elevation 60 º with a -158 dBW received power is assumed. For forming the space-time correlation matrix in (5.22), 1 ms digitized samples are considered (generally much less samples are needed for high power interfering signals). According to (5.57), the filter is able to mitigate all interfering signals and to have a distortionless response in the desired signal direction. It is assumed that the interfering signals are CW tones and the wideband interfering signal is white Gaussian noise with 10 MHz bandwidth centered at L1 carrier frequency. The characteristics of interfering signals are tabulated in Table 5-1.

Table 5-1: Signals characteristics used in the first simulation

	Received power (dBW)	Interference Type	Centre Frequency (Hz) L1=1575.42 MHz	Elevation (degree)	Azimuth (degree)
Interference 1	-100	NB	L1-525	45	180
Interference 2	-100	NB	L1-645	25	210
Interference 3	-100	NB	L1+825	37.5	270
Interference 4	-100	NB	L1+300	50	330
Interference 5	-100	NB	L1+50	60	285
Interference 6	-100	NB	L1+685	30	60
Interference 7	-100	NB	L1-405	20	90
Interference 8	-100	WB (10MHz)	L1-100	5	15

Figure 5-2 shows the gain patterns as a function of the azimuth and elevation angles for different frequencies corresponding to the carrier offset of the incident interfering signals with respect to the L1 carrier frequency as given in Table 5-1. As it can be observed, in the space-time processing, the different gain patterns are obtained for different frequencies. By applying the optimal gain vector obtained in (5.26), for each interfering signal a null has been steered toward its direction in a particular frequency. Therefore, the signals arriving from the same direction can be still distinguished in the frequency domain by a space-time process. For the wideband interfering signal, a null should be placed in its entire frequency band. This is shown in Figure 5-3 in which the gain patterns with respect to frequency and azimuth angle for different elevations are shown. At an elevation of 5^0 where the wideband interfering signal is received a null is steered toward that direction for all frequencies. It can be observed that the beamformer puts deep nulls in the direction of the interference signals (approximately 50 dB attenuation). These attenuations plus the attenuation due to the despreading process lead to the complete suppression of the interfering signals.

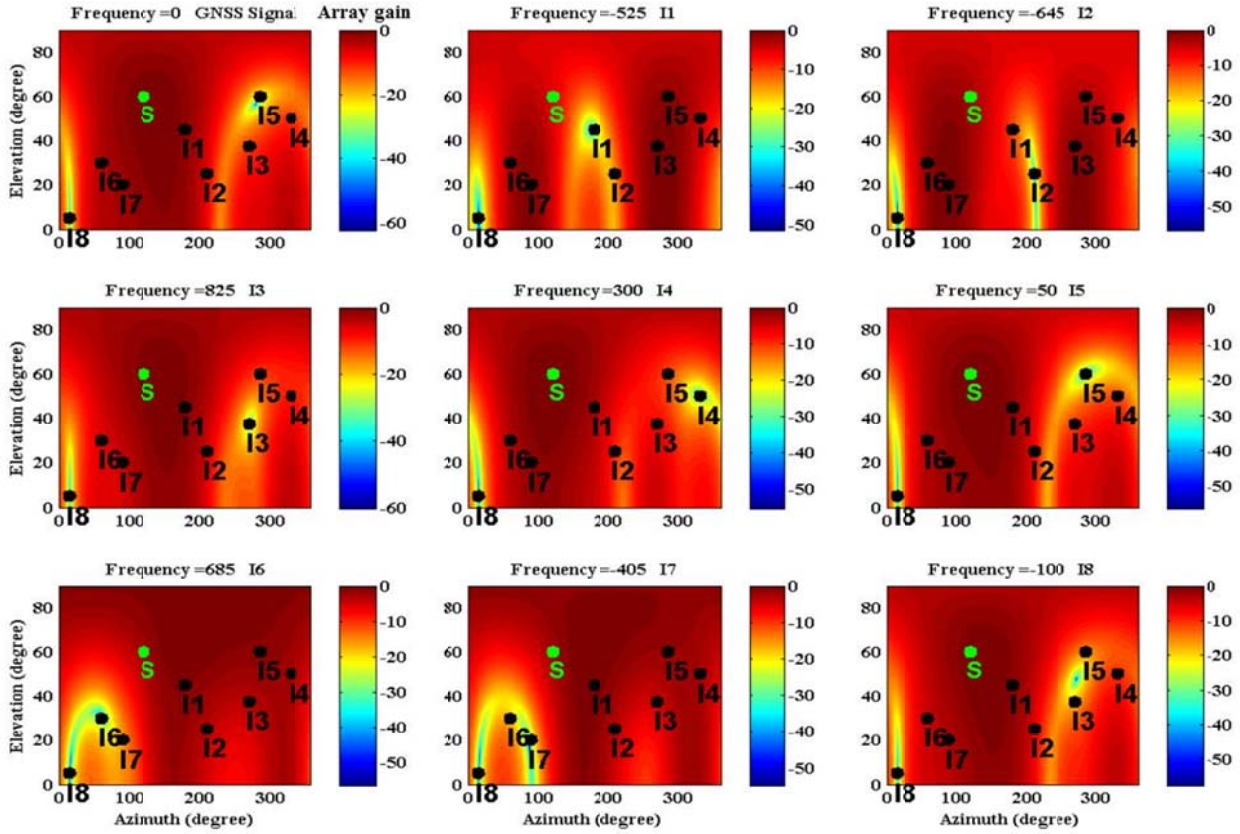

Figure 5-2: Gain patterns with respect to azimuth and elevation for different frequencies

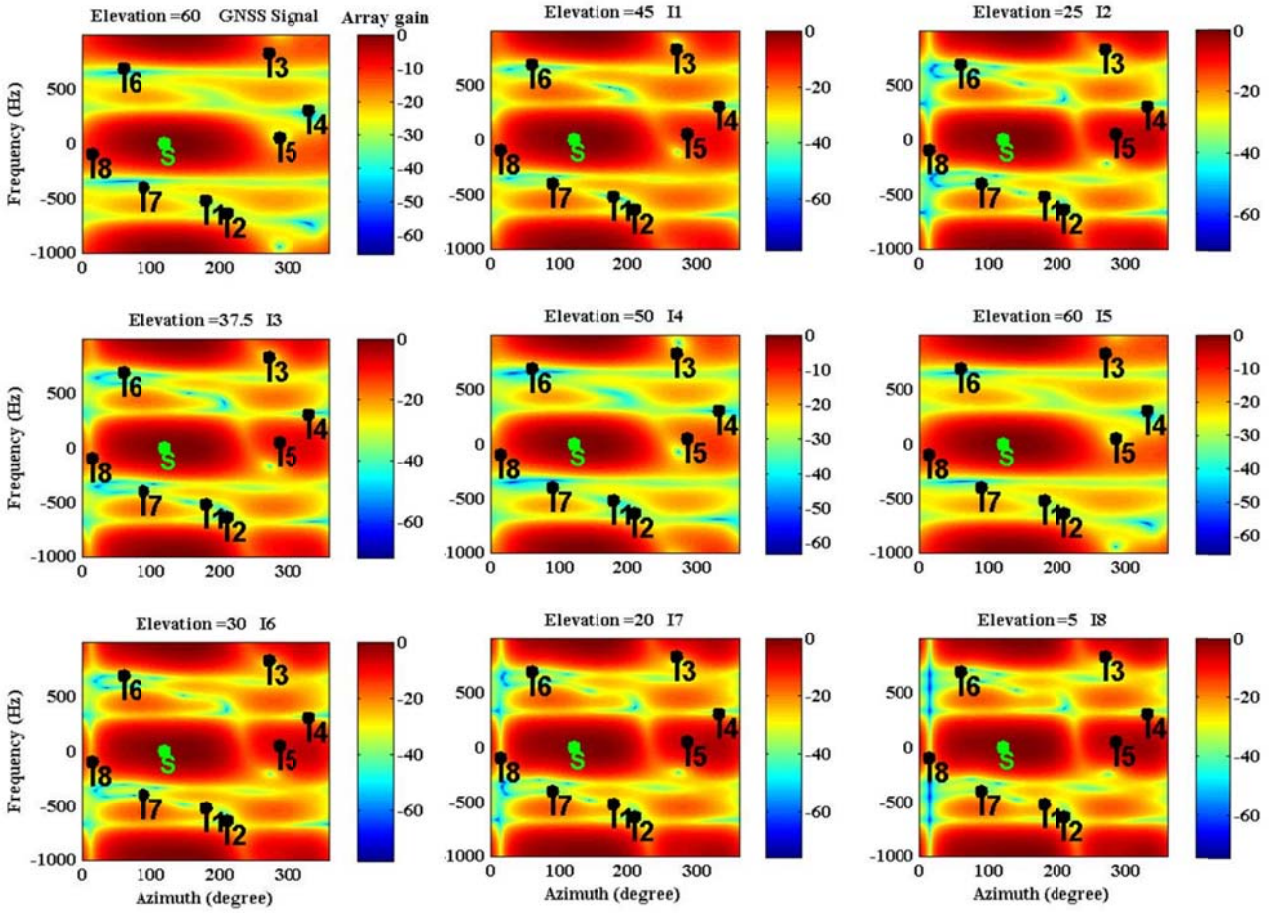

Figure 5-3: Gain patterns with respect to azimuth and frequency for different elevation angles

B. Comparison with conventional space-time filters

The second simulation scenario evaluates the performance of the proposed method and compares it with conventional space-time filters. In this scenario, eight narrowband sinusoidal interfering signals with different interference frequency span (IFS) have been considered. Herein, IFS is defined as a frequency bandwidth in which the interfering

signals are randomly distributed. Therefore, the lower the value of IFS, the higher the correlation between the interfering signals. For the following simulations, IFS varies from 20 Hz to 20 MHz corresponding to a highly correlated interference scenario to an uncorrelated interference scenario, respectively. Monte-Carlo simulations were performed for 1000 runs to calculate the interference-to-noise ratio (INR) and SINR versus IFS. The power of all interfering signals is the same and equal to -100 dBW and their incident direction are randomly chosen in a sector with elevation 0 to 45˚ for all azimuth angles. The interference carrier frequency is randomly distributed over a bandwidth equal to IFS centered on the L1 carrier frequency. In each run, the INR and SINR are calculated from the following formulas:

$$
\begin{aligned}
INR &= 10Log\frac{\vec{h}^H E\left\{\mathcal{B}\mathcal{B}^H\right\}\vec{h}}{N_0 B_W \vec{h}^H \vec{h}} \\
SINR &= 10Log\frac{\vec{h}^H E\left\{\mathcal{A}\mathcal{A}^H\right\}\vec{h}}{N_0 B_W \vec{h}^H \vec{h} + \vec{h}^H E\left\{\mathcal{B}\mathcal{B}^H\right\}\vec{h}}
\end{aligned}
\tag{5.74}
$$

where vectors and matrices are defined in (5.30). In (5.74), N_0 is the noise spectral density ratio with a typical value of -204 dBW/Hz and B_W is the frequency bandwidth of the receiver input filter. For a GPS signal with the received power of -158 dBW and B_W=20 MHz, the pre-correlation SNR is -27 dB.

For this simulation, four different space-time filtering methods were considered as follows:

a. Method 1: The first space-time filter was designed based on the power minimization technique (e. g. Church et al 2007, Lu et al 2006, McDonald et al 2004, Myrick et al 2000). This technique has been widely employed as a simple space-time filter since the knowledge of GNSS signal steering vectors is not required. However, this method induces some distortion in the cross correlation function. The optimization problem for this case can be expressed as

$$\begin{aligned} \underset{\vec{h}}{Min}\ & \vec{h}^H \mathbf{R}_{\tilde{r}} \vec{h} \\ & \mathbf{e}_1^H \vec{h} = 1 \end{aligned} \tag{5.75}$$

where

$$\underset{NK\times 1}{\mathbf{e}_1} = \begin{bmatrix} 1 \\ 0 \\ \vdots \\ 0 \end{bmatrix} \tag{5.76}$$

b. Method 2: Second space-time filter was designed based on a fully distortionless constraint (e. g. Konovaltsev et al 2008, Myrick et al 2001). The optimization problem is the same as (5.23) where $L_p = 1$ (periodicity is not employed).

c. Method 3: The third method's optimization problem is the same as Method 1, where only one column constraint is considered in the optimization problem. In this method it is assumed that the GNSS signal steering vectors are known (e. g. Church et al 2007, Myrick et al 2001). In this filter, only the first group of tap gains is required to pass the GNSS signal undistorted, which means $\mathbf{h}_{0,0}$ in Figure 5-1. Consequently, other taps may pass the signal through the filter and cause distortion on the cross correlation function. The optimization problem for this case is

$$\begin{aligned} \underset{\vec{h}}{Min}\ & \vec{h}^H \mathbf{R}_{\vec{r}} \vec{h} \\ & \mathbf{e}_2^H \vec{h} = 1 \end{aligned} \tag{5.77}$$

where

$$\underset{NK\times 1}{\mathbf{e}_2} = \begin{bmatrix} \mathbf{a}_m \\ \underset{N\times 1}{\mathbf{0}} \\ \vdots \\ \underset{N\times 1}{\mathbf{0}} \end{bmatrix} \tag{5.78}$$

d. Method 4: The last space-time filter employs the periodicity in the structure of the filter and uses the steering vector of the GNSS signals as proposed in this chapter

Table 5-2 summarizes the specification of different space-time filtering methods.

Table 5-2: Methods characteristics

	Constraint	K	L_p	DOF
Method 1	$\mathbf{e}_2^H \vec{\boldsymbol{h}} = 1,\ \underset{NK\times 1}{\mathbf{e}_1} = \begin{bmatrix} 1 \\ 0 \\ \vdots \\ 0 \end{bmatrix}$	6	0	$NK-1=17$
Method 2	$\mathbf{C}_{const.}^H \vec{\boldsymbol{w}} = \mathbf{f}$ $\underset{NK\times K}{\mathbf{C}_{const.}} = \begin{bmatrix} \underset{N\times 1}{\mathbf{a}_m} & \mathbf{0} & \cdots & \mathbf{0} \\ \mathbf{0} & \mathbf{a}_m & \ddots & \vdots \\ \vdots & \ddots & \ddots & \mathbf{0} \\ \mathbf{0} & \cdots & \mathbf{0} & \mathbf{a}_m \end{bmatrix}, \underset{K\times 1}{\mathbf{f}} = \begin{bmatrix} 1 \\ 0 \\ \vdots \\ 0 \end{bmatrix}$	6	0	$NK-K=12$
Method 3	$\mathbf{e}_2^H \vec{\boldsymbol{h}} = 1\ \underset{NK\times 1}{\mathbf{e}_2} = \begin{bmatrix} \mathbf{a}_m \\ \underset{N\times 1}{\mathbf{0}} \\ \vdots \\ \underset{N\times 1}{\mathbf{0}} \end{bmatrix}$ -	6	0	$NK-1=17$
Method 4	$\mathbf{C}_{const.}^H \vec{\boldsymbol{w}} = \mathbf{f}$ $\underset{NL_pK\times K}{\mathbf{C}_{const.}} = \begin{bmatrix} \underset{NL\times 1}{\mathbf{d}} & \mathbf{0} & \cdots & \mathbf{0} \\ \mathbf{0} & \mathbf{d} & \ddots & \vdots \\ \vdots & \ddots & \ddots & \mathbf{0} \\ \mathbf{0} & \cdots & \mathbf{0} & \mathbf{d} \end{bmatrix}, \underset{K\times 1}{\mathbf{f}} = \begin{bmatrix} 1 \\ 0 \\ \vdots \\ 0 \end{bmatrix}, \mathbf{d} = \underset{L_p}{\mathbf{1}} \otimes \mathbf{a}_m$	6	3	$NKL_p - K = 39$

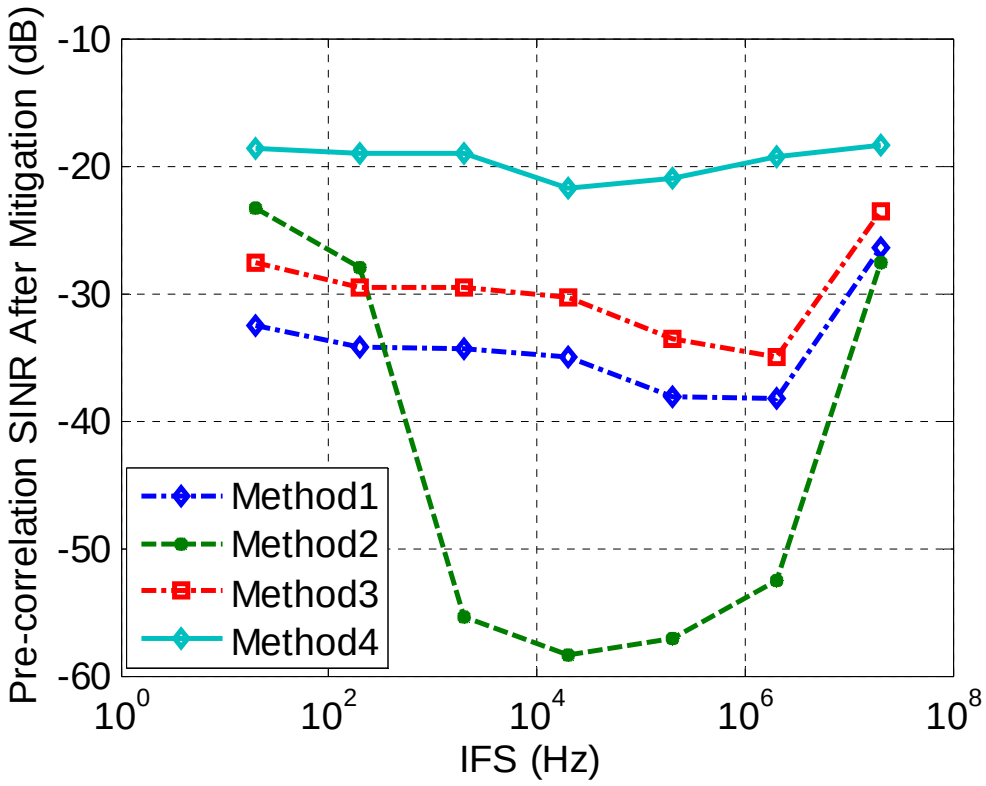

Figure 5-4: SINR versus IFS

Using Monte-Carlo simulations, pre-correlation SINR versus IFS values for different methods are plotted in Figure 5-4. The SINR values for Method 4 achieve almost 8 dB and 12 dB gain in comparison to Method 1 and 3, which is due to employing the periodicity and the GNSS signal steering vector. Method 2 has the worst performance. Although both Method 2 and Method 4 employ the fully distortionless constraint in the optimization problem, the condition in (5.51) is not met for Method 2 for a wide range of IFS values. This is due to rank deficiency happening in the optimization problem, which is explained in formulas (5.52) to (5.55). Therefore, Method 2 is not able to suppress interference for a wide range of IFS and the SINR is significantly decreased for this range.

Figure 5-5 graphically illustrates the relative amount of the GNSS signal amplitude passed through the filter versus IFS and delay (chips) for the four methods. Each point of the diagram stands for a particular IFS and delay and its value is calculated as $\mathbf{h}_{0,k}^{H}\mathbf{a}_{m}$. The delay is equal to kT_s where k varies from 0 to $K-1$ (for $K=6$ and $T_s=0.05\mu s$, the delay varies from 0 to approximately 0.25 chip in the diagram). For Method 4 in which the periodicity is employed, the value for each point is calculated as $\sum_{l=0}^{L_p-1}\mathbf{h}_{l,k}^{H}\mathbf{a}_{m}$. This illustration can be employed as a metric for the amount of distortion. However, it should be noted that this metric does not characterize the SINR performance and the injected interference into the system. In fact, this metric demonstrates the distortion on the cross correlation function under perfect interference suppression.

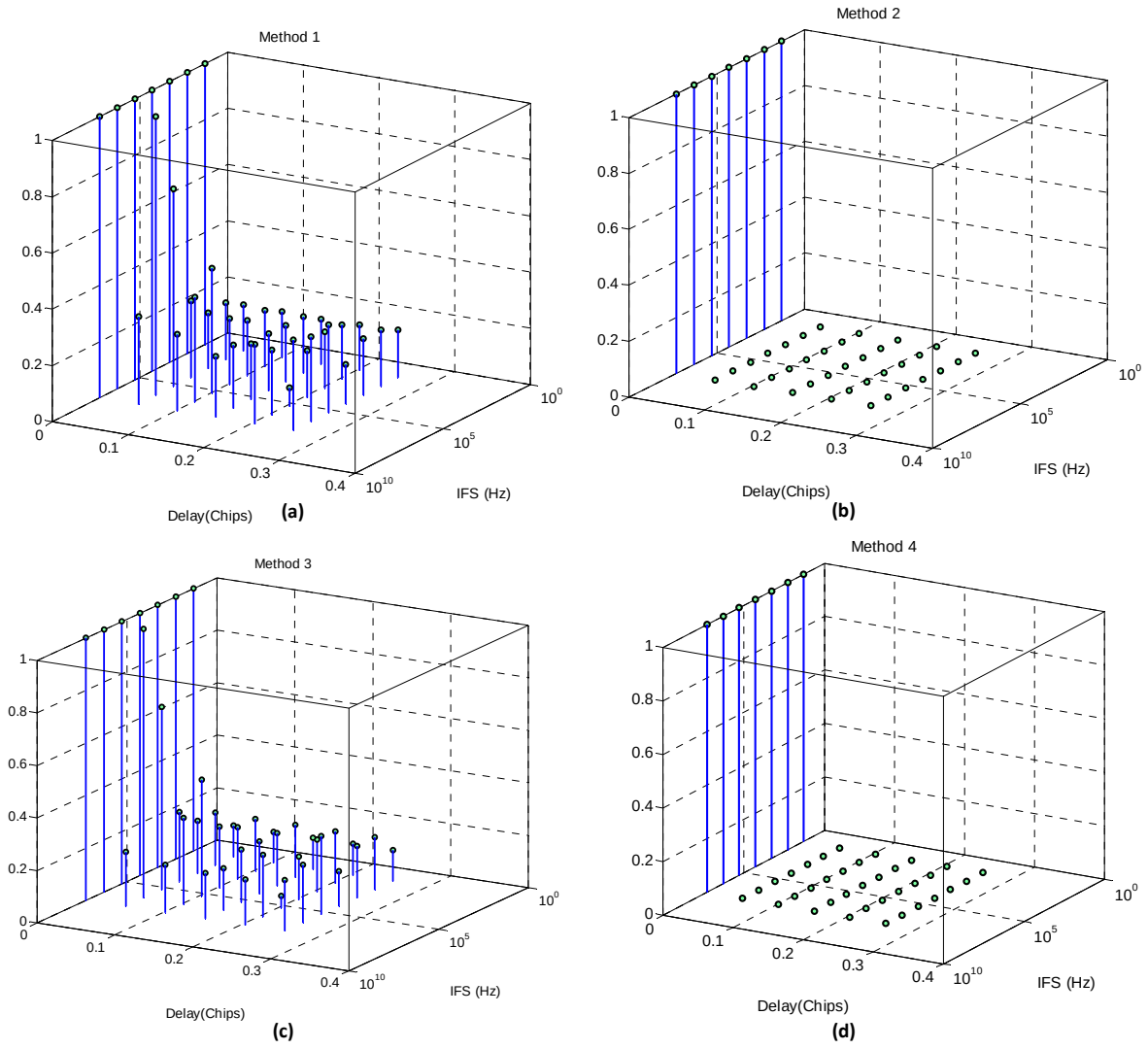

Figure 5-5: The relative amount of the GNSS signal amplitude passed through the filter versus IFS and delay for a) Method 1, b) Method 2, c) Method 3, d) Method 4

As expected, Method 1 and 3 induce biases and distortions (see Figure 5-5.a and Figure 5-5.c) although they can successfully mitigate the interference. As mentioned and as it can be seen in Figure 5-5.b, the optimal gain vector in Method 2 is obtained based on a distortionless constraint but as shown in Figure 5-4, it fails to mitigate the interference for

a wide range of IFS values. On the other hand, it can be seen that Method 4 employing the periodicity in the structure of the filter outperforms other methods in providing not only the SINR gain but also a distortionless response.

C. Performance evaluation of the proposed space-time filter

In the next simulation set, the enhancement due to employing the periodicity was studied for the proposed distortionless space-time filter. By performing Monte-Carlo simulations with 1000 runs, the performance is evaluated for different numbers of L_p employed in the filter design. Figure 5-6 and Figure 5-7 plot the INR and SINR versus IFS for four cases where in all cases $K = 6$ and L_p varies from 1 to 4. The interference scenario is the same as the previous simulation set. As observed, when the periodicity is not used, the INR and SINR performance may be significantly degraded. As mentioned, this is due to rank deficiency happening in the optimization problem. These plots show how by employing more GNSS signal periods in the structure of the filter, this issue can be alleviated and a more robust space-time filter can be achieved. This filter can suppress interference signals without distorting the cross correlation function.

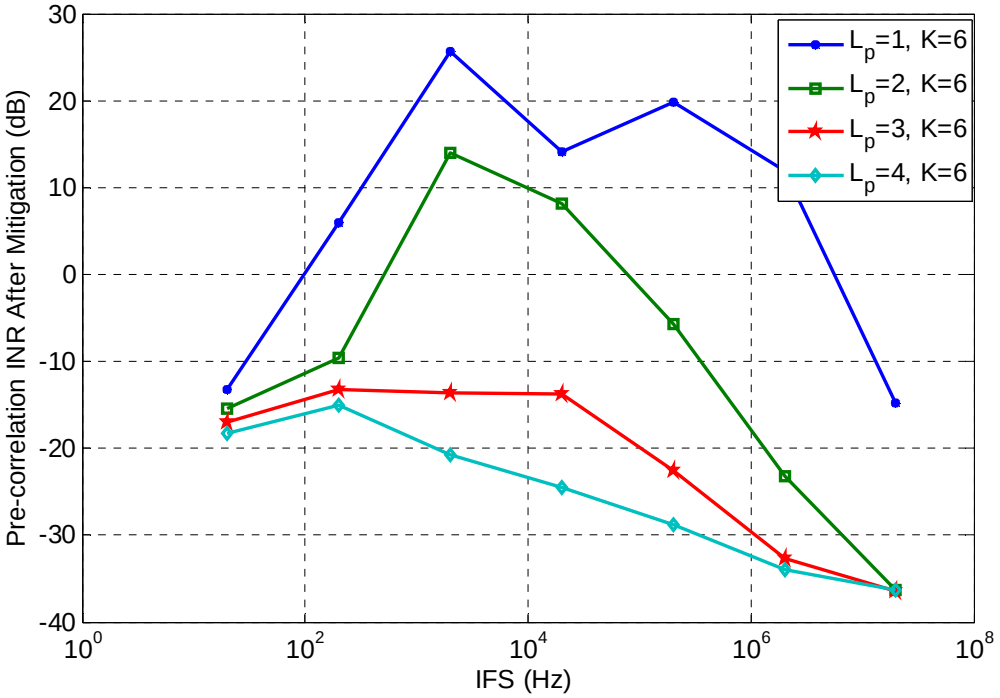

Figure 5-6: INR versus IFS

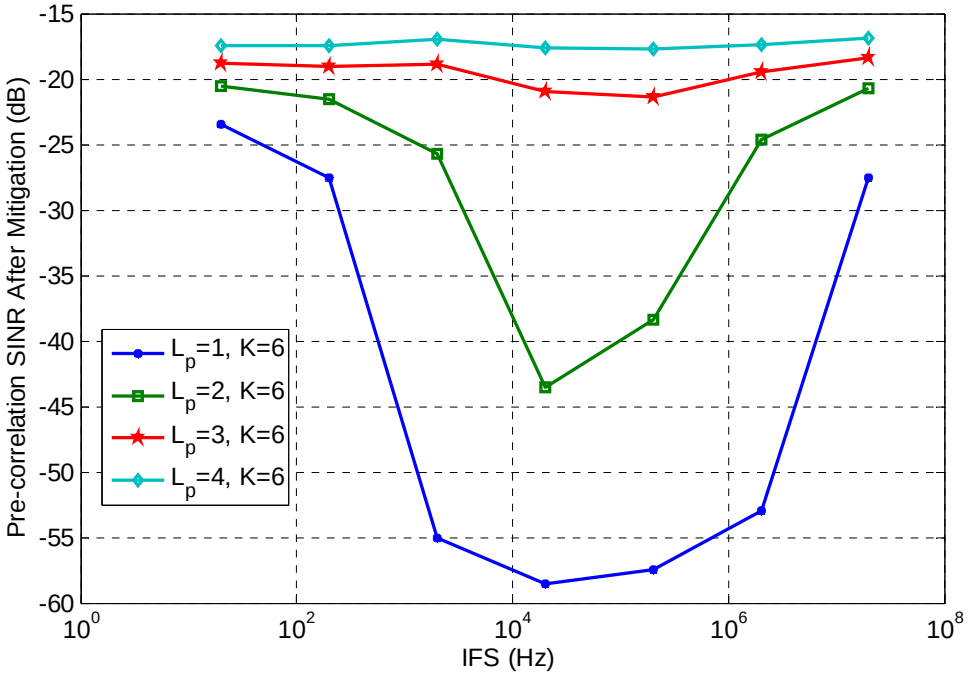

Figure 5-7: SINR versus IFS for L_p=1, 2, 3 and 4

D. Performance of the blind space-time filter

In this simulation, the performance of the blind filter obtained in (5.70) is compared to the one employing the steering vectors. For both cases, $K = 1$ and $L_p = 6$. Figure 5-8 shows the SINR for these two filters. The filters do not induce any distortion due to the time processing; however, in the case of the blind filter, since the steering vector of the desired signals is not considered, unintentional attenuation in the direction of the desired signals cannot be avoided. Therefore, the overall SINR is lower than the one employing the steering vectors of the signals in designing the filter. These SINR values are calculated for 20 MHz input filter bandwidth. For a coherent integration time of 1 ms, the post SINR for the case of unknown steering vector and known steering vector increases to approximately 15 and 25 dB, respectively.

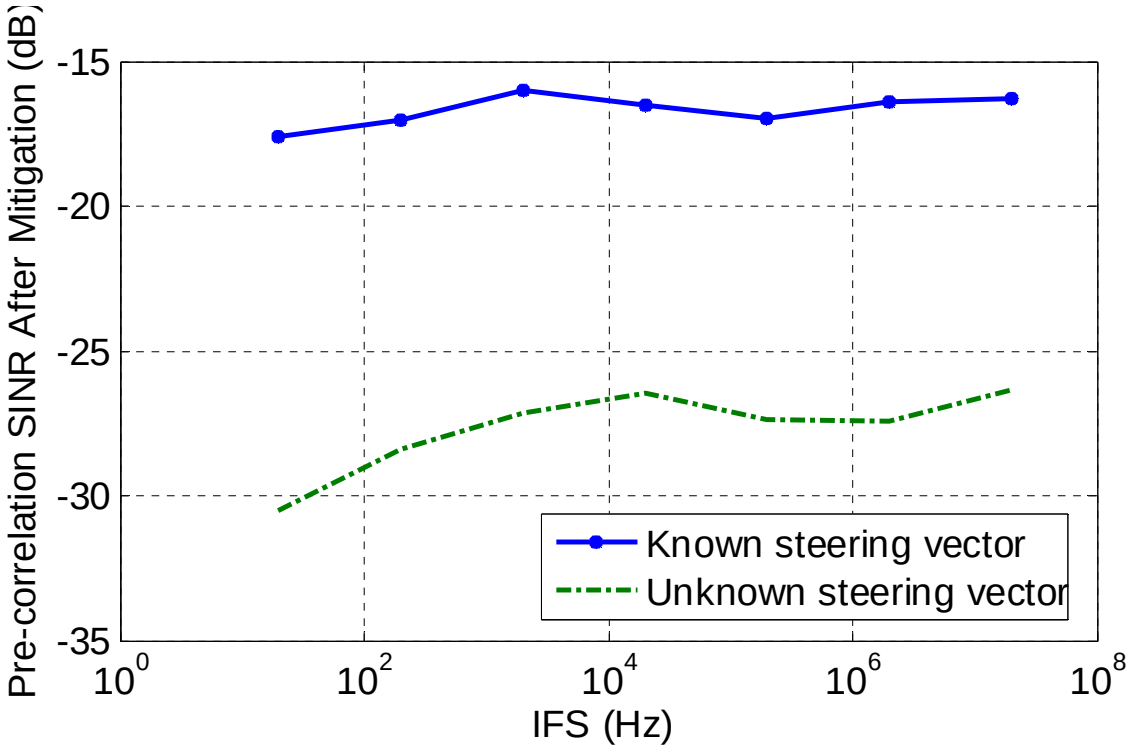

Figure 5-8: SINR versus IFS for the proposed method for the known steering vector and unknown steering vector cases

E. Real data measurements:

Finally, a mixed simulated and real signal test is applied to the proposed technique to verify the applicability of this technique under some imperfect conditions. The interfering signals are generated and added to real GPS signals in software. Figure 5-9 shows the proposed test scenario where a three-element antenna array was placed on a rooftop in order to receive GPS L1 signals. The received signals then passed through the three-channel RF front-end. Seven CW tones were considered for this test (see Table 5-1) and they were added to the collected digitized GPS samples.

In order to evaluate the distortion amount, the cross correlation function for different cases is shown over 100 observations. In Figure 5-10.a, the cross correlation function for interference-free signals is shown. In this case, the main lobe of the antenna array is steered toward the GPS LOS direction. Figure 5-10.b and Figure 5-10.c show the cross correlation functions after applying the proposed method for $K = 2,\ L_p = 1$ and $K = 1,\ L_p = 2$, respectively, where the average INR for CW interference signals is 40 dB. It can be observed that employing the periodicity avoids both distortion and SINR degradation. By increasing INR to 50 dB, the space-time filter with $K = 2,\ L_p = 1$ almost fails (see Figure 5-10.d) whereas in the $K = 1,\ L_p = 2$ case the distortion effect is much less (see Figure 5-10.e). Figure 5-10.f shows the cross correlation function for a filter with $K = 1,\ L_p = 3$ where the average INR is 50 dB. It can be observed that for this case, by employing three periods, the cross correlation functions are not considerably distorted where degradation in SINR values is not observable.

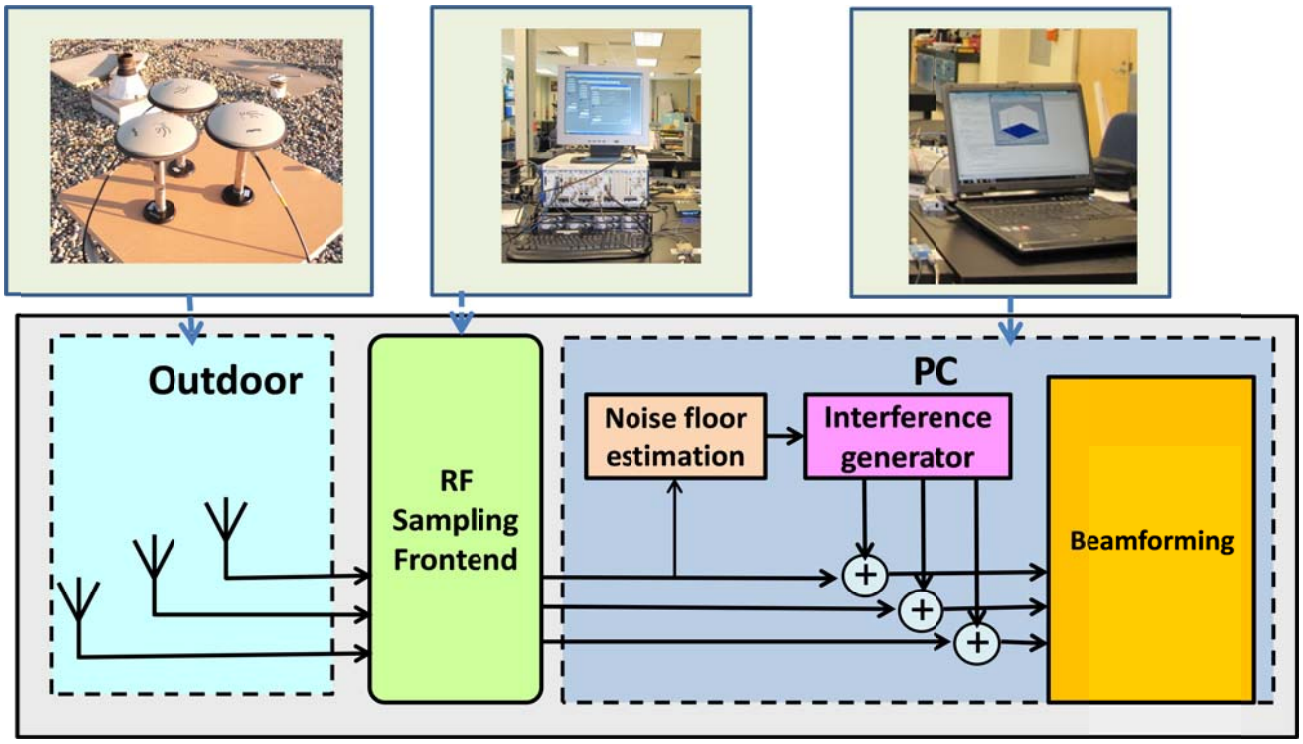

Figure 5-9: Proposed test setup

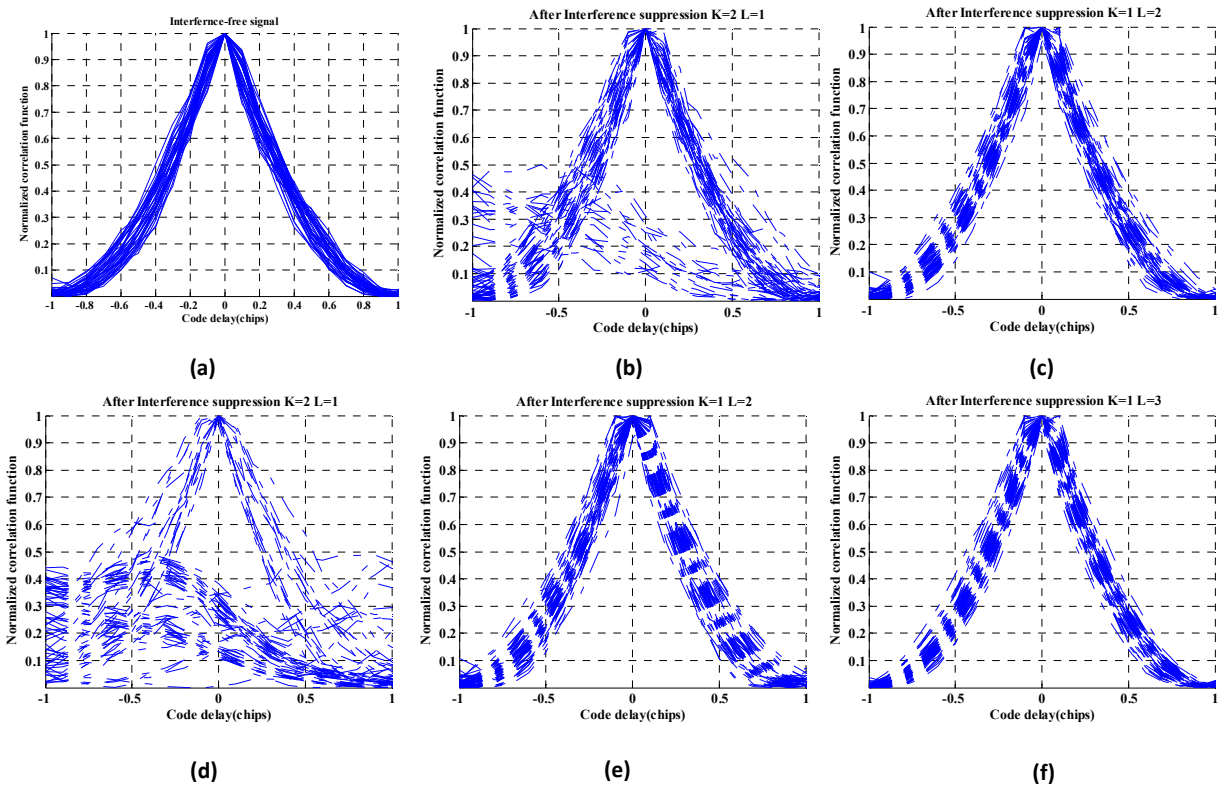

Figure 5-10: Cross correlation functions for a) Interference-free signal b) K=2, L_p =1, INR= 40 dB c) K=1, L_p=2, INR= 40 dB d) K=2, L_p =1, INR= 50 dB e) K=1, L_p =2, INR= 50 dB f) K=1, L_p =3, INR= 50 dB

5.5 Summary

This chapter studied a distortionless space-time processing filter for GNSS signals. In contrast to STAP methods in other applications, the distortion and bias caused by space-time processing may not be neglected in GNSS applications. Theoretical analyses along with several simulations were provided to evaluate the performance of the distortionless space-time filtering for GNSS interference mitigation applications. Moreover, the periodicity of GNSS signals was employed as an effective approach to increase the DOF

of the space-time filter for suppressing narrowband band interfering signals such as CW tone jammers or harmonics of signals originating unintentionally from any electronic devices in GNSS frequency bands without decreasing the SINR which may cause the failure of the filter. Several simulations and a practical test were performed to verify the effectiveness of the proposed method in real situations.

Chapter Six: SPOOFING MITIGATION BASED ON ANTENNA ARRAY PROCESSING

The civilian GNSS signal structures are publicly known and they are received with low power on the Earth's surface. These make GNSS signals susceptible to spoofing attacks. Hence, the requirement for proper mitigation techniques becomes a must in current and future GNSS receivers for robust, accurate and reliable positioning. This chapter proposes a new anti-spoofing technique using an antenna array.

6.1 Introduction

Spoofing countermeasure using an antenna array is one of the most powerful techniques that have been devised against this threat (Daneshmand et al 2013c, Daneshmand et al 2012b, Daneshmand et al 2011, Nielsen et al 2011, Nielsen et al 2010, Montgomery et al 2009, McDowell 2007, Hartman 1996). These techniques generally rely on the fact that a spoofer transmits several PRN codes from the same antenna whereas the authentic signals are transmitted from different satellites with different directions. The studied methods generally operate after acquisition and tracking stages of a GNSS receiver and they need to separately acquire and track all authentic and spoofing signals. This may impose a high computational complexity to the receiver. In addition, some of these techniques depend on precise array calibration which in turn increases the computational complexity. Moreover, most of the previously proposed techniques completely fail in multipath environments where the reflections of the spoofing signal are also received by the antenna array.

Both spoofing and authentic signals use the direct sequence spread spectrum (DSSS) modulation and their power is far below the noise floor when they are received by the target receiver's antenna elements. Moreover, in multipath environments, not only should the LOS spoofing signal be mitigated but also its reflections should be removed. Although these components usually have lower power than the LOS component, they may still mislead receivers if they are not mitigated properly. In multipath environments such as urban canyons, multipath components or the indirect signal with delays of the order of 500 ns exist and this amount may increase to 10 μs for hilly and mountainous places (Steingass & Lehner 2004, Jahn et al 1996). Although for the GPS L1 C/A code this is around 0.5 to 10 chips, for military codes and modernized GNSS signals such as L1/L2 P(Y) and L1/L2 M, L5, E6B, E5a, E5b which employ higher chip rates, this delay ranges from a few chips for suburban and urban environments to tens of chips in mountainous environments. Moreover, since all spoofing PRN codes experience the same multipath channel, even if the spoofing LOS component is removed, its multipath component leads to the same fake position and timing solutions targeted by the spoofer. In fact, this common delay due to the multipath propagation is absorbed in the clock term and it does not affect the position and timing solutions. However, as mentioned, a spoofer is a point source transmitting several PRN codes, each of which have a comparable power level to that of the authentic signals. Therefore, the overall spatial power of the spoofing signal (before despreading) is considerably higher than that of the authentic ones (the same fact for their multipath components). By considering this fact, this chapter

proposes a method to distinguish the spoofing signal and its reflections from authentic ones by performing spatial-temporal processing.

The rest of the chapter is organized as follows: In Section 6.2, the problem formulation is presented. In Section 6.3, the proposed spoofing mitigation technique is discussed in three subsections namely space-time correlation matrix formation, spoofing signal channel coefficients estimation and null steering. In Section 6.4, simulation results are presented and, finally, Section 6.6 summarizes the chapter.

6.2 Problem formulation

Assume that an antenna array has an arbitrary configuration with N elements. Several authentic GNSS signals and one spoofing signal[1] plus its multipath components are received by this antenna array. For simplicity in the problem formulation, one sample per chip is assumed (this method can be extended to the multi-rate/multi-antenna scenario). Again for the sake of simplicity, it is assumed that the antenna array is calibrated (the method is applicable for non-calibrated array as well). Moreover, assume that the maximum possible multipath delay (order of the multipath channel) with respect to the LOS signal for desired and undesired signals is equal to L_{ch} chips, which is an integer number. The received $N \times 1$ baseband signal vector of all incident signals including their multipath components can be expressed as (Ding & Li 2000)

[1] The spoofing signal consists of several PRN codes.

$$\underset{N\times 1}{\mathbf{r}_i} = \sum_{m=0}^{M}\sum_{l=0}^{L_{ch}} \bar{\mathbf{a}}_l^m s_{i-l}^m + \boldsymbol{\eta}_i \tag{6.1}$$

where s_{i-l}^m is the sample of mth signal for the ith time index received with the delay of l compared to its LOS signal component. M is the number of authentic GNSS signals. Without loss of generality, the index m equal to zero stands for the spoofing signal. In (6.1), $\boldsymbol{\eta}_i$ is spatial-temporal zero-mean white noise vector and $\bar{\mathbf{a}}_l^m$ is an $N \times 1$ vector that represents the channel coefficients for the signal component whose delay is l chips compared to the LOS component of the mth incident signal. In fact, for the mth signal, $\bar{\mathbf{a}}_l^m$ is related to the combination of the steering vectors of those signal components that have the same delay l (see Figure 6-1).

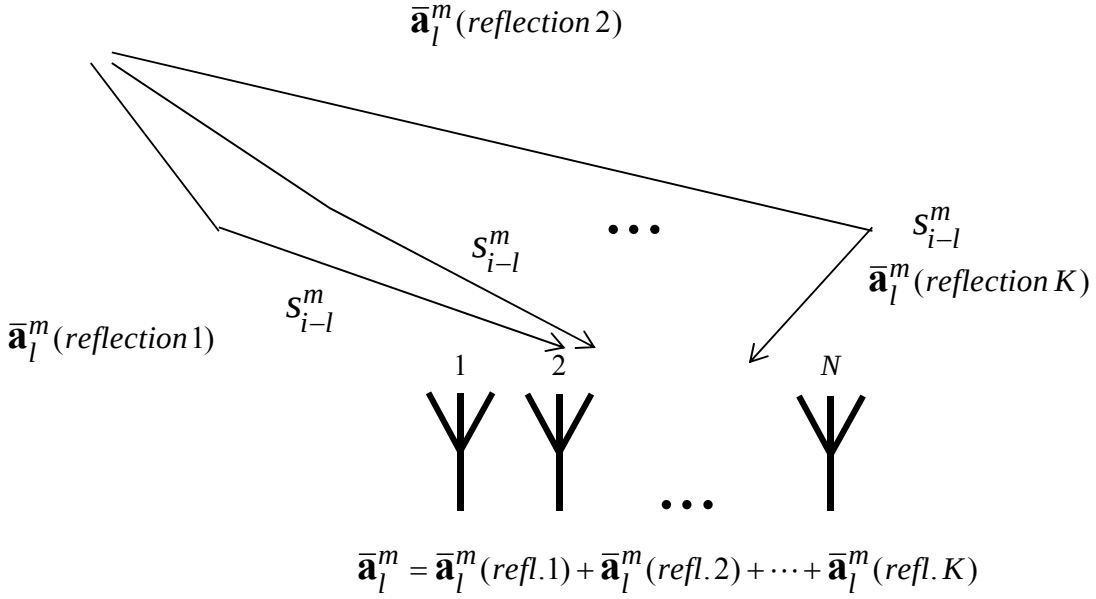

Figure 6-1: *K* reflections with the same delay *l* originated from the *m*th signal

Herein, the problem of interest is to find an optimal gain vector to satisfy the following conditions:

$$\begin{aligned} &\mathbf{w}^H \overline{\mathbf{a}}_l^0 = 0 \quad if \ \left(\overline{\mathbf{a}}_l^0\right)^H \overline{\mathbf{a}}_l^0 > \lambda_T \qquad l = 0,1,...L_{ch} \\ &\left\|\mathbf{w}\right\| = 1 \end{aligned} \tag{6.2}$$

where λ_T is a threshold which can be set from the relative values of the estimated channel coefficients. The constraint in (6.2) avoids the trivial solution, which is an all-zero vector. By applying this gain vector to the received antenna array signal vector, the spoofing signal and its multipath reflections are suppressed as

$$\mathbf{w}^H \mathbf{r}_i = \sum_{m=0}^{M} \sum_{l=0}^{L_{ch}} \mathbf{w}^H \overline{\mathbf{a}}_l^m s_{i-l}^m + \mathbf{w}^H \boldsymbol{\eta}_i = \underbrace{\sum_{l=0}^{L_{ch}} \mathbf{w}^H \overline{\mathbf{a}}_l^0 s_{i-l}^0}_{\approx 0} + \underbrace{\sum_{m=1}^{M} \sum_{l=0}^{L_{ch}} \mathbf{w}^H \overline{\mathbf{a}}_l^m s_{i-l}^m}_{Authentic\ signals} + \mathbf{w}^H \boldsymbol{\eta}_i \tag{6.3}$$

6.3 Proposed method

Herein, a spatial processing approach in conjunction with the time domain processing is utilized to estimate the spoofing LOS and its multipath channel coefficients which then can be employed to nullify the spoofing signal and its reflections. In doing so, a spatial-temporal processing with three stages is proposed. In the first stage, a space-time correlation matrix is formed from both temporal and spatial digitized samples. In the second stage, a blind channel estimation technique based on second order statistics (SOS) is employed to estimate the channel coefficients. It is shown that the spatial power dominance of the spoofing signal leads to easy decomposition of the channel coefficients of the spoofing signal and its multipath components from authentic GNSS signals by

analyzing the space-time correlation matrix. In the final stage, first by setting a threshold, the channel coefficients corresponding to the potential reflections of the spoofing signal can be detected. The estimated channel coefficients convey the spatial information of the incident signals. Therefore by having them, the spoofing signal and its multipath components can be nullified by the null steering process. All these three stages are performed before the despreading process which significantly decreases the processing time. Furthermore, this method does not require array calibration. These features make this method suitable for real-time GNSS applications and, thus, it can be either employed as a pre-processing technique for conventional GNSS receivers or easily integrated into the next-generation of receivers to deal with GNSS spoofing in multipath environments. The proposed method is introduced in the following subsections.

6.3.1 Space-time correction matrix formation

In (6.1), $\mathbf{r}_i$ can be expressed in a more compact form as

$$\underset{N\times 1}{\mathbf{r}_i} = \sum_{l=0}^{L_{ch}} \mathbf{A}_l \mathbf{s}_{i-l} + \boldsymbol{\eta}_i \tag{6.4}$$

where

$$\underset{N\times(M+1)}{\mathbf{A}_l} = \left[\bar{\mathbf{a}}_l^0 \quad \bar{\mathbf{a}}_l^1 \quad \cdots \quad \bar{\mathbf{a}}_l^M\right], \quad l = 0,1,...,L_{ch}$$

$$\underset{(M+1)\times 1}{\mathbf{s}_i} = \begin{bmatrix} s_i^0 \\ s_i^1 \\ \vdots \\ s_i^M \end{bmatrix}. \tag{6.5}$$

Assume that the vector $\vec{\mathbf{r}}_i$ is formed from K_s consecutive snapshots $(K_s \geq L_{ch})$ as

$$\vec{\mathbf{r}}_i = \begin{bmatrix} \mathbf{r}_i \\ \mathbf{r}_{i-1} \\ \vdots \\ \mathbf{r}_{i-(K_s-1)} \end{bmatrix}_{NK_s\times 1}. \tag{6.6}$$

It can be verified that

$$\vec{\mathbf{r}}_i = \mathcal{A}\vec{\mathbf{s}}_i + \boldsymbol{\eta}_i \tag{6.7}$$

where $\mathcal{A}$ is a block Toeplitz matrix defined as

$$\underset{NK_s\times(M+1)(L_{ch}+K_s)}{\mathcal{A}} = \begin{bmatrix} \mathbf{A}_0 & \mathbf{A}_1 & \cdots & \mathbf{A}_{L_{ch}} & \mathbf{0} & \cdots & \cdots & \mathbf{0} \\ \underset{N\times(M+1)}{\mathbf{0}} & \mathbf{A}_0 & \mathbf{A}_1 & \cdots & \mathbf{A}_{L_{ch}} & \ddots & \ddots & \mathbf{0} \\ \mathbf{0} & \ddots & \ddots & \ddots & \ddots & \ddots & \ddots & \vdots \\ \vdots & \ddots & \mathbf{0} & \mathbf{A}_0 & \cdots & \mathbf{A}_{L_{ch}-1} & \mathbf{A}_{L_{ch}} & \mathbf{0} \\ \mathbf{0} & \cdots & \cdots & \mathbf{0} & \mathbf{A}_0 & \cdots & \mathbf{A}_{L_{ch}-1} & \mathbf{A}_{L_{ch}} \end{bmatrix} \tag{6.8}$$

and

$$\vec{\mathbf{s}}_i = \begin{bmatrix} \mathbf{s}_i \\ \mathbf{s}_{i-1} \\ \vdots \\ \mathbf{s}_{i-L_{ch}-K_s+1} \end{bmatrix}_{(M+1)(L_{ch}+K_s)\times 1} \qquad \vec{\boldsymbol{\eta}}_i = \begin{bmatrix} \boldsymbol{\eta}_i \\ \boldsymbol{\eta}_{i-1} \\ \vdots \\ \boldsymbol{\eta}_{i-L_{ch}-K_s+1} \end{bmatrix}_{NK_s\times 1}. \tag{6.9}$$

Noise and the received signals are assumed to be independent. Hence, the space-time correlation matrix can be formed as

$$\underset{NK_s\times NK_s}{\mathbf{R}_{\vec{\mathbf{r}}}} = E\left\{\vec{\mathbf{r}}_i\vec{\mathbf{r}}_i^H\right\} = \mathcal{A}E\left\{\vec{\mathbf{s}}_i\vec{\mathbf{s}}_i^H\right\}\mathcal{A}^H + \sigma^2\,\underset{NK_s}{\mathbf{I}} \tag{6.10}$$

where σ^2 is the variance of the noise.

In (6.10), $\mathbf{R}_{\vec{\mathbf{r}}}$ can be approximately estimated by averaging over K_{win} consecutive windows of the received temporal-spatial samples as

$$\mathbf{R}_{\vec{\mathbf{r}}} \approx \frac{1}{K_{win}}\sum_{i=0}^{K_{win}-1}\vec{\mathbf{r}}_i\vec{\mathbf{r}}_i^H. \tag{6.11}$$

6.3.2 Spoofing signal channel coefficients estimation

In order to identify the channel coefficients of the spoofing signal and its multipath components, the well-known techniques used for blind channel estimation based on SOS can be applied. There are many SOS-based methods among which linear prediction algorithms (LPA) are of particular interests for the problem at hand since they are less sensitive to the overestimation of the channel order. In other words, they can be one of the best options for spoofing multipath identification and mitigation applications since the order of the channel is not usually known. LPAs were first proposed by Slock (1994)

and Abed-Meraim et al (1995). To improve performance, many modified versions of LPA were presented by Ding (1997), Tong & Zhao (1998), Tsatsanis & Xu (1999) and others. In this chapter, the outer product decomposition algorithm (OPDA) proposed by Ding (1997) is developed for the case of mitigation of a spoofing signal and its multipath components.

For simplicity's sake, in the rest of the analysis, it is assumed that the PRN codes of the spoofing signal and the authentic one are uncorrelated. (i. e. they either have different PRN codes or their corresponding delays are different). Therefore, due to the autocorrelation and cross correlation properties of the PRN codes, the correlation between each pair (including both spoofing and authentic PRN codes) of them is negligible. Hence, $E\left\{\vec{\mathbf{s}}_i\vec{\mathbf{s}}_i^H\right\}$ can be assumed as a block diagonal matrix as

$$E\left\{\vec{\mathbf{s}}_i\vec{\mathbf{s}}_i^H\right\} = \underset{(M+1)(L_{ch}+K_s)\times(M+1)(L_{ch}+K_s)}{\mathcal{A}} = \begin{bmatrix} \underset{(M+1)\times(M+1)}{\bar{\mathbf{\Lambda}}} & \mathbf{0} & \cdots & \mathbf{0} \\ \mathbf{0} & \bar{\mathbf{\Lambda}} & \ddots & \vdots \\ \vdots & \ddots & \ddots & \mathbf{0} \\ \mathbf{0} & \cdots & \mathbf{0} & \bar{\mathbf{\Lambda}} \end{bmatrix}. \tag{6.12}$$

Assume that $\mathbf{A}_{ch}$ is defined as

$$\underset{NK_s\times(M+1)}{\mathbf{A}_{ch}} = \begin{bmatrix} \underset{N\times(M+1)}{\mathbf{A}_0} \\ \mathbf{A}_1 \\ \vdots \\ \mathbf{A}_{L_{ch}} \\ \underset{N\times 1}{\mathbf{0}} \\ \vdots \\ \mathbf{0} \end{bmatrix} = \begin{bmatrix} \overline{\mathbf{a}}_0^0 & \overline{\mathbf{a}}_0^1 & \cdots & \overline{\mathbf{a}}_0^M \\ \overline{\mathbf{a}}_1^0 & \overline{\mathbf{a}}_1^1 & \ddots & \overline{\mathbf{a}}_1^M \\ \vdots & \vdots & \ddots & \vdots \\ \overline{\mathbf{a}}_{L_{ch}-1}^0 & \overline{\mathbf{a}}_{L_{ch}-1}^1 & \ddots & \overline{\mathbf{a}}_{L_{ch}-1}^M \\ \underset{N\times 1}{\mathbf{0}} & \mathbf{0} & \ddots & \mathbf{0} \\ \vdots & \vdots & \ddots & \vdots \\ \mathbf{0} & \mathbf{0} & \cdots & \mathbf{0} \end{bmatrix}. \tag{6.13}$$

The first column of $\mathbf{A}_{ch}$ includes all the sufficient information needed for suppressing the spoofing signal and its reflections. By developing the OPDA introduced by Ding (1997) for the case that the diagonal elements of $\overline{\mathbf{\Lambda}}$ in (6.12) are not equal (due to different power of the incident signals), it can be shown that the first column of $\mathbf{A}_{ch}$ can be estimated by performing the following analysis.

Assume that $\mathbf{A}_h$ is a block Hankel matrix of size $K_sN \times (L_{ch} + K_s)(M+1)$ and defined as

$$\underset{K_sN\times(L_{ch}+K_s)(M+1)}{\mathbf{A}_h} \triangleq \begin{bmatrix} \mathbf{A}_0 & \mathbf{A}_1 & \cdots & \mathbf{A}_{L_{ch}-1} & \mathbf{A}_{L_{ch}} & \mathbf{0} & \cdots & \mathbf{0} \\ \mathbf{A}_1 & \mathbf{A}_2 & \cdots & \mathbf{A}_{L_{ch}} & \mathbf{0} & \mathbf{0} & \cdots & \mathbf{0} \\ \vdots & \vdots & \ddots & & & & & \\ \mathbf{A}_{L_{ch}-1} & \mathbf{A}_{L_{ch}} & & \ddots & & \vdots & & \\ \mathbf{A}_{L_{ch}} & \mathbf{0} & & & \ddots & & & \\ \underset{N\times(M+1)}{\mathbf{0}} & \mathbf{0} & & \vdots & & \ddots & & \\ \vdots & \vdots & & & & & \ddots & \\ \mathbf{0} & \mathbf{0} & & & & & & \mathbf{0} \end{bmatrix}. \tag{6.14}$$

where $\mathbf{A}_l$, $l = 0,1,...,L_{ch}$ are defined in (6.13). Furthermore, assume that $\mathbf{R}_h$ is another block Hankel matrix defined as

$$\underset{K_s N \times N K_s}{\mathbf{R}_h} \triangleq \begin{bmatrix} \mathbf{R}_0 - \sigma^2 \mathbf{I} & \mathbf{R}_1 & \cdots & \mathbf{R}_{K_s-1} \\ \mathbf{R}_1 & \mathbf{R}_2 & \underset{N\times N}{\mathbf{0}} & \vdots \\ \vdots & \ddots & \ddots & \vdots \\ \mathbf{R}_{K_s-1} & \mathbf{0} & \cdots & \mathbf{0} \end{bmatrix} \tag{6.15}$$

where $\underset{N\times N}{\mathbf{R}_i}, i = 0,1,2, \ldots, K_s - 1$ can be estimated from partitioning the correlation matrix in (6.10) as

$$\mathbf{R}_{\bar{\mathbf{r}}} = \begin{bmatrix} \underset{N\times N}{\mathbf{R}_0} & \mathbf{R}_1 & \cdots & \mathbf{R}_{K_s-1} \\ \mathbf{R}_1^H & \mathbf{R}_0 & \cdots & \mathbf{R}_{K_s-2} \\ \vdots & \ddots & \ddots & \vdots \\ \mathbf{R}_{K_s-1}^H & \mathbf{R}_{K_s-2}^H & \cdots & \mathbf{R}_0 \end{bmatrix}. \tag{6.16}$$

By performing some matrix manipulations, it can be concluded that (Ding & Li 2000)

$$\mathbf{R}_h = \mathbf{A}_h \mathcal{A} \mathcal{A}^H . \tag{6.17}$$

Moreover, it can be verified that (Ding 1997)

$$\mathcal{A}^{\frac{1}{2}} \mathcal{A}^H \left(\mathcal{A} \mathcal{A} \mathcal{A}^H \right)^{\#} \mathcal{A} \mathcal{A}^{\frac{1}{2}} = \mathbf{I}. \tag{6.18}$$

Let $\boldsymbol{\Delta}$ be defined as

$$\underset{NK_s \times NK_s}{\boldsymbol{\Delta}} \triangleq \mathbf{R}_h (\mathbf{R}_{\bar{\mathbf{r}}} - \sigma^2 \mathbf{I})^{\#} \mathbf{R}_h{}^H. \tag{6.19}$$

Considering (6.19) along with (6.18) and (6.17), $\boldsymbol{\Delta}$ can be obtained as

$$\boldsymbol{\Delta} = \mathbf{A}_h \boldsymbol{\mathcal{A}} \boldsymbol{\mathcal{A}}^H \left(\boldsymbol{\mathcal{A}} \boldsymbol{\mathcal{A}} \boldsymbol{\mathcal{A}}^H \right)^{\#} \boldsymbol{\mathcal{A}}^H \boldsymbol{\mathcal{A}} \mathbf{A}_h^H = \mathbf{A}_h \boldsymbol{\mathcal{A}} \mathbf{A}_h^H . \tag{6.20}$$

Considering (6.20) and performing some matrix manipulations, it can be verified that (Ding & Li 2000, Ding 1997)

$$\boldsymbol{\Delta} - \mathbf{J}^N \boldsymbol{\Delta} \left(\mathbf{J}^N \right)^H = \mathbf{A}_{ch} \bar{\boldsymbol{\Lambda}} \mathbf{A}_{ch}^H \tag{6.21}$$

where $\mathbf{J}$ is a shifting matrix defined as

$$\mathbf{J} = \begin{bmatrix} 0 & 1 & 0 & \cdots & 0 \\ 0 & 0 & 1 & \ddots & 0 \\ \vdots & \ddots & \ddots & \ddots & \vdots \\ 0 & 0 & 0 & \ddots & 1 \\ 0 & 0 & 0 & \cdots & 0 \end{bmatrix} \tag{6.22}$$

and $\mathbf{J}^N$ means $\mathbf{J}$ power N .Therefore, considering (6.19), $\mathbf{A}_{ch} \bar{\boldsymbol{\Lambda}} \mathbf{A}_{ch}^H$ can be estimated from only the SOS which is the spatial-temporal elements of the correlation matrix. In the next step, by performing a singular value decomposition (SVD) of $\mathbf{A}_{ch} \bar{\boldsymbol{\Lambda}} \mathbf{A}_{ch}^H$ the spoofing signal channel coefficients can be estimated. To this end, it should be noticed that the first element of $\bar{\boldsymbol{\Lambda}}$ is significantly higher than the other diagonal elements. This is due to the fact that all spoofing PRNs are coming from the same direction (the same for the reflection components) whereas the authentic PRNs are transmitted from different satellites and are received from different directions. The diagonal elements of $\bar{\boldsymbol{\Lambda}}$ are the summations of the variance (power) of each incident signal and its reflections. Hence, the

diagonal element corresponding to the spoofing signal and its reflection is significantly larger than the other elements. This is also verified by performing a simulation in Section 6.4. Hence, under a spoofing attack, $\mathbf{A}_{ch}\overline{\mathbf{\Lambda}}\mathbf{A}_{ch}^{H}$ can be approximated as

$$\mathbf{A}_{ch}\overline{\mathbf{\Lambda}}\mathbf{A}_{ch}^{H} \simeq \begin{bmatrix} \overline{\mathbf{a}}_0^0 \\ \overline{\mathbf{a}}_1^0 \\ \vdots \\ \overline{\mathbf{a}}_{L_{ch}}^0 \\ \underset{N\times 1}{\mathbf{0}} \\ \vdots \\ \mathbf{0} \end{bmatrix} \sigma_{sp}^2 \begin{bmatrix} \overline{\mathbf{a}}_0^0 \\ \overline{\mathbf{a}}_1^0 \\ \vdots \\ \overline{\mathbf{a}}_{L_{ch}}^0 \\ \mathbf{0} \\ \vdots \\ \mathbf{0} \end{bmatrix}^H . \tag{6.23}$$

where σ_{sp}^2 is the power of the spoofing signal. Therefore, $\overline{\mathbf{a}}_l^0,\ l = 0,1,...,L_{ch}$ can be estimated by obtaining the singular vector corresponding to the largest singular value of matrix $\mathbf{\Delta} - \mathbf{J}^N \mathbf{\Delta} \left(\mathbf{J}^N\right)^H$.

6.3.3 Null steering

After estimating $\overline{\mathbf{a}}_l^0,\ l = 0,1,...,L_{ch}$, by comparing absolute value of each $\overline{\mathbf{a}}_l^0$ to a threshold denoted by λ_T [1], delays and their corresponding channel coefficients at which there are potential reflections of the spoofing signal can be detected. In fact, $\overline{\mathbf{a}}_l^0$ is deemed as a steering vector of a signal component or combination of the steering vectors of several signal components received with the same delay l if

[1] This threshold can be determined from the relative values of the estimated channel coefficients and is not discussed herein.

$$\left(\bar{\mathbf{a}}_l^0\right)^H \bar{\mathbf{a}}_l^0 > \lambda_T, l = 0,1,...,L_{ch}. \tag{6.24}$$

Assume that M_{sp} potential delays are detected and the corresponding channel coefficients are put in a $N \times M_{sp}$ matrix defined as $\mathbf{B}$. The matrix $\mathbf{P}_\perp$, which is the orthogonal projection to the spoofing subspace, can be obtained as

$$\underset{N\times N}{\mathbf{P}_\perp} = \mathbf{I} - \mathbf{B}(\mathbf{B}^H\mathbf{B})^{-1}\mathbf{B}^H. \tag{6.25}$$

Thus, the spoofing signal and its reflection are removed from the received antenna array signals if this orthogonal projection matrix is applied to the received signal vector as

$$\bar{\mathbf{r}}_i = \mathbf{P}_\perp^H \mathbf{r}_i = \sum_{m=0}^{M}\sum_{l=0}^{L_{ch}} \mathbf{P}_\perp^H \bar{\mathbf{a}}_l^m s_{i-l}^m + \mathbf{P}_\perp^H \boldsymbol{\eta}_i = \underbrace{\sum_{l=0}^{L_{ch}} \mathbf{P}_\perp^H \bar{\mathbf{a}}_l^0 s_{i-l}^0}_{\approx 0} + \sum_{m=1}^{M}\sum_{l=0}^{L_{ch}} \mathbf{P}_\perp^H \bar{\mathbf{a}}_l^m s_{i-l}^m + \mathbf{P}_\perp^H \boldsymbol{\eta}_i. \tag{6.26}$$

It is straightforward to verify that by applying $\mathbf{P}_\perp$ to $\bar{\mathbf{r}}_i$, the spoofing signal is removed and the first term in (6.26) becomes negligible. Hence, the optimal gain vector $\mathbf{w}$ satisfying (6.2) is $\mathbf{P}_\perp\boldsymbol{\beta}$ where $\boldsymbol{\beta}$ is an arbitrary unit vector.

For the case of an open sky or in the presence of only non-resolvable multipath components ($L_{ch} = 0, K_s = 1$), the computation complexity reduces considerably. The correlation matrix in (6.10) reduces to

$$\underset{N\times N}{\mathbf{R}_\mathbf{r}} = E\left\{\mathbf{r}_i\mathbf{r}_i^H\right\} = \mathbf{A}_0 E\left\{\mathbf{s}_i\mathbf{s}_i^H\right\}\mathbf{A}_0{}^H + \sigma^2 \underset{N\times N}{\mathbf{I}} \tag{6.27}$$

which only consists of spatial samples. In this case, the channel coefficients of the spoofing signal $\bar{\mathbf{a}}_0^0$ can be estimated from the following eigenvalue problem

$$\underset{\|\boldsymbol{\mu}\|=1}{Max}\ \boldsymbol{\mu}^H \mathbf{R}_{\mathbf{r}} \boldsymbol{\mu} \tag{6.28}$$

where $\boldsymbol{\mu}$ is equal to the eigenvector corresponding to the largest eigenvalue of $\mathbf{R}_{\mathbf{r}}$. Hence, the orthogonal projection to the spoofing subspace can be obtained as

$$\underset{N\times N}{\mathbf{P}_{\perp}} = \mathbf{I} - \boldsymbol{\mu}(\boldsymbol{\mu}^H \boldsymbol{\mu})^{-1} \boldsymbol{\mu}^H. \tag{6.29}$$

It is worth mentioning that the second largest eigenvector of $\mathbf{R}_{\mathbf{r}}$ maximizes the power of the authentic signal components. Therefore, choosing this vector as the array gain vector allows the power of the authentic signals to pass through the beamformer as much as possible whereas the spoofing signal is suppressed. In an open-sky environment, the computation complexity can be reduced even more and also extra analyses can be performed in order to maximize the power of individual authentic signals (Daneshmand et al 2012, Daneshmand et al 2011b).

The summary of the proposed technique is:

1 Construct the spatial-temporal correlation matrix $\mathbf{R}_{\bar{\mathbf{r}}}$ from (6.11)

2 Compute $\boldsymbol{\Delta}$ from (6.19)

3 Perform SVD of $\boldsymbol{\Delta} - \mathbf{J}^N \boldsymbol{\Delta} \left(\mathbf{J}^N\right)^H$ to obtain the largest singular vector in order to estimate the channel coefficients of the spoofing signal.

4 Compare the estimated spoofing channel coefficients with the threshold in (6.24) and construct matrix $\mathbf{B}$.

5 Compute the orthogonal projection $\mathbf{P}_{\perp}$ from (6.25) and apply it to the received signal vector.

The block diagram of the proposed method is shown in Figure 6-2. As it can be observed, the whole process is performed before the acquisition and tracking stages in a GNSS receiver. Therefore, the computational burden and the processing time are significantly reduced compared to those methods operating after the despreading process. Furthermore, the proposed method can be employed as an in-line stand-alone unit operating independently from the receiver structure or it can be implemented inside the new generation receivers capable of suppressing spoofing.

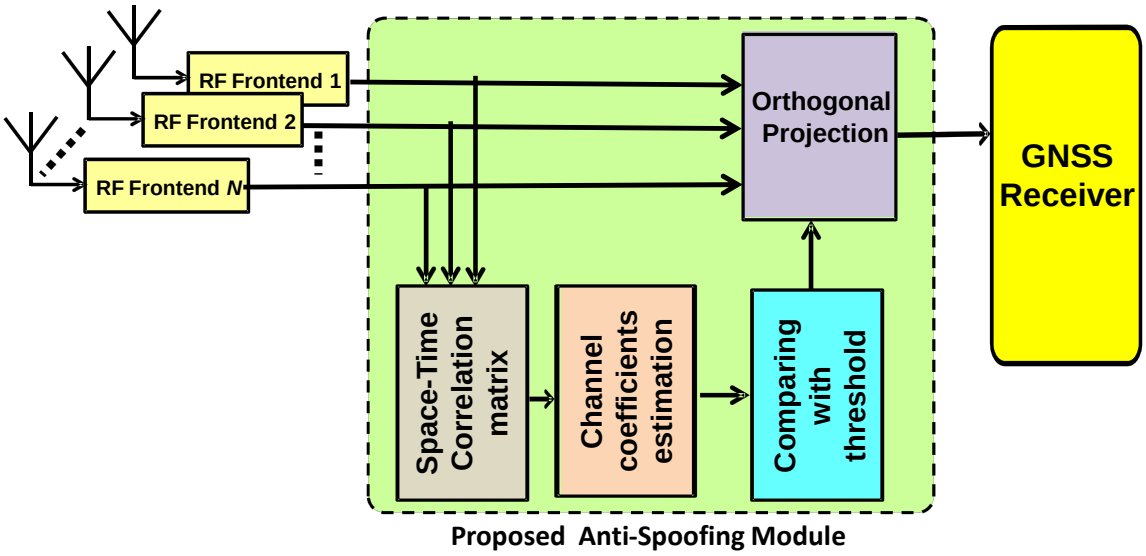

Figure 6-2: Block diagram of the proposed spoofing mitigation module

6.4 Simulation results

In this section, several simulations are performed to show the effectiveness of this algorithm and evaluate its performance. For all examples, the interfering signal is a single-source spoofing signal that consists of nine fake GPS L1 C/A PRN codes. In addition, nine authentic GPS L1 C/A signals are assumed[1]. The average power of the authentic signals is chosen to be -158 dBW. Sampling rate is chosen to be 1.023 MHz (one sample per chip). An antenna array with four elements is used and the antenna configuration is a square with a half GPS L1 wavelength spacing between adjacent elements. 1000 samples are used to form the space-time correlation matrix. In all simulations, K_s is selected as 10 chips, which is assumed to be greater than the order of the multipath channel.

For the first simulation, it is assumed that the average power of the PRN codes for the LOS spoofing signal is -155 dBW and it is received at an azimuth and elevation of 45° and only one reflection of the spoofing signal exists, which is received at an azimuth of 150° and elevation of 15° with a delay equal to three chips with an average power of 2 dB lower than that of the LOS component.

Figure 6-3 shows the absolute values of the normalized estimated channel coefficients of the LOS and the multipath component of the spoofing signal versus the number of chip

---

[1] As mentioned before, multipath with a delay more than one chip rarely happens for the L1 C/A code. However, for simplicity, this code is considered for simulations. Since this approach does not depend on the structure of the spreading code, the same result is expected for military codes and modernized GNSS signals such as L1 and L2 P(Y) and M, L5, E6B, E5a, E5b, which employ higher chip rates. The multipath channel order for these signals ranges from the order of a few chips for urban canyons to tens of chips in mountainous environments.

delays and antenna element number. Therefore, each point stands for a channel coefficient associated to a specific delay and antenna element. It can be observed that the spoofing signal and its multipath reflection can be easily distinguished. Figure 6-4 shows the polar beam pattern of the proposed method after the null steering stage. It can be seen that deep nulls have been steered toward the direction of the spoofing signal and its reflection.

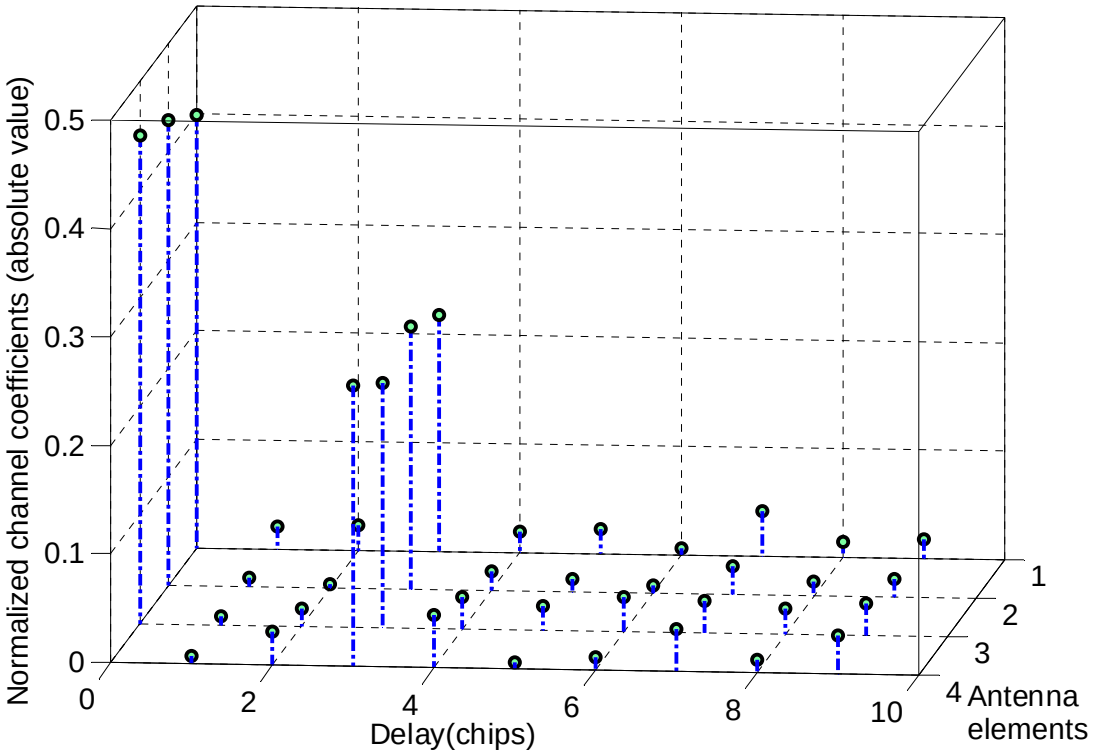

Figure 6-3: The absolute values of the estimated channel coefficients for the LOS and one multipath component of the spoofing signal

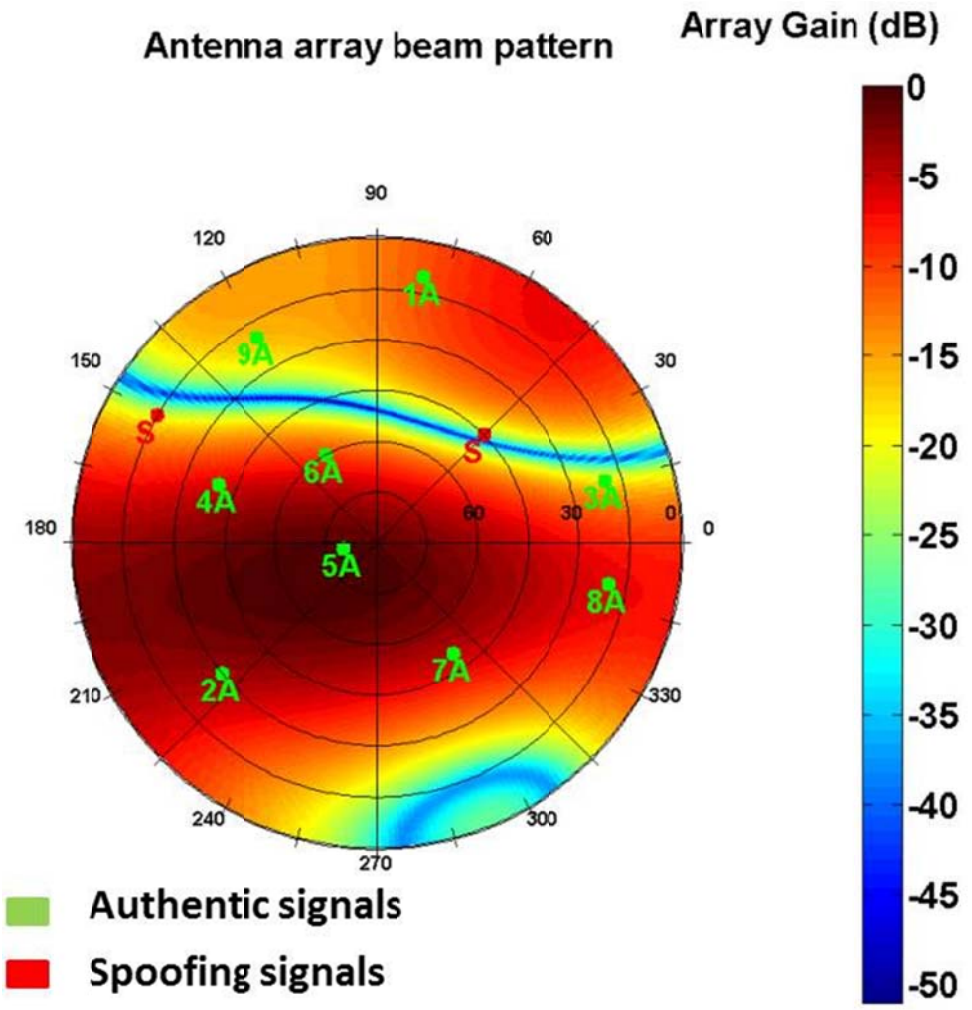

Figure 6-4: Polar beam pattern with respect to azimuth and elevation (the LOS spoofing signal and one multipath component)

Figure 6-5 shows the normalized cross ambiguity functions (CAF) before and after spoofing mitigation for one of the common PRNs. It is observed that before spoofing mitigation (Figure 6-5a) the authentic signal peak is weaker than the spoofing one and also the presence of the spoofing signal and its reflection has increased the receiver noise floor which can result in the deterioration of the authentic signal acquisition. After

spoofing mitigation, the correlation peaks of the spoofing signal and its reflection are removed and only the authentic one remains.

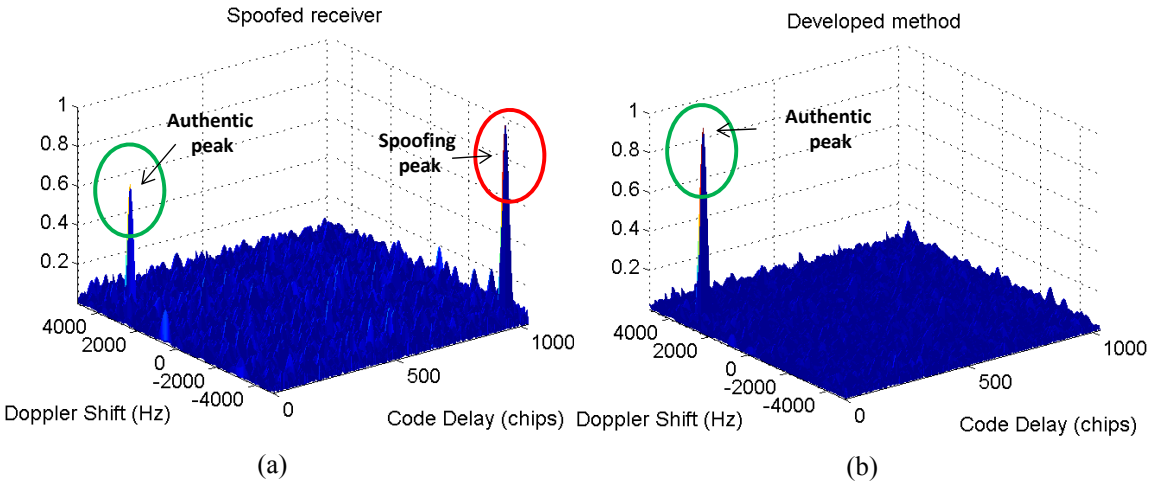

Figure 6-5: Normalized CAFs (a) before spoofing mitigation (b) after spoofing mitigation

In the second example, two multipath components are assumed. The first multipath component is the same as the previous example and the second one is received at an azimuth of 300° and elevation of 10° with a delay equal to five chips with a power of 2 dB less than the LOS spoofing component. The channel coefficients and the beam pattern are shown in Figure 6-6 and Figure 6-7, respectively. It can be observed that the channel coefficients related to the potential spoofing reflections can be easily distinguished and, therefore, three nulls can be steered toward the directions of the LOS and two multipath reflections. The maximum available number of nulls to suppress the spoofing signal and its reflection is equal to $N-1$.

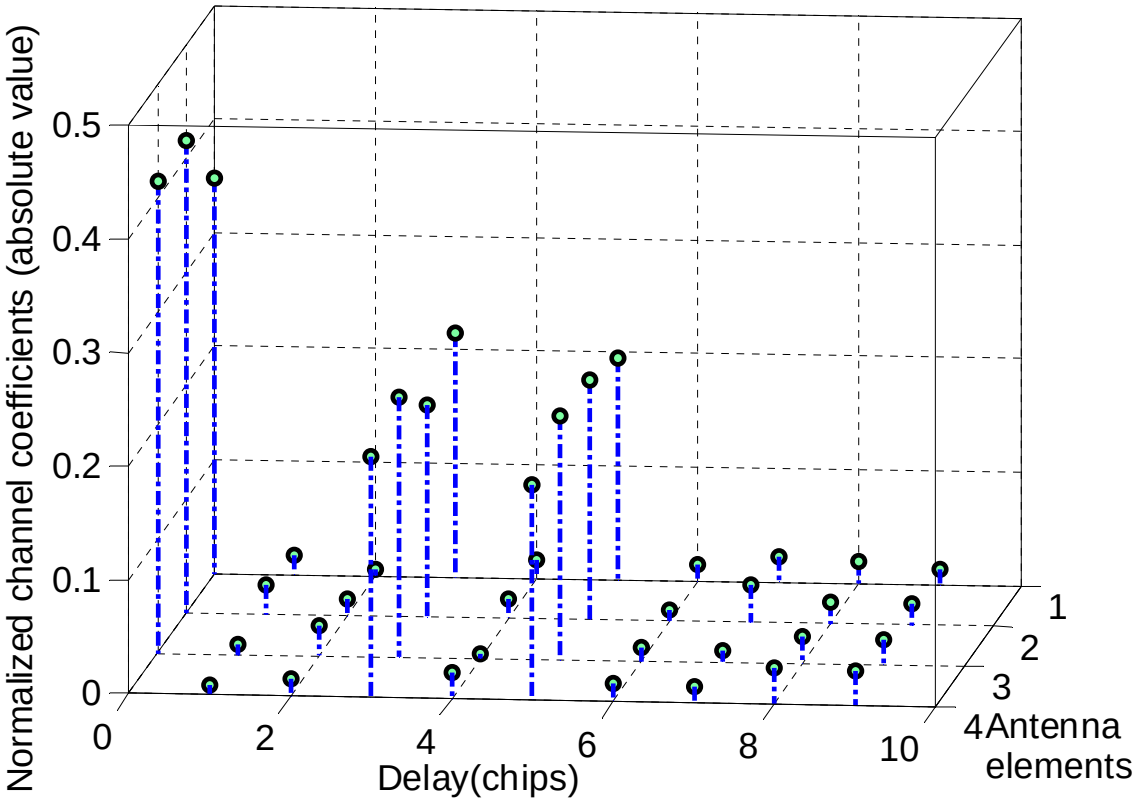

Figure 6-6: Absolute values of estimated channel coefficients for the LOS and two multipath components of the spoofing signal

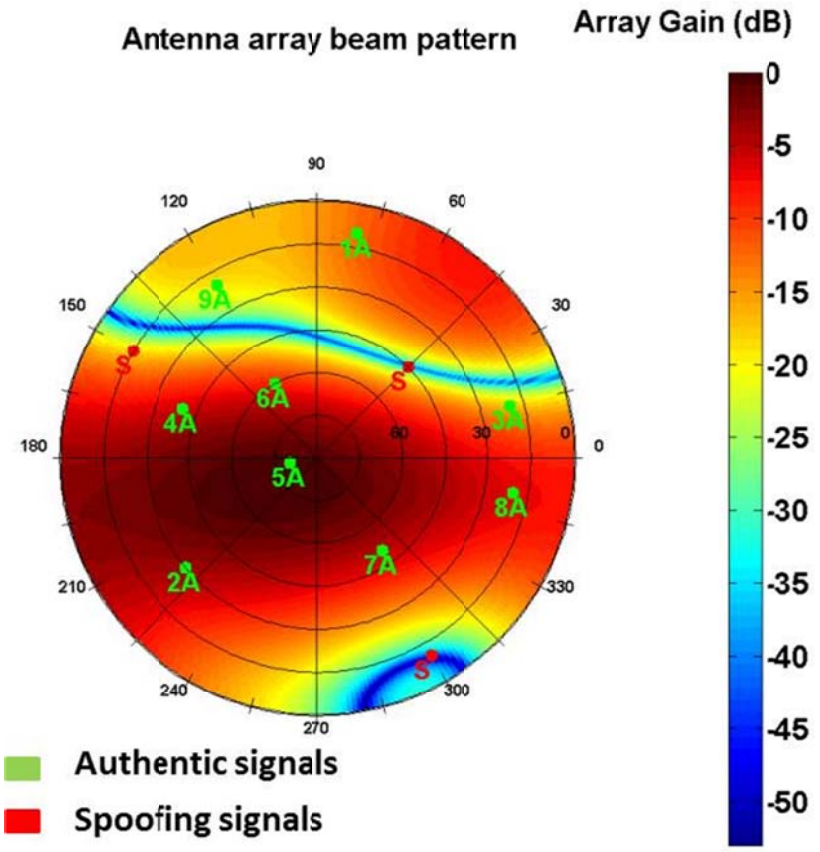

Figure 6-7: Polar beam pattern with respect to azimuth and elevation (the spoofing LOS signal and two multipath components)

The next simulation evaluates the validation of approximation in (6.23). For simplicity, $L_{ch} = 0,\ K_s = 1$ and only a LOS spoofing component is assumed. In Figure 6-8, a Monte-Carlo simulation is performed to show the result for the inner product between vectors of the estimated channel coefficient from (6.23) and the actual one ($\bar{\mathbf{a}}_0^0$) after normalization as a function of the spoofing to authentic power ratio (SAPR). SAPR is the ratio of the average power of spoofing PRNs to average power of authentic signals. This simulation is performed for 10,000 runs and in each run nine authentic signals impinge on the

antenna array from different random azimuth and elevation angles and their corresponding C/N_0 is assumed to be 45 dB-Hz. The simulation has been repeated for different numbers of spoofing PRNs which is shown with N_{spoof}. It is observed that the inner product between the two vectors approaches unity as the SAPR increases. Essentially, the spoofing attack can be considered as a threat if its power is equal to or is higher than the authentic signals power (i.e. SAPR $\geq$ 0 dB). It is observed that the inner product of these two vectors is higher than 0.9 for different numbers of simulated spoofing PRNs for the region where a spoofing attack can considered as a threat.

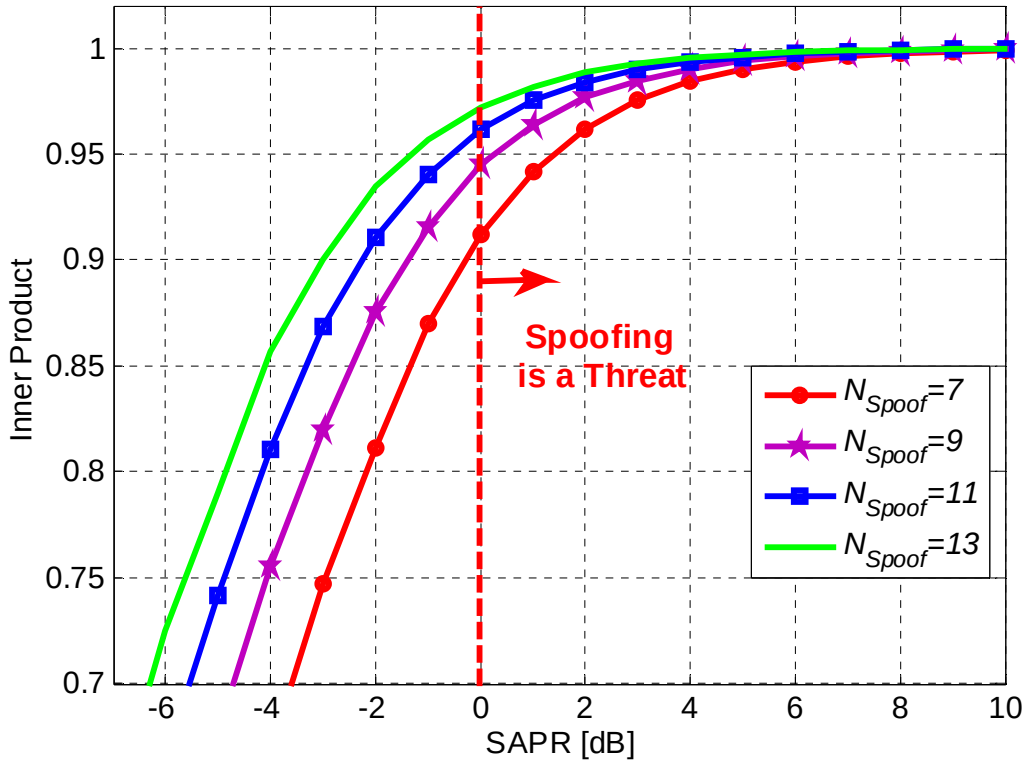

Figure 6-8: Inner product of the estimated channel coefficient vector and the actual one as a function of SAPR

In the final simulation, in order to show the overall improvement of the proposed method, a Monte-Carlo simulation is performed over 1000 runs for different spoofing power levels. Figure 6-9 shows the average SNR of the PRN codes for the authentic signals, the spoofing LOS and its multipath component as a function of the average input power of the spoofing PRN codes for both a single antenna receiver and the proposed spoofing mitigation technique. The multipath delay is randomly selected between 0 to 5 chips in each run and its average power is 3 dB lower than that of the LOS spoofing component. The transmit direction, the code delay and the Doppler frequency shift of the spoofing and authentic PRN codes are randomly changed during each run. The SNRs are calculated as the ratio of average authentic/spoofing PRN powers (after applying the null steering stage) to the output power of a noise floor estimator that correlates the received signal with a normalized fictitious PRN over 1 ms (Kaplan & Hegarty 2006). In the case of the single antenna receiver, it is observed that the authentic signals' SNR decreases as the input spoofing power increases. This is due to the higher receiver noise floor due to the cross correlation terms caused by the higher power spoofing PRNs. At the same time, the SNR of the spoofing PRNs for both the LOS and multipath components increases as the power of the spoofing PRNs increases. In this case, a conventional receiver will mistakenly acquire the spoofing correlation peak instead of the authentic one. Considering the proposed null steering method, it is observed that as the spoofing power increases the average SNR of the authentic signals almost remains constant while the spoofing SNR for both LOS and multipath components is always far below the detection threshold. Hence, this method not only attenuates the spoofing correlation peaks of the

LOS and its multipath components but also significantly reduces the effect of spoofing cross correlation terms that increase the receiver noise floor.

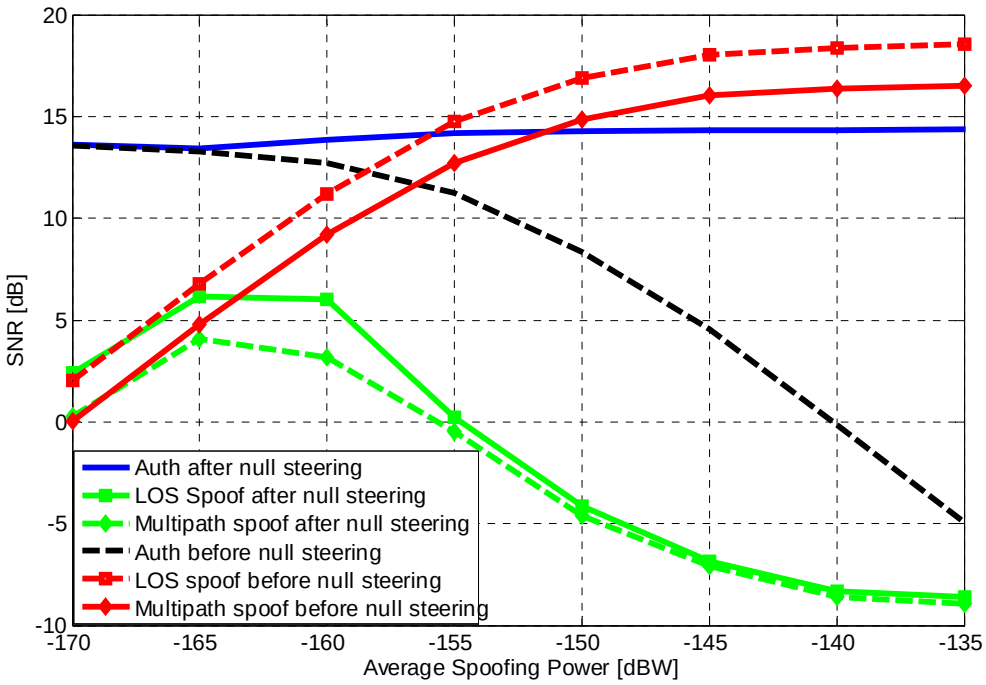

Figure 6-9: Authentic and spoofing SNR before and after spoofing mitigation as a function of average input spoofing power

6.5 Experimental results

Due to frequency regulations, special considerations are necessary when testing the performance of anti-spoofing techniques in the presence of real GNSS signals. Some previous work has suggested indoor signal re-transmission or combining the recorded spoofing signals to the received authentic ones without any propagation (Montgomery et al 2009, Humphreys et al 2008).

In order to show the effectiveness of the proposed method under some imperfect conditions, a real data test was performed. Figure 6-10 shows the test scenario where a three-element antenna array was placed in a laboratory where a spoofing signal (GPS L1 C/A) and one multipath component were generated by a hardware simulator. The delay of the multipath component was chosen as 3.1 chips. The generated signals were propagated by two highly directional antennas from different directions and received by the antenna array and then passed through a three-channel RF front-end. Previously recorded GPS L1 signals (collected by the same antenna configuration under open sky condition) were then added to the collected spoofing samples in software. This scenario models a spoofing attack in an environment where one resolvable multipath component and several non-resolvable ones also exist.

Figure 6-10: Real data collection test setup

In the second stage of the proposed method, the channel coefficients of the spoofing signal are estimated. Absolute values of estimated channel coefficients for the LOS and its multipath components of the spoofing signal are shown in Figure 6-11. As expected, in addition to the LOS component, the recognizable channel coefficients for the delay of 3 (stronger) and 4 (weaker) chips show the presence of a reflection of the spoofing signal, which corresponds to the delay of 3.1 chips set in the hardware simulator.

Figure 6-12 shows the antenna array polar beam pattern after the null steering stage. Although the array was not calibrated and therefore, the beam pattern is not directly related to the direction of the incident signals, two deep nulls can be recognized, which are related to the direction of the spoofing signal and its reflection.

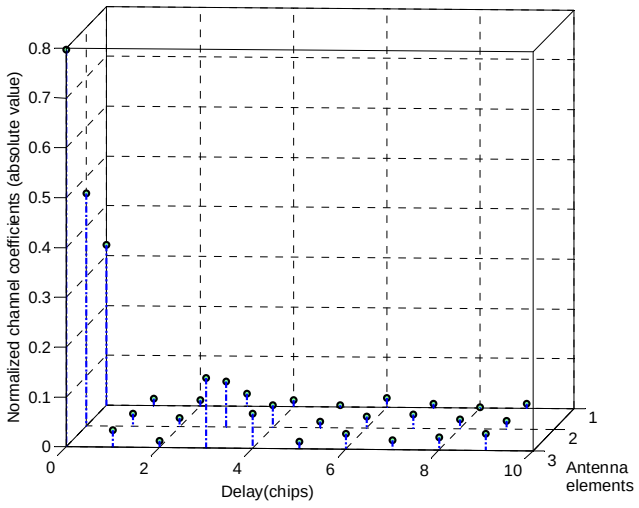

Figure 6-11: Absolute values of estimated channel coefficients for the LOS and its multipath components of the spoofing signal

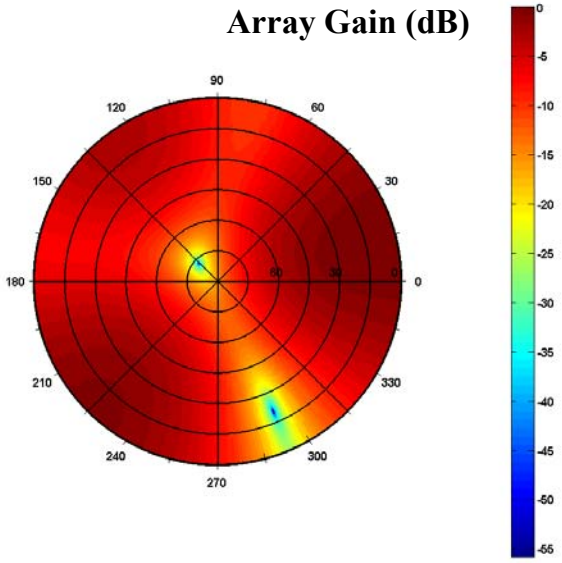

Figure 6-12: Antenna array polar beam pattern

Figure 6-13 shows the CAF for PRN 7, which is a common PRN for the authentic and spoofing scenarios, before and after spoofing mitigation. In Figure 6-13a, the CAF before spoofing mitigation is shown. It is observed that the presence of the spoofing signal and its reflection has increased the receiver noise floor, which results in the complete deterioration of the authentic signal acquisition. In Figure 6-13b, the CAF after mitigation of the spoofing LOS signal is shown. In this case, although the authentic peak can be seen, it is not strong enough compared to the spoofing multipath peak to be acquired. Figure 6-13c shows the CAF after nullifying the LOS and multipath components of the spoofing signal. In this case, the spoofing signal and its reflection are suppressed and furthermore, the elevated noise floor caused by the spoofer is discarded such that the authentic signal can be detected in the acquisition process.

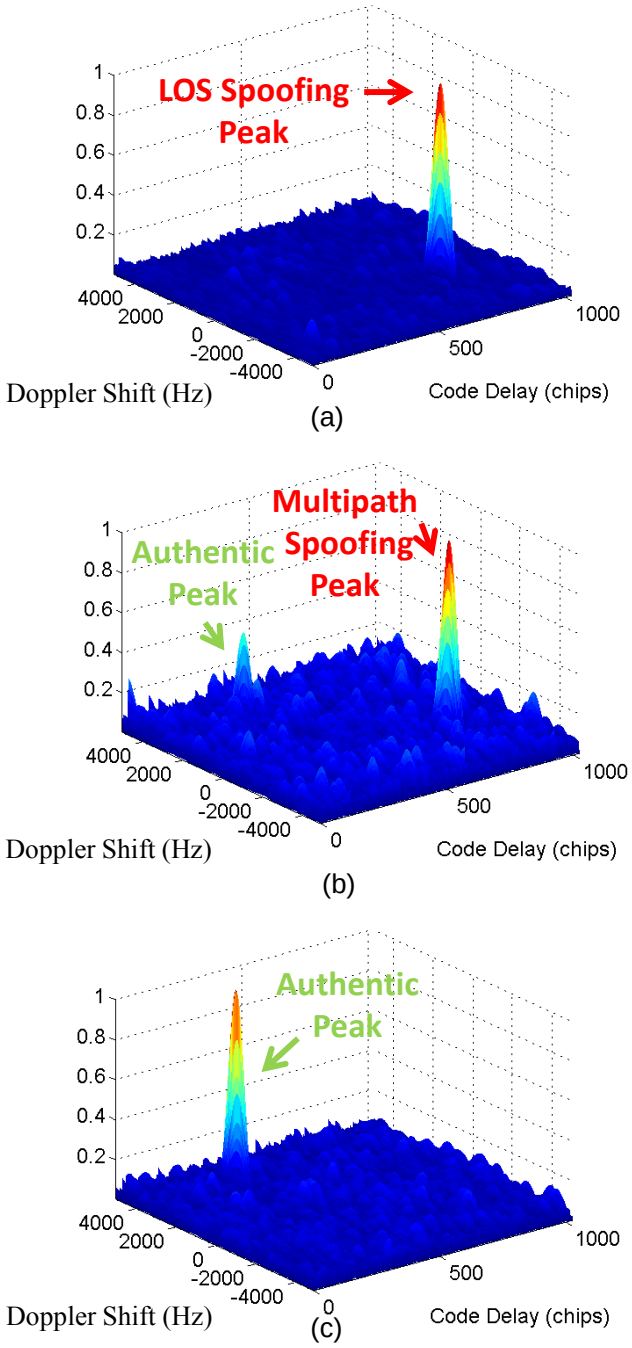

Figure 6-13: Normalized CAF of PRN10 (a) before spoofing mitigation (b) after LOS spoofing mitigation (c) after mitigation of LOS and multipath components of the spoofing signal

In order to further investigate the effectiveness of the proposed technique in the position domain, the intermediate frequency samples were analyzed using the GSNRx™ GNSS software receiver (Petovello et al 2008). This receiver operates on the sampled IF GNSS signals in order to extract position, velocity and timing (PVT). For various cases, the results verified that not only could the spoofing LOS component result in fake PVT solutions, but also the multipath component was able to mislead the receiver into generating fake PVT solutions. However, after nullifying both spoofing LOS and multipath components, the correct PVTs were obtained by the software receiver.

6.6 Summary

This chapter proposed a spoofing mitigation method based on a spatial-temporal process that has a low computational complexity and processing time without requiring separate despreading of different PRN codes. This is in contrast with conventional spoofing mitigation techniques, which first require despreading of all PRN codes and then detection and mitigation of spoofing signals. The proposed space-time processing method removes the spoofing signal LOS component as well as its multipath reflections and decreases the elevated noise floor caused by the spoofer. Although the problem is formulated for the calibrated antenna array, the directions of the incident signals are not required for this method and it can be easily verified that this technique is also applicable for non-calibrated array. These features make this method suitable for real-time applications and it can be either employed as an inline standalone pre-processing unit for

conventional GPS receivers or easily integrated into the next generation of low cost GPS receivers. It can also be easily extended to other GNSS signal structures such as Galileo.

Chapter Seven: CONCLUSIONS AND RECOMMENDATIONS

This chapter provides the conclusions of this thesis regarding antenna array capabilities and considerations for suppressing different types of interference. Recommendations for possible future work in this context are then presented to further extend and develop the proposed methods.

7.1 Conclusions

The following conclusions can be drawn from this research.

7.1.1 GNSS multipath mitigation

The nature of multipath signals results in their high correlation with the LOS signal and they are also received with low power. Therefore, a successful multipath mitigation approach should be performed after the despreading process in acquisition and tracking stages of a GNSS receiver. Although the despreading process completely suppresses the resolvable multipath components, it is not useful for non-resolvable ones.

In Chapter 3, it was shown that both the coherent and correlated multipath components could degrade the performance of conventional beamformers or even cause a complete failure in beamforming. It was shown that coherent multipath components caused rank deficiency of the temporal correlation matrix and the correlated components resulted in the signal cancelation phenomenon. It was also shown that a successful beamformer should alleviate both issues in order to combat multipath propagation and to provide a distortionless response in the direction of the desired signals. Based on these facts,

Chapter 3 proposed a new method to deal with the correlated and coherent multipath components which employs a combination of pre-spatial filtering and spatial smoothing techniques. This method used several overlapping subarrays and the spatial smoothing technique to avoid the rank deficiency of the temporal correlation matrix and then, by pre-gaining and taking the difference between signals of the subarrays, excluded the LOS signal power from the optimization problem and consequently avoided the signal cancelation phenomenon. This method requires prior knowledge of the LOS signal steering vector and consequently of the antenna array orientation, which may limit its applicability in some situations. Moreover, employing the overlapping subarrays requires at least one antenna element per each additional subarray. This method is able to mitigate multipath for both static and kinematic scenarios by putting deep nulls in the direction of the multipath components in the antenna array beam pattern.

Another new method proposed in Chapter 4 for dealing with coherent and correlated multipath components employs a moving antenna array to decorrelate the coherent multipath components and then spatial pre-filtering to estimate the multipath subspace and completely nullify the multipath signals. Furthermore, a moving antenna array was implemented in order to synthesize a bigger antenna array and consequently to increase the degree of freedom of the antenna array without increasing the number of physical antenna elements. Although this method outperforms the previous approach in terms of the degree of freedom, it is only applicable in kinematic scenarios such as vehicular applications. Prior knowledge about LOS steering vectors is required for this method as well.

7.1.2 GNSS high power narrowband and wideband interference mitigation

One effective approach utilized in this thesis to deal with high power narrowband and wideband interference signals is to mitigate them before despreading in the spatial domain processing. It was shown that contrary to the time and frequency domain processing, a wideband interfering signal could be suppressed in the spatial processing domain by steering a null toward its direction regardless of its time and frequency characteristics.

Research conducted in Chapter 5 showed that besides the superior advantages of combining the spatial and temporal processing domains in interference mitigation, the distortion and bias caused by such processing should be carefully considered. In the method proposed in Chapter 5, the periodicity of GNSS signals was employed as an effective approach to design a distortionless space-time filter in which the degree of freedom is increased for suppressing narrowband interfering signals such as intentional tone jammers or harmonics originating from any electronic systems and amplifiers operating in non-linear regions. It was shown that the conventional space-time techniques may not completely suppress distortion and at the same time avoid the severe degradation in SINR due to rank deficiency in the optimization problem. The use of the periodic feature of GNSS signals in the space-time filter structure suppressed interference without causing distortion on the cross correlation function and rank deficiency in the optimization problem. Prior knowledge about the steering vector of the LOS signal is required in this method. Another similar approach suggested in this chapter did not

require this prior information and was referred to as the blind beamformer. This algorithm takes advantage of the periodicity to increase the degree of freedom but the SINR decreased compared to the previous algorithm due to unintentional attenuation of the GNSS signals.

7.1.3 GNSS spoofing mitigation

Although a spoofing signal is similar to GNSS multipath components in many aspects, the spatial characteristics of a spoofing signal makes it possible to distinguish it from authentic signals before the despreading process and put a null in its direction in the antenna array beam pattern. This significantly reduces the processing time and computational complexity. A method was proposed based on space-time processing to mitigate the spoofing signal and its multipath components without requiring to despread different PRN codes of spoofing and authentic signals. The proposed space-time processing method suppresses the spoofing signal LOS component and its multipath reflections and reduces the elevated noise floor caused by the spoofer. There is no need to antenna array calibration or knowledge about the spoofing and authentic steering vectors. These features make this method suitable for real-time applications and, therefore, it can be either employed as a standalone pre-processing unit connected between a GNSS receiver and the antenna array or it could be easily integrated into the next generation receivers.

7.2 Recommendations

Considering the presented theoretical, simulations and experimental results obtained herein, the following recommendations for future work can be made:

1 In this thesis, simulations and practical tests were limited to GPS L1. Although the facts on which the proposed methods were developed are the same for other GNSS signals, different modifications and considerations may be required for each case. Applying the modified methods for other GNSS signals, simulating and performing real data tests are recommended as a further development of the research conducted herein. Especially, testing the anti-spoofing method proposed in Chapter 6 would be interesting for military codes and modernized GNSS signals such as L1/L2 P(Y) and L1/L2 M, L5, E6B, E5a, E5b codes which employ higher chip rates and in multipath environments such as urban canyons their multipath delay might be several chips.

2 In many parts of this research, the steering vectors of the LOS GNSS signals are required as a priori knowledge. In order to verify the applicability and effectiveness of most methods, calibration was not needed; however, for an evaluation of these methods in the position domain, a calibrated antenna array is required, which means that knowledge about the array configuration and orientation is needed. Using the GNSS signals for calibration, along with an

inertial measurement unit (IMU) to measure antenna array orientation, is recommended in order to evaluate the proposed methods in the position domain.

3 In Chapter 5, a distortionless space-time processing technique based on the periodicity of GNSS signals was proposed. It was assumed that the data bits and Doppler frequencies were removed beforehand. The knowledge of the steering vectors was required for best performance. These facts may limit the applicability of this technique. This problem could be resolved by investigating a multi-stage interference suppression unit. This unit would consist of three stages which employ Methods 1, 3 and 4 in Section 5.4. The main features of these methods are repeated here as follows:

a. Method 1: By employing the space-time power minimization approach, interference is suppressed and the DOF of the filter increases although the cross correlation function may be considerably distorted.

b. Method 3: The steering vectors of the GNSS signals are employed in the structure of the space-time filter. The cross correlation functions are still distorted; however, the amount of distortion is less compared to the Method 1. Moreover, employing the spatial information of the incident signals leads to an increase in the SINR.

c. Method 4: By employing the inherent periodicity of the GNSS signals, a distortionless space-time filter can be obtained. This method requires the

knowledge of the steering vectors and Doppler frequencies of the GNSS signals.

In the first stage of the recommended interference suppression unit, Method 1 would be employed for interference suppression. Although the cross correlation functions are distorted, the accuracy is good enough to acquire and track the GNSS signals. In this stage, aiding from IMU sensors, position solutions and satellite positions extracted from almanac data, the steering vectors of the GNSS signal could be estimated. Then, the interference suppression unit enters into the second stage. In this stage, Method 3 for interference mitigation would be employed, which utilizes knowledge about the GNSS signal steering vectors estimated in the first stage to reduce the amount of distortion on the cross correlation functions. Therefore, more accurate estimates of Doppler frequencies and steering vectors of GNSS signals could be obtained. Afterwards, by removing data bits and Doppler frequencies, the interference suppression unit enters the third stage. In this stage, Method 4 would be used for interference suppression, which employs the periodic feature of the GNSS signals in the structure of the space-time filter and therefore, the distortion in the cross correlation functions would be reduced to an insignificant level for high precision GNSS applications.

4 The methods proposed in this thesis are based on space or space-time processing techniques and it is implicitly or explicitly assumed that the environment is stationary. This may limit the application of these methods. Although adaptive

antenna array processing is not considered in this thesis, the proposed method can be developed and extended to the adaptive cases in which changes in the environment are followed. Generally, there are two adaptive approaches, namely block adoption and continuous adoption. For a non-stationary environment block adoption is preferred whereas the latter is usually used when statistics are time varying. For the block adoption, the correlation matrix and the calculated weights are recomputed periodically. In the continuous adoption, LMS and RLS adaptive methods can be employed (Van Veen & Buckley 1988).

5 In order to evaluate the proposed methods in the position domain, proper software and hardware implementation are required. A portable multi-channel RF front-end with synchronized channels provides the opportunity for performing more tests and evaluations on the introduced methods. This RF front-end can provide row IF samples for further processing in any GNSS software receivers supporting antenna array processing. Therefore, implementing the proposed methods into these software receivers provides an opportunity to further evaluate the proposed methods in many practical applications. Moreover, if in addition to the multi-channel RF front-end, the hardware platform is also equipped with a digital processing core such as a DSP or FPGA, methods such as the anti-spoofing technique introduced in Chapter 6, which does not need to be implemented inside the GNSS receiver structure, could be tested and evaluated independently from GNSS receivers.

References

Abed-Meraim, K., P. Duhamel, D. Gesbert, L. Loubaton, S. Mayrargue, E. Moulines and D. Slock (1995) "Prediction error methods for time-domain blind identification of multichannel FIR filter," *In Proceedings of the IEEE International Conference on Acoustics, Speech, and Signal Processing (IEEE ICASSP 1995)*, 9-12 May, Detroit, MI, pp. 1968-1971

Agamata, B. N. (1991) "Time Domain Adaptive Filter Implementation of a Minimum Variance Distortionless Response (MVDR) Beamformer for a Sensor Array" In *Proceedings of the 4th International Technical Meeting of the Satellite Division of The Institute of Navigation (ION GPS 1991)*, 11-13 September, Albuquerque, NM, pp. 443-452

Amin, M. G. and W. Sun (2005) "A novel interference suppression scheme for global navigation satellite systems using antenna array," *IEEE Journal on Selected Areas in Communications*, vol 23, no 5, May, pp. 999-1012

Amin, M. G., L. Zhao and A. R. Lindsey (2004) "Subspace array processing for the suppression of FM jamming in GPS receivers" *IEEE Transactions on Aerospace and Electronic Systems*, vol 40, no 1, January, pp. 80-92

Applebaum, S. P. (1976) "Adaptive arrays" *IEEE Transactions on Antennas and Propagation*, vol 24, no 5, September, pp. 585-598

Backen, S., D. M. Akos, and M. L. Nordenvaad (2008) "Post-Processing Dynamic GNSS Antenna Array Calibration and Deterministic Beamforming," in *Proceedings of the 21st International Technical Meeting of the Satellite Division*, 16-19 September, Savannah, GA, pp. 2806-2814

Badke B., and A. Spanias (2002) "Partial band interference excisions for GPS using frequency-domain exponents" *In Proceedings of the IEEE International Conference on Acoustics, Speech, and Signal Processing (IEEE ICASSP 2002)*, 13-17 May, Orlando, FL, pp. 3936-3939

Basta, N., A. Dreher, S. Caizzone, M. Sgammini, F. Antreich, G. Kappen, S. Irteza, R. Stephan, M. A. Hein, E. Schafer, A. Richter, M. A. Khan, L. Kurz, and T. G. Noll (2012) "System Concept of a Compact Multi-Antenna GNSS Receiver," *7th German Microwave Conference (GeMiC)*, 12-14 March, Ilmenau, Germany, pp. 1-4

Borio D. (2008) *A Statistical Theory for GNSS Signal Acquisition,* Doctoral Thesis, Dipartimento di Elettronica, Politecnico di Torino, Italy

Borio, D. (2010) "GNSS Acquisition in the Presence of Continuous Wave Interference", *IEEE Transactions on Aerospace and Electronic Systems*, vol 46, no 1, January, pp. 47–60

Brennan, L. E. and L. S. Reed (1973) "Theory of Adaptive Radar" *IEEE Transactions on Aerospace and Electronic Systems*, vol 9 no 2, March, pp. 273-252

Bresler, Y., V. U. Reddy, and T. Kailath (1988) "Optimum beamforming for coherent signal and interferences" *IEEE Transactions on Acoustic, Speech, Signal Processing*, vol 36, no 6, June, pp. 833-843

Broumandan, A., and T. Lin (2008) "Performance of GNSS Time of Arrival Estimation Techniques in Multipath Environments" *Proceedings of ION GNSS 2008*, 16-19 September Savannah, GA, USA, pp. 632–643

Broumandan, A., J. Nielsen, and G. Lachapelle (2008) "Practical results of high resolution AOA estimation by the synthetic Array," In *IEEE Vehicular Technology Conference*, 21-24 September, Calgary AB, Canada, pp. 1-5

Broumandan, A., Nielsen, J., and G. Lachapelle (2010) "Signal detection performance in rayleigh multipath fading environments with a moving antenna", *IET Signal Processing*, vol. 4, no. 2, April, pp. 117–129

Brown, A. (2000) "Multipath Rejection Through Spatial Processing," in *Proceedings of ION GPS 2000*, 19-22 September, Salt Lake City, UT, pp. 2330 - 2337

Brown, A. and N. Gerein (2001) "Test Results of a Digital Beamforming GPS Receiver in a Jamming Environment," in *Proceedings of ION GPS 2001*, 11-24 September, Salt Lake City UT, pp. 894-903

Buckley, K. M. and L. J. Griffiths (1986) "An adaptive generalized sidelobe canceller with derivative constraints" *IEEE Transactions on Antennas Propagation*, vol AP-34, March, pp.311-319

Capon, J. (1969) "High-Resolution Frequency-Wavenumber Spectrum Analysis," in *Proceedings of the IEEE*, vol 57, no 8, August, pp. 1408-1419

Chang, C. L., and J. C. Juang (2010) "Performance analysis of narrowband interference mitigation and near-far resistance scheme for GNSS receivers," *Signal Processing, Elseveir*, vol 90, no 9, September, pp. 2676-2685

Chang, L. and C. Yeh (1992) "Performance of DMI and eigenspace-based beamformers" *IEEE Transactions on Antennas Propagation*, vol 40, no 11, November, pp. 1336-1347

Church, C. M. and I. J. Gupta (2009) "Calibration of GNSS Adaptive Antennas," in *Proceedings of the 22nd International Meeting of the Satellite Division of The Institute of Navigation*, 22-25 September, Savannah, GA, pp. 344-350

Church, C., I. Gupta and A. O'Brien (2007) "Adaptive Antenna Induced Biases in GNSS Receivers," *Proceedings of the 63rd Annual Meeting of The Institute of Navigation*, 23-25 April, Cambridge, MA, pp. 204-212

Citron, T. K. and T. Kailath (1984) “An improved eigenvector beamformer,” *Acoustics, Speech, and Signal Processing, IEEE International Conference on ICASSP 84*, 19-21 March, San Diego CA, pp. 718-721

Closas, P., C., Fernandez-Prade, and J. A. Fernandez-Rubio(2006) “Bayesian DLL for Multipath Mitigation in Navigation Systems Using Particle Filters,” In *Proceeding of IEEE ICASSP 06*, 14-19 May, Toulouse, France, pp. 129-132

Cuntz, M., A. Konovaltsev, M. Sgammini, C. Hattich, G. Kappen, M. Meurer, A. Hornbostel, and A. Dreher, (2011) “Field Test: Jamming the DLR Adaptive Antenna Receiver,” in *Proceedings of the 24th International Technical Meeting of The Satellite Division of the Institute of Navigation (ION GNSS 2011)*, 20-23 September, Portland, OR, pp. 384-392

Daneshmand, S., A. Broumandan and G. Lachapelle (2011a) “GNSS Interference and Multipath Suppression Using Array Antenna,” *in Proceedings of the 24th International Technical Meeting of the Satellite Division of the Institute of Navigation (ION GNSS 2011)*, 20-23 September, Portland, OR, pp. 1183-1192

Daneshmand, S., A. Broumandan, J. Nielsen and G. Lachapelle (2013a) “Interference and multipath mitigation utilising a two-stage beamformer for global navigation satellite systems applications” *IET Radar, Sonar and Navigation Journal,* vol 7, no 1, January, pp. 55-66

Daneshmand, S., A. Broumandan, N. Sokhandan and G. Lachapelle (2013b) “GNSS Multipath Mitigation with a Moving Antenna Array” *Published in IEEE Transactions on Aerospace and Electronic Systems*, vol 49, no 1, January, pp. 693-698

Daneshmand, S., A. Jafarnia, A. Broumandan and G. Lachapelle (2011b) “A Low Complexity GNSS Spoofing Mitigation Technique Using a Double Antenna Array” *GPS World*, vol 22, no 12, December, pp. 44-46

Daneshmand, S., A. Jafarnia, A. Broumandan and G. Lachapelle (2013c) "GNSS spoofing mitigation in multipath environments using space-time processing" *accepted to the European navigation conference (ENC) 2013*, 23-25 April, Vienna, Austria, 10 pages

Daneshmand, S., A. Jahromi, A. Broumandan and G. Lachapelle (2012) "A Low-Complexity GPS Anti-Spoofing Method Using a Multi-Antenna Array" *in Proceedings of the 25th International Technical Meeting of The Satellite Division of the Institute of Navigation (ION GNSS 2012)*, 17-21 September, Nashville TN, 11 pages

De Lorenzo, D. S. (2007), *Navigation accuracy and interference rejection for GPS adaptive antenna arrays*, Doctoral Thesis, Department of aeronautics and astronautics, Stanford University

De Lorenzo, D. S., F. Antreich, H. Denks, A. Hornbostel, C. Weber and P. Enge (2007) "Testing of Adaptive Beamsteering for Interference Rejection in GNSS Receivers," *Proc. of ENC GNSS 2007*, 29 May-1 June Genf, Switzerland, 11 pages

De Lorenzo, D. S., J. Gautier, J. Rife, P. Enge and D. Akos (2005) "Adaptive Array Processing for GPS Interference Rejection," *Proceedings of the 18th International Technical Meeting of the Satellite Division of The Institute of Navigation (ION GNSS 2005)*, 13-16 September 2005, Long Beach, CA, pp. 618-627

De Lorenzo, D. S., J. Rife, J., P. Enge, and D. M. Akos (2006) "Navigation Accuracy and Interference Rejection for an Adaptive GPS Antenna Array" In *Proceedings of the 19th International Technical Meeting of the Satellite Division of the Institute of Navigation (ION GNSS 2006)*, 26-29 September, Fort Worth, TX, pp. 763-773

De Lorenzo, D. S., S. C. Lo, P. K. Enge and J. Rife (2012) "Calibrating adaptive antenna arrays for high-integrity GPS," *GPS solution*, vol 16, no 2, April, pp. 221-230

Deergha Rao, K., and M. N. S. Swamy (2006) "New approach for suppression of FM jamming in GPS receivers" *IEEE Transactions on Aerospace and Electronic Systems*, vol 42, no 4, October, pp. 1464-1474

Ding, Z. (1997) "Matrix Outer-Product Decomposition Method for Blind Multiple Channel identification," *IEEE Transactions on Signal Processing*, vol 45, no 12, December, pp. 3053-3061

Ding, Z. and Y. Li (2000) *Blind equalization and identification*, Marcel Dekker, Inc., New York, Basel

Draganov, S., M. Harlacher, L. Haas, M. Wenske and C. Schneider (2011) "Synthetic aperture navigation in multipath environments," *IEEE Trans. Wireless Communications*, vol 18, no 2, April, pp. 52-58

Duvall, K. M. (1983) *Signal cancellation in adaptive antennas: The phenomenon and a remedy*, PhD Thesis, Department of electrical Engineering, Stanford University, USA

Er, M. H. and A. Cantoni (1985) "An alternative formulation for an optimum beamformer with robustness capability" In *Communications, Radar and Signal Processing, IEE Proceedings*, vol 132, no 6, October, pp. 447-460

Evans, J. E., J. R. Johnson, and D. F. Sun (1982) *Application of advanced signal processing techniques to angle of arrival estimation in ATC navigation and surveillance systems*, Technical Report No. 582, M.I.T. Lincoln Laboratory, Lexington, Massachusetts, 386 pages

Falcone, K., N. B. Jarmale, F. Allen and J. Clark (2000) "GPS Anti-Jam for CAT II Landing Applications," *Proceedings of the 13th International Technical Meeting of the Satellite Division of The Institute of Navigation (ION GPS 2000)*, 19-22 September, Salt Lake City, UT, pp. 1301-1308

Falcone, K., N. B. Jarmale, F. Allen, and J. Clark (2000) "GPS Anti-Jam for CAT II Landing Applications," In *Proceedings of the 13th International Technical Meeting of the Satellite Division of The Institute of Navigation (ION GPS 2000)*, 19-22 September, Salt Lake City, UT, pp. 1301-1308

Fante, R. L., and J. J. Vaccaro (1998a) "Cancellation of jammers and jammer multipath in a GPS receiver", *IEEE Aerospace and Electronic Systems Magazine*, vol. 13, no. 13, November, pp. 25–28

Fante, R. L., and J. J. Vaccaro (1998b) "Cancellation of jammers and jammer multipath in a GPS receiver," *Position Location and Navigation Symposium, IEEE 1998*, 20-23 April, Palm Springs, CA, pp. 622–625

Fante, R. L., and J. J. Vaccaro (2000) "Wideband Cancellation of Interference in a GPS Receive Array," *IEEE Transactions on Aerospace and Electronic Systems*, vol 36, no 2, April, pp. 549–564

Fante, R. L., M. P. Fitzgibbons and K. F. McDonald (2004) "Effect of Adaptive Array Processing on GPS Signal Crosscorrelation" *Proceedings of the 17th International Technical Meeting of the Satellite Division of The Institute of Navigation (ION GNSS 2004)*, 21-24 September, Long Beach, CA, , pp. 579-583

Feldman, D. D. and L. J. Griffiths (1991) "A constraint projection approach for robust adaptive beamforming," *Acoustics, Speech, and Signal Processing, IEEE International Conference on ICASSP 91*, 14-17 April, Toronto ON, pp.1381–1384

Feldman, D. D. and L. J. Griffiths (1994) "A projection approach for robust adaptive beamforming," *IEEE Transactions on Signal Processing*, vol 42, no 4, April, pp. 867–876

Friedlander, B. (1988) “A signal subspace method for adaptive interference cancellation,” *IEEE Transactions on Acoustic, Speech, Signal Processing*, vol 36, no 12, December, pp. 1835–1845

Frost, O. L. (1972) “An Algorithm For Linearly Constrained Adaptive Array Processing,” *proceedings of the IEEE*, vol 60, no 8, August, pp. 926-935

Garin, L. and J. M. Rousseau (1997) “Enhanced strobe correlator multipath rejection for code & carrier,” in *Proceedings of the 10th International Technical Meeting of the Satellite Division of the Institute of Navigation (ION GPS ’97)*, 16-19 September, Kansas City MO, USA, pp. 559–568

Godara, L. C. (1990) “Beamforming in the presence of correlated arrivals using structured correlation matrix” *IEEE Transactions on Acoustic, Speech, Signal Processing*, vol 38, no 1, January, pp. 1-15

Grabowski, J. C. (2012) “Personal Privacy Jammers” in *GPS World Magazine*, April, vol. 23, no. 4, pp. 28-37

Gupta, I. J. and T. D. Moore (2004) “Space-Frequency Adaptive Processing (SFAP) for Radio Frequency Interference Mitigation in Spread-Spectrum Receivers”, *IEEE Transactions on Antennas and Propagation*, vol 52, no 6, June, pp. 1611-1615

Gupta, I. J., J. R. Baxter, S. W. Ellingson, H. G. Park, H. S. Oh, and M. G. Kyeong (2003) “An experimental study of antenna array calibration” in *IEEE Transactions on Antennas and Propagation*, vol 51, no 3, March, pp. 664-667

Haber, F. and M. Zoltowski (1986) “Spatial spectrum estimation in a coherent signal environment using an array in motion,” *Transactions on Antennas and Propagation*, vol 34, no 3, March, pp. 301–310

Haimovich, A. M. and Y. Bar-Ness (1988) "Adaptive antenna arrays using eigenvector methods," *In IEEE Antennas and Propagation Society International Symposium*, 6-10 June, Syracuse NY, pp. 980-983

Haimovich, A. M. and Y. Bar-Ness (1991) "An eigen analysis interference canceller," *IEEE Transactions on Acoustic, Speech, Signal Processing*, vol 39, no 1, January, pp. 76–84

Hartman, R. G. (1995) *Spoofing detection system for a satellite positioning system* US Patent 5557284, 13 pages

Hatke, G. F. (1998) "Adaptive array processing for wideband nulling in GPS systems," in *Proceedings of 32th Asilomar Conference Signals, Systems & Computers*, 1-4 November, Pacific Grove CA, pp. 1332–1336

Humphreys, T. E., B. M. Ledvina, M. L. Psiaki, B. W. O'Hanlon and P. M. Kintner (2008) "Assessing the Spoofing Threat: Development of a Portable GPS Civilian Spoofer" *ION GNSS 21st. International Technical Meeting of the Satellite Division*, 16-19 September, Savannah, GA, pp. 2314-2325

Hung, E. K. L. and R. M. Turner (1983) "A fast beamforming algorithm for large arrays" *IEEE Transactions on Aerospace Electronic Systems*, vol 19, no 4, July, pp. 598-607

Hwang S. S., and J. J. Shynk (2006) "Multicomponent receiver architectures for GPS interference suppression" *IEEE Transactions on Aerospace and Electronic Systems*, vol 42, no 2, April, pp. 489-502

Irsigler, M. and B. Eissfeller (2003) "Comparison of multipath mitigation techniques with consideration of future signal structures," in *Proceedings of the 16th International Technical Meeting of the Satellite Division of the Institute of Navigation*, 9-12 September, Portland OR, USA pp. 2584–2592

Jafarnia-Jahromi, A., A. Broumandan, J. Nielsen and G. Lachapelle (2012) “GPS Vulnerability to Spoofing Threats and a Review of Antispoofing Techniques” *in the International Journal of Navigation and Observation*, vol 2012, 16 pages

Jahn, A., H. Bischl and G. Heiss (1996) “Channel Characterisation for Spread Spectrum Satellite Communications, Spread Spectrum Techniques and Applications”, in *Spread Spectrum Techniques and Applications Proceedings IEEE 4th International Symposium*, 22-25 September, Mainz, pp. 1221-1226

Jang, J., M. Paonni, and B. Eissfeller (2012) “CW Interference Effects on Tracking Performance of GNSS Receivers”, *IEEE Transactions on Aerospace and Electronic Systems,* vol 48, no 1, January, pp. 243–258

Kalyanaraman, S. K., M. S. Braasch and J.M Kelly (2006), “Code tracking architecture influence on GPS carrier multipath” *IEEE Transactions on Aerospace and Electronic Systems,* vol 42, no 2, April, pp. 548-561

Kaplan, E. D. and C. J. Hegarty (2006) *Understanding GPS Principles and applications 2nd edition*, Artech House, Boston, London

Kappen, G., C. Haettich and M. Meurer (2012) "Towards a robust multi-antenna mass market GNSS receiver" in *Position Location and Navigation Symposium (PLANS), IEEE/ION*, 23-26 April, Myrtle Beach, SC, pp. 291-300

Kelly, J. M., M. S. Braasch (1999) “Mitigation of GPS Multipath via Exploitation of Signal Dynamics,” *Proceedings of the 55th Annual Meeting of The Institute of Navigation*, 27-30 June, Cambridge, MA, pp. 619-624

Kim, S. J. and R. A. Iltis (2004) “STAP for GPS receiver synchronization” *IEEE Transactions on Aerospace and Electronic Systems*, vol 40, no 1, January, pp. 132-144

Kirsteins, I. P. and D. W. Tufts (1985) "On the probability density of signal-to-noise ratio in an improved adaptive detector" *In Proceedings of the IEEE International Conference on Acoustics, Speech, and Signal Processing (IEEE ICASSP 1985)*, April, Tampa, Florida, pp. 572-575

Konovaltsev, A., D. S. De Lorenzo, A. Hornbostel and P. Enge (2008) "Mitigation of Continuous and Pulsed Radio Interference with GNSS Antenna Arrays," *Proceedings of the 21st International Technical Meeting of the Satellite Division of The Institute of Navigation (ION GNSS 2008)*, 16-19 September, Savannah, GA, pp. 2786-2795

Krim, H. and M. Viberg (1996) "Two Decades of Array Signal Processing Research," *IEEE Signal Processing Magazine*, vol 13, no 4, July, pp. 67-94

Ledvina, B. M., W. J. Bencze, B. Galusha and I. Miller (2010) "An In-Line Anti-Spoofing Device for Legacy Civil GPS Receivers" Institute of Navigation ITM, 26-28 January, San Deigo, CA, pp. 698 – 712.

Lu, D., Q. Feng and R. B. Wu (2006) "Survey on Interference Mitigation via Adaptive Array Processing in GPS" *in Electromagnetics Research Symposium 2006*, 26-29 March, Cambridge, USA, pp.722-727

Madhani, P., H., P. Axelrad, K. Krumvieda and J. Thomas (2003) "Application of successive interference cancellation to the GPS pseudolite near-far problem" *IEEE Transactions on Aerospace and Electronic Systems*, vol 39, no 2, April, pp. 481-488

McDonald, K. F., P. J. Costa and R. L. Fante (2006) "Insights into Jammer Mitigation Via Space-Time Adaptive Processing," *Proceedings of IEEE/ION PLANS 2006*, 25-27 April, San Diego, CA, pp. 213-217

McDonald, K. F., R. Raghavan, and R. Fante (2004) "Lessons Learned Through the Implementation of Space-Time Adaptive Processing Algorithms for GPS Reception in

Jammed Environments," *IEEE PLANS Conference Proceedings*, 26-29 April, pp. 418-428

McDowell, C. E. (2007) *GPS Spoofer and Repeater Mitigation System using Digital Spatial Nulling*, US Patent 7250903 B1, 7 pages

McGraw, G. A. and M. S. Braasch (1999) "GNSS multipath mitigation using gated and high resolution correlator concepts," in *Proceedings of The National Technical Meeting of the Satellite Division of the Institute of Navigation*, 25-27 January, San Diego CA, USA, pp. 333-342

McGraw, G. A., C. McDowell, J. M. Kelly (2006) "GPS Anti-Jam Antenna System Measurement Error Characterization and Compensation," In *Proceedings of the 19th International Technical Meeting of the Satellite Division of the Institute of Navigation (ION GNSS 2006)*, 26-29 September, Fort Worth, TX, pp. 705-714

McGraw, G.A., S. Y. Ryan Young, and K. Reichenauer (2004) "Evaluation of GPS Anti-Jam System Effects on Pseudorange and Carrier Phase Measurements for Precision Approach and Landing," In *Proceedings of the 17th International Technical Meeting of the Satellite Division of the Institute of Navigation (ION GNSS 2004)*, 21-24 September, Long Beach, CA, pp. 2742-2751

Melvin, W. L. (2004) "A STAP Overview" *IEEE Aerospace and Electronic Systems Magazine*, vol 19, no 1, January, pp. 19-35

Moelker, D. J. (1997) "Multiple antennas for advanced GNSS multipath mitigation and multipath direction finding," in *Proceedings of ION GPS 1997*, 16-19 September, Kansas City MO, pp. 541-550

Moelker, D. J., E. van der Pol and Y. Bar-Ness (1996) "Adaptive antenna arrays for interference cancellation in GPS and GLONASS receivers" In *IEEE Position Location and Navigation Symposium*, 22-26 April, Atlanta, GA, pp. 191-198

Montgomery, P. Y., T. E. Humphreys and B. M. Ledvina (2009) "Receiver-Autonomous Spoofing Detection: Experimental Results of a Multi-antenna Receiver Defense against a Portable Civil GPS Spoofer" *ION 2009 International Technical Meeting*, 26-28 January, Anaheim, CA, pp. 124-130

Motella, B., S. Savasta, D. Margaria, and F. Dovis (2011) "Method for Assessing the Interference Impact on GNSS Receivers", *IEEE Transactions on Aerospace and Electronic Systems*, vol. 47, no 2, April, pp. 1416–1432

Myrick, W. L., J. S. Goldstein, and M. D. Zoltowski (2001)"Low Complexity Anti-jam Space-Time Processing for GPS," " *In Proceedings of the IEEE International Conference on Acoustics, Speech, and Signal Processing (IEEE ICASSP 2001)*, 7-11 May, Salt Lake City, UT, pp. 2233-2236

Myrick, W. L., M. Zoltowski, and J. S. Goldstein (2000) "Exploiting conjugate symmetry in power minimization based pre-processing for GPS: reduced complexity and smoothness," in *Acoustics, Speech, and Signal Processing, IEEE International Conference on ICASSP 2000*, 5-9 June, Istanbul, Turkey, pp. 2833-2836

Ng, B. C. and C. M. S. See (1996) "Sensor-array calibration using a maximum-likelihood approach," in *IEEE Transactions on Antennas and Propagation*, vol 44, no 6, June, pp. 827-835

Nielsen, J., A. Broumandan and G. Lachapelle (2011) "GNSS Spoofing Detection for Single Antenna Handheld Receivers" *Journal of Navigation*, vol 58, no 4, Winter, pp. 335-344

Nielsen, J., A. Broumandan and G. Lachapelle, (2010) "Spoofing Detection and Mitigation with a Moving Handheld Receiver" in *GPS World magazine*, vol 21, no 9, September, pp. 27-33

O'Brien, A. J. and I. J. Gupta (2011) "Mitigation of adaptive antenna induced bias errors in GNSS receivers" *IEEE Transactions on Aerospace and Electronic Systems*, vol 47, no 1, January,pp. 524-538

Paulraj, A. J. and C. B. Papadias (1997) "Space-time processing for wireless communications" *IEEE Signal Processing Magazine*, vol 49, no 6, November, pp. 49-83

Petovello M., C. O'Driscoll, G. Lachapelle, D. Borio, and H. Murtaza (2008) "Architecture and Benefits of an Advanced GNSS Software Receiver" *Journal of Global Positioning Systems*, vol 7, no 2, December, pp. 156–168

Pickholtz, R. L., D. L. Schilling, and L. B. Milstein (1982) "Theory of spread-spectrum communications-a tutorial" *IEEE Transaction on Communication*, vol. 30, no. 5, May, pp. 855-884

Pillai, S. U. and B. H. Kwon (1989) "Forward/backward spatial smoothing techniques for coherent signal identification," *IEEE Transactions on Acoustic, Speech, Signal Processing*, vol 37, no 1, January, pp. 8-15

Poisel, R. (2004) *Modern communications jamming principles and techniques,* 1st ed., Artech House, Boston, Massachusetts

Raghunath, K. J., and V. U. Reddy (1992) "Finite data performance analysis of MVDR beamformer with and without spatial smoothing" *IEEE Transactions on Signal Processing*, vol 40, no 11, November, pp. 2726-2736

Ramos, J. and M. Zoltowski and M. Urgos (1996) "Robust blind adaptive array, a prototype for GPS" *IEEE International Symposium on Phased Array Systems and Technology*, 15-18 October, Boston, MA, pp. 406-410

Rensburg, C. V., and B. Friedlander (2004) "The Performance of a Null-Steering Beamforming in Correlated Rayleigh Fading," *IEEE Transaction on Signal Processing*, vol. 52, no. 11, November, pp. 3117-3125

Sahmoudi, M. and M. G. Amin (2007) "Optimal Robust Beamforming for Interference and Multipath Mitigation in GNSS Arrays," in *Acoustics, Speech, and Signal Processing, IEEE International Conference on ICASSP 2007*, 15-20 April, Honolulu HI , pp. 693-696

Sahmoudi, M., and M. G. Amin (2008) "Fast Iterative Maximum-Likelihood Algorithm (FIMLA) for Multipath Mitigation in the Next Generation of GNSS Receivers" *IEEE Transaction on Wireless Communication*, vol 7, no 1, November, pp. 4362-4373

Seco-Granados G., J. A. Fernández-Rubio, and C. Fernández-Prades (2005) "ML estimator and hybrid beamformer for multipath and interference mitigation in GNSS receivers" *IEEE Transactions on Signal Processing*, vol 53, no 10, March, pp. 1194-1208

Shan, T. J. and T. Kailath (1985) "adaptive beamforming for coherent signals and interference," *IEEE Transactions on Acoustic, Speech, Signal Processing*, vol 33, no 3, June, pp. 527–534

Slock, D. (1994) "Blind fractionally-spaced equalization, perfect reconstruction filter banks and multichannel linear prediction," *In Proceedings of the IEEE International Conference on Acoustics, Speech, and Signal Processing (IEEE ICASSP 1994)*, 19-22 April, pp. 585-588

Steingass, A. and A. Lehner (2004) "Measuring the Navigation Multipath Channel A Statistical Analysis," in *Proceedings of the 17th International Technical Meeting of the Satellite Division of The Institute of Navigation (ION GNSS 2004)*, Long Beach, CA, 21-24 September 2004, pp. 1157-1164.

Sun, W. and M. G. Amin (2005a) "A self-coherence anti-jamming GPS receiver" *IEEE Transactions on Signal Processing*, vol 53, no 10, October, pp. 3910–3915

Sun, W. and M. G. Amin (2005b) "Maximum signal-to-noise ratio GPS anti-jam receiver with subspace tracking," *Acoustics, Speech, and Signal Processing, IEEE International Conference on ICASSP 2005*, 18-23 March, Philadelphia, PA, USA, pp. 1085–1088

Tong, L. and Q. Zhao (1998) "Blind channel estimation by least squares smoothing," *In Proceedings of the IEEE International Conference on Acoustics, Speech, and Signal Processing (IEEE ICASSP 1998)*, 12-15 May, Seattle, WA, pp. 2121-2124

Townsend, B. R. and P. Fenton (1994) "A Practical approach to the reduction of pseudorange multipath errors in a L1 GPS receiver," in *Proceedings of the 7th International Technical Meeting of the Satellite Division of the Institute of Navigation (ION-GPS '94)*, 20-23 September, Salt Lake City, Utah, USA, pp. 143–148

Townsend, B., D. J. R. Van Nee, P. C. Fenton, and K. J. Van Dierendonck (1995) "Performance evaluation of the multipath estimating delay lock loop," *Navigation Journal of the Institute of Navigation*, vol 42, no 3, Fall, pp. 503-514

Tsai, C. J., J. F. Yang, and T. H. Shiu (1995) "Performance analyses of beamformers using effective SINR on array parameters" *IEEE Transactions on Signal Processing*, vol 43, no 1, January, pp. 300-303

Tsatsanis, M. K. and Z. Xu (1999) "Constrained Optimization Methods for Direct Blind Equalization," *IEEE Journal on selected areas in communications*, vol 17, no 3, March, pp. 424-433

Van Dierendonck, A. J., P. J. Fenton, and T. Ford (1992) "Theory and performance of narrow correlator spacing in a GPS receiver," *Journal of the Institute of Navigation*, vol 39, no 3, Fall,pp. 265–283

Van Nee, D. J. V. (1992) "The Multipath Estimating Delay Lock Loop," in *Proceedings of the IEEE 2nd International Symposium on Spread Spectrum Techniques and Applications*, November 29- December 2, Yokohama, Japan, pp. 39-42

Van Trees, H. L. (1966) “Optimum Processing for passive sonar arrays” in *Processing of IEEE Ocean Electronics symposium*, August 29-31, Honolulu, Hawaii, pp. 41-65

Van Trees, H. L. (2002) *Optimum Array Processing, Detection, Estimation, and Modulation Theory Part IV*, John Wiley & Sons, New York, pp. 428-699

Van Veen, B. D. and K. M. Buckley (1988) “Beamforming: a versatile approach to spatial filtering,” *IEEE ASSP Magazine*, vol 5, no 2, April, pp.4-24

Wen, H., P. Y. Huang, J. Dyer, A. Archinal and J. Fagan (2005) “Countermeasures for GPS Signal Spoofing” *ION GNSS 18th International Technical Meeting of the Satellite Division*, 13-16 September, Long Beach, CA, pp. 1285 – 1290

Widrow, B., K. M. Duvall, R. P. Gooch, and W. C. Newman (1982) “Signal cancellation phenomena in adaptive antennas: Causes and cures” *IEEE Transactions on Antennas and Propagation*, vol 30, no 4, May, pp. 469-478

Youn, W. S. and C. K. Un (1994) “Robust adaptive beamforming based on the eigen structure method” *IEEE Transactions on Signal Processing*, vol 42, no 6, June, pp. 1543-1547

Yu, J. L. and C. C. Yeh (1995) “Generalized eigenspace-based beamformers” *IEEE Transactions on Signal Processing*, vol 43, no 11, November, pp. 2453-2461

Zoltowski, M. D. (1988) “On the performance analysis of the MVDR beamformer in the presence of correlated interference” *IEEE Transactions on Acoustic, Speech, Signal Processin*g, vol 36, no 6, June, pp. 945-947

Zoltowski, M. D., and Gecan, A. S (1995) “Advanced adaptive null steering concepts for GPS”, *Military Communications Conference, MILCOM 95, IEEE*, 5-8 November, San Diego, CA, USA, , pp. 1214-1218

APPENDIX A: LAGRANGIAN METHOD

The method of Lagrange multipliers is employed to solve the following linear constraint optimization problem (Van Trees 2002, Frost 1972)

$$\underset{\mathbf{w}}{Min}\ \mathbf{w}^H\mathbf{R}\,\mathbf{w}, \qquad \mathbf{C}^H\mathbf{w}=\mathbf{f} \tag{A.1}$$

where $\mathbf{R}$ is an $N\times N$ positive definite matrix. $\mathbf{w}$ is a desired gain vector. $\mathbf{C}$ is an $N\times M$ constraint full column rank matrix ($N>M$) and $\mathbf{f}$ is an $M\times 1$ vector. In this minimization, the Lagrangian is formed as (Van Trees 2002)

$$\underset{M\times 1}{\mathrm{L}(\mathbf{w},\boldsymbol{\lambda}_L)}=\mathbf{w}^H\mathbf{R}\mathbf{w}+\boldsymbol{\lambda}_L^H(\mathbf{C}^H\mathbf{w}-\mathbf{f})+(\mathbf{w}^H\mathbf{C}-\mathbf{f}^H)\boldsymbol{\lambda}_L. \tag{A.2}$$

where $\boldsymbol{\lambda}_L$ is the Lagrange multiplier vector. Taking the complex gradient of $\mathrm{L}(\mathbf{w},\boldsymbol{\lambda}_L)$ with respect to $\mathbf{w}$ and setting the result equal to zero results in

$$\mathbf{w}^H\mathbf{R}+\boldsymbol{\lambda}^H\mathbf{C}^H=\underset{1\times N}{\mathbf{0}} \tag{A.3}$$

which is a least-squares problem. The solution is obtained as

$$\mathbf{w}^H=-\boldsymbol{\lambda}_L^H\mathbf{C}^H\mathbf{R}^{-1} \tag{A.4}$$

By substituting $\mathbf{w}$ in constraint in (A.1), the Lagrange multiplier is obtained as

$$\boldsymbol{\lambda}_L^H=-\mathbf{f}^H\left(\mathbf{C}^H\mathbf{R}^{-1}\mathbf{C}\right)^{-1}. \tag{A.5}$$

Hence the optimal gain vector is obtained as

$$\mathbf{w} = \mathbf{R}^{-1}\mathbf{C}\left(\mathbf{C}^{H}\mathbf{R}^{-1}\mathbf{C}\right)^{-1}\mathbf{f}. \tag{A.6}$$